



National Library
of Canada

Acquisitions and
Bibliographic Services Branch

395 Wellington Street
Ottawa, Ontario
K1A 0N4

Bibliothèque nationale
du Canada

Direction des acquisitions et
des services bibliographiques

395, rue Wellington
Ottawa (Ontario)
K1A 0N4

Votre file - Votre référence

Our file - Notre référence

NOTICE

The quality of this microform is heavily dependent upon the quality of the original thesis submitted for microfilming. Every effort has been made to ensure the highest quality of reproduction possible.

If pages are missing, contact the university which granted the degree.

Some pages may have indistinct print especially if the original pages were typed with a poor typewriter ribbon or if the university sent us an inferior photocopy.

Reproduction in full or in part of this microform is governed by the Canadian Copyright Act, R.S.C. 1970, c. C-30, and subsequent amendments.

AVIS

La qualité de cette microforme dépend grandement de la qualité de la thèse soumise au microfilmage. Nous avons tout fait pour assurer une qualité supérieure de reproduction.

S'il manque des pages, veuillez communiquer avec l'université qui a conféré le grade.

La qualité d'impression de certaines pages peut laisser à désirer, surtout si les pages originales ont été dactylographiées à l'aide d'un ruban usé ou si l'université nous a fait parvenir une photocopie de qualité inférieure.

La reproduction, même partielle, de cette microforme est soumise à la Loi canadienne sur le droit d'auteur, SRC 1970, c. C-30, et ses amendements subséquents.

Canada

UNIVERSITY OF ALBERTA

PROPERTIES OF THE LITHOSPHERE IN
SOUTHERN BRITISH COLUMBIA AND ALBERTA
FROM SEISMIC EXPERIMENTS

BY

Michael John Andrew Burianyk



A thesis submitted to the Faculty of Graduate Studies and Research in partial fulfillment
of the requirements for the degree of Doctor of Philosophy

IN

Geophysics

Department of Physics

Edmonton, Alberta

Fall 1994



National Library
of Canada

Acquisitions and
Bibliographic Services Branch

395 Wellington Street
Ottawa, Ontario
K1A 0N4

Bibliothèque nationale
du Canada

Direction des acquisitions et
des services bibliographiques

395, rue Wellington
Ottawa (Ontario)
K1A 0N4

Vous l'avez vu. Vous l'avez vu.

Vous l'avez vu. Vous l'avez vu.

The author has granted an irrevocable non-exclusive licence allowing the National Library of Canada to reproduce, loan, distribute or sell copies of his/her thesis by any means and in any form or format, making this thesis available to interested persons.

L'auteur a accordé une licence irrévocable et non exclusive permettant à la Bibliothèque nationale du Canada de reproduire, prêter, distribuer ou vendre des copies de sa thèse de quelque manière et sous quelque forme que ce soit pour mettre des exemplaires de cette thèse à la disposition des personnes intéressées.

The author retains ownership of the copyright in his/her thesis. Neither the thesis nor substantial extracts from it may be printed or otherwise reproduced without his/her permission.

L'auteur conserve la propriété du droit d'auteur qui protège sa thèse. Ni la thèse ni des extraits substantiels de celle-ci ne doivent être imprimés ou autrement reproduits sans son autorisation.

ISBN 0-315-95155-9

Canada

Name Michael John Andrew BURIANYK

Dissertation Abstracts International is arranged by broad, general subject categories. Please select the one subject which most nearly describes the content of your dissertation. Enter the corresponding four-digit code in the spaces provided.

Geophysics
SUBJECT TERM

0373
SUBJECT CODE

U·M·I

Subject Categories

THE HUMANITIES AND SOCIAL SCIENCES

COMMUNICATIONS AND THE ARTS
Architecture 0729
Art History 0377
Cinema 0900
Dance 0378
Fine Arts 0357
Information Science 0723
Journalism 0391
Library Science 0399
Mass Communications 0708
Music 0413
Speech Communication 0459
Theater 0465

EDUCATION
General 0515
Administration 0514
Adult and Continuing 0516
Agricultural 0517
Art 0273
Bilingual and Multicultural 0282
Business 0688
Community College 0275
Curriculum and Instruction 0727
Early Childhood 0518
Elementary 0524
Finance 0277
Guidance and Counseling 0519
Health 0680
Higher 0745
History of 0520
Home Economics 0278
Industrial 0521
Language and Literature 0279
Mathematics 0280
Music 0522
Philosophy of 0998
Physical 0523

Psychology 0525
Reading 0535
Religious 0527
Sciences 0714
Secondary 0533
Social Sciences 0534
Sociology of 0340
Special 0529
Teacher Training 0530
Technology 0710
Tests and Measurements 0288
Vocational 0747

LANGUAGE, LITERATURE AND LINGUISTICS

Language
General 0679
Ancient 0289
Linguistics 0290
Modern 0291
Literature
General 0401
Classical 0294
Comparative 0295
Medieval 0297
Modern 0298
African 0316
American 0591
Asian 0305
Canadian (English) 0352
Canadian (French) 0355
English 0593
Germanic 0311
Latin American 0312
Middle Eastern 0315
Romance 0313
Slavic and East European 0314

PHILOSOPHY, RELIGION AND THEOLOGY

Philosophy 0422
Religion
General 0318
Biblical Studies 0321
Clergy 0319
History of 0320
Philosophy of 0322
Theology 0469

SOCIAL SCIENCES

American Studies 0323
Anthropology
Archaeology 0324
Cultural 0326
Physical 0327
Business Administration
General 0310
Accounting 0272
Banking 0770
Management 0454
Marketing 0338
Canadian Studies 0385
Economics
General 0501
Agricultural 0503
Commerce-Business 0505
Finance 0508
History 0509
Labor 0510
Theory 0511
Folklore 0358
Geography 0366
Gerontology 0351
History
General 0578

Ancient 0579
Medieval 0581
Modern 0582
Black 0328
African 0331
Asia, Australia and Oceania 0332
Canadian 0334
European 0335
Latin American 0336
Middle Eastern 0333
United States 0337
History of Science 0585
Law 0398
Political Science
General 0615
International Law and Relations 0616
Public Administration 0617
Recreation 0814
Social Work 0452
Sociology
General 0626
Criminology and Penology 0627
Demography 0938
Ethnic and Racial Studies 0631
Individual and Family Studies 0628
Industrial and Labor Relations 0629
Public and Social Welfare 0630
Social Structure and Development 0700
Theory and Methods 0344
Transportation 0709
Urban and Regional Planning 0999
Women's Studies 0453

THE SCIENCES AND ENGINEERING

BIOLOGICAL SCIENCES

Agriculture
General 0473
Agronomy 0285
Animal Culture and Nutrition 0475
Animal Pathology 0476
Food Science and Technology 0359
Forestry and Wildlife 0478
Plant Culture 0479
Plant Pathology 0480
Plant Physiology 0817
Range Management 0777
Wood Technology 0746
Biology
General 0306
Anatomy 0287
Biostatistics 0308
Botany 0309
Cell 0379
Ecology 0329
Entomology 0353
Genetics 0369
Limnology 0793
Microbiology 0410
Molecular 0307
Neuroscience 0317
Oceanography 0416
Physiology 0433
Radiation 0821
Veterinary Science 0778
Zoology 0472
Biophysics
General 0786
Medical 0760

EARTH SCIENCES

Biogeochemistry 0425
Geochemistry 0996

Geodesy 0370
Geology 0372
Geophysics 0373
Hydrology 0388
Mineralogy 0411
Paleobotany 0345
Paleoecology 0426
Paleontology 0418
Paleozoology 0985
Palynology 0427
Physical Geography 0368
Physical Oceanography 0415

HEALTH AND ENVIRONMENTAL SCIENCES

Environmental Sciences 0768
Health Sciences
General 0566
Audiology 0300
Chemotherapy 0992
Dentistry 0567
Education 0350
Hospital Management 0769
Human Development 0758
Immunology 0982
Medicine and Surgery 0564
Mental Health 0347
Nursing 0569
Nutrition 0570
Obstetrics and Gynecology 0380
Occupational Health and Therapy 0354
Ophthalmology 0381
Pathology 0571
Pharmacology 0419
Pharmacy 0572
Physical Therapy 0382
Public Health 0573
Radiology 0574
Recreation 0575

Speech Pathology 0460
Toxicology 0383
Home Economics 0386

PHYSICAL SCIENCES

Pure Sciences

Chemistry
General 0485
Agricultural 0749
Analytical 0486
Biochemistry 0487
Inorganic 0488
Nuclear 0738
Organic 0490
Pharmaceutical 0491
Physical 0494
Polymer 0495
Radiation 0754
Mathematics 0405
Physics
General 0605
Acoustics 0986
Astronomy and Astrophysics 0606
Atmospheric Science 0608
Atomic 0748
Electronics and Electricity 0607
Elementary Particles and High Energy 0798
Fluid and Plasma 0759
Molecular 0609
Nuclear 0610
Optics 0752
Radiation 0756
Solid State 0611
Statistics 0463

Applied Sciences

Applied Mechanics 0346
Computer Science 0984

Engineering
General 0537
Aerospace 0538
Agricultural 0539
Automotive 0540
Biomedical 0541
Chemical 0542
Civil 0543
Electronics and Electrical 0544
Heat and Thermodynamics 0348
Hydraulic 0545
Industrial 0546
Marine 0547
Materials Science 0794
Mechanical 0548
Metallurgy 0743
Mining 0551
Nuclear 0552
Packaging 0549
Petroleum 0765
Sanitary and Municipal 0554
System Science 0790
Geotechnology 0428
Operations Research 0796
Plastics Technology 0795
Textile Technology 0994

PSYCHOLOGY

General 0621
Behavioral 0384
Clinical 0622
Developmental 0620
Experimental 0623
Industrial 0624
Personality 0625
Physiological 0989
Psychobiology 0349
Psychometrics 0632
Social 0451



UNIVERSITY OF ALBERTA

RELEASE FORM

NAME OF AUTHOR: Michael John Andrew Burianyk

TITLE OF THESIS: Properties of the Lithosphere in Southern British Columbia
and Alberta From Seismic Experiments

DEGREE: Ph.D.

YEAR THIS DEGREE GRANTED: 1994

Permission is hereby granted to the University of Alberta Library to reproduce single copies of this thesis and to lend or sell such copies for private, scholarly or scientific research purposes only.

The author reserves all other publication and other rights in association with the copyright in the thesis, and except as hereinbefore provided neither the thesis nor any substantial portion thereof may be printed or otherwise reproduced in any material form whatever without the author's prior written permission.



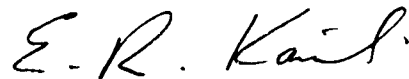
3-11105 9th Ave.
Edmonton, Alberta
T6J 6Z4

August 30, 1994


UNIVERSITY OF ALBERTA

FACULTY OF GRADUATE STUDIES AND RESEARCH

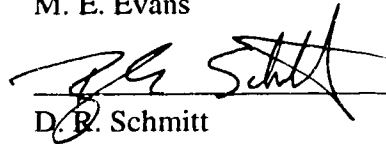
The undersigned certify that they have read, and recommend to the Faculty of Graduate Studies and Research for acceptance, a thesis entitled Properties of the Lithosphere in Southern British Columbia and Alberta From Seismic Experiments submitted by Michael John Andrew Burianyk in partial fulfillment of the requirements for the degree of Doctor of Philosophy in Geophysics.



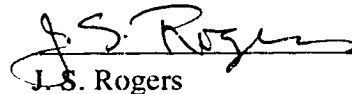
E. R. Kanasewich



M. E. Evans



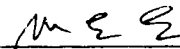
D. R. Schmitt



J. S. Rogers



P. Erdmer



S. B. Smithson

August 30, 1994

Dedication

To Natasha and Mark. I would have finished this a lot earlier without you - but it would not have been worthwhile.

Abstract

Modern techniques of seismic recording and analysis have been used to determine the physical structure and properties of the lithosphere in western Canada as part of the Lithoprobe project. Three dimensional seismic structure is included in the study and integrated with measurements of heat flow, electrical conductivity, geologic and other seismic data.

Travel time and amplitude analysis of wide-angle seismic records from the southeastern Canadian Cordillera show that the crust is similar to the Basin and Range province. It is relatively thin (35 km) and has a low average velocity (6.2 km s^{-1}). Major findings include correlations between velocity trends and large geological structures in the upper and middle crust, and a pervasive low velocity zone over much of the southeastern Cordillera. The relatively low velocities observed correlate well with the high heat flow within the region which is a likely cause of crustal velocity reversals. The uniformly low velocities through the mid-crust to upper mantle also suggest that a heat source lies below the lithosphere.

Broadside recording in the southeastern Cordillera has allowed relatively high resolution mapping of crustal thickness and average velocity which are correlatable to each other as well as to the Bouguer gravity and heat flow data. A previously unidentified deep seismic arrival is evident on one broadside record and allows the interpretation of depth to the asthenosphere.

Seismicity in Western Canada was interpreted by the innovative mapping of earthquake energy emissions. The two main super-terrane of the Cordillera appear as aseismic regions surrounded by seismically active areas interpreted earlier as suture zones. Major faults are highlighted, as are indications of the extent of the North American craton and the location of seismic gaps.

Innovative field procedures resulted in the acquisition of relatively inexpensive, high quality, crustal seismic reflection and associated three-dimensional and wide-angle data from Alberta. The reflection data images a Proterozoic collisional orogen within the Canadian craton. The three-dimensional data image a mid-crustal feature while preliminary analysis of the wide-angle records gives the first indications of the velocity structure of central Alberta.

Acknowledgements

This has been a long and complex effort. Along the way, there have been many people who have helped me and contributed much to this final product. Without exaggeration I can say that it couldn't have been done without their efforts.

First, I would like to thank my supervisor, Professor E. R. Kanasewich. Ernie has given me tremendous opportunities and the moral and material support to exploit them. I am sure that few graduate students have ever had the wealth of experience that I have under his tutelage. Besides that I have also profoundly benefited from the wealth of scientific ideas that Ernie has generated.

The untimely passing of Prof. R. St. J. Lambert was felt deeply. It was not simply the hole left in my graduate committee; I greatly miss his erudition and his sincere interest in my work.

Charles McClouglan and Len Tober have been constants in my studies at the U of A Department of Physics. Charles was instrumental in most of the earlier computer work for data editing, processing and display and cartography. He was also ready, able and willing to discuss every topic imaginable, and did so to my delight. Len is the very model of what a technician should be. I have spent a lot of time with him in the field and am very thankful for the depth of his experience and his willingness to share it.

More recently, Norman Udey has been the critical factor in the evolution of our computer and graphics capabilities. Through Norman's endeavors, I have been able, almost seeming effortlessly, to leap over several generations of computer technology. Norman's work laid the groundwork for Edward Thommes who wrote the FORTRAN code for the direct to PostScript `insight_to_ps` program for seismic data plotting. Jim MacKinnon must also be mentioned for his work in keeping the computer systems running.

It has been the nature of most of my work that there was little opportunity for direct collaboration with my fellow graduate students. Nonetheless, I have been happy in my associations with my lab mates. In particular, Dai Nanxun and Sotiris Kapotas were always ready for consultation on all matters scientific or not.

On the other hand, the recent Alberta Transect reflection work has allowed me to help, and more importantly, to be helped by Gilbert Dubuc and Lu Rong. I am grateful to both of them, but especially Gilbert for his initial work on the interpretation of the 3-D data volume. Fotios Kalantzis has helped all of us with his advice on the use of those software packages of his creation and/or expertise

Also, Doug Schmitt, though a tenured professor, hasn't yet quite been able to make the mental transition from graduate student. I am thankful for the many discussions on scientific and other matters I have had with him.

As principal organizer of LITHOPROBE's SCoRE '90 program, I would like to express my gratitude to the 40 some colleagues, from the Universities of Alberta, British Columbia, Saskatchewan, and Victoria, and from the Geological Survey of Canada (Ottawa) and the United States Geological Survey (Menlo Park), who participated in the field work. Among them I must single out Jim Luetgert of USGS from whose field experience I benefited greatly and Lyndsey Brady and Greg Purdue who did a tremendous job for me that entire summer. I am also grateful to Mal Stelck, Principal and Pat Jacklin, Campus Manager of Selkirk College in Castlegar, British Columbia (along with John Adams and Leslie Anderton) for their donation of laboratory space (and kind help and support) for that experiment. I would also like to acknowledge and thank Chevron Canada Resources Limited of Calgary for the loan of their Trimble GPS instrument.

Much of the data interpretation was carried out by use of the various versions of the computer programs *rayinvr* and *tramp* written by Colin Zelt. To Colin, and to his brother Barry, I am also indebted for their advice on the use of *rayinvr* and guidance in refraction seismic interpretation in general. I have also benefitted from the counsel of George Spence, Don White, Dave Forsyth, Ron Clowes, Bob Ellis, Trevor Lewis, Gary Fuis, S. B. Smithson, T. L. Pratt and an anonymous reviewer of certain earlier parts of this work. James Viau and Jean-Francois Lemieux are also to be thanked for their work on some especially tedious, but nonetheless important, calculations and graphics. I am also deeply grateful to Kris Vasudevan, Rolf Maier and other past employees of the Lithoprobe Seismic Processing Facility for their help and advice over the years.

During my time at the University of Alberta, I have been supported by various Graduate Assistantships from the Department of Physics. I thank them for that support and the opportunity to interact with undergraduate students. I am also obliged for major scholarships I have held, the Province of Alberta Graduate Fellowship and the Amoco Canada Postgraduate Scholarship in Geophysics as well as the CSEG scholarship.

Finally, I am gratified to have been able to be associated with the LITHOPROBE program. Canadians can rest assured that their tax dollars have been wisely invested.

Table of Contents

1	Introduction	1
1.1	Background	1
1.2	Seismic Methods	4
1.3	Geological and Geophysical Framework	15
1.4	Outline	25
2	Cordilleran Seismic Refraction/Wide-Angle Reflection Experiment	28
2.1	Background	28
2.2	Data Acquisition	29
2.3	Data Characteristics	38
2.4	Data Modelling	51
2.5	Interpretation	67
2.6	Discussion	80
2.7	Summary	90
3	Three-dimensional Cordilleran Refraction/Wide-Angle Reflection Analysis	93
3.1	Background and Data Acquisition	93
3.2	Data Characteristics	93
3.3	Interpretation of split-spread record	100
3.4	Measurement of crustal thickness from broadside records	102
3.5	Sub Moho arrivals and mantle structure	112
3.6	Summary	118
4	Seismic Power Density and Seismicity in Western Canada	120
4.1	Background	120
4.2	Western Canadian seismicity	121
4.3	Seismic power density map	124
4.4	Seismicity and tectonic elements	125
4.5	Summary	132
5.	Alberta basement transect seismic reflection	133
5.1	Background	133
5.2	Two-dimensional profiling	135
5.3	Three-dimensional data	143
5.4	Velocity determination using long offset expanding spread data	147
5.5	Summary	156
6.	Conclusions	159
6.1	Cordilleran Wide-Angle Experiments	159
6.2	Cordilleran broadside experiment	161
6.3	Seismic Power Density	161

6.4 Alberta Basement reflection experiments	162
Bibliography	164
Appendices	176
1 SCoRE '90 Schedule	176
2 SCoRE '90 Participants	177
3 SCoRE '90 Shotpoint List	178
4 Number of Shotholes and Quantity of Explosives	179
5 Detailed Shothole Locations and Shot Times	179
6 SCoRE '90 Shotpoint Environmental Requirements	185
7 SCoRE '90 Receiver Site Names	185
8 Deployment and Shooting Schedule	186
9 SCoRE '90 Shot Profiles	187

List of Tables

Table		Page
4.1	Large Earthquakes on the west coast.	129
5.1	Crustal velocity function for line 7 ESP.	157

List of Figures

Figure	Page
1.1 Southern Alberta and British Columbia and LITHOPROBE transects	2
1.2 Schematic seismograms.	4
1.3 The seismic reflection method.	6
1.4 The seismic refraction method.	9
1.5 Multiple wide-angle seismic records.	12
1.6 Broadside seismic experiments.	14
1.7 Terranes and Tectonic Elements of Western Canada.	16
1.8 Major morphogeological tectonic belts of western Canada.	18
1.9 Geological domains of Central Alberta and seismic reflection lines.	19
2.1 Morphogeological belts of the Cordillera and the SCoRE profiles.	31
2.2 Velocity sensitivity of the seismographs.	36
2.3 SCoRE'90 Line 8 shot 32.	39
2.4 SCoRE'90 Line 8 shot 32 with picks.	40
2.5 SCoRE'90 Line 8 shot 37.	41
2.6 SCoRE'90 Line 8 shot 37 with picks.	42
2.7 SCoRE'90 Line 7 shot 23.	43
2.8 SCoRE'90 Line 7 shot 23 with picks.	44
2.9 SCoRE'90 Line 7 shot 30.	45
2.10 SCoRE'90 Line 7 shot 30 record section with picks.	46
2.11 Synthetic seismograms for Line 8.	47

2.12	Normalized energy vs. source-receiver offset for Line 7 P_g arrival.	54
2.13	Ray paths and traveltimes/distance curves from Line 8.	55/56
2.14	Ray paths and traveltimes/distance curves from Line 7.	59
2.15	Normalized energy vs. source-receiver offset from Line 7 reflections.	65
2.16	Final velocity model for SCoRE'90 line 8.	68
2.17	Final velocity model for SCoRE'90 line 7.	69
2.18	Migrated and coherency-filtered vibrator reflection line 6.	72
2.19	Line 8 final velocity model compared with the interpreted reflectivity.	73
2.20	Migrated and coherency-filtered vibrator reflection lines 7-11.	78
2.21	Line 7 final velocity model compared with the interpreted reflectivity.	79
2.22	Velocity depth columns for several regions of western North America.	81
2.23	Schematic of Line 7 final velocity model and crustal isotherms.	89
3.1	Lithoprobe's SCoRE '90 broadside recording.	94
3.2	SP 32 broadside record.	95
3.3	SP 35 broadside record.	96
3.4	SP 61 broadside record.	97
3.5	SP 37 broadside record.	98
3.6	Amplitude vs. offset curves.	101
3.7	Theoretical and observed traveltimes fit for SP 37 'split-spread' record.	103
3.8	Final velocity model for SP37 broadside record.	104
3.9	In-line and corresponding broadside traces for SP 35 and 61.	105
3.10	Example of interpretation of broadside data for depth to Moho.	107
3.11	Depth to Moho in the southeastern Canadian Cordillera.	108

3.12	Average crustal velocity in the southeastern Canadian Cordillera.	109
3.13	Bouguer gravity in the southern Canadian Cordillera.	110
3.14	Parts of SP 32 in-line and broadside records.	113
3.15	Hypothetical deepening of the Moho on Line 8.	115
3.16	Blowup of SP 32 in-line record.	116
3.17	SP 32 deep broadside arrivals straddling the in-line intersection.	117
4.1	The seismicity in western Canada and adjacent regions for 1964-1988.	122
4.2	Earthquake events reported in the period prior to 1964.	123
4.3	Seismic power density of western Canada for period 1964 to 1988.	126
4.4	Seismic power density of western Canada and tectonic elements.	127
4.5	Cross sections showing the depth of earthquakes	130
5.1	Magnetic field over Alberta with the seismic reflection lines.	134
5.2	The standard seismic reflection spread geometry.	136
5.3	The standard seismic reflection geometry.	137
5.4	Array overlaps ensure continuity.	140
5.5	Three-dimensional field acquisition.	144
5.6	Three-dimensional reflection grid.	146
5.7	Migrated and coherency filtered line 2.	148
5.8	Migrated and coherency filtered lines 3.	149
5.9	Structure map of the top of the mid-crustal horizontal reflector.	150
5.10	Structure map of the bottom of the mid-crustal horizontal reflector.	151
5.11	Structure map of the bottom of the crust.	152
5.12	Expanding spread profile geometry.	154

5.13	Migrated and coherency filtered line 7.	155
5.14	Plots of Alberta Basement Line 7 ESP velocities.	158

1. Introduction

1.1 Background

This work describes three seismic studies of the earth's crust and lithosphere in areas of western Canada using state of the art instrumentation and methods of computer analysis. Two of the three studies are LITHOPROBE experiments; one a set of refraction/wide-angle seismic profiles from the southeastern Canadian Cordillera in British Columbia and the second a near vertical incidence seismic reflection data set over the Alberta plains (Figure 1.1). The third study utilizes earthquake databases to investigate crustal characteristics over western Canada as a whole.

LITHOPROBE is described as "Canada's national, collaborative, multidisciplinary Earth science research project" [Clowes, 1993]. It is a consortium of Canadian Universities, federal and provincial research agencies and private industry whose goal is to determine the basic geologic structure of Canada by geophysical and geological probing of the crust and upper mantle - i.e the 'lithosphere'. It is funded by NSERC, the Geological Survey of Canada and by other public and private funding. The Lithoprobe program is one of Canada's scientific Centres of Excellence whose yearly budget is at a current level of 5 million dollars. The bulk of this funding is for seismic profiling, but there are separate budgets for electromagnetic studies and supporting geosciences such as geochemistry, geochronology, geological surface mapping, rock physical properties and so on.

LITHOPROBE is divided into various transects which are carefully planned to investigate integrated geological provinces. The Southern Cordillera Transect was a part of Phase I and II and was established to study the Canadian Cordillera in southern British Columbia. It is in the final stages of completion and consolidation. The Alberta

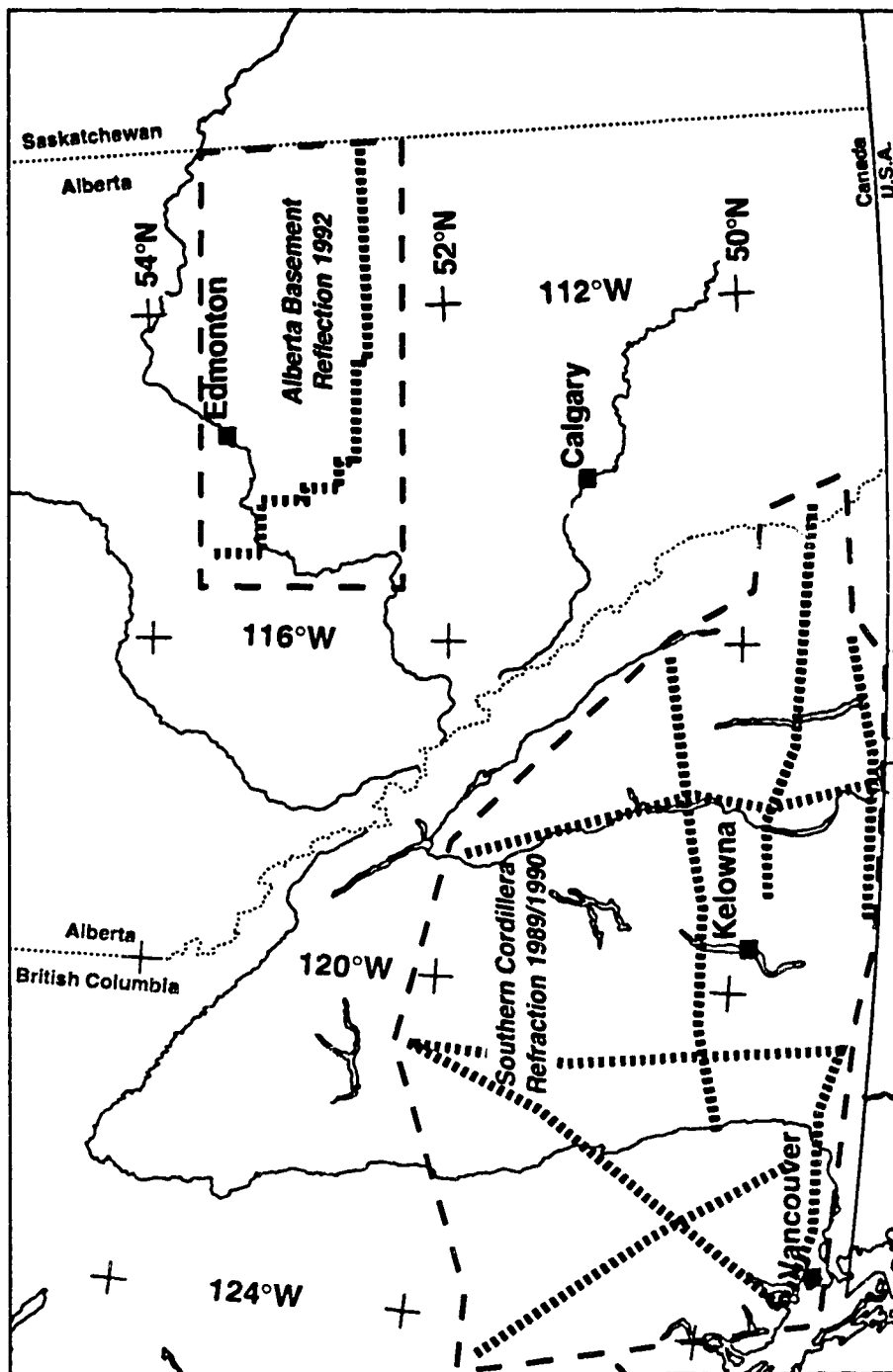


Figure 1.1 Map of southern Alberta and British Columbia showing the general locations of LITHOPROBE's 1992 Alberta Basement Reflection program and the 1989/90 Southern Cordillera Refraction Experiments.

Basement transect, set up to explore the crystalline rocks (the 'basement') beneath the sedimentary cover of Alberta, is one of the latest projects in Phase III.

1.2 Seismic Methods

All types of experimental, or observational, seismology have as their basis the 'seismogram'. A seismogram is a graph, measured at a specific location, usually at the earth's surface, of elastic and anelastic waves propagating through the earth. Seismograms are most often graphically portrayed as 'wobble-traces' - plots of oscillations specifying the amplitude ('x-axis'), phase and frequency of the seismic wave arrivals measured with respect to the time ('y-axis') of the seismic arrivals (Figure 1.2a). Several seismograms can be plotted together as record sections with the amplitude axis also serving as the spatial dimension with respect to the distance between the seismic source and recording location (Figure 1.2b).

Observational seismology can be divided into two types. One kind uses fixed location seismometer arrays to record natural seismic sources - earthquakes mainly [Milne, 1899, Bullen, 1963]. These seismic signals can be studied to ascertain either the characteristics of the source (the principal domain of earthquake seismology), the parameters (crustal layering and velocities) of the earth between the source and receivers or the state of the crust as shown by the location and timing of earthquakes (known as seismicity). The other variety of seismology is known as controlled-source (or explosion) seismology [Mallet, 1848; Mallet, 1851; Abbot, 1878], and involves the use of artificial sources (explosives, mechanical vibrators, marine airguns, etc.) and a large number of mobile, usually linear, arrays of seismometers. This type would include the so-called refraction method [Mallet, 1861; Mintrop, 1931], until recently the most important technique for crustal studies [Meissner, 1986; Fowler, 1990], and the reflection

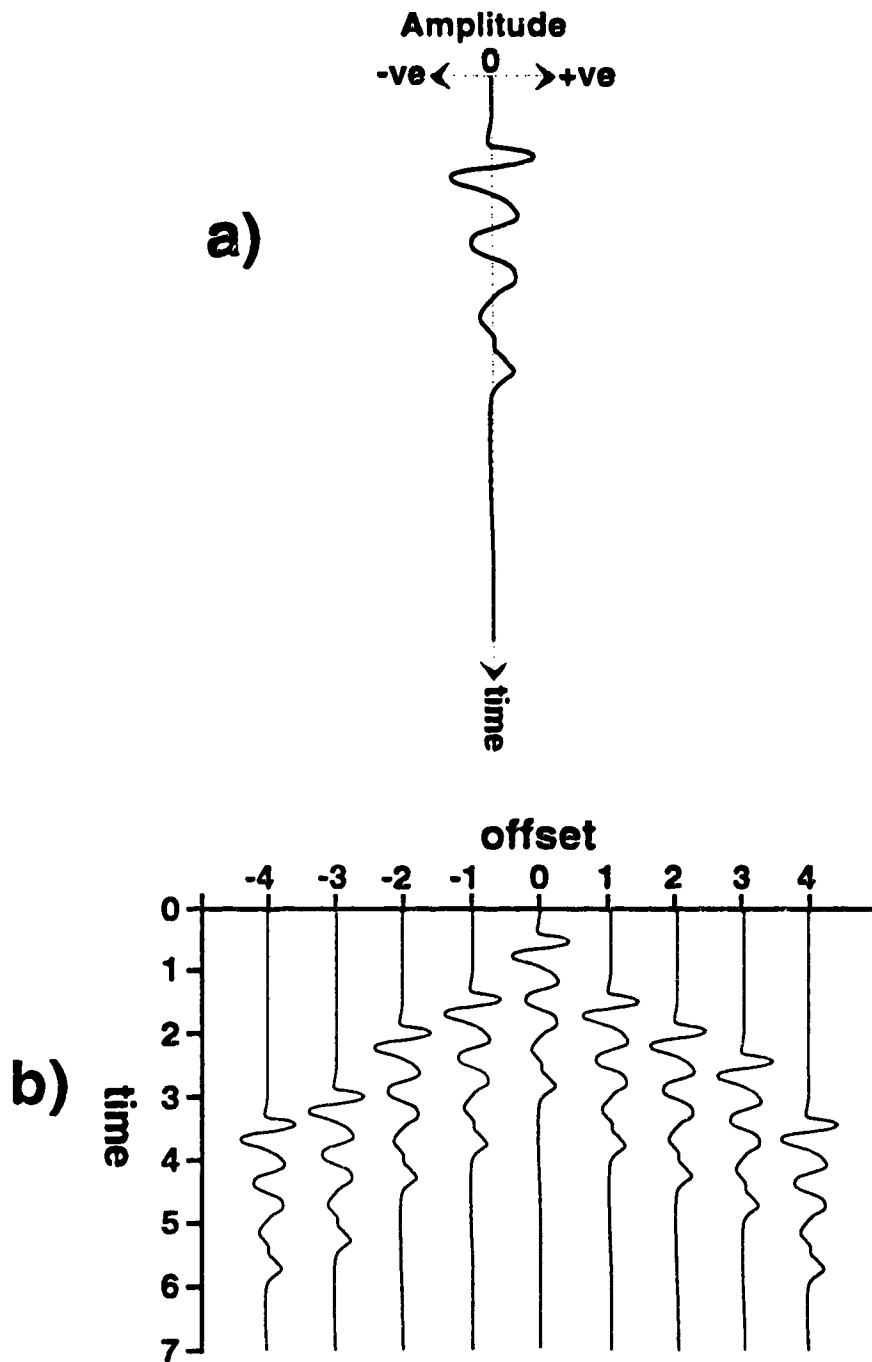


Figure 1.2 Schematic seismograms. A seismogram, a) is a recording of the measurement of ground motion with time due to seismic wave arrivals at a particular location. A set of seismograms, b) can be plotted as a seismic record section in relation to their distance from the seismic source.

method [Fessenden, 1917; Karcher, 1987] which dominates the petroleum exploration industry to this day [Telford *et al.*, 1990; Dobrin and Savit, 1988].

Of the non-explosion type of seismology, only seismicity studies are dealt with in this work. Seismicity [Gutenberg and Richter, 1949] describes the geography and distribution of earthquakes and their relationships with the tectonic stresses in a region. The known characteristics of earthquakes which are determined by analysis of signals recorded at seismic observatories - time of occurrence, depth, location and magnitude - are compiled by such government organizations as the Geological Survey of Canada and the U.S. Geological Survey, in readily accessible data bases. The magnitude of an earthquake can be quantitatively related to the amount of energy it radiates [Gutenberg and Richter, 1956]. Most continental earthquakes, away from lithospheric plate boundaries, are relatively shallow, occurring above the 'brittle/ductile' crustal transition in the mid crust and as such give a broad picture of the state of stress of the crust. Any seismicity studies are limited by the uncertainties in location due to poorly known regional velocity models and the small number and limited distribution of earthquake observatories.

The seismic reflection method [Fessenden, 1917; Karcher, 1987], also known as near vertical incidence seismic profiling, has been in development for the past 70 years as a tool in petroleum exploration. It has been applied to deep crustal studies since the 1950s [Junger, 1951; Kanasewich and Cumming, 1965] and has become so successful a tool that several national programs, such as the U.S. CoCorp, British BIRPS and French ECORS, have been developed strictly around it. It should be noted however, that Canada's LITHOPROBE program uses seismic reflection techniques only as the main method of an interdisciplinary approach to crustal studies.

The reflection technique can be characterized by several features that distinguish it from other controlled source methods (Figure 1.3a). The intervals between receiver

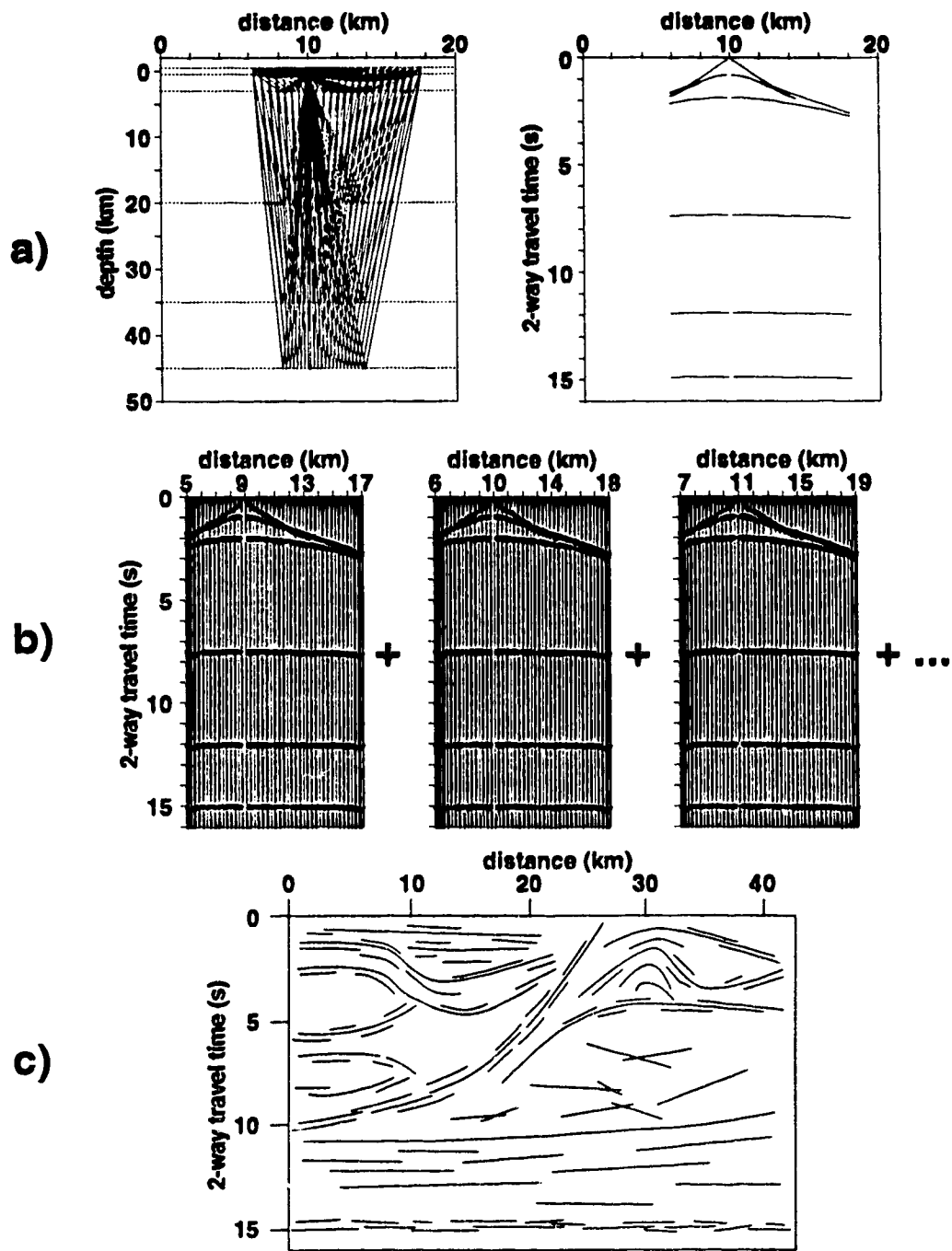


Figure 1.3 The seismic reflection method. a) ray paths and travel-time curves for a seismic reflection experiment. Note the distance scale, especially with respect to Figure 1.4. Ray paths have near vertical angles of incidence resulting in poor velocity estimation using travel time curves. b) Reflection experiments are composed of a great number of overlapping record sections which are, after various data corrections are summed into c) seismic profiles which give a detailed image of the reflectivity (assumed to mirror geology) of the crust.

stations are predominantly tens of meters, with source intervals usually only two to four times greater. The receivers are generally arrays of seismometers (currently numbering 240 to 480) laid out in patterns in such a way as to minimize both random ambient and coherent source generated noise. The arrays are interdependently connected to a single digital recording system. The seismic sources have relatively high frequency content (maxima over 100 hz) with wide bandwidths (4-5 octaves). Sources on land can be explosives (up to several kilograms) in shallow boreholes or standard petroleum industry mechanical vibrators (44,000 lb peak force). Data acquisition results in a large number of several second long, highly redundant seismic records, each containing a large number of individual seismograms (Figure 1.3b). These data are amenable to very specialized data processing techniques, including static and dynamic alignments, summation of common midpoint seismograms and two-dimensional filtering and image processing methods such as migration [Schoenberger, 1984; Yilmaz, 1987].

The final form of the data are cross-sections of the earth (Figure 1.3c) that display the 'reflectivity' of the crustal profile plotted in terms of the traveltime of the seismic waves from source to reflector and back to the receiver ('two-way travel time'). Occasionally, assuming or knowing the seismic velocities, the sections may be converted to, and plotted, in depth. Reflectivity is due to impedance contrasts within the earth which have been thought to be generated by, among other things, lithologic contrasts, banding within fault zones, layered intrusions, anisotropy and trapped fluids. Though it is not always clear, in crustal studies, what the seismic waves are reflecting from, reflection profiles are commonly interpreted to present an image of the sub-surface structural geology - illuminating the geologic layering and geometry of faults, shear zones, crustal ramps and other structures.

These data, in terms of general seismology, are of high resolution - laterally due to the small source and receiver intervals and temporally, or in depth, due to the high

signal frequency and broad bandwidth. As well, reflection data is considered by some to be much less ambiguous than other seismic data, relating a sequence of events from the crust, reflectors, uniquely to a sequence of arrivals on the records [Meissner, 1986]. Nonetheless, it must be pointed out that for deep crustal data reflectivity is rarely continuous over much more than a fraction of the profile - correlating one reflection segment to another is not always straight forward. Seismic reflection data are also relatively insensitive to velocity changes in the subsurface. The short aperture array which gives such high lateral resolution of reflectivity samples only that small portion of the seismic wave field that has travelled essentially directly down and back up - that is, only near vertical incidence rays are recorded. The wider angle seismic rays which carries most of the information on velocities are not measured. Some velocity information is retrievable, but it is of low resolution. As a rule, the resolving velocity power of reflection profiling decreases as the ratio of aperture length to depth of investigation.

Reflection seismic exploration procedures are evolving in ways to increase the amount of information on crustal properties that can be obtained. The acquisition of three-dimensional reflection recording is becoming common place in the petroleum industry and has very lately been applied to crustal studies [Chapter 5]. Use of longer recording spreads in specialized crustal experiments has increased the resolution of velocity measurements [Chapter 5].

Seismic refraction [Mintrop, 1931], better termed wide-angle profiling, or in Europe, Deep Seismic Sounding (DSS) [Zverev, 1967; Giese *et al.*, 1976], is perhaps the other end of the seismic exploration spectrum (Figure 1.4). This method has been principally used for large scale crustal studies [Meissner, 1986], but also in miniature in very shallow engineering and mining applications [Milsom, 1989].

In wide-angle profiling receiver intervals are on the order of a kilometer while shot intervals are measured in tens of kilometers (Figure 1.4a). The receivers are usually

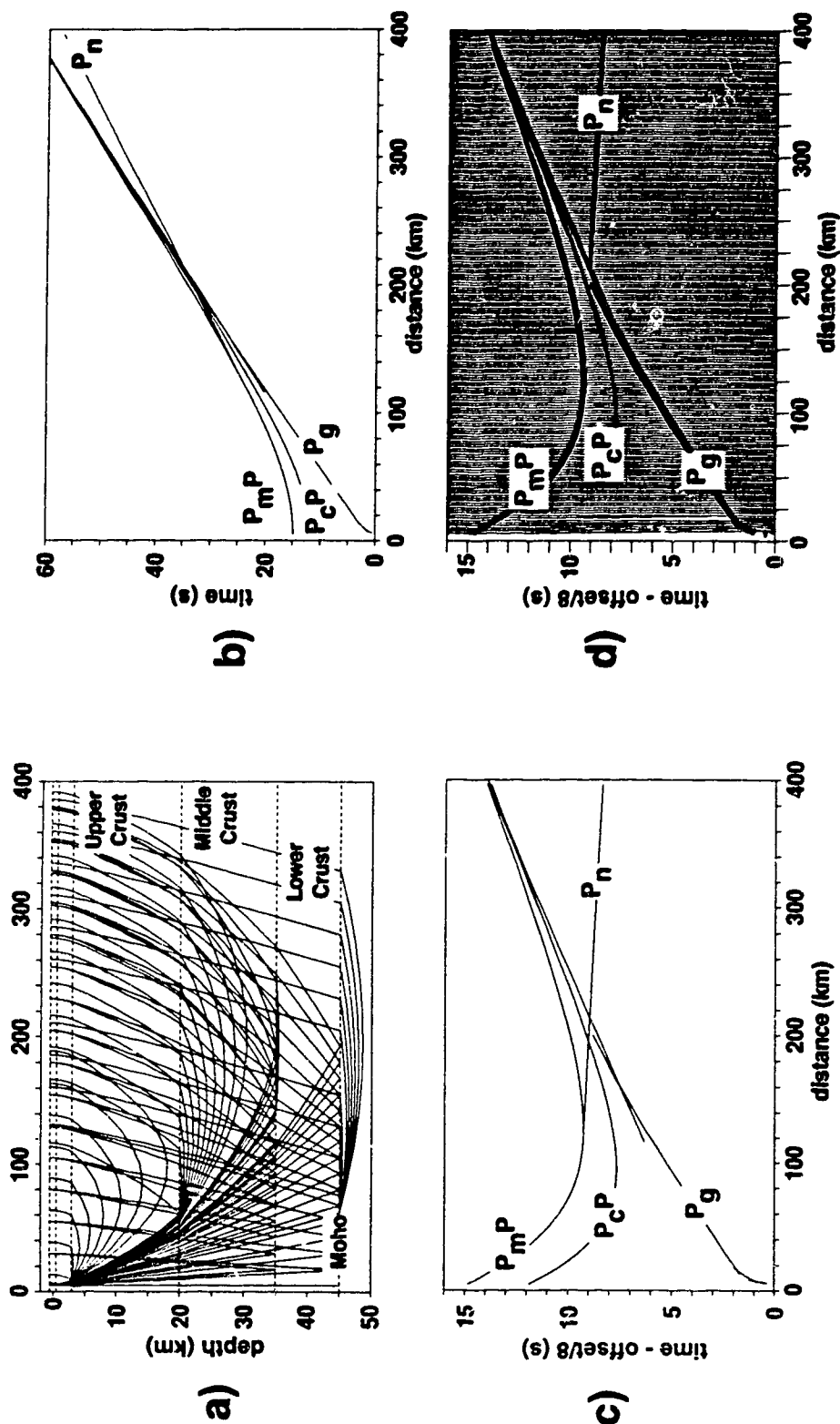


Figure 1.4 The seismic refraction method. a) ray paths for a wide-angle experiment. Note the distance scale here and on subsequent panels, especially in relation to Figure 1.3. b) travel-time curves for the preceding ray path diagram. Note the long time scale. c) reduced travel-time plot of preceding panel. The time scale is much smaller and the different seismic arrivals are more differentiated. d) reduced travel-time synthetic seismic record of the preceding panels. The amplitude characteristics of different arrivals are noticeable and can be exploited in an interpretation. The arrival identifications are as in the text.

several hundred single seismometer/digital recorders, independently deployed along profiles hundreds of kilometers long. Sources are exclusively large explosive charges (hundreds to thousands of kilograms) in boreholes. Though the sources themselves are frequency rich [Jarchow *et al.*, 1990] attenuation of higher frequencies by long crustal travel times limits the frequency content of the recorded signals to 0-20 Hz. A relatively small number of redundant and reversed seismic records are recorded for many tens of seconds (Figure 1.4b). Seismometer/receiver locations must be measured accurately to less than 100m and start of recording time measured within microseconds relative to shot location and time. Data are usually compressed and stored in reduced time format - the seismograms shifted towards zero time on the basis of their distance from the source (Figure 1.4c).

Unlike reflection profiling which depends on summation of redundant data for high S/N, data quality in refraction experiments depends strongly on shot size, wave propagation efficiency and local noise and coupling characteristics at the receiver sites. The acquisition geometries and conditions also limit the amount of data processing that can be applied. Acquisition geometries and the particular seismic signals recorded preclude the common-midpoint stacking that is so effective in reflection work. Variable receiver intervals and gaps, resulting from difficulty in accessing sites over long distances, limits the effectiveness of two-dimensional filtering and analysis techniques. Usually, digital processing is limited to bandpass filtering and various amplitude gaining procedures. One major complication is that independent recording, and often the use of different instrumentation within the same experiment, necessitates much post-acquisition data editing and merging.

The resulting data sets are composed of separate record sections, or 'shot profiles', for each shotpoint (Figure 1.4d). The first seismic arrivals, relatively unimportant in reflection data, are important and prominent signals on wide-angle

profiles. These first arrivals are the seismic rays which travel directly from the shotpoint through the crust, usually in curved ray paths, to the receiver and are given the designation P_g . With long shot-receiver offsets (150-200 km or more), direct first arrivals from the upper mantle, P_n rays, are easily recorded. Prominent secondary arrivals can include other direct path seismic energy, usually very prominent wide-angle reflections from the base of the crust, labelled P_mP , and often other less prominent wide-angle reflections originating within the crust and upper mantle. All of these arrivals can also exhibit variations in their amplitude characteristics.

Compared to reflection data, refraction seismic is of low resolution. Long source/receiver spacing and limited temporal bandwidths means that the method is relatively insensitive to reflectivity. However, the strength of the technique lies in its extreme sensitivity to the elastic velocities of the material the waves propagate through. The travel-times from source to receiver of the direct waves give direct indications of the rock velocities and complete measurement of wide-angle reflection move-out curves provides high quality velocity constraints. Multiple shotpoints over a profile provide different angles of illumination allowing modern data sets to be treated in much the same way as in tomographic techniques (Figure 1.5).

Simple analysis of refraction data can be accomplished by measurement of the slopes and intercepts of direct arrival travel time curves for which abundant details are found in most introductory seismology texts [Telford *et al.*, 1990; Dobrin and Savit, 1988]. Serious analysis of crustal shot profiles, however, is done by various seismic modelling techniques. The most important modelling procedure used is ray-tracing based on Asymptotic Ray Theory [Cerveny *et al.*, 1977] because of its computational speed, the ability to easily control the types of seismic signals modelled and the ease with which inversion techniques can be applied [Kanasewich and Chiu, 1985; Huang *et al.*, 1986; Zelt and Smith, 1990]. Other modelling methods are used, but suffer from disadvantages such as slow computation times as with finite difference methods or being limited to one-

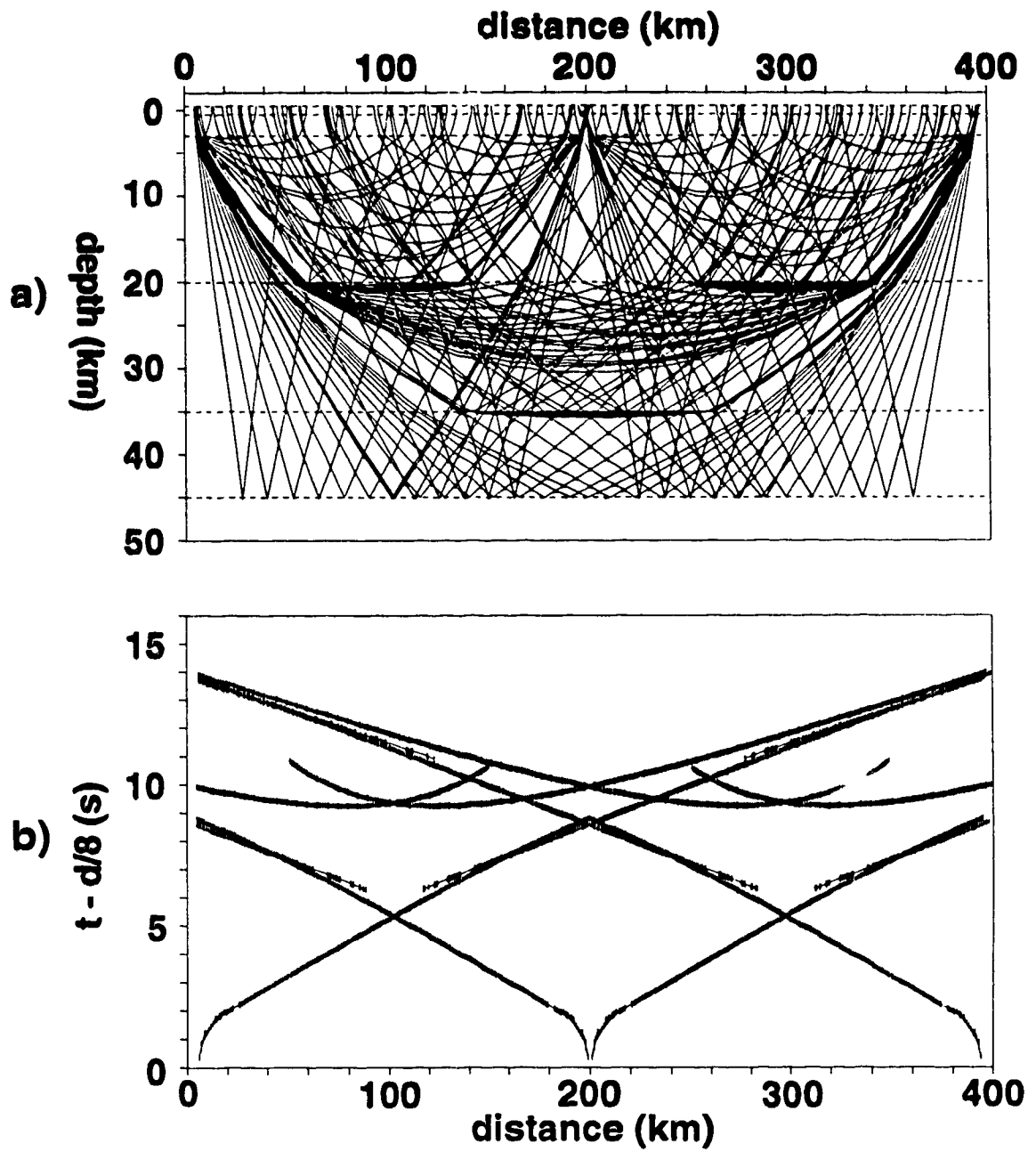


Figure 1.5 Multiple wide-angle seismic records sampling similar parts of the earth from different angles can give detailed images of the velocity structure. a) ray paths through a crustal velocity model. b) theoretical ray paths (curves) matched to travel-time picks (short vertical lines) from experimental data.

dimensional models as with the reflectivity method [*Fuchs and Muller, 1971*].

The basic interpretational approach, with any modelling method, is that of computing theoretical seismic travel time curves, corresponding to those arrivals identified in the data, from a given crustal velocity model (Figure 1.5b). The velocity model is changed until the required degree of fit between computed and actual travel times is achieved. The amplitude characteristics of the recorded waves, sensitive to velocity gradients and seismic attenuation, can be analysed as well and this is where the finite difference or reflectivity algorithms can be superior to ray-tracing methods. The forward modelling approach described above can be somewhat automated by mathematically minimizing the misfit between theoretical and field data with respect to a parameterized model [*Menke, 1989*]. A recent example of this technique is the work of *Zelt and Smith* [1991].

The final model is usually represented graphically by a crustal profile showing layering and velocity variations. The velocity structure is primarily due to lithology and mineralogy, but is generally modified by depth, pressure, heat, and presence of fluids.

Wide-angle experiments, even since the early 20th century, have also included fan, or broadside, shooting (Figure 1.6). Extensions to this have culminated in the fully 3-D 'Kanasewich Triangle' [*Kanasewich et al., 1987; Zelt et al., 1992*] experiment, while regular broadside records are commonly recorded in most crustal experiments. An important trend in wide-angle work is an increase in the number of receivers and shots along with decrease in shot and receiver intervals [*Murphy et al., 1993*] resulting in higher resolution of crustal properties. Increasingly, three component data are being recorded and shear wave arrivals are being interpreted.

The present day reflection and refraction techniques are end members of a continuum of seismic exploration methods and represent the trade-off between geological structure, as implied by reflectivity, and velocity resolution, which can have implications

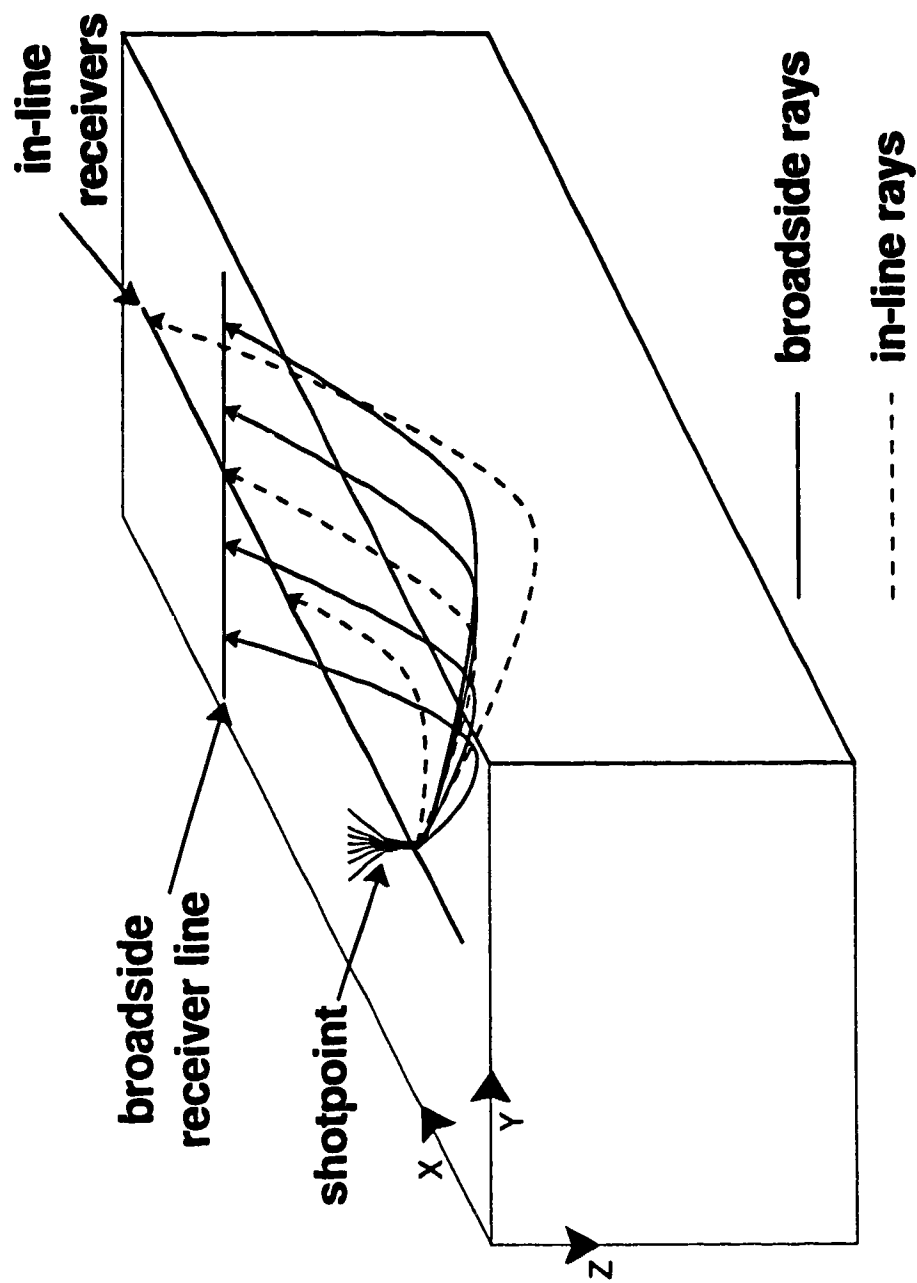


Figure 1.6 Broadside seismic experiments. As opposed to in-line experiments, broadside or fan shots are recorded by receivers along a perpendicular line and add three-dimensionality to seismic work.

for lithology and composition. Also, the reflection method uses vertical incidence arrivals, while the refraction method senses more horizontal rays, which implies different responses to anisotropic media. Common practice in the LITHOPROBE transects is to conduct the refraction shooting coincidentally with the reflection work. As they do measure different aspects of the same parameters of elasticity of the lithosphere, they are fully complementary to one another, though not always in an obvious way.

1.3 Geological and Geophysical Framework

Geologic work on the structure of continental crust revolves around the concepts of 'craton' and 'terrane'. A craton is that part of a continent which has remained coherent and relatively rigid since Precambrian time [*Hoffman*, 1988]. Terranes are geological blocks having some common autochthonous stratigraphic units and are bounded by major faults [*Schermer et al.*, 1984]. Though the concept of terrane has been defined by work on Phanerozoic rocks, recently it has been extended to distinct blocks within cratons, where it is sometimes cognate with the phrase 'geological province' [*Williams et al.*, 1991]. Distinct terranes, but with particular relationships, can be grouped into 'superterranes' [*Monger and Price*, 1982; *Monger*, 1984]. The current location of terranes may be remote from where they were originally formed ('exotic' or 'suspect' terranes) or they may have formed on the edge of the existing craton and suffered small amounts of motion along transcurrent or thrust faults [*Coney et al.*, 1980].

Our study areas include central Alberta, the southeastern Cordillera as well as the whole of western Canada in general. The terranes and tectonic elements of Western Canada and the adjacent regions of the United States of America and the floor of the Pacific Ocean are presented in Figure 1.7. The map, stripped of Phanerozoic sedimentary cover, is based on recent attempts to decompose the continent into its constituent terranes

using surface mapping, interpretation of potential fields and systematic geochronological studies [Ross *et al.*, 1991; Villeneuve *et al.*, 1993; Hoffman, 1988; Hoffman, 1989; Gabrielse and Yorath, 1989; Atwater and Severinghaus, 1989; R. A. Burwash, personal communication]. Figure 1.8 is a map showing the major morphogeological tectonic belts of western Canada, from Wheeler *et al.* [1991] and Gabrielse and Yorath [1989]. These tectonic belts can be associated with the so-called superterrane of the Cordillera.

On the terrane map (Figure 1.7) east of the Rocky Mountains (in blue), the shading of the Precambrian Canadian Shield refer to conservatively interpreted ages. Red colored sections include stable Archean cratonic terranes. Orange is used to characterize juvenile Proterozoic rocks, interpreted by some to be orogenic suture zones between older cratonic masses [Hoffman, 1988; Hoffman, 1989; Ross *et al.*, 1991; Villeneuve, 1993]. Yellow colored elements are considered to be undetermined in age [R. A. Burwash, personal communication]. Note that lineations in the craton just east of the Cordillera, such as the Great Slave Lake Shear Zone and the Snowbird Fault run southwest to northeast.

West of the Rockies, the much younger Cordilleran rocks trend northwest to southeast. The colors are coded to the various related groups of superterrane [Gabrielse and Yorath, 1989], such as the Insular Superterrane on the west coast and the Intermontane Superterrane in the British Columbia interior (seen more easily on Figure 1.8).

The near-vertical seismic reflection data was acquired in central Alberta [Ross *et al.*, in submission]. On the eastern part of this central Alberta study area, at the Saskatchewan border, is the Archean Hearne Province (Figure 1.9). Here, the Hearne is characterized by a positive magnetic anomaly trending north, the Eyehill High, along with the Loverna Block. To the northwest of the Hearne province lie several terranes which all trend northeast. Directly next to the Hearne is the Proterozoic, low grade

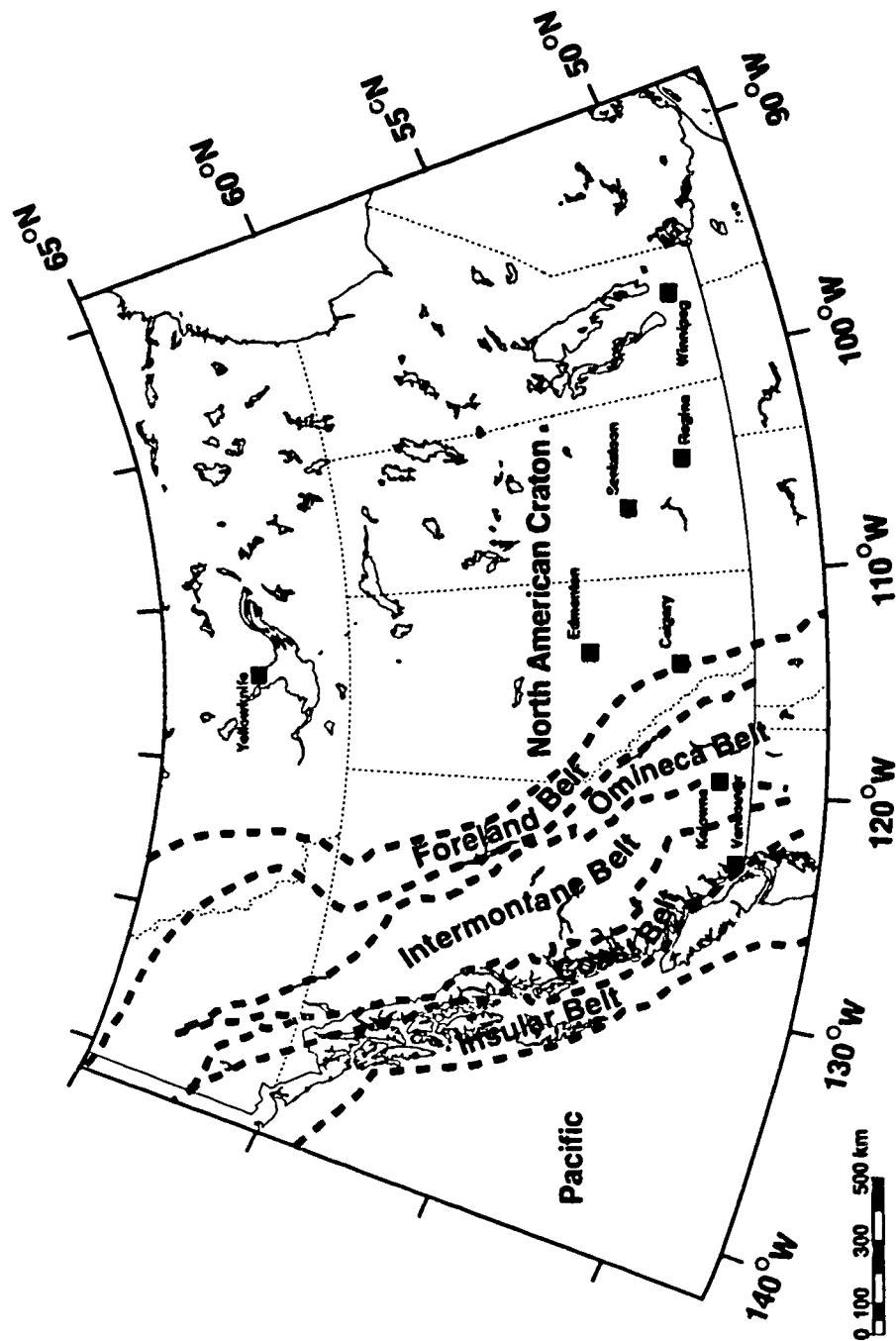


Figure 1.8 Major morphogeological tectonic belts of western Canada, from Wheeler et al. [1991] and Gabrielse and Yorath [1989]. These tectonic belts can be associated with the so-called superterrane of the Cordillera.

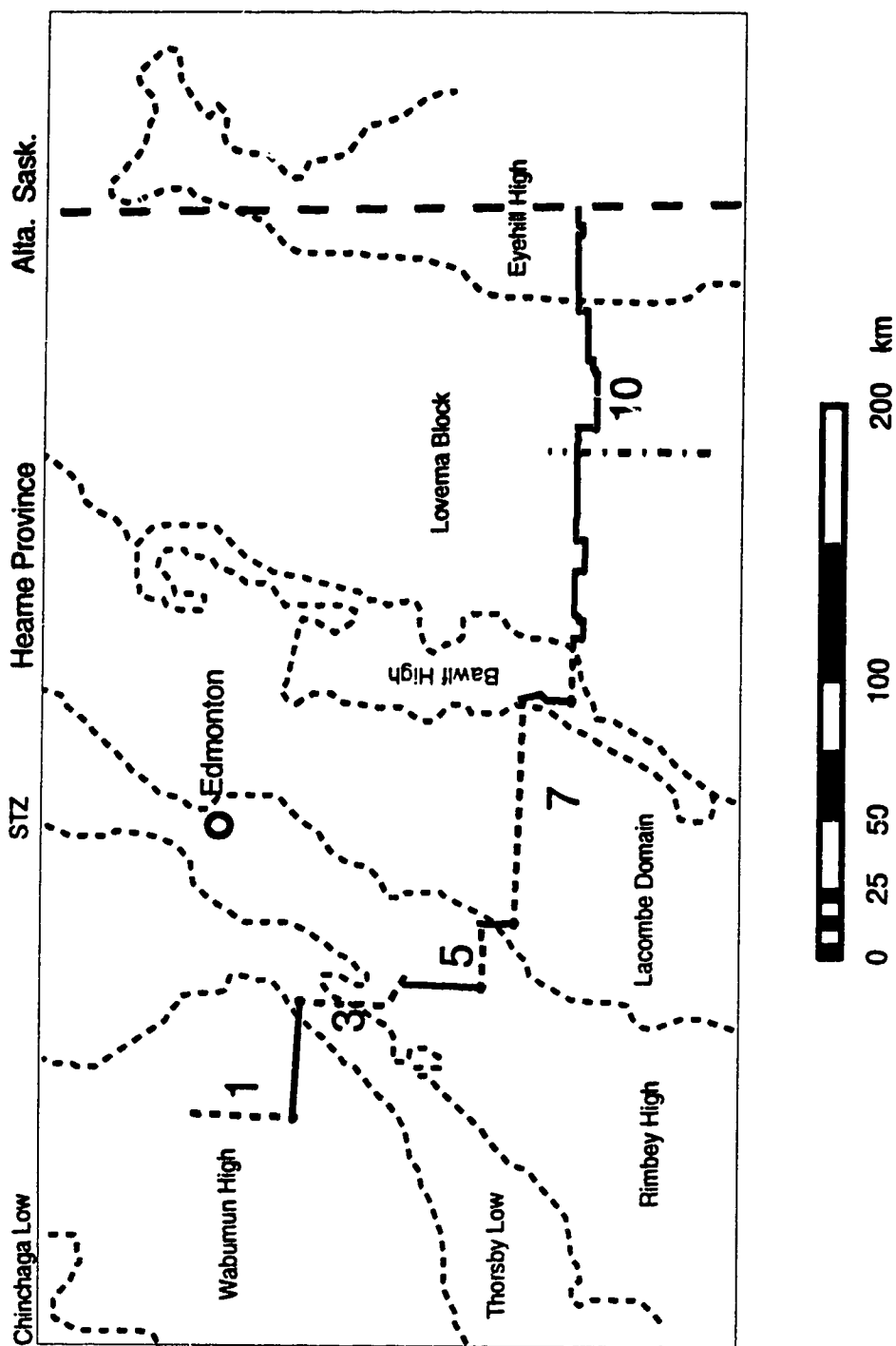


Figure 1.9 Detailed map of basement geological domains of Central Alberta with respect to Alberta Basement seismic reflection lines. The interpreted geologic domains to the east of the Thorsby Low are all part of the Heame Province as seen in Figure 1.7.

metamorphic Lacombe Domain. Further northwest is the Rimbey High that extends from the Snowbird zone to beneath the Rocky mountain foothills and is interpreted to be a juvenile magmatic belt. The following terrane, the Thorsby Low, is thought to be the ductile southern extension of the Snowbird Tectonic Zone in Saskatchewan. Finally, in the westernmost of the study area, is the Wabamun High whose age is early Proterozoic and whose magnetic characteristics suggest another magmatic belt.

Compared to the immense amount of seismic reflection data (predominantly proprietary) collected by petroleum companies, there has been relatively little geophysical crustal data collected on the Canadian craton in western Canada. Only with the current LITHOPROBE transects has there been an opportunity to acquire high quality geophysical measurements. The cratonic terranes and lineaments described above have been interpreted with the help of aeromagnetic and gravity measurements which are only now being adequately completed to cover all areas. Historically, though, there have been a few large scale experiments which have given some insights into the crustal properties of the cratonic crust. *Chandra and Cumming* [1972] and *Kanasewich et al.* [1987] present seismic velocity structures of the North American craton in Western Canada using seismic refraction data from southern Alberta, Saskatchewan and Manitoba. They find that, generally, the crust is 45 km thick. The upper crust has velocities up to 6.4 km/s and a 15 km thick middle crust has velocities of 6.6 km/s. The lower crust begins below 35 km and has a 7.1 km/s velocity. The upper mantle velocity is 8.2 km/s.

The seismic refraction/wide-angle reflection data set was collected in the southeastern Canadian Cordillera (Figure 1.7, west of the Rocky Mountains). Here it has been recognized for the better part of two decades that the region is composed of a great many terranes, some of which have been interpreted as having been displaced far from their places of origin [*Monger and Ross*, 1971; *Monger and Irving*, 1980; *Coney et al.*, 1980]. The geological evolution of the Canadian Cordillera, according to *Gabrielse and*

Yorath [1989], is characterized by the accretion of various types of terranes to the Mesozoic-Cenozoic continental margin and Cretaceous-Cenozoic displacements of these terranes along dextral transcurrent faults. All of this is a direct consequence of the interactions between the North American and the various Pacific ocean lithospheric plates that have occurred in the last two hundred million years [*Atwater*, 1970; *Atwater*, 1989; *Engelbreton et al.*, 1985; *Debiche et al.*, 1987].

During the Late Triassic, just before any collisions had disturbed the miogeoclinal successions of the continental margin, there was already a history of interactions and amalgamations between many of the Cordilleran terranes in the Pacific ocean [*Gabrielse and Yorath*, 1989]. One of these super-terranes, the Intermontane Superterrane, collided with North America in mid-Jurassic time. It is believed that this collision produced the Foreland Belt (i.e. the Rocky Mountains) and a plutonic, metamorphic complex (the Omineca Crystalline belt) described as a 'welt' [*Monger et al.*, 1982] marking the suture zone.

Similarly, in mid-Cretaceous time the Insular Superterrane suffered its collision with North America (which now included the Intermontane Superterrane), forming at least in part, the rocks of the Coast Plutonic Complex as another area of suture.

There is a fair amount of evidence, mostly palaeomagnetic [*Monger and Irving*, 1980; *Irving and Wynne*, 1991], that these superterranes may have collided with North America considerably south of their present locations. Subsequent displacements were accomplished by motion along dextral, transcurrent faults; for example the Northern Rocky Mountain-Tintina Fault system [*Gabrielse*, 1985]. Paleontological data [*Monger and Ross*, 1971] also suggests northward translation of terranes. There is little doubt, geologically speaking, that such transcurrent motions occurred, but the present argument is over the amount of translation - a few hundred kilometers or a few thousand [*Price and Carmichael*, 1986]. At any rate, *Avé Lallemant and Oldow* [1988] suggest that the displacement of what they term 'transpressional' terranes along transcurrent faults on

either side of the plate boundaries is an expression of oblique plate convergence.

The entire history of the Cordillera, then, can be summarized as the oblique convergence of oceanic plates with the North American craton. The oceanic plates carried previously amalgamated superterrane which collided with North America, causing eastward directed thrusting and folding (i.e. shortening) of continental shelf sediments (now the Rocky Mountains), and northward translation of the joined terranes (Intermontane and Insular Superterrane) and intervening zones (Omineca and Coast Plutonic belts) leaving the present Cordilleran geomorphological situation.

The seismic refraction/wide-angle profiles are situated within the southern Omineca Crystalline Belt and the southern Intermontane Belt (Figure 1.7, Figure 1.8). The southern Intermontane Belt is bounded on the west by the Fraser Fault, while the eastern border, shared with the Omineca Belt, is the Okanagan Valley Fault (OVF). Here, the Intermontane Belt is entirely composed of the Quesnelia terrane (Qn) - Triassic-Jurassic arc volcanics and volcanoclastics overlain by Jurassic arc-derived clastics [Wheeler *et al.*, 1991]. In the Omineca Belt the seismic profiles cross rocks of the Kootenay terrane (Ko) - highly deformed and metamorphosed Proterozoic to Triassic clastics with some volcanics and limestones locally intruded by mid-Palaeozoic plutons [Wheeler *et al.*, 1991]. North American continental shelf material [Wheeler *et al.*, 1991] lies in the eastern third of the Omineca within the Purcell Mountain Range. Normal fault and shear zones in both the southern Omineca and Intermontane Belts suggest extension during Eocene time [Gabrielse and Yorath, 1989].

Carr *et al.* [1987] have described normal faults and shear zones associated with a metamorphic core complex of the Omineca belt which suggest extension during Eocene time. The metamorphic core complexes in the Omineca Belt are related to those in the U.S. Cordillera and Basin and Range [Armstrong, 1982]. Parrish *et al.* (1988) look at the geochronology and structure of other Omineca features to document about 80% crustal

stretching in a major portion of the southern Omineca Belt including northern Washington. *Oldow et al.* (1989) calls this the Omineca-Okanagan domain of the Cordilleran extensional province. Though the documented extension occurred much earlier than the tectonic activity in the Great Basin region of the Basin and Range domain [*Eaton, 1982*], *Lambert and Chamberlain* [1988] have commented that some of the Omineca extensional regime dates from more recent times and is simply a northern continuation of the Basin and Range.

The seismic refraction profiles also cross two major Cordilleran thrust faults, the Monashee Décollement (MD) and the Okanagan Valley Fault (OVF). The Monashee Décollement, within the Omineca Belt, marks the top of metasediments and Proterozoic gneissic basement rocks, the Monashee Complex (Mo), considered to be part of the North American craton [*Wheeler et al., 1991; Read and Brown, 1981*]. The MD dips south-southwest on the southwestern end of the Monashee Complex, its dip changing to north-northwest at the northern end. The OVF, the local boundary between the Omineca and Intermontane Belts, is a south-southwest striking thrust fault generally dipping to the west. The Nicola Horst, or Nicola Batholith, bounded by the Coldwater (CWF) and Quilchena Creek (QCF) Faults [*Wheeler and McFeely, 1991*] is also profiled by the seismic lines.

There was little seismic work done in southeastern British Columbia until the late 1960s and early 1970s [*Berry et al., 1971*]. Then, low resolution Cordilleran refraction data [*Forsyth et al., 1974; Berry and Forsyth, 1975*] was interpreted to suggest crustal thicknesses within the Intermontane and western Omineca Belt of 32-40 km, an average crustal velocity of 6.4 km s^{-1} and an upper mantle velocity below 8.1 km s^{-1} . Later, *Cumming et al.* [1979] described two east-west partially reversed refraction profiles across the southeastern Cordillera through the Intermontane and Omineca Belts, oblique to the two SCoRE '90 strike lines (Line 7 and Line 9 - Figure 1.1). Their results indicate that the Moho dips gently eastward from 30 km depth within the Intermontane Belt to

more than 40 km just west of the Foreland Belt. Upper crustal velocities are 6.2 km s^{-1} to a depth of 20 km while a 12-15 km thick lower crust has a velocity of 6.9 km s^{-1} . The upper mantle velocity is 7.8 km s^{-1} . *Cumming et al.* [1979] correlate the thin crust and low velocities with the region's relatively high heat flow.

During the period 1985 to 1988, LITHOPROBE acquired high quality vertical incidence seismic reflection data throughout the southern Canadian Cordillera [*Cook et al.*, 1988, 1992]. This data set has revealed a highly reflective and complex crust with many deep reflectors whose up-dip projections are readily correlatable with surface geology. Several east-west reflection lines are partially coincident with the east-west refraction profiles and one north-south segment of the reflection coverage matches part of a north-south refraction line. On these reflection profiles, *Cook et al.* [1992] interpret prominent reflections to be the Monashee Décollement which is thought to be the top of the North American Craton and dips listrically to the west from near surface into the deep crust. Their model suggests that the craton beneath the Cordillera is highly attenuated and extends to the Fraser River Fault. The Okanagan Valley Fault, used in this area as the boundary between the Intermontane and Omineca Belts, is also interpreted to be a major, westerly dipping, listric shear zone extending to the Fraser Fault. There is also considerable reflectivity associated with the Nicola Horst and its bounding faults. Much of the reflectivity in the sections, not associated with the shear zones, is sub-horizontal. The reflection Moho, assuming a single, homogeneous crustal velocity of 6.0 km s^{-1} , is calculated to be at a depth of 35 km.

There have also been recent, non-seismic, geophysical studies carried out under LITHOPROBE's Southern Cordillera Transect. *Lewis et al.* [1992] study thermal data from the southeastern Cordillera and conclude that the Intermontane/Omineca Belt region is a single province of relatively high heat flow, indicating a warm thin lithosphere. *Jones et al.* [1992] describe magnetotelluric work that shows the crust in the Omineca Belt to be conductive while the Intermontane Belt is less so. They relate the changes in

conductivity to correlations with the heat flow. *Majorowicz and Gough* (1991) find low magnetotellurically derived resistivity values in the Intermontane and Omineca belts. Coupled with moderately high heat flow values in this region [*Davis and Lewis*, 1984; *Lewis et al.*, 1985; *Lewis et al.*, 1992], *Majorowicz and Gough* [1991] conclude that this is confirmation of a previous hypothesis of a mantle upflow in the region [*Kanasewich*, 1966; *Gough*, 1986; and *Kanasewich et al.*, 1987] possibly related to present Basin and Range tectonics

1.4 Outline

Chapter 2 of this work describes the acquisition, analysis and interpretation of two intersecting in-line seismic refraction/wide-angle reflection profiles in the southeastern Canadian Cordillera. These data are a part of SCoRE (Southern Cordillera Refraction Experiment) '90 of LITHOPROBE's Southern Cordillera Transect seismic program (Figure 1.1). The data reveal the crust of the southeast cordillera to be thin and of relatively low velocity in relation to surrounding crust in northwest North America. There is a marked correlation between low velocity regions in the upper crust with the known traces of crustal fault and shear zones. A major horst structure identified from surface geologic mapping is imaged by the seismic data as a high velocity plug in the upper and mid-crust. The velocity characteristics of the neighboring Coast Belt to the west are found to be very different from that of the Omineca/Intermontane region. But, there is little significant difference between the Omineca and Intermontane Belts. A prominent low velocity zone (LVZ) is recognized within the mid crust of the southeast cordillera. The LVZ correlates with crustal isotherms, leading to the conclusion that the region's temperature characteristics modify the velocity structure. Seismic signals from below the crust/mantle boundary define layering in the upper mantle.

Chapter 3 describes the analysis and interpretation of 3-dimensional seismic broadside records from SCoRE '90 (Figure 1.1). The unique geometry of the shotpoints and receivers allowed the recording of seismic signals from deeper in the lithosphere that were not evident on the two-dimensional in-line profiles. Some of the arrivals are from the base of the crust and allow for a higher resolution of a three-dimensional Moho structure, but the most interesting and prominent signals suggest that the previously established upper mantle layer is the top of another low velocity zone and thus is the bottom of the lithosphere.

Chapter 4 describes innovative seismicity studies of western Canada. A power density map is used to summarize the seismic emissions over a 25 year interval. The power output from seismic events is obtained by using an energy-magnitude relation for earthquakes, summing the energy for all events whose hypocenters occur within a half degree square over a period when reliable information is available and dividing by the area and the observational time. The result in Watts m^{-2} are contoured on a logarithmic base to obtain a map showing quantitatively those areas that are most active and which may be correlated with particular lineaments, faults or terranes and the parts that show seismic gaps which may be an indicator of areas with large strain accumulations. Regions which are naturally inactive seismically because strain is being relieved in other ways or because the stress is modest are more easily identified. This form of presentation is very useful in displaying the seismicity in the stable continental interior and making correlations with zones of weakness in the crystalline basement.

The most active areas off the coast of western North America have seismic power emissions equal to 10^{-4} W m^{-2} which is comparable to the average heat flow measurements in many parts of the world. There are striking trends associated with the Coast Plutonic Complex, the region of the Fraser River Fault and the Northern Rocky Mountain Trench. Seismic gaps occur in the power density field and are of particular interest since one coincides with a large metropolitan center. This area would appear to

be a potential site for an earthquake in the magnitude range 6 to 7. Less prominent belts of aseismicity are found in the Insular Superterrane and west of the very active Nahanni area of the Northwest Territories. Northeast-southwest seismically active zones in eastern British Columbia and western Alberta may be related to zones of weakness in the crystalline basement and appear to indicate that the western edge of the craton extends up to or just beyond the Arrow Lakes.

Chapter 5 discusses LITHOPROBE's seismic reflection profiles acquired across central Alberta (Figure 1.1). Along with the usual deep crustal reflection profiles, we recorded two experimental data sets. Using the same field equipment and surveyed stations, a three-dimensional data set and a long-offset expanding spread profile were recorded. The excellent data quality of the regular reflection profiling allowed the imaging of crustal structures below the Phanerozoic sedimentary cover which indicated the presence of a 1.8 billion year old orogenic belt underneath central Alberta. In the three-dimensional data volume we have been able to map a bright reflector at mid-crustal levels and have outlined the three-dimensional structure of the Moho over the three-dimensional grid. Preliminary analysis of the expanding spread data has produced a one-dimensional velocity-depth profile over an area with no previous crustal velocity information.

Chapter 2 Cordilleran Seismic Refraction/Wide-Angle Reflection Experiment

2.1 Background

The seismic refraction method is the only remote-sensing geophysical technique that can provide detailed information on the velocities and depths of crustal and lithospheric features. SCoRE '90 [Burianyk *et al.*, 1992] is the final phase of the Southern Cordillera Refraction Experiment of LITHOPROBE's Southern Cordillera Transect [Clowes, 1993] to study the crustal structure of southern British Columbia. This experiment, along with the first refraction program, SCoRE '89 [Zelt *et al.*, 1990; 1992; 1993], complements the seismic reflection data acquired in 1985 and 1988 [Cook *et al.*, 1988; 1992 and Varsek *et al.*, 1993]. Thus, the SCoRE seismic refraction program is one of the most important elements of the interdisciplinary LITHOPROBE program.

The general objectives of this refraction and wide angle reflection experiment are to study the velocity field, crustal structure, spatial range of terranes, geometry of faults and the western extent of the cratonic basement in the southern Canadian Cordillera. This is to be accomplished by the integrated interpretation with the seismic reflection data and other geophysical/geological studies. In this respect, SCoRE '90 was planned to cover the same regions as did the 1985/88 seismic reflection profiles [Cook *et al.*, 1988, 1992 and Varsek *et al.*, 1993]. The seismic line along the Coast Plutonic Complex, Line 10, is in an area where good quality refraction data were unavailable before. The lines in the eastern Cordillera, (7, 8, 9 and the broadside records) span a region in which pre-existing refraction data are old, sparse and of very low resolution.

Since the beginning of the Mesozoic, the margin of the North American continent has grown by 500 km due to accumulation of sedimentary and volcanic rock and the accretion of crustal blocks ('terranes') and magmatic bodies by plate tectonic processes

[*Gabrielse and Yorath, 1988; Oldow et al., 1989*]. The main emphasis of LITHOPROBE's Southern Cordillera Transect has been on the integrated interpretation of geophysical, geological and geochemical data to understand the processes and events of this westward growth of North America.

The first part of the chapter describes the acquisition, editing and processing of the entire SCoRE '90 data set. The remaining part of the chapter discusses the analysis and interpretation of two of the SCoRE '90 profiles, Line 8 [*Kanasewich et al., 1994*] and Line 7 [*Burianyk and Kanasewich, in submission*] (Figure 2.1). Line 8 is the north-south set of refraction/wide angle reflection profiles sub-parallel to geologic strike in the Cordilleran Omineca Belt. Seismic Line 7 is comprised of a set of east-west shot records perpendicular to geologic strike across the Intermontane and Omineca Belts. It intersects the north-south Line 8 and the similarly orientated Line 1 of SCoRE '89 [*Zelt et al., 1992*] along the Intermontane Belt. Line 7 is thus a vital link between the SCoRE '89 and SCoRE '90 programs.

2.2 Data Acquisition

SCoRE '90 began on August 6, 1990 and continued until August 25, 1990 (see Appendix 1 - SCoRE '90 Schedule). Bases were set up in Vancouver, Clearwater Lake and Castlegar, British Columbia. The experiment involved personnel from the Universities of Alberta, British Columbia, Saskatchewan and Victoria and from the Continental Geoscience Division and Geophysics Division of the Geological Survey of Canada (GSC) in Ottawa and the United States Geological Survey (USGS) in Menlo Park (see Appendix 2 - SCoRE '90 Participants).

The author, representing the University of Alberta Seismology Laboratory, had responsibility for planning and execution of the eastern portion of the experiment (about 85% - Lines 7, 8, 9, spatial array and broadside array) while the Department of

Geophysics and Astronomy at the University of British Columbia dealt with the western part (Line 10). The Geological Survey of Canada was closely involved with the planning of the program and ran the field laboratory during the experiment. The U. S. Geological Survey also provided practical advice.

During the experiment a total of 29 shotpoints were recorded by 300 vertical component seismic instruments. The data were acquired as four reversed profiles, each 340 km or longer, several broadside records and a small spatial array. To as great a degree as possible, the refraction lines were coincident with the earlier LITHOPROBE seismic reflection profiles.

SCoRE '90 was conducted over almost the entire width of the Canadian Cordillera south of 52° latitude. Figure 2.1 is a map of the Cordillera with the locations of the seismic profiles along with the distribution of selected geologic terranes and morphogeological belts ('superterranes'). The westernmost profile, Line 10, runs northwest-southeast for about 350 km across the Coast Plutonic Complex. Two profiles, Line 7 and 9, run east-west, covering much of the Intermontane Belt (Quesnelia, Stikinia and Cache Creek terranes), the Omineca Crystalline Belt (coincident with the Quesnelia, Kootenay and Monashee terranes) and into the Purcell Range and Rocky Mountains (Foreland Belt). Line 7 runs for over 400 km from the Fraser River to the Rocky Mountain Trench near Radium Hot Springs. The first shotpoint of Line 9 is just east of Kelowna and continues 360 km eastward into the Crowsnest Pass in Alberta. Line 8 is a 340 km strike line paralleling the Columbia River system/Arrow Lakes. Its northernmost shotpoint is just south of the Mica Creek Dam and the line extends through Revelstoke, Castlegar and on to the US border. Line 6, the broadside line, consists of an east-west line of receivers deployed just north of the US border and centered at Castlegar. Line 5 was the name given to the spatial array of between 8 to 18 receivers located around Castlegar.

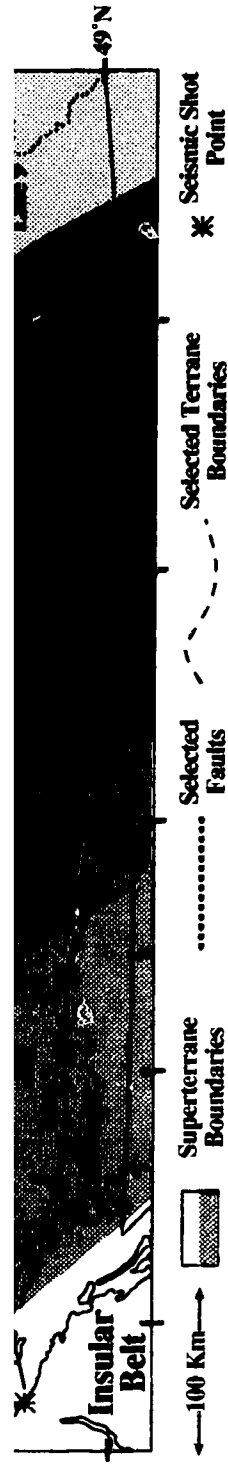


Figure 2.1 Map of morphogeological belts and selected terranes of the Cordillera and the SCoRE seismic profiles. Abbreviations are: Quesnellia (Qn), Stikinia (St), Cache Creek (CC), Kootenay (Ko), Monashee Complex (Mo), Monashee Décollement (MD), North American continental margin rocks (NA), Coldwater Fault (CWF), Quilchena Creek Fault (QCF), Purcell Fault (PF), Rocky Mountain Trench (RMT). The terrane and tectonic data are after Wheeler et al. [1991] and Wheeler and McFeely [1991].

Each of the four linear profiles of the experiment had from 6 to 8 shotpoints, some of which were recorded simultaneously by the broadside and spatial arrays. Large, usually 1800 kilogram, shots were detonated at each end of the four main profiles. Medium (800 kilogram) shots were fired in the approximate middle of each line. Smaller (200 or 400 kilogram), sources were used elsewhere to provide detailed information on shallow crustal heterogeneities. Shot point spacing was a nominal 50 km. This interval was lowered to 25 km in areas of special interest.

Each shotpoint had one to three drill holes (20 cm in diameter) containing charges of 'Nitropel' (an easily loaded nitroglycerine based pellet explosive). A shotpoint site rated for 200 to 800 kg had only one drill hole. An 1800 kg or larger site had at least two drill holes with a maximum of 900 kg of explosives per hole. The depths of the holes were 100' (30 m) for 200 and 400 kg and 140' (42.4 m) for 700, 800 and 900 kg of explosives.

The shotpoints were numbered consecutively following the numbering scheme of SCoRE '89 (Zelt *et al.*, 1990). Thus, shotpoint 23 of Line 7 was the first shot of SCoRE '90. The numbering of the lines was to follow that of SCoRE '89 as well. Line 7, the first line of SCoRE '90, followed Line 6, the last profile of the 1989 experiment. This rule was violated, however, in regards to the broadside line ('Line 6') and the spatial array ('Line 5') which should not be confused with Lines 5 and 6 of SCoRE '89.

Line 7 had seven shotpoints - numbered 23, 24, 25, 27, 28, 29, and 30. There were nine shots for Line 8 - 32, 33, 34, 35 61A, 61B, 69, 36 - and 37 - and eight for Line 9 - 38, 36, 75, 40, 41, 42, 43, and 44. The location for shotpoint 36 was used twice, once for Line 8 and a second time for Line 9, providing a tie between the two profiles. Shot point 61 was planned as a tie between Lines 7 and 8 (61A for Line 7, 61B for Line 8), but both 200 kg shots were eventually fired for Line 8 only. The result was three records - 61A and 61B separately, and 61AB stacked. Line 10 had 6 shotpoints - 46 to 51

inclusive. Details of the shotpoints, including locations, shot times, amount drilled and quantity of explosives used, are given in Appendix 3 - SCoRE '90 Shot point List, Appendix 4 - Number of Shotholes and Quantity of Explosives and Appendix 5 - Detailed Shothole Locations and Shot Times.

Shot point locations were first provisionally picked from NTS 1:50 000 and 1:250 000 topographic maps, and then based on several criteria (Appendix 6 - SCoRE '90 Shot point Environmental Requirements) were scouted, marked, surveyed and logged.

Recorder separation varied from 1 to 3 km. An interval of 1 km was used where it was thought the denser coverage was warranted, while 3 km was used in less critical areas. Tentative receiver locations were determined by drawing a straight line between the shotpoint locations on a 1:50 000 NTS topographic map, marking off the appropriate 1 or 3 km interval, then projecting the position horizontally onto the available system of roads. On this basis, the receiver positions were scouted, surveyed, marked and logged.

The shots were recorded by 180 GSC/LITHOPROBE PRS-1s and 120 USGS FM cassette recorders (SCRs) in four 'deployments' [Asudeh *et al.*, 1994]. The first deployment (DEP1) consisted of the records of Line 10, the second (DEP2) of the data for Line 7 and part of the spatial array, the third (DEP3) of Line 8 and broadside data and the fourth (DEP4) of Line 9 and the remaining spatial array traces. Detailed receiver site name information, is found in Appendix 7 - SCoRE '90 Receiver Site Names. Appendix 8 - Deployment and Shooting Schedule, contains details of the timing of the shots for each deployment.

During the planning of SCoRE '90 there were several environmental concerns that had to be addressed. The most critical consideration from the start was locating shotpoints in areas far enough away from any habitation. Federal COGLA rules were used and are given in Appendix 6. All shot locations were found to be satisfactory and were permitted by the appropriate provincial authorities (both B.C. and Alberta). Obtaining provincial approval was relatively straight forward, requiring the acquisition of

provincial geophysical exploration licenses and the filing of detailed shotpoint reports.

In addition, the entire program had to be approved by the Office of Environmental Affairs (OEA) of Energy, Mines and Resources Canada. This required the filing (by GSC) of an Environmental Assessment Report which included a complete list of shot locations and other details, an account of provincial permitting, list of townships within which shots were to be detonated as well as a description of the type of explosive and blasting procedure.

Approval by OEA was readily granted, on certain conditions. These included more stringent rules on the location and drilling of shotpoints. These conditions are summarized in Appendix 6.

Another condition was that the public be informed of the project through letters to mayors of municipalities and information releases to the local press. Accordingly a letter was drafted by LITHOPROBE Secretariat outlining the aims of LITHOPROBE's studies and mailed to the affected municipalities.

Apart from these matters, the other overriding concern was to return the shot sites to their original state. After the experiment great effort was expended in visiting shot holes and arranging for local contractors to repair any damage (mainly filling in craters).

All of the shotpoint locations and 94% the receiver sites were located by use of GPS (Global Positioning System) navigational instruments. These hand held devices receive signals from US military navigational satellites and are able to locate the user to within several meters, depending on conditions. Occasionally it was difficult to get a GPS position due to poor satellite visibility at certain locations. In those few cases, locations and elevations were read from 1:50 000 NTS topographic maps. On Line 10, several sites were surveyed with Loran C, then a correction (from redundant Loran C/GPS measurements) applied to make them comparable to the GPS readings. The accuracy of the GPS measurements is about 50 m in location and 20 m in altitude.

Locations from topographic maps is about 100-150 m for location and 65 m in elevation.

All data traces contain the shot and receiver locations (in latitude and longitude) and elevations (in meters) in the SEG-Y-LDS headers. In addition, there are digital files containing modified SEGPI [SEG, 1983; Asudeh *et al.*, 1993] format receiver and shot locations for all lines (positions given in latitude and longitude and UTM coordinates).

The GSC/LITHOPROBE PRS-1s are programmed ('downloaded') by the program lithoSEIS operated on microcomputers running DOS. The downloading procedure programs the seismograph units to record during specified time windows. Data are stored in solid state memory which is later 'uploaded' to computer memory via lithoSEIS again [Asudeh *et al.*, 1993].

The USGS instruments are also programmed to turn on at given times. The data stored on cassette tapes are later played back and digitized in a field lab using IBM AT compatible computers [see Murphy, 1988 and Kohler, 1990 for details].

The relative velocity responses of both GSC and USGS instruments are both similar. The response is essentially flat from 2 to 20 Hz (Figure 2.2). Both units used the same geophone - Mark Products L4A 2 Hz seismometers. The GSC sampling rate was 120 samples/second while the analog USGS data were digitized at 200 samples/second.

After the completion of the field work, the data were available on 9-track digital tape in SEG-Y-LDS format [SEG, 1980; Spencer *et al.*, 1989] in two separate sets. GSC data were delivered in SEG-Y format 1 (i.e. 4 byte floating point - Real*4) at 120 Hz sampling rate, -1s to 59 s (i.e. with respect to shot time) and in amplitude units of nanometers/second. The USGS delivered -1 s to 39 s of data at 200 Hz sampling rate in SEG-Y format 3 (2 byte fixed point - Integer*2) and with various amplitude gains. The basic processing, merging and header addition and corrections was done by the University of Alberta Seismology Laboratory, benefiting from the previous experience of

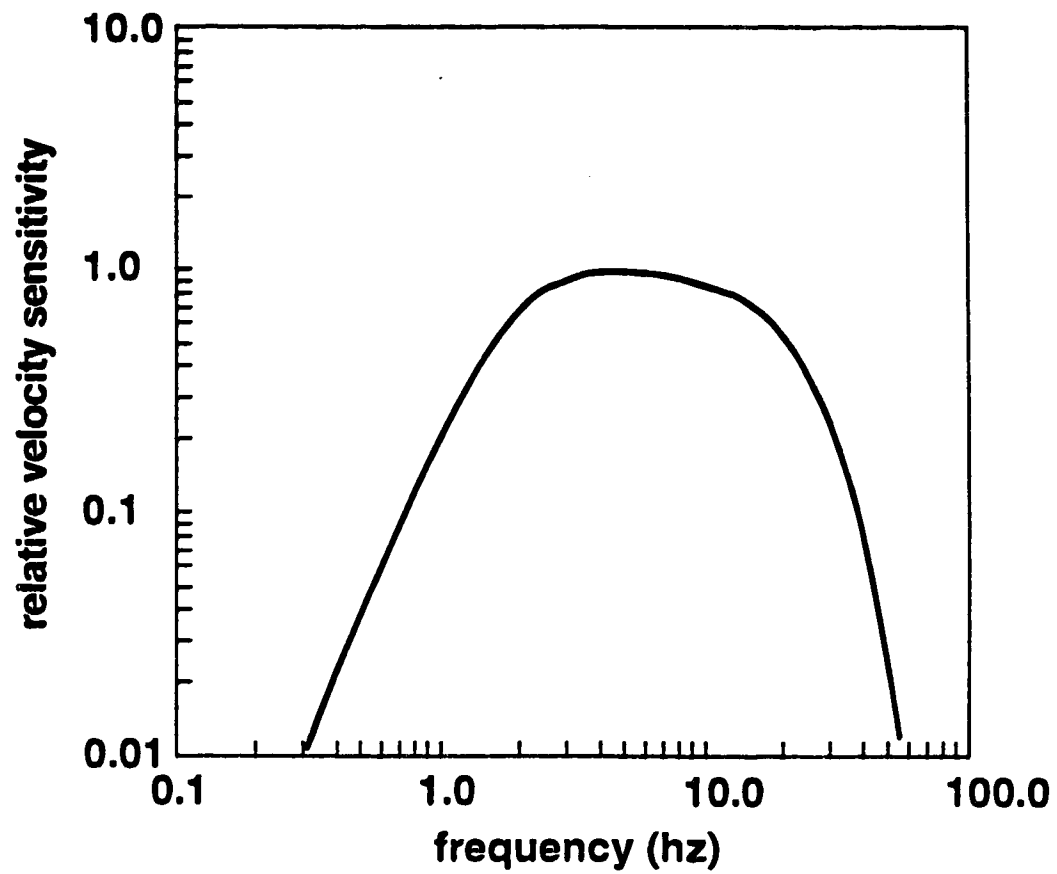


Figure 2.2 Relative velocity sensitivity of the GSC PRS-1 and USGS SCR seismographs.

Zelt et al. [1990].

To merge the two data sets required processing of the USGS data to be made compatible with the GSC data. This included re-digitizing (to 120 Hz from 200 Hz), gain correction to units of nanometers/second and reformatting from SEG-Y format 3 to format 1 (2 byte integer to 4 byte floating point). Also, 20 seconds of data (zero valued samples) were added to make each USGS trace the same length as GSC traces.

In addition, some of the header information required additions and corrections. Specific updates and alterations were the shot and receiver site locations. Based on these, source-receiver offsets, source-receiver azimuths (i.e. direction from shot to receiver) had to be updated as well. Changes in site locations also necessitated shifting of the reduced time traces (with a reduction velocity of 8 km/s) and thus the trace start time values in the headers.

To summarize, the USGS data were processed (re-digitized, amplitude scaled, format converted and trace lengthened) to be made compatible with the GSC data set. Headers on both GSC and USGS traces were edited to correct shot and receiver site locations and their dependent values. Traces were shifted to their proper reduced times and trace start time in the headers were corrected. No processing was done to the GSC data other than trace shifting and header updates.

The final archive data set is on two digital 9-track tapes (6250 BPI), stored at the LITHOPROBE Seismic Processing Facility at the University of Calgary. Shot records from Line 8 and 9 are on Tape 1 while Lines 7, 10, 5 and 6 are on Tape 2. There are 60 seconds of 120 Hz digitally sampled data per trace, representing times from -1 s to 59 s. Each shot record is a separate SEG-Y-LDS file. The data traces are sorted according to source-receiver distance, starting at either the north or west side of the line.

Trace header word #2 (bytes 5-8) is the sequential trace order on the basis of the final sort order. Trace header word #4 (bytes 13-16) gives the absolute receiver id

(identical to the character string in bytes 225-228 - this is consistent with USGS practice). Trace header value 'cor' (bytes 185-186) can be used to shift the trace back or forward in order to align it relative to zero time (i.e. shot time).

Plots of all shot records interpreted in this study are shown in Appendix 9 - SCoRE '90 Data Profiles.

2.3 Data Characteristics

Figures 2.3 to 2.10 are plots, with color coded amplitudes, of four of the Line 7 and 8 shot records (reduced at 8 km s^{-1}). Shot point 32 (Figure 2.3 and 2.4) is an end-on profile located at the extreme north end of Line 8 while Shot point 37 (Figure 2.5 and 2.6) is an end-on profile on the south end of the line. Both shots have a charge size of 1800 kg. Shot point 23 (Figure 2.7 and 2.8) is an 1800-kg end-on shot located on the west end of Line 7, while Shot point 30 (Figure 2.9 and 2.10) is the end-on 1800-kg shot at the east end. Appendix 9 shows all of the data records for the two lines.

Plotting of amplitude spectra of subsets of the data shows that though there is occasionally energy as high as 18-20 Hz, the predominant frequency of the signal wavelet is 5-8 Hz with most of the energy contained within the 4-14 hz range. The data have been bandpass filtered, generally with a 2-to 18-Hz window, and the amplitudes are scaled by multiplying by trace offset. The traces are displayed in variable area format with true amplitude scaling.

The features of the entire Line 7 and 8 data sets can be discussed with reference to the four shotpoints in Figures 2.3 to 2.6, and more clearly, to the SP 32 and SP 37 synthetic shot records in Figure 2.11. The profiles are characterized by three distinct first arrival branches. On Line 8 the near offset first arrival from the surface layer (P_s) has an apparent velocity of $5.5 \pm 0.2 \text{ km s}^{-1}$ and can be observed at offsets from 0 km to a maximum of 35 km. On Line 7, P_s has highly variable apparent velocities between 2.0

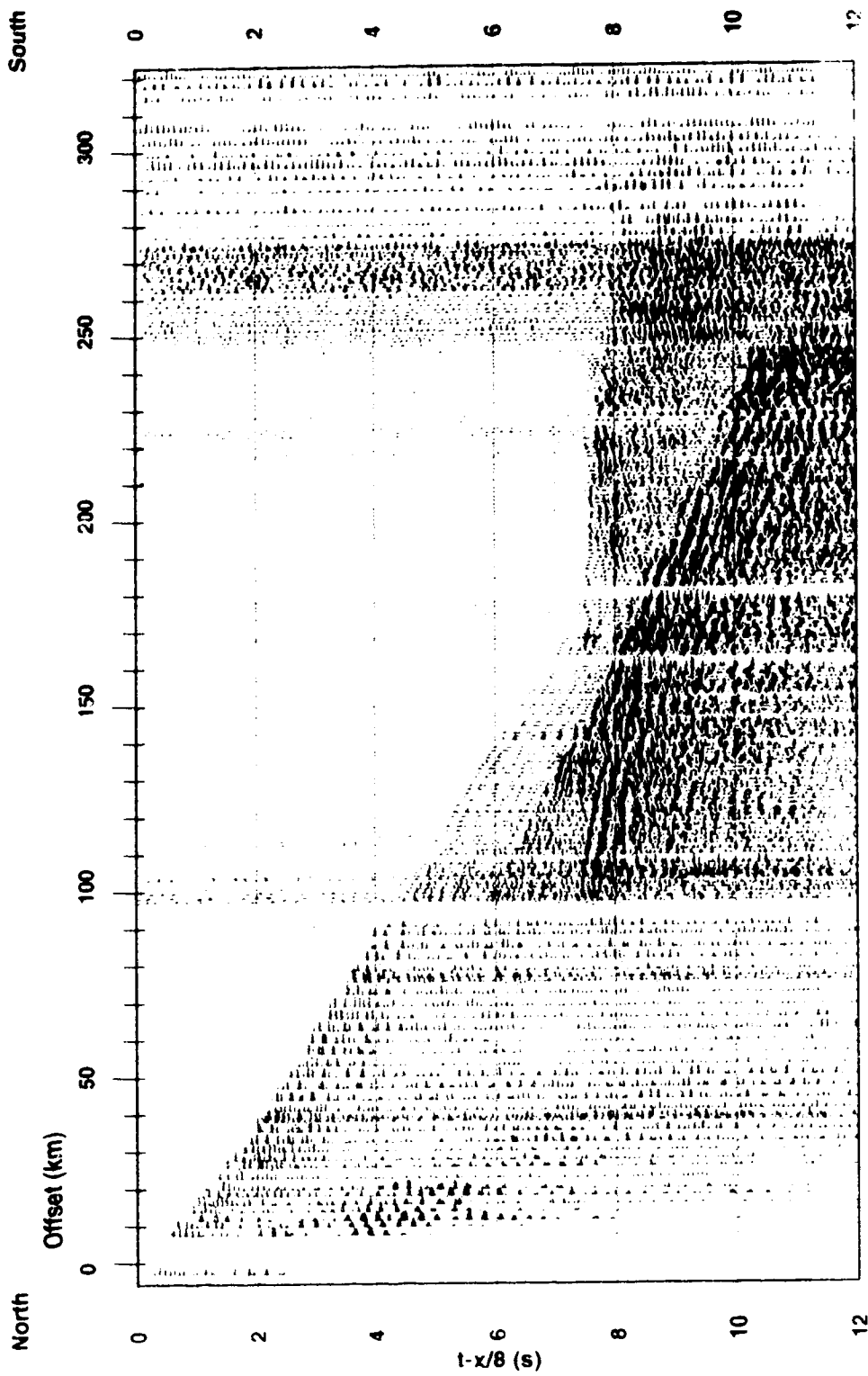


Figure 2.3 SCoRE'90 Line 8 shot 32 (northernmost shotpoint) record section (1800-kg charge size) with 8 km s-l reducing velocity and with true relative amplitudes. This is one of the highest data quality records. The colors are coded to positive amplitude: red represents the highest amplitudes, then yellow, green and blue for smallest positive amplitudes. Poor data quality on the south end corresponds to the older generation seismographs of the U.S.G.S.

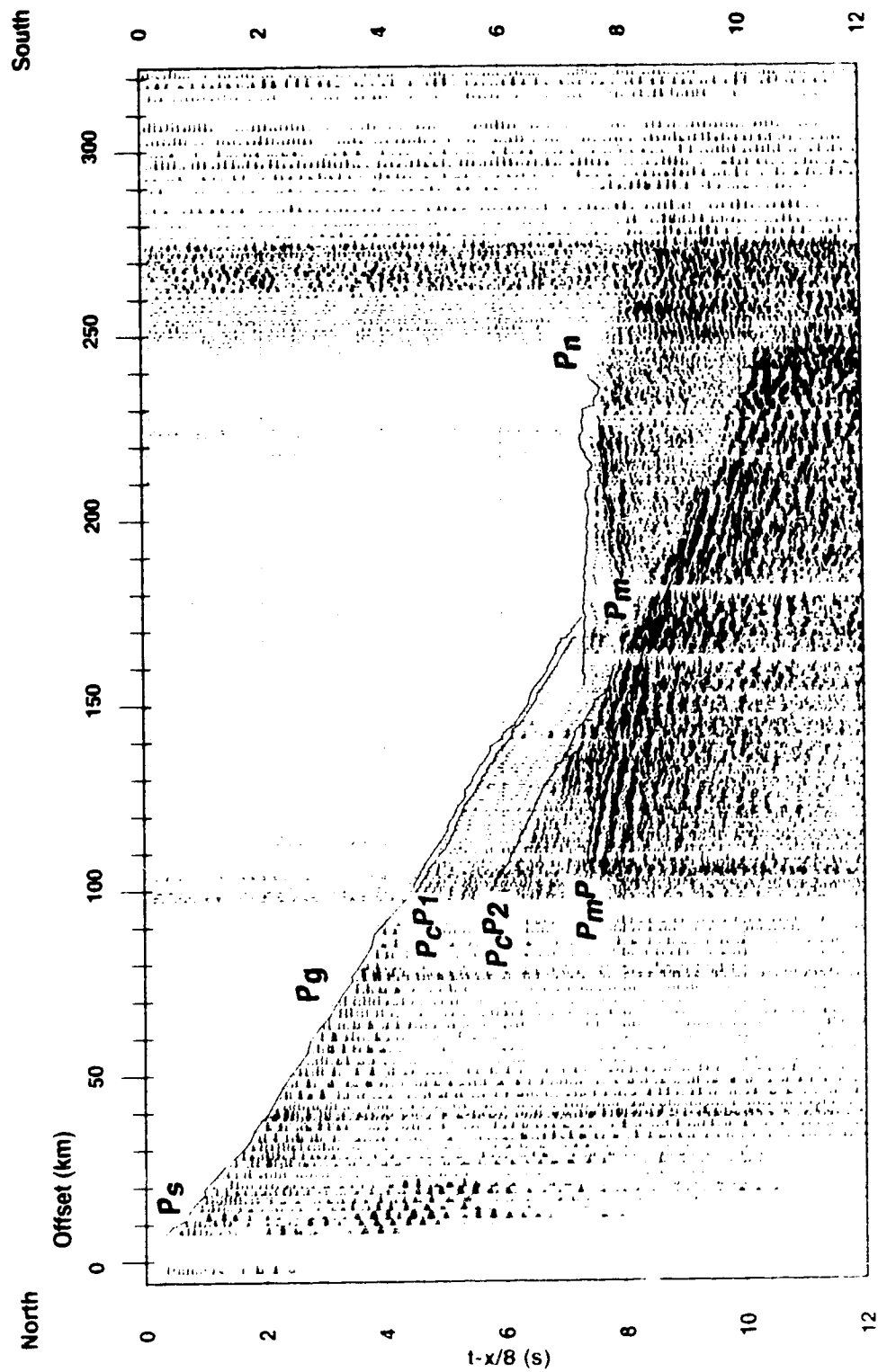


Figure 2.4 SCoRE'90 Line 8 shot 32 record section with interpreted arrival picks. The correlated time picks are shown as solid lines.

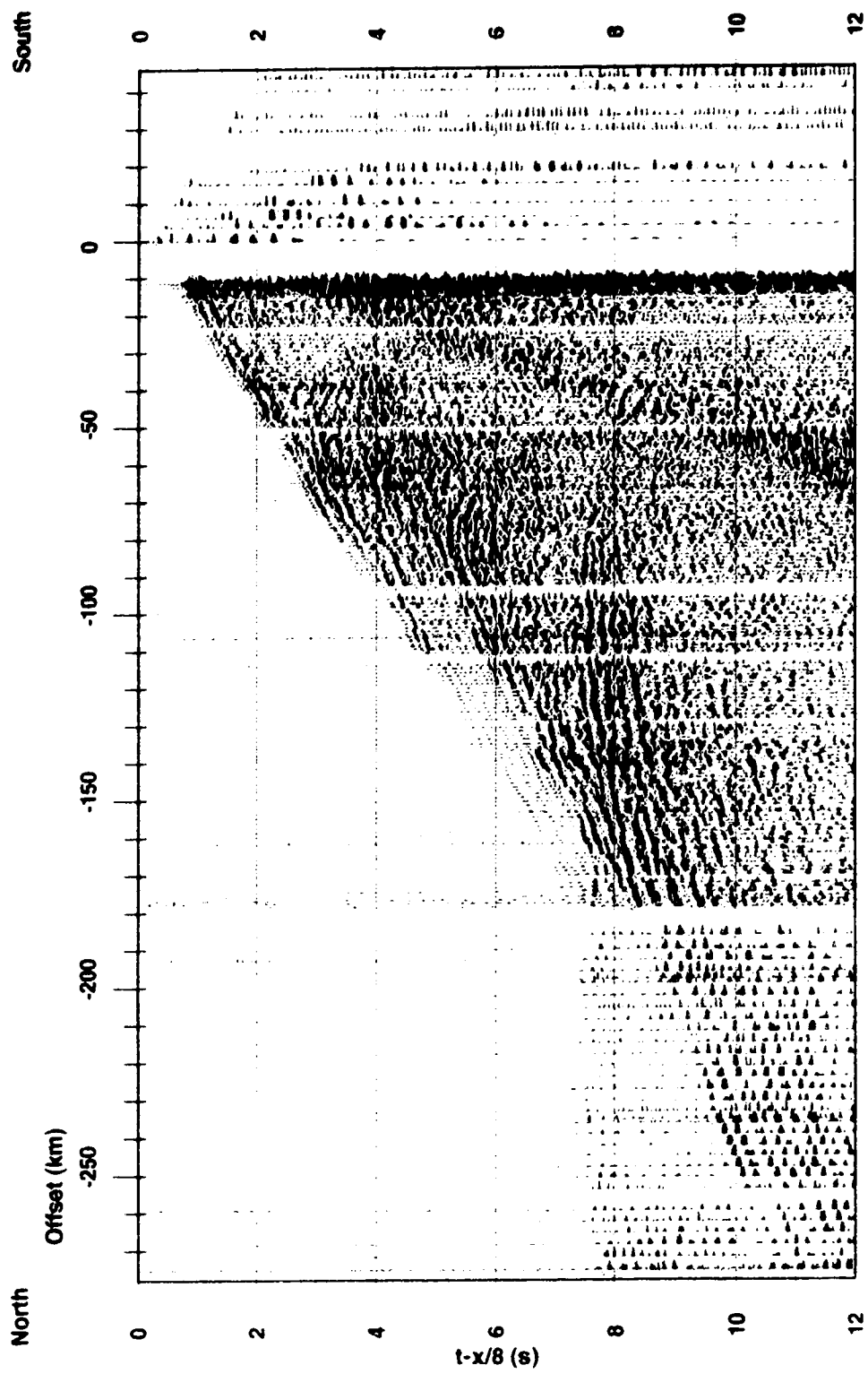


Figure 2.5 SCoRE'90 Line 8 shot 37 (southernmost shotpoint) record section (1800-kg charge size) with 8 km s⁻¹ reducing velocity and with true relative amplitudes. Details as for Figure 2.3.

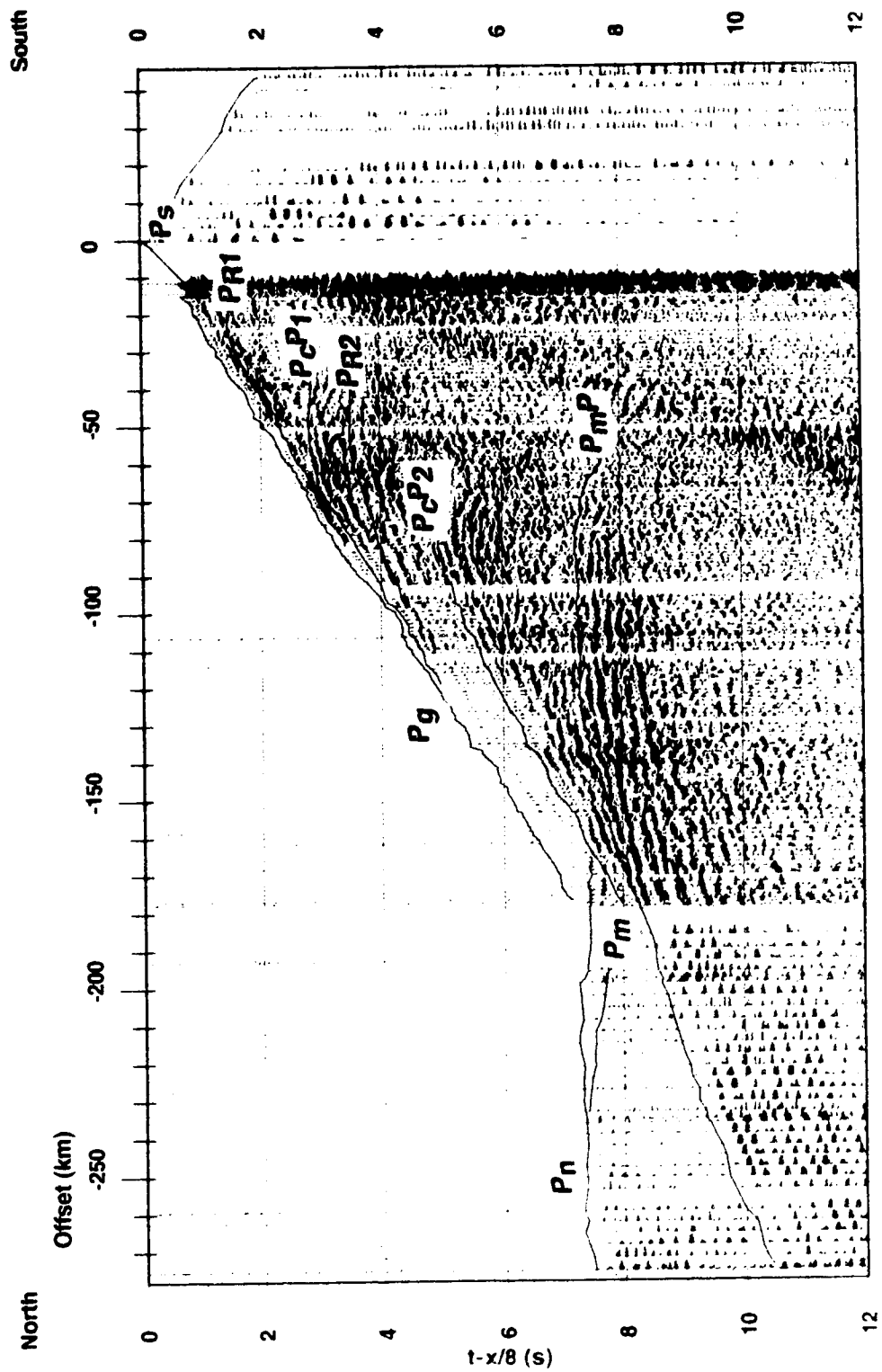


Figure 2.6 SCoRE'90 Line 8 shot 37 record section with interpreted arrival picks.

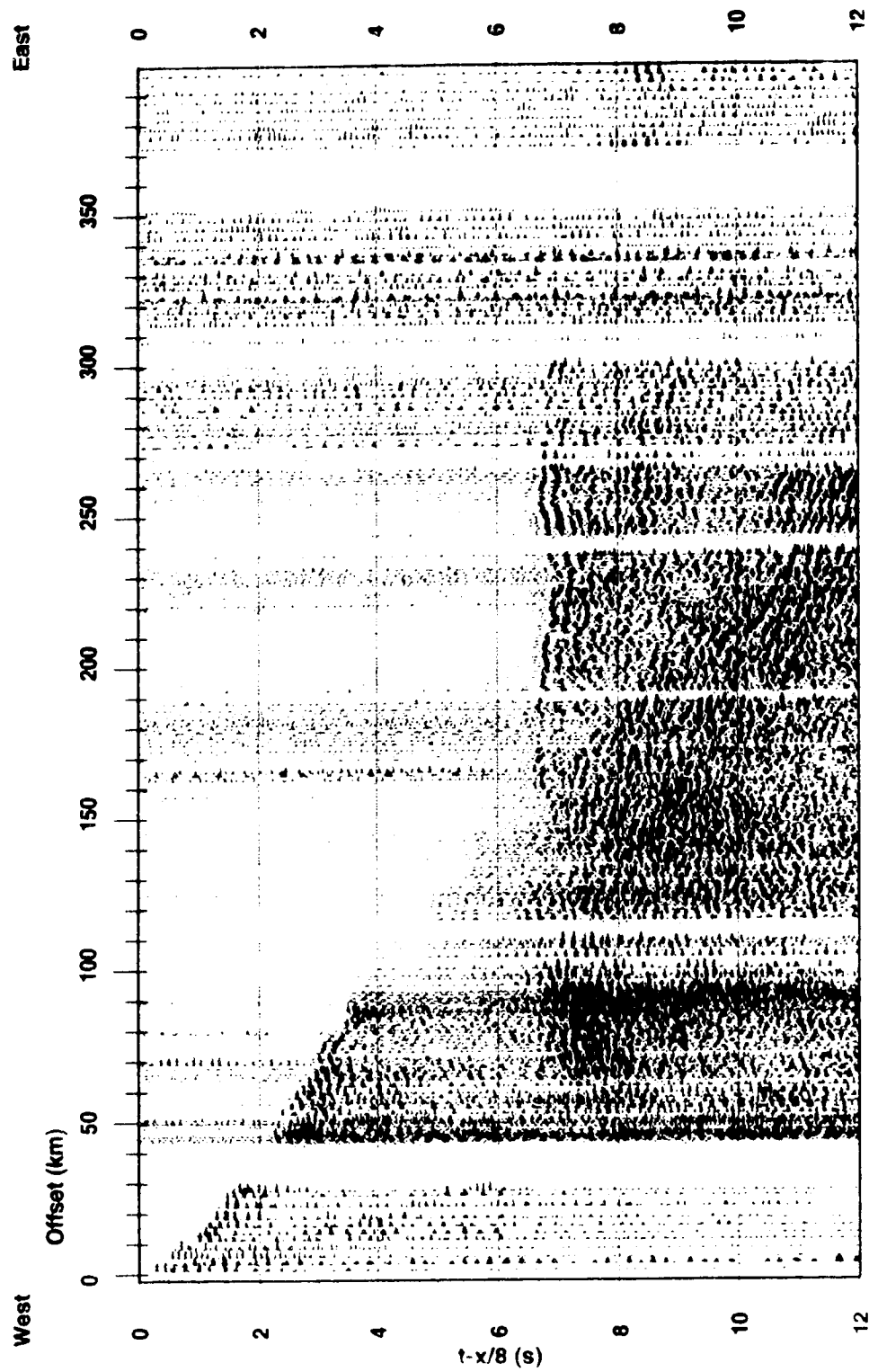


Figure 2.7 SCoRE'90 Line 7 shot 23 (westernmost shotpoint) record section (1800-kg charge size) with 8 km s⁻¹ reducing velocity and with true relative amplitudes. Details as for Figure 2.3.

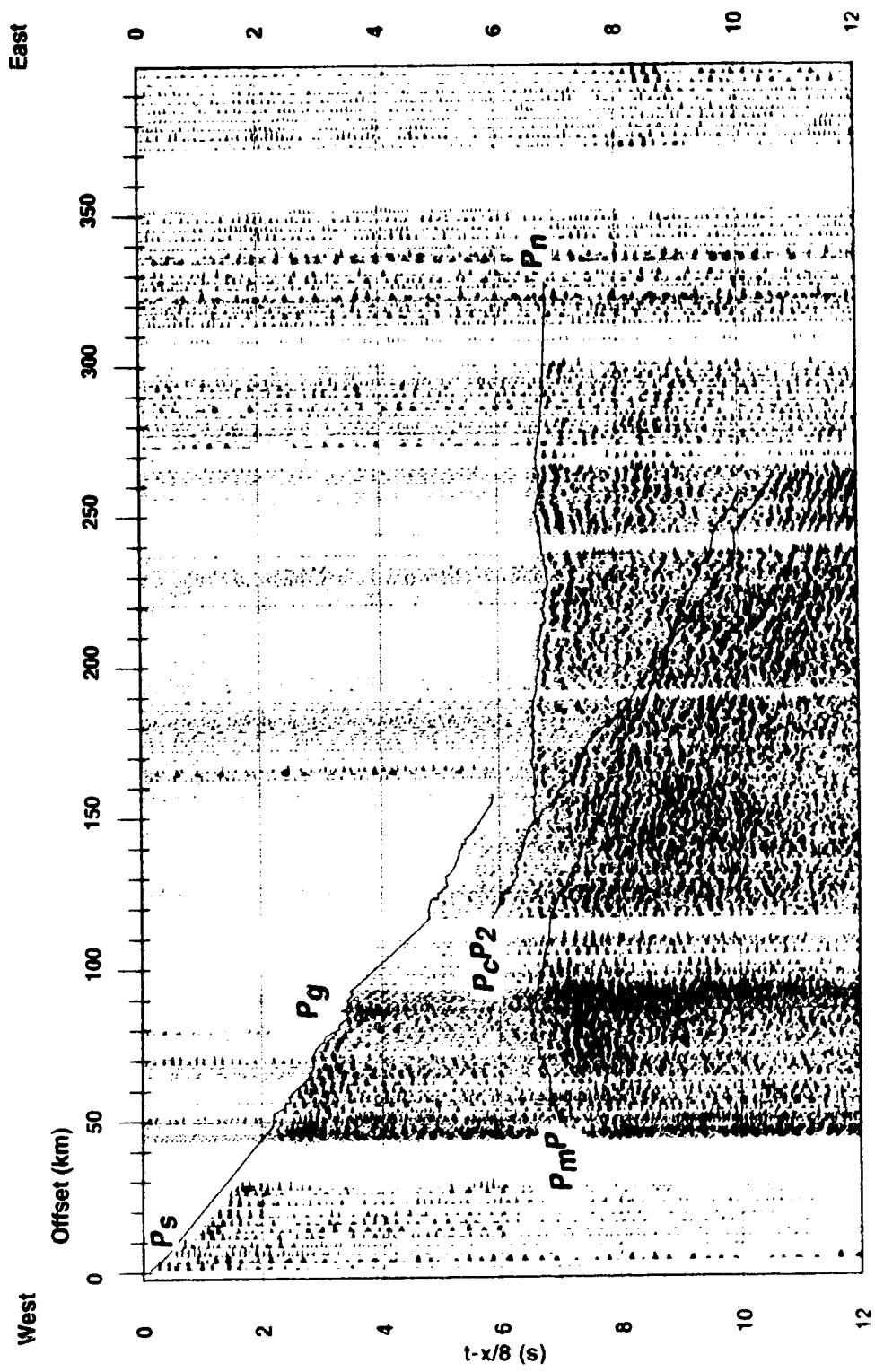


Figure 2.8 SCoRE'90 Line 7 shot 23 record section with interpreted arrival picks.

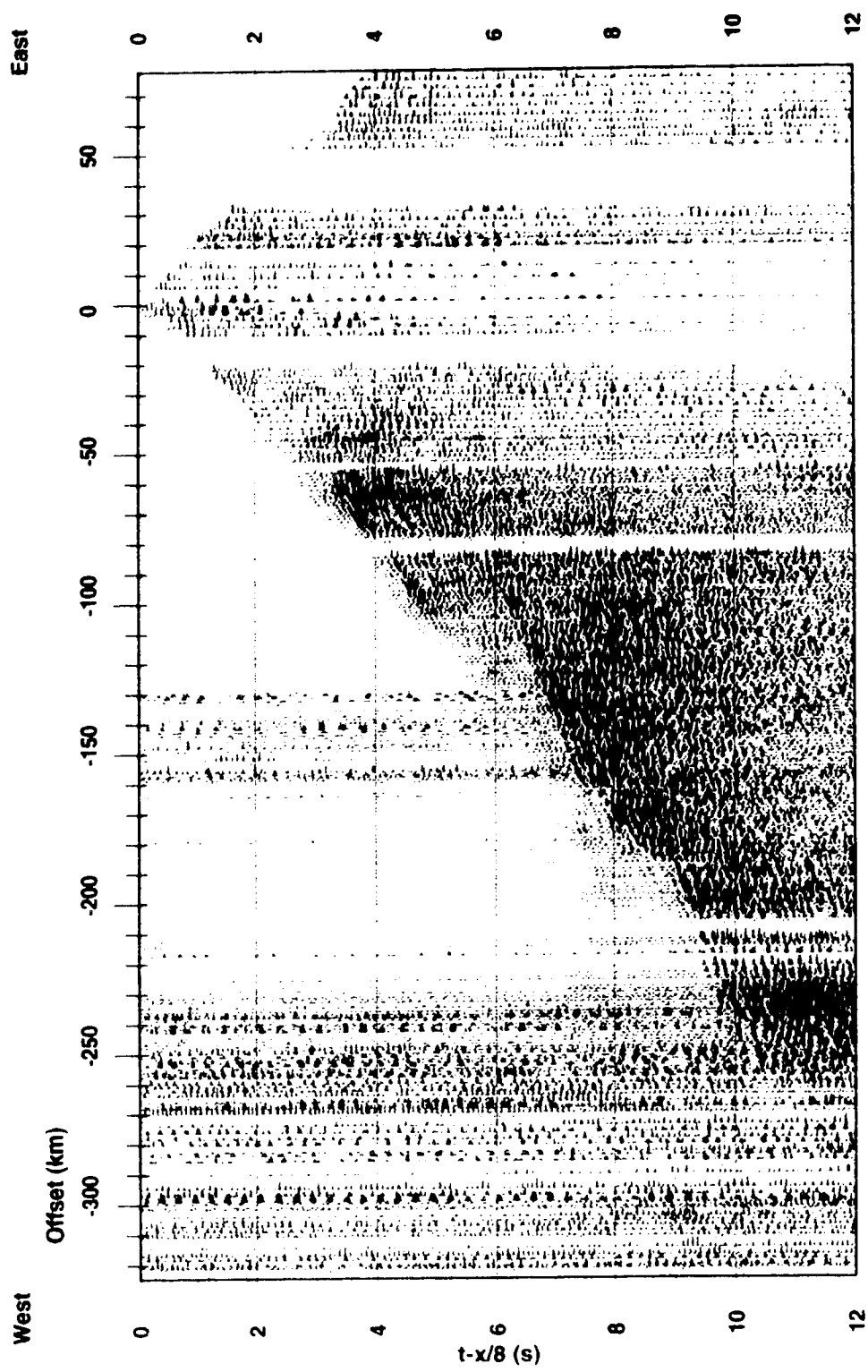


Figure 2.9 SCoRE'90 Line 7 shot 30 (easternmost shotpoint) record section (1800-kg charge size) with 8 km s⁻¹ reducing velocity and with true relative amplitudes. Details as for Figure 2.3.

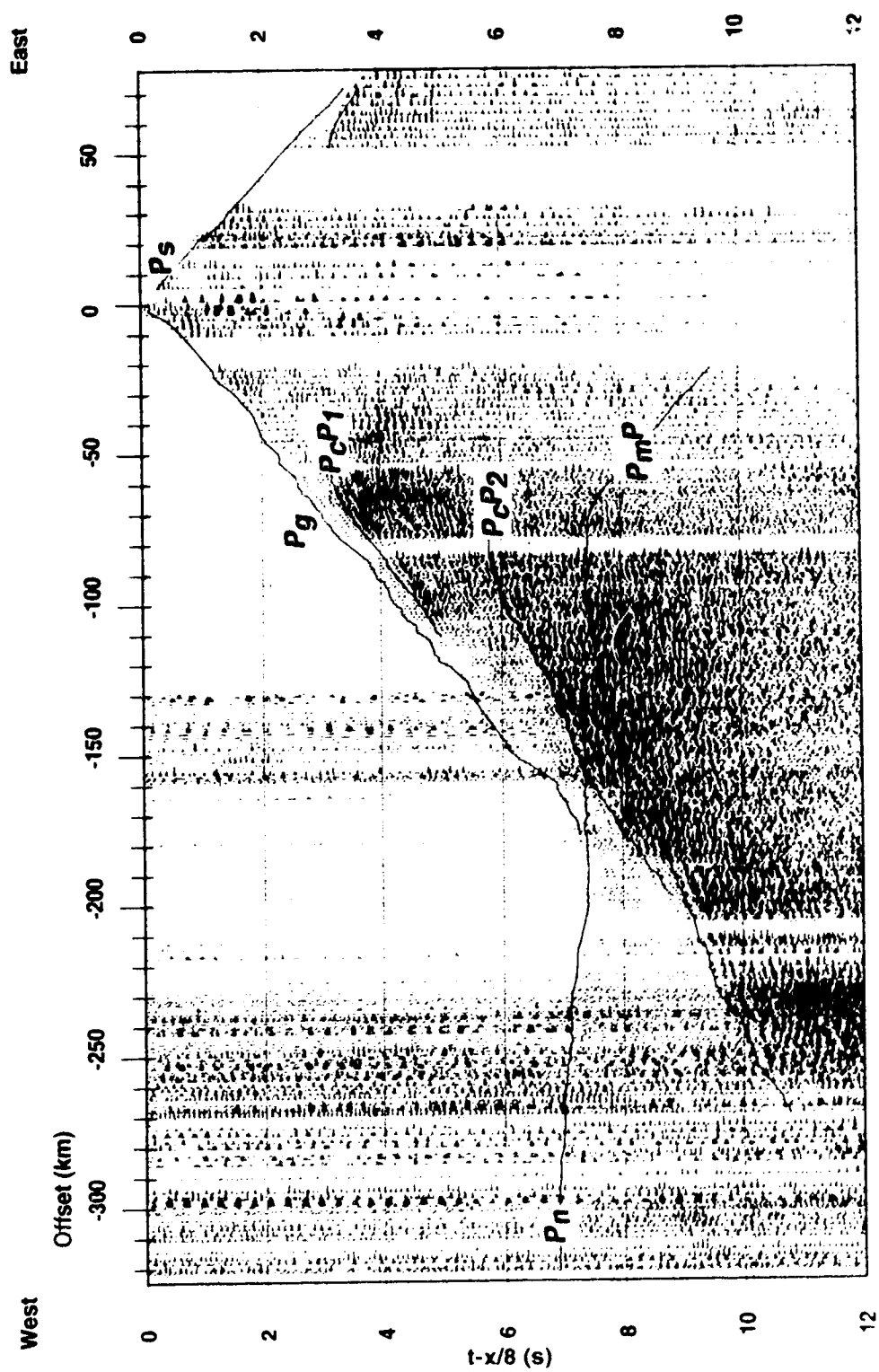


Figure 2.10 SCoRE'90 Line 7 shot 30 record section with interpreted arrival picks.

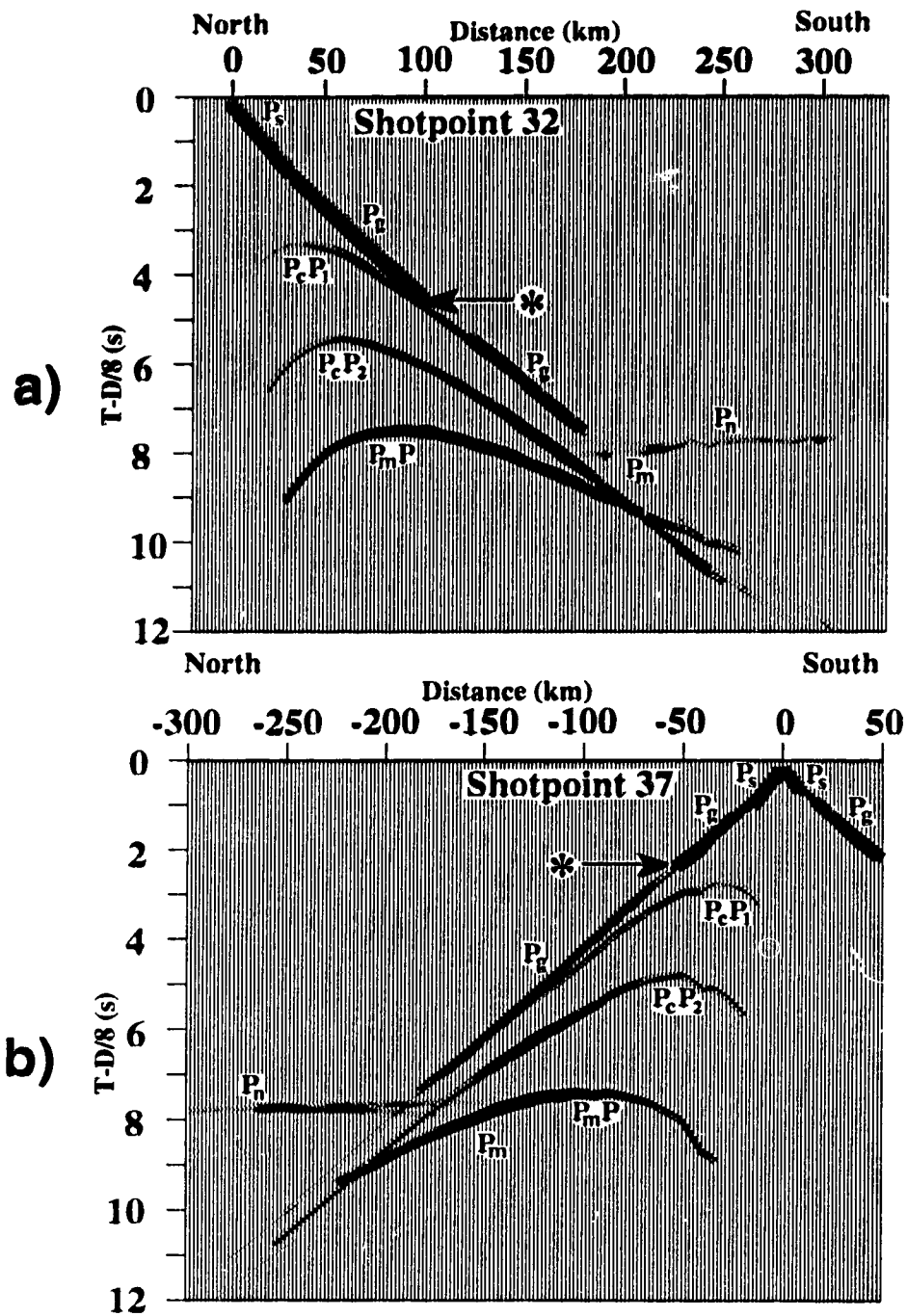


Figure 2.11 Synthetic seismograms for Line 8 from the final velocity models (Figure 2.16) illustrating seismic arrivals generally identified on SCoRE '90 data: P_s - shallow direct arrival; P_g - crustal direct arrival; P_n - mantle direct arrival; P_cP_1 - crustal wide-angle reflection (WAR); P_cP_2 - deeper crustal WAR; P_mP - Moho WAR; P_m - mantle WAR; * - indicates P_g amplitude change.

and 5.5 km s^{-1} and are generally observed at offsets from 0 km to a maximum of 10 km.

The second branch has an apparent velocity of $6.1 \pm 0.1 \text{ km s}^{-1}$ and is identified as P_g . This phase has first arrival times beginning at 1-2 s (reduced time) down to 7.5 s and is observed between offset ranges of 0 to 160 km on both lines.

The strong P_n phase, or refracted waves from just beneath the Moho, exhibits a fairly consistent 7.9 km s^{-1} velocity. The first arrival offset for the P_n branch is between 160-175 km. Sometimes on Line 8 and rarely on Line 7, this phase can be discerned as a secondary arrival between 140 and 175 km offset.

A marked decrease in amplitude of the P_g branch with shot-receiver offset is observed on some records. This phase often disappears completely before the P_n crossover point. Assuming that P_g are the refracted, or turning, rays in the crust, this amplitude decrease is an indication that deeper in the upper crust, vertical velocity gradients are very low. These amplitude changes occur at similar offset ranges, which is more indicative of the structure at depth than to local, shallow lateral heterogeneities, and so may be analysed to obtain information on vertical velocity gradients.

All records display a distinct but complex wide-angle reflection at about 7.5 s reduced traveltime at 100 km offset. We interpret this phase as P_mP (i.e., reflection from the Moho). It is likely, due to the complex multiphase nature of the reflected signal, that the first pick of the phase is a reflection from the top of a Moho transition zone. This is fully consistent with the seismic reflection data [Cook *et al.*, 1992], which show an intricate, layered character in the lowermost crust (see Figures 2.18 and 2.20).

Shot point 32 (Figure 2.3 and 2.4) displays a conspicuous secondary arrival from well beneath the Moho with an apparent velocity of 8.6 km s^{-1} designated $P_{m'}$. Other Line 8 records have less convincing, but nevertheless visible, indications of apparent velocities of 8.3 to 8.6 km s^{-1} . These are either wide-angle reflections or refraction/head wave phases from upper mantle layering. Initial modeling suggests that it would be

difficult to unravel reflected signals from corresponding refracted ones at the offsets available, but the relatively strong amplitudes on shotpoint 32 are a good argument to consider them as wide-angle reflections. This arrival cannot be identified on any Line 7 records.

Besides having prominent P_mP arrivals, many of the records have weaker wide-angle reflections from the middle and lower crust and are labeled as P_cP_1 and P_cP_2 . These reflections provide important constraints on crustal geometries and velocities. Correlation is a problem with these reflections near crossovers at offsets greater than 175 km. The shallower reflection, P_cP_1 , is visible on shotpoints 32, 34, and 37 on Line 8 and only on SP 30 on Line 7. The more prominent and deeper reflection, P_cP_2 is seen on all of the shot records of Line 8 and on SP 23, 25, 27 and 30 of Line 7.

It is possible to identify very shallow reflections, labeled as P_{R1} and P_{R2} on the three southernmost shotpoints of Line 8. They can be associated with upper crustal shear zones as interpreted on the reflection data [Cook *et al.*, 1992].

There are other secondary arrivals that are apparent in the data records. For example, on shotpoint 32 (Figure 2.3 and 2.4) there appear to be several correlatable events between the P_cP_1 and P_cP_2 arrivals. Correlation and modeling of these arrivals, however, proved to be difficult. That is, no combination of velocities and structures could be found to adequately fit their traveltimes curves. These signals are considered to be scattered energy due to local heterogeneities and three-dimensional effects, analyzable only with more specialized modeling techniques and more complex models.

As a rule, the characteristics of the seismic arrivals of Line 7 are similar to those of the Line 8 records. The main difference is that Line 7 data has a much lower signal to noise ratio. This may be due to the lower efficiency of seismic energy propagation across geologic strike as opposed to along strike. As such, the identification and correlation of phases for Line 7 is more ambiguous and time picks are less numerous and reliable.

Determination and correlation of phases were facilitated by multiple plotting of sections in color and with various maximum amplitude and time/distance scales. After correlation, time picking was performed using interactive software. For first arrivals, the initial part of the pulse was picked, while for wide-angle reflections, the initiation of high energy was used as a pick determinant.

Uncertainties in traveltimes were estimated for each traveltimes branch on every shot record and serve as a grade of the quality of the picks. In general, shots with larger explosive charges resulted in higher quality records, both in number of observations and in lower uncertainties (note the richer content of signals on shotpoints 32 and 37 in Figures 2.3 and 2.4 contrasted to the signals of smaller charged shotpoints shown in Appendix 9). The overall quality (both in terms of uncertainties and in number of observations) of the arrivals and their time picks can be graded, from highest to lowest: P_g and P_s , P_mP , P_n , P_cP_2 , P_cP_1 , P_{R1} , P_{R2} , P_m . Uncertainties ranged from ± 0.05 s (about ± 0.3 km) for the most reliable P_g and P_s picks, to ± 0.1 (about ± 0.6 km) for the higher-quality P_cP_2 and P_mP reflections, and to ± 0.15 - 0.2 s for the less dependable arrivals. The average uncertainties for first arrivals (refracted events) was less than ± 0.1 s (Line 8) and less than ± 0.08 s (Line 7) while for the wide-angle reflections, the average was ± 0.12 - ± 0.14 s.

There is also a prominent change in data quality across shot records. This is most noticeable on the shotpoint 32 record (Figure 2.3 and 2.4) at offset distances of 250 km and greater. Here the drop in data quality is correlated with a change in instrumentation type. Also, as seen on the shotpoint 37 profile (Figure 2.5 and 2.6), the arrivals on the northernmost 100 km are less easy to correlate due to the change from 1 km receiver spacing to 3 km.

The seismic characteristics of the lithosphere within the Omineca Belt are determined mainly by the P_g waves, sampling the upper crust; the ubiquitous P_cP_2 reflector, constraining velocities in the middle crust and defining a mid/lower crust

boundary; P_m determining lower crustal velocities and crustal thickness and P_n giving velocities in the shallow mantle. All the other, lesser arrivals simply modify the details of the main interpretation.

2.3 Data Modelling

The traveltimes for Line 7 and 8 have been modeled using the two-dimensional inversion method of *Zelt and Smith* [1992] which performs damped least squares inversion of ray-traced traveltimes through an appropriately parameterized crustal model. The difference between predicted and actual arrival times yields traveltime residuals that are inverted along with velocity and depth derivatives to provide an updated model. The inversion code provides detailed statistics of how well the model fits the data and estimates of the resolution of the revised velocity and depth parameters.

The inversion algorithm assumes a two-dimensional isotropic medium. The velocity model is composed of layers whose boundaries are made up of linear, arbitrarily dipping segments defined by depth nodes. Model velocities are specified by velocity nodes placed at the top and bottom of each layer. The boundary depth and layer velocity nodes can be generally placed in such a way as to construct a relatively complex, laterally and vertically heterogeneous velocity structure with a minimum number of model parameters.

As the asymptotic ray arrival times are calculated, the algorithm tabulates the number of arrivals that were able to be traced to observation points, the root-mean square (RMS) traveltime residual and the normalized χ^2 misfit. This statistical measure of goodness of fit depends somewhat upon the estimated error in the observed times. In general, normalized χ^2 values of 1.0 and less are considered a good fit between data and calculated values.

On inverting for depth and/or velocity nodes, the estimated resolution of these

parameters is given. Resolution estimates lie between 0.0 and 1.0 and indicate the amount of linear dependence of the inverted model, or the relative number of rays that independently sample each parameter. Empirically, resolution values greater than 0.5 indicate that parameters are resolved and reliable [Zelt and Smith, 1992].

During data modeling, a layer stripping approach was used. The main criteria for choosing a final model was minimizing the RMS traveltime residual and the χ^2 misfits while maximizing the number of rays able to be traced to the observation points. On Line 8, qualitative amplitude modeling (i.e., visual comparison of synthetic seismograms with real seismic traces) was also used to obtain constraints on velocity gradients in the upper crust and as indications of the size of velocity discontinuities in the lower crust. This was accomplished by a modification of the ray-tracing synthetic seismogram algorithm of Zelt and Ellis [1988], which uses the same model parameterization as the inversion routines of Zelt and Smith [1992]. For Line 7, the more quantitative procedure of analysis of amplitude-offset curves by computing the smoothed seismic energy along picked arrivals and plotting versus shot-receiver offset was used.

The following sections describe the modelling for upper, middle and lower crust, and upper mantle for each line. Line 8 was modelled and interpreted first [Kanasewich *et al.*, 1994], Line 7 [Burianyk and Kanasewich, in submission] following several months after. Therefore, there are some differences in the ways the two profiles were evaluated.

Upper Crust Line 8

The first step was to find a velocity model for the surface layer from P_s . Using the topography of the seismic line as the surface boundary, and an arbitrary bottom boundary placed at a depth of 1.5 km, a single set of upper and lower velocity nodes were changed over a range of values and forward modeled for traveltimes. These tests revealed that values of 5.5 km s^{-1} to 5.8 km s^{-1} gave the best fit (i.e., a velocity gradient

of approximately 0.15 km s^{-1}). At that point, velocity nodes were added at each shotpoint. Boundary depths were adjusted in order to trace only P_s arrivals. An inversion, keeping the previously found gradients constant, resulted in a model where rays were traced to all appropriate receiver locations. The resolution for some of the velocity parameters are low, due to the few rays available, but the overall fit is very good - for 58 traveltimes an RMS traveltime misfit of 0.04 s and a χ^2 fit of 0.5 were obtained for the final surface layer model. Figure 2.13 a shows the combined P_s and P_g travel-time picks, calculated rays and traveltime curves and overall fit characteristics. Figure 2.12 displays the relevant traveltime curves, time picks, and ray paths along with the fit characteristics (number of data points fit, RMS traveltime residuals and χ^2 values) of all arrivals discussed for Line 8.

On the basis of gross changes in amplitude character in the P_g phase (See Figure 2.11), two layers with differing velocity gradients were defined with no velocity discontinuities across the boundary. Localized velocity models for pairs of reversed shotpoints were constructed by forward modeling of both traveltimes and amplitudes along with inversion of traveltimes. The local models were used to construct an initial two-dimensional upper crustal model, placing velocity and depth nodes at the shotpoint locations. The model was inverted for all shots simultaneously. Since boundary parameters were poorly resolved, only the velocity nodes were inverted. Gradients and depths were adjusted on the basis of forward amplitude modeling and the result inverted again to reach an acceptable fit based on ray coverage and traveltime fit (Figure 2.13 a) and amplitude character (Figures 2.7). For 1104 traveltime observations, an RMS traveltime misfit of 0.1 s (compared to an average arrival time uncertainty of 0.1 s) and a normalized χ^2 fit of 1.0 were obtained.

The remainder of the upper crust is minimally constrained by wide-angle reflections ($P_c P_f$) found on three shot records (Figure 2.13 b). We define this reflector as the bottom of the upper crust. Since first arrival characteristics suggest that there

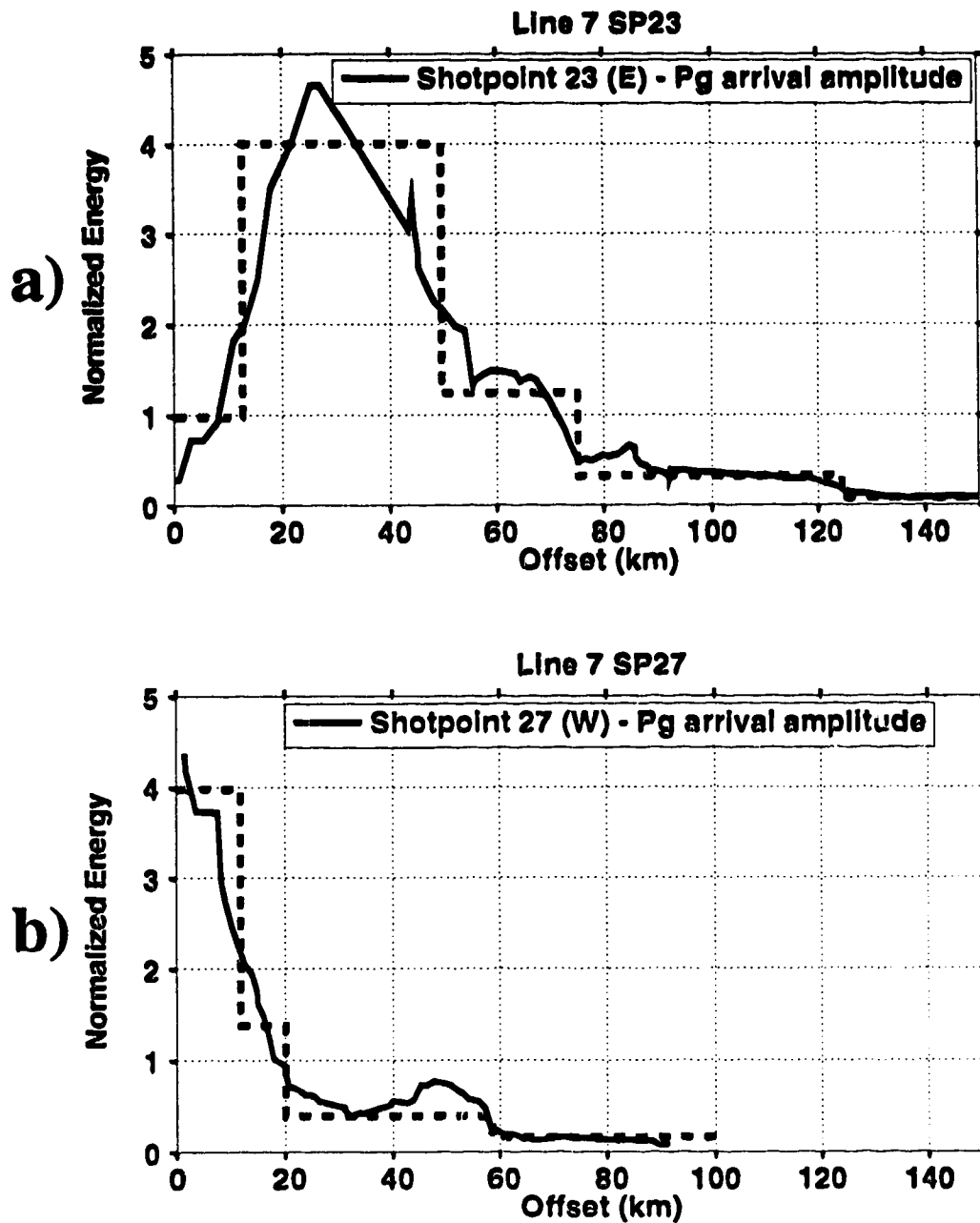


Figure 2.12 Examples of the normalized energy vs. source-receiver offset for Line 7 SP 23 (east) and Line 7 SP 27 (west) for the Pg arrival. The blocked-off amplitude curve constrains the relative velocity gradients in layers below the shotpoint. Relative differences in velocity gradients are equated to the relative difference in amplitudes in each blocked off amplitude regime (equivalent to a distinct layer).

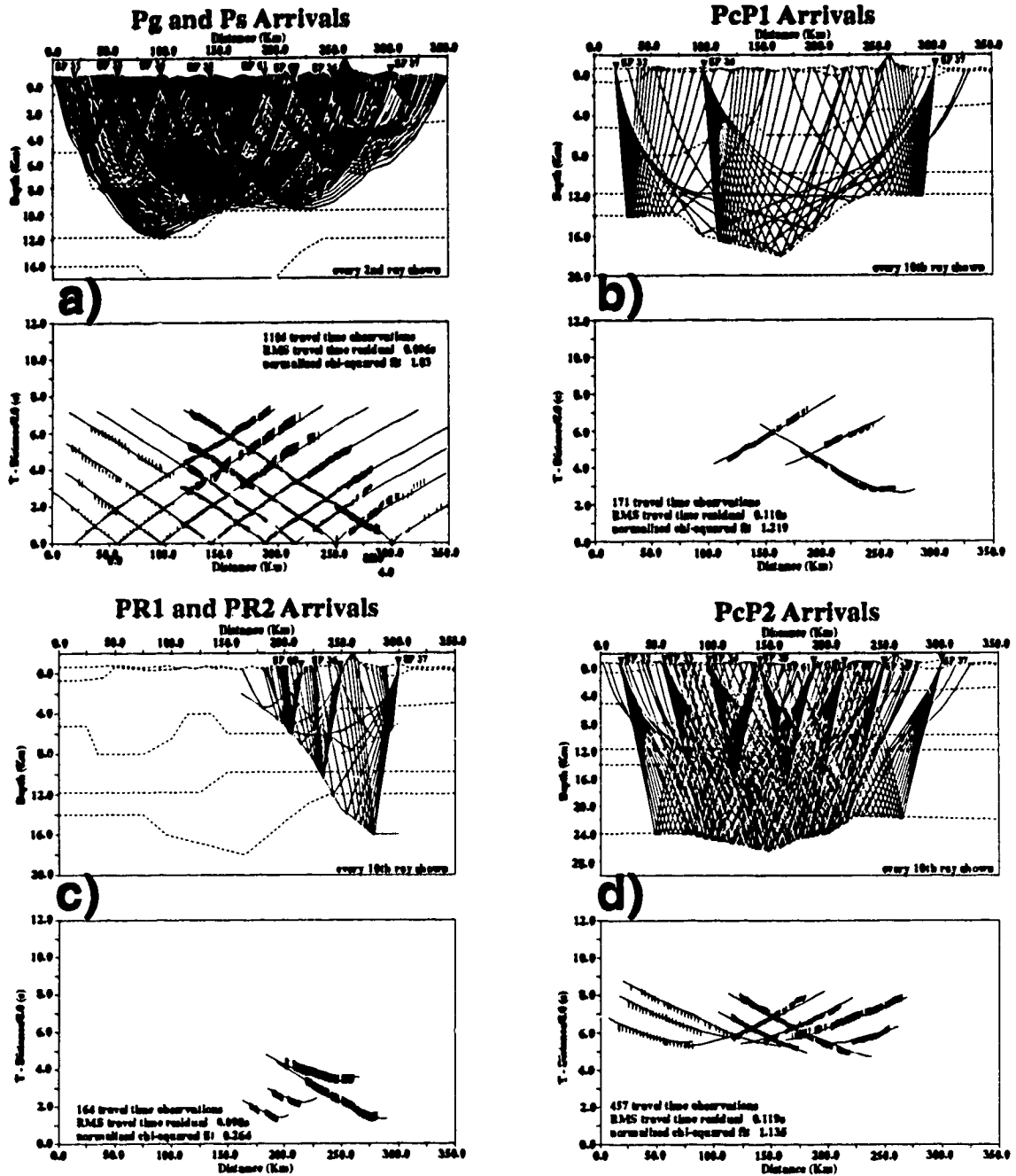


Figure 2.13 Ray coverage and traveltime curves for various arrivals of Line 8 using the final velocity model (Figure 2.12 a). Traveltime picks are shown by vertical bars whose lengths are in proportion to estimates of time pick uncertainty. Smooth lines are calculated traveltime curves. (a) Ps and Pg upper crustal arrivals (b) PcP1 WAR from the bottom of the upper crustal layer. (c) PR1 and PR2 intra-crustal reflectors. (d) PcP2 WAR from the bottom of the middle crust - continued on next page

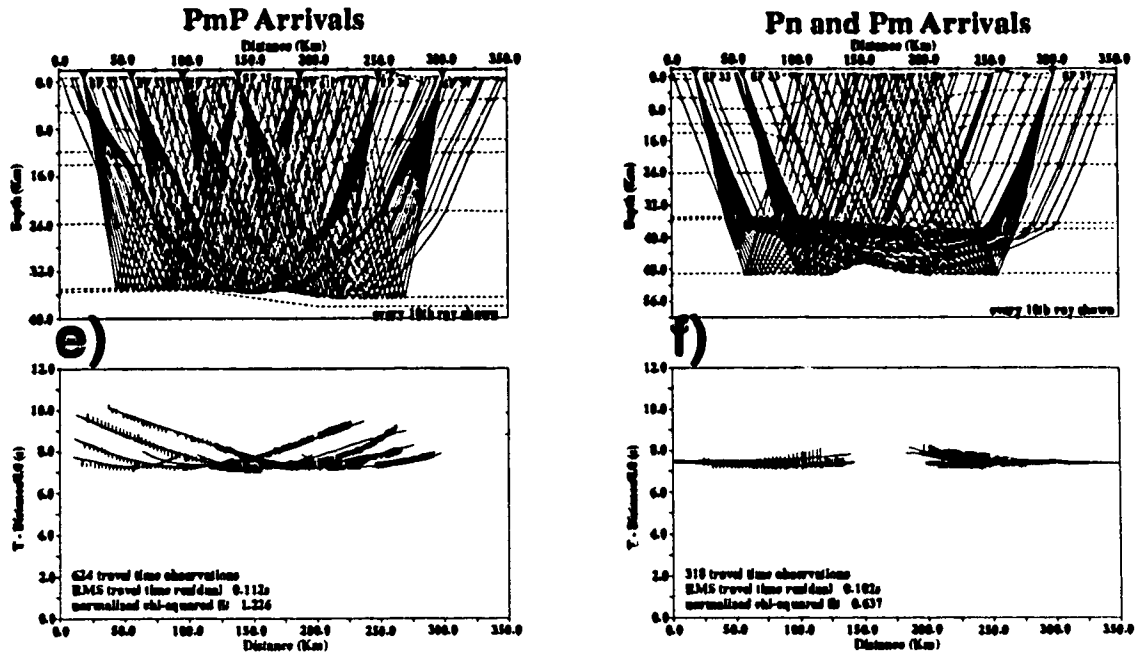


Figure 2.13 Continued from previous page (e) PmP WAR from the top of the crust/mantle transition zone (Moho) and (f) Pn and Pm arrivals from the upper mantle. Vertical exaggerations for the ray path diagrams are (a) 15:1 (b) 10:1 (c) 10:1 (d) 7:1 (e) 5:1 (f) 3.5:1.

is a negligible velocity gradient below depths of 10-12 km, this region above the reflector was modeled with a constant velocity and with no velocity contrast at the top of the layer. Thus only depths to the bottom of the upper crust are inverted for. For 171 traveltimes, the model gives an RMS traveltime misfit of 0.1 s (average uncertainty is 0.1 s) and a normalized χ^2 fit of 1.2.

Upper Crust Line 7

The upper crust was modelled almost exclusively by the P_S and P_G direct arrivals. The bottom of the upper crust, and some of the deepest velocities were modelled by a reflection from a single shotpoint and by use of constraints from intersecting profiles.

We analyzed the first arrival amplitudes on all shot records and found that only the three largest shotpoints (SP 23, SP 27 and SP 30) showed any amplitude variation. The amplitude-offset curves suggested that there were a number of relatively distinct amplitude regimes (Figure 2.12). By assuming that each amplitude regime was caused by a layer within the profile with a characteristic linear vertical velocity gradient, it was possible to construct a simple depth model of several layers with relative velocity gradients. Absolute velocities and gradients along with the thickness of layers were arrived at by calibrating with previous results from Line 8 and *Zelt et al.* [1992] and with preliminary forward travel-time modelling. The result was an initial, 5 layer model, with no velocity discontinuities except between the shallow surface layer (layer 1) and layer 2, and velocity gradients and layer thicknesses fixed by the amplitude-offset characteristics. This was the starting model for subsequent inverse modelling.

Initially, velocity nodes were placed in each layer, underneath every shotpoint. The P_S and P_G arrivals were inverted simultaneously and the model was inverted for all shots simultaneously. Again, since boundary parameters were not resolved by the rays, only the velocity nodes were inverted. Velocities and depths were adjusted on the basis

of forward modelling and the result inverted again. This iterative procedure was followed until an acceptable fit based on ray coverage and travel-times was reached. During the modelling, velocity gradients were sometimes changed slightly to obtain smaller traveltime residuals.

Additional velocity nodes were added between shotpoint locations to increase the resolution of the model and to reduce the model misfit. All of the nodes were resolved very well - well above the 0.5 value for well-resolved parameters. For 755 out of 767 observations, the RMS travel-time residual was 0.1 s (compared to an average pick uncertainty of 0.08 s) and the normalized χ^2 value was 1.2 (Figure 2.14 a).

Much of the remainder of the upper crust is unconstrained by the data. A wide-angle reflection ($P_c P_I$), that was earlier defined on Line 8 as the bottom of the upper crust was identified only on one shot record (SP 30, Figure 2.9 and 2.10). We also used as constraints the velocity values and depths from Line 8 and Zelt *et al.* [1992] where those profiles intersected ours. Thus, we end up with a small but non-zero velocity gradient in the lowest part of the upper crust and a well constrained boundary only east of the intersection with Line 8 and in the region surrounding the intersection with Line 1. Using those constraints, the inversion for the one shot record give us for 57 arrivals and RMS traveltime residual of 0.03 s (average uncertainty of 0.1 s) and a normalized χ^2 of 0.1 (Figure 2.14 b), indicating an excellent fit to the data.

intra-crustal Reflections Line 8

The P_{R1} and P_{R2} reflections are found in the region where, based on the vertical-offset reflection interpretation of Cook *et al.* [1992], one might expect to see evidence of upper crustal shear zones, especially the Monashee Décollement. The absence of evidence, from P_g waves, of juxtaposed geologic blocks with differing seismic properties is consistent with discrete zones being the source of the P_{R1} and P_{R2} reflections. That is, these reflections can be interpreted to be from impedance contrasts within fault zones that

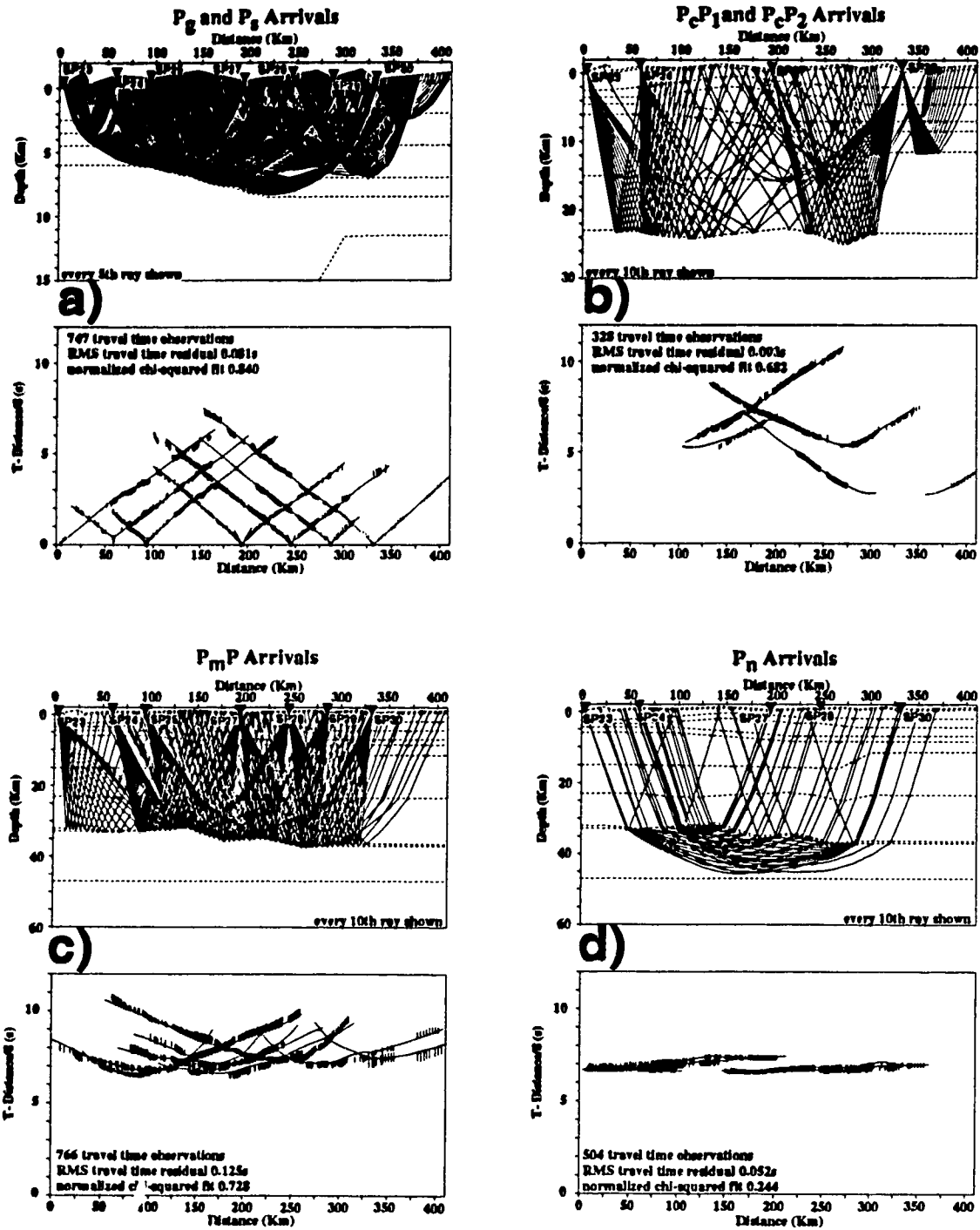


Figure 2.14 Ray paths and traveltime/distance curves from final velocity model of Line 7 (Figure 2.12 b). Description is the same as for Figure 2.9. a) P_s and P_g direct arrivals, b) P_cP_1 and P_cP_2 WAR c) P_mP WAR from Moho and d) P_n direct arrivals from upper mantle.

cut across the previously determined velocity structure. No intra-crustal reflectors were identified on Line 7.

These reflections are of limited lateral extent (P_{R2} is found on the three southernmost record while P_{R1} can be identified only on shotpoint 37) and are thus used to define an image but have little constraint on velocity parameters. These reflectors are used to interpret wide-angle reflections of limited extent and represent a spatial image similar to vertical-incidence reflection images whose velocity structures are not determined. The velocity field determined from the P_g analysis is assumed and only the geometry of the reflectors is inverted for.

On inversion, for 164 traveltimes and an average uncertainty of 0.2 s, an RMS traveltimes misfit of 0.1 s and a χ^2 fit of 0.3 were obtained. Note that the low χ^2 value of fit (Figure 2.13 c) with an average traveltimes residual is due to the high uncertainties estimated for picking the arrival times of the reflections.

Middle Crust Line 8

The $P_c P_1$ wide-angle reflection was used above to mark the bottom of the upper crustal layer, and in turn is taken to be the top of a distinct mid crustal layer. The bottom of this mid-crustal layer is vividly marked by the $P_c P_2$ wide-angle reflection. This reflection is clearly seen on all Line 8 shot records and is especially apparent on the two large end shotpoints (Figures 2.3 and 2.4). Special care was taken with the interpretation of this reflector since earlier analyses indicated anomalously low velocities in the mid crust. The quality of the picks is good. There are 457 observations used in the analysis, providing excellent multi-path ray sampling of the layer.

The first step in defining this mid crustal layer was simple forward modeling of $P_c P_2$ traveltimes using a flat reflector at various depths and a single constant velocity for the entire layer with a range of values. The results of these tests favored a thin layer and

a low velocity, a bottom interface at 26 km and a velocity of 6.3 km s^{-1} . Then, several depth nodes were added to the model. Several starting models with the best fit single velocity value for the range of layer thicknesses were inverted for simultaneous structure and velocity. The results for all eight starting models were remarkably similar, an average velocity of 6.0 km s^{-1} with a standard deviation of 0.1 and depth nodes (between 18 and 26 km) differing by less than 2%. Clearly, the data favor relatively low velocities. These preliminary results were used for subsequent inversion tests to determine the optimum number and placing of velocity and depth nodes to gain the highest resolution. These inversions tests included changing the inversion damping factor which reduces variations in the model parameters at the cost of decreased resolution. The aim was to gain the best fit to the traveltimes using reasonable and smoothly varying velocities, while maintaining reasonable resolution. The resulting inversion gave the highest velocities with the lowest acceptable parameter resolution (varying from 0.4 to 0.6) with an RMS residual of 0.1 s and χ^2 of 0.8. As velocity values are quite low (5.9 to 6.1 km s^{-1}), the analysis was continued by using the standard error resulting from the previous inversion to smooth the lateral velocity changes. This increased the misfit slightly. The velocities were then increased in all nodes by 0.5 km s^{-1} , held constant, and inverted only for depth to improve the fit. It was found that every increase in the velocities degraded the fit. Only the first stage increase of 0.5 km s^{-1} resulted in a satisfactory fit. The final model fit (Figure 2.13 d) shows velocities between 6.0 and 6.1 km s^{-1} . This velocity model for the distinct middle crustal layer has the highest possible velocities that give an acceptable traveltime fit. As such, this model represents the most conservative estimate of mid crustal velocities. The final model for 457 traveltime observations was an RMS traveltime misfit of 0.1 s (with average uncertainty of 0.1 s) and a χ^2 fit of 1.1.

Since the $P_c P_f$ arrivals are not as reliable as the $P_c P_2$ reflections, it could be asked how the velocity model in the middle crust would change without an explicit

bottom to the upper crust. Further forward and inverse modeling was conducted assuming that the boundary defined by $P_c P_1$ did not exist. In this case the middle crust required negative velocity gradients, velocities were still below 6.1 km s^{-1} and the position of the middle crust/lower crust boundary nodes changed by less than ± 2 km.

Middle Crust Line 7

Having defined a bottom to the upper crustal layer, the thickness and average velocity of the mid-crust can be determined from the $P_c P_2$ reflector, which is a reliable arrival on four shot records. The 271 time picks sample the layer uniformly and from a range of angles. During the analysis of Line 8 above, great care was taken in the modelling of this arrival since indications were that the mid-crust was a low velocity zone. Conservative interpretation of that data confirmed average velocities no higher than 6.1 km s^{-1} .

Inverse modelling tests were done on the $P_c P_2$ reflectors to ascertain the general velocity characteristics and it was found that the data favored a thin layer with low velocities over a thicker layer with higher velocities. Inversion with several velocity and depth nodes resulted in a well-resolved layer (resolution values $\gg 0.5$), with an RMS traveltimes residual of 0.1 s (uncertainty of 0.1 s) and a normalized χ^2 value of 1.0 (Figure 2.14 b). Test inversions without a boundary to the mid-crust (i.e. no explicit bottom to the upper crust) result in similar velocities and little change (± 2 km) in the position of the lower boundary.

Lower Crust and Upper Mantle Line 8

Amplitude modeling of the $P_c P_2$ reflection constrained the velocity contrast at the top of the lower crustal zone (Figure 2.11). Comparing the observed amplitude character

with synthetic seismograms indicated that the critical point for $P_c P_2$ was consistent with a velocity of 6.4-6.5 km s⁻¹ at the top of the lower crustal layer. For the upper mantle, the complex coda of the $P_m P$ reflection (Figures 2.3 and 2.4) suggests a crust/mantle transition zone and so a thin high velocity layer was included at the bottom of the crust. Again, amplitude modeling of $P_m P$ reflection critical point constrained this velocity to 7.6-7.7 km s⁻¹ (Figures 2.7). Initially, amplitude modeling included reflections from both the top and bottom of the zone, but tests showed that the bottom reflection had no effect on the analysis. An initial upper mantle velocity of 7.9 km s⁻¹, the apparent velocity of the P_n arrivals, was used as the upper mantle velocity, with a starting gradient of 0.02 s⁻¹. The P_m arrival was modeled as a wide-angle reflection from an intra-mantle interface, or steep velocity gradient, at about 48 km depth.

After construction of the starting model, inversion tests determined the optimum number and location of depth and velocity parameter nodes. Holding constant the amplitude-constrained velocities at the top of the lower crust, the inverted $P_m P$ arrivals determined values for the velocities at the bottom of the crust and the position of the bottom crustal boundary. No attempt was made to invert traveltimes for the crust/mantle transition, as P_n rays would not be able to resolve the velocities within this thin layer; on inversion the starting velocities were held constant. The P_n arrivals were used to invert for upper mantle velocity and to constrain the bottom of the transition zone. The depth to the intra-mantle reflector was obtained from inversion of P_m . There were 624 data points for the $P_m P$ inversion, 232 for P_n , and 86 observations for P_m (Figures 2.13 e and f).

For $P_m P$, the final model gave an RMS traveltime misfit of 0.1 s (average uncertainty is 0.1 s) and a χ^2 fit of 1.2. The result for the 232 P_n arrivals (with average uncertainty of 0.108 s) had an RMS traveltime misfit of 0.07 s and a χ^2 fit of 0.7. For the P_m arrivals, the 86 arrivals gave an RMS traveltime misfit of 0.2 s (average uncertainty is 0.2 s) and a χ^2 fit of 0.6. Again, the good χ^2 fit is due to the relatively large uncertainty

given this arrival.

Lower Crust and Upper Mantle Line 7

The $P_m P$ arrival (reflection from the bottom of the crust) defined the top of the Moho transition zone and the average velocity in the lower crust. In addition, amplitude modelling of the $P_c P_2$ reflection constrained the velocity contrast at the top of the lower crust. Comparing the observed amplitude-offset curves with those from synthetic seismograms (Figure 2.15 a) indicated that the critical point for $P_c P_2$ was consistent with a velocity of $6.4\text{--}6.5 \text{ km s}^{-1}$ at the top of the lower crustal layer. For the upper mantle, the complex coda of the $P_m P$ reflection suggests a crust/mantle transition zone (as does the interpretation of Zelt *et al.*, 1992 and for Line 8 above) and thus a thin high velocity layer was included at the bottom of the crust. Again, amplitude modelling of $P_m P$ reflection critical point (Figure 2.15 b) constrained this velocity to $7.5\text{--}7.6 \text{ km s}^{-1}$. An initial upper mantle velocity of 7.9 km s^{-1} - the apparent velocity of the P_n arrivals - was used as the upper mantle velocity, with a starting gradient of 0.02 s^{-1} .

After construction of the starting model, inversion tests determined the optimum number and location of depth and velocity nodes. Holding constant the amplitude-constrained velocities at the top of the lower crust, the inverted $P_m P$ arrivals determined values for the velocities at the bottom of the crust and the position of the bottom crustal boundary. No attempt was made to invert traveltimes for the crust/mantle transition as P_n rays would not be able to resolve the velocities within this thin layer - on inversion, these starting velocities were held constant. The P_n arrivals were used to invert for upper mantle velocity and to constrain the bottom of the transition zone. There were 845 data points for the $P_m P$ inversion with an RMS traveltime residual of 0.1 s (0.1 s average uncertainty) and χ^2 of 0.9 (Figure 2.14 c), and 505 observations for P_n giving an RMS traveltime residual of 0.05 s and a normalized χ^2 of 0.3 (Figure 2.14 d). All velocity and

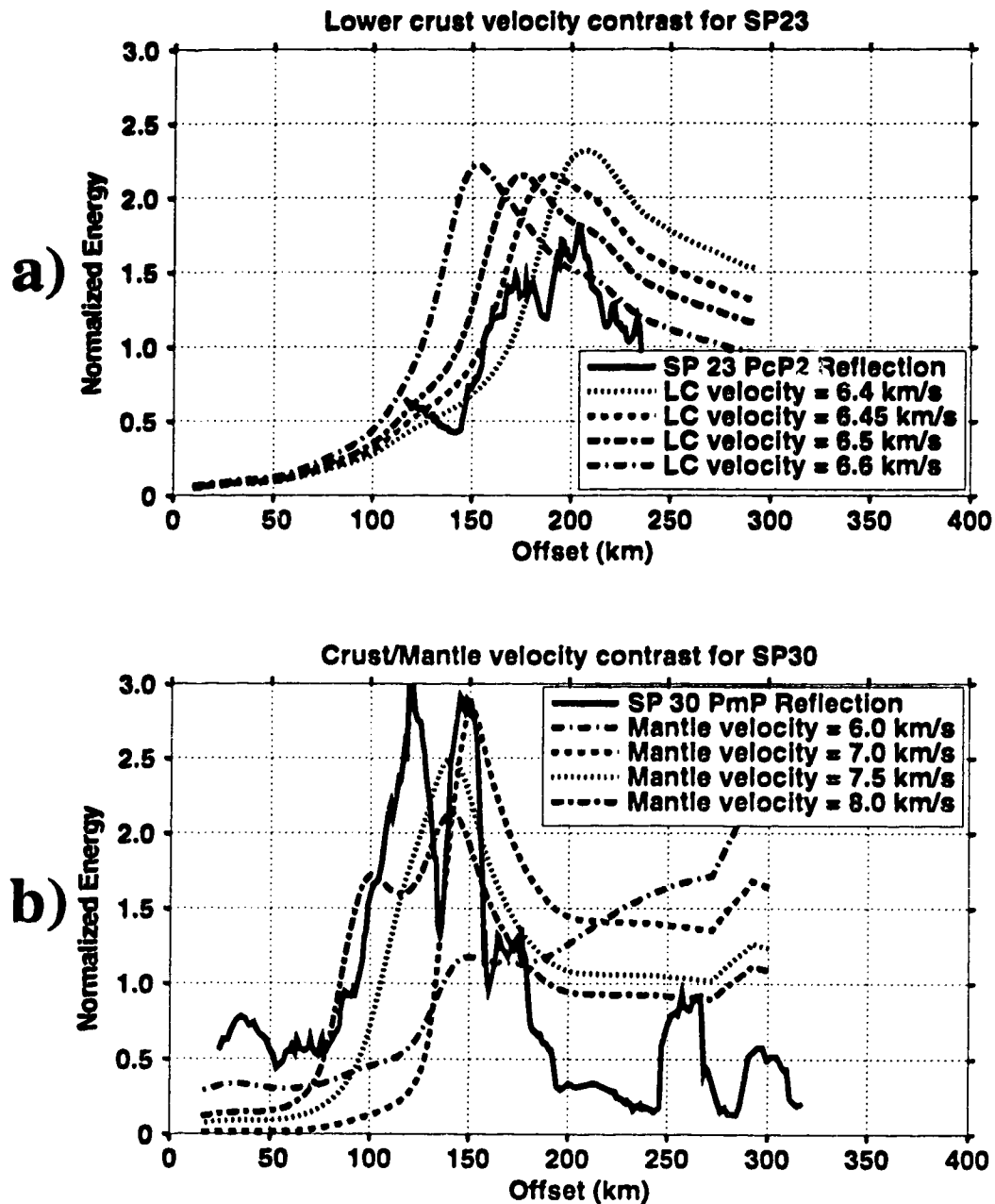


Figure 2.15 Two examples of the normalized energy vs. source-receiver offset. a) The PcP2 wide-angle reflection on SP 23. A comparison between the PcP2 amplitudes and modelled amplitudes shows that, assuming a previously defined mid-crustal velocity, velocities at the top of the lower crust are most compatible with values of 6.5-6.6 km s⁻¹. b) The PmP wide-angle reflection on SP 30. For PmP, the data suggests mantle transition velocities of 7.5-7.7 km s⁻¹.

depth nodes for the upper crust and position of the bottom of the crust were well resolved (resolution values > 0.7). Velocity nodes at the top of the mantle were also well resolved, with the resolution falling off for deeper parameters (≥ 50 km) with decrease in ray coverage.

Horizontal Resolution and Model Uncertainty

For the entire model of Line 8, with 2878 observations, the overall fit is characterized by an RMS traveltimes residual of 0.11 s (compared to the overall travel-time pick uncertainty of 0.11 s) and a χ^2 misfit of 1.0. For the entire model of Line 7 with 2377 observations, the overall fit is described by an RMS travel-time residual of 0.1 s (compared to the overall travel-time pick uncertainty of 0.1 s) and a χ^2 misfit of 0.7.

In the upper crust, the velocity nodes, placed at least at the shotpoint locations, all had high resolution values (≥ 0.9). Thus the upper crust velocities have a horizontal resolution of at least the shotpoint spacing, 50 to 25 km. Line 7 resolution is often better, since the modelling was done with velocity nodes between shotpoints as well. The resolution of the bottom boundary of the upper crust layer is of that order as well for Line 8, but there is little resolution of it on Line 7 with its poor constraints. In the middle crust, the horizontal velocity and structural variations at the bottom of the layer are resolved to 40 km. In the lower crust, lateral velocity and boundary depth nodes at the bottom of the crust are well resolved to 25 km as a result of the relatively higher number of rays, from a wide variety of angles, constraining the parameters. The velocities within the transition zone are not constrained by the traveltimes at all, and the bottom of the layer is poorly resolved, laterally and vertically, indicating that this is a nonessential part of the model. The upper mantle velocities have a lateral resolution of 40 km. The structure of the intra-mantle reflector on Line 8 is poorly resolved, due to few arrivals. Though these P_m arrivals do provide evidence of intra-mantle layering, there is little that

can be said other than it occurs at an approximate depth of 45-50 km.

Uncertainties of velocities and depths of the model were tested by perturbing the model parameters [Zelt and Smith, 1992]. As well, some parts of the models were independently analysed more than once and values were continually compared with intersecting lines. On the basis of these analyses it was estimated that velocity parameters have errors of $\pm 0.1 \text{ km s}^{-1}$, while depth uncertainties are of the order of $\pm 1.0 \text{ km}$. However, other studies of similar data in this region [C. A. Zelt and D. J. White, manuscript in preparation] suggest that the parameters may have higher uncertainties, $\pm 0.2 \text{ km s}^{-1}$ in velocity and $\pm 2.0 \text{ km}$ in depth, especially in deeper sections. Comparison of our Line 8 model with the intersection of a model from the east-west line 9 [C. A. Zelt and D. J. White, manuscript in preparation] and our Line 7 with Line 1 of Zelt *et al.* [1992] also suggest that errors in velocity are $\pm 0.1 \text{ km s}^{-1}$ and could be as much as $\pm 0.2 \text{ km s}^{-1}$ and that uncertainties in depth could be as much as $\pm 2 \text{ km}$. The higher uncertainties pertain to deeper sections of the model.

2.5 Interpretation

Line 8

The final model for Line 8 is shown in Figure 2.16. The details of the velocity field for this profile is shown as iso-velocity lines while wide-angle reflection boundaries are presented as solid lines. Thick broken lines indicate shear zones interpreted from localized wide-angle reflections. The color shading is coded to velocity values as indicated. The interpreted profile can be grouped into four distinct broad areas: upper crust, middle crust, lower crust, and mantle. In some of these areas further distinctions may be made. In all, eight discrete layers have been interpreted.

The upper crust can be divided into four zones, each with distinctive velocity and velocity gradients but no evidence for sharp velocity discontinuities at the zone

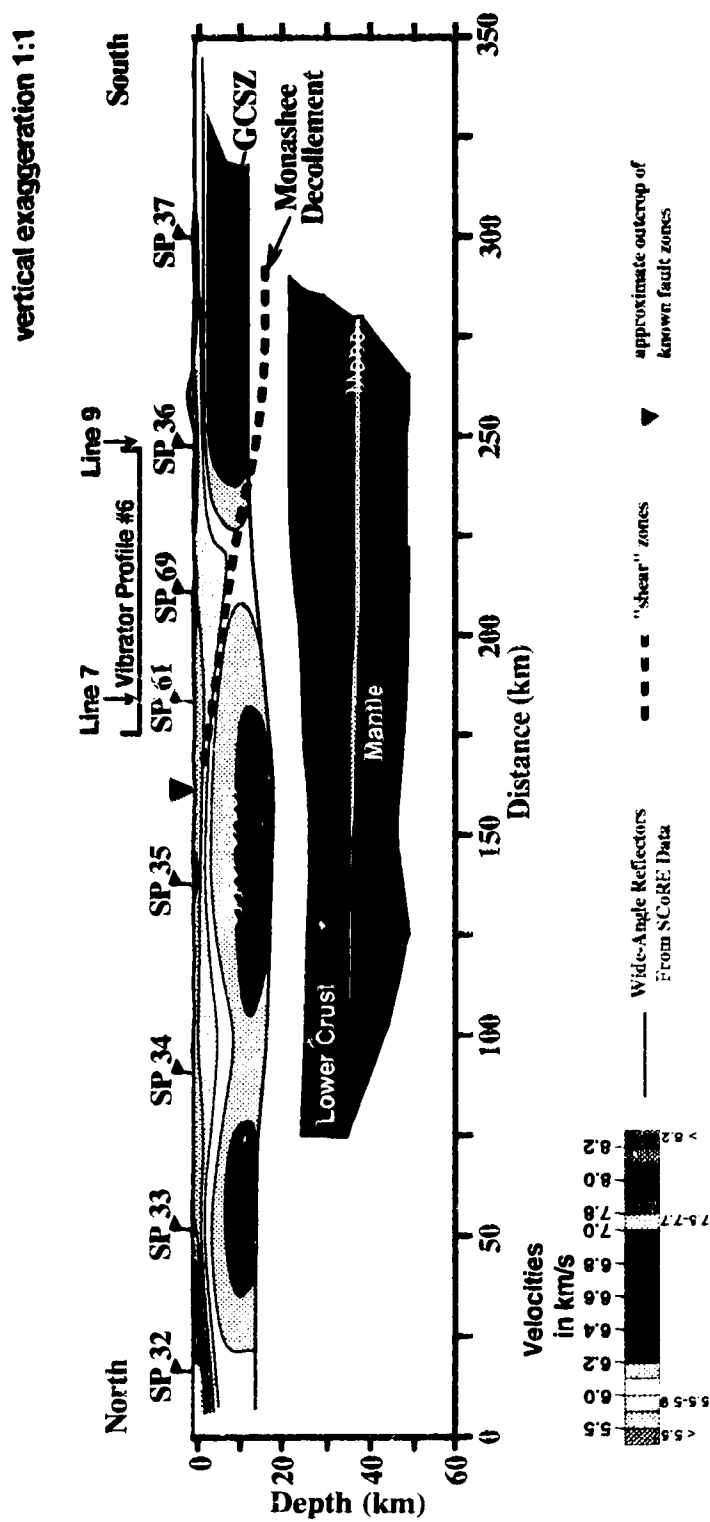


Figure 2.16 Final velocity model for SCoRE'90 line 8. Velocity ranges for the profiles are color coded as given in the legend.

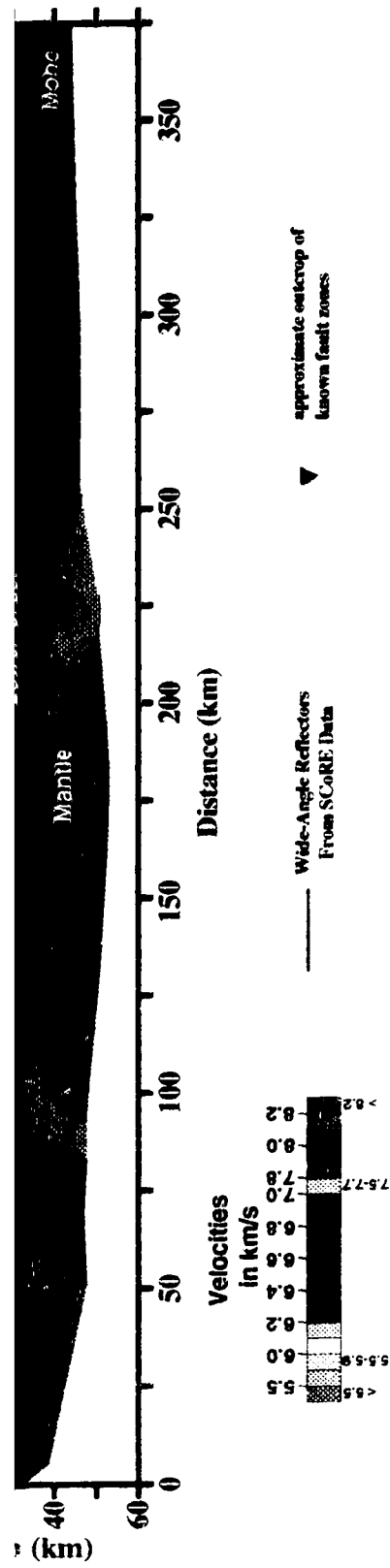


Figure 2.17 Final velocity model for SCoRE'90 line 7. Velocity ranges for the profiles are color coded as given in the legend.

boundaries. These zones are not to be taken as distinct layers, but only as indications of a gross change in the linear vertical velocity gradient - hence the iso-velocity display of Figure 2.16. The thin surface layer has a mean velocity of 5.5 km s^{-1} with a relatively high gradient of 0.11 s^{-1} . The next three layers, have average thicknesses of 5.5 and 3.5 km, respectively, average velocities of 6.0, 6.2, and 6.2 km s^{-1} with respective average gradients of 0.06, 0.01, and 0.0 s^{-1} . Thus within the upper crust, velocities increase and velocity gradients decrease with depth. The bottom of the upper crustal layer is between 12 and 18 km depth. Also in the upper crust, two shear zones, are imaged on the south end of the profile between shotpoints 35 and 37 (Figure 2.16). Based on comparisons with the seismic reflection interpretation [Cook *et al.*, 1992], the lower fault (Figure 2.16) corresponds roughly with the Monashee Décollement while the shallower one is in agreement with the position of the Gwillim Creek Shear Zone (GCSZ on Figure 2.16). The "Monashee Décollement" reflector on our profile dips to the south and flattens out at 16 km depth.

The middle crust is interpreted as a distinct seismological layer with respect to the upper and lower crust. It is between 7 and 10 km thick and has a relatively low velocity ranging from 6.0 to 6.1 km s^{-1} . We have taken great care to obtain the highest possible velocities (i.e., most conservative) that will fit the data, and it is clear that this layer exhibits a characteristic lower velocity than that of the upper crust. On this basis, we call this zone the mid crustal Low Velocity Zone (LVZ). The top of the lower crust has depths from 21.5 to 26 km. Velocities range from 6.4 - 6.5 km s^{-1} at the top to 6.5 - 6.8 km s^{-1} at the base. Its thickness is 11 km on average and it has a mean velocity gradient of 0.02 s^{-1} . The bottom of the crust, the top of the crust/mantle transition zone, is located at a depth ranging from 35 to 37 km. The top of the Moho has a slight dip from north to south. Velocities within the Moho transitional zone are ~ 7.6 - 7.7 km s^{-1} , as constrained by reflection amplitudes. The thickness of the transition region is variable, generally 1 to

2 km, but is very poorly constrained by the data.

There is an intra-mantle boundary, or abrupt velocity change at an approximate depth of 48 km, again not well constrained. This boundary defines an upper mantle zone with a thickness of 10 to 14 km and velocities averaging 7.9 km s^{-1} at the top and 8.1 km s^{-1} at the bottom. The imaged portion of the upper mantle between 35 and 50 km has an average velocity of 8.0 km s^{-1} with a velocity gradient of 0.012 s^{-1} . It is tempting to interpret the intra-mantle boundary as the top of the asthenosphere, especially considering the thin lithosphere in the region [Wickens, 1971, 1977]. However, inferring a positive or negative velocity contrast is very difficult on the low signal-to-noise ratio P_m arrival.

Generally, the model shows the crust of the Canadian Cordillera in the Omineca Belt to be characterized by slight lateral changes in velocity, with a thickness of 35 to 37 km. Velocities range up to a maximum of 6.3 km s^{-1} in the upper crust, less than 6.1 km s^{-1} in the mid-crust and $6.4\text{-}6.8 \text{ km s}^{-1}$ in the lower crust. The upper mantle layer has velocities starting at 7.9 km s^{-1} and averaging 8.0 km s^{-1} . The average crustal velocity is between 6.2 and 6.3 km s^{-1} , slightly lower than the most common mean crustal velocity of 6.3 km s^{-1} , but similar to the Basin and Range [Smithson *et al.*, 1981].

Figure 2.18 is the migrated and coherency-filtered line 6 data, from Lithoprobe's near-vertical incidence reflection program [Cook *et al.*, 1992] which is coincident with part of Line 8 (see position of Vibrator Profile 6 on Figures 2.12 a). Fig. 2.19 is a comparison between the interpretation of Cook *et al.* [1992], shown by (white) dashed lines, and the velocity model from this study, given by solid lines and iso-velocity colors. For the comparison, note that Cook *et al.* [1992] used a single average crustal velocity for depth conversion and that the depths given by the present work have an uncertainty of at least $\pm 1.0 \text{ km}$. It is evident that our "Monashee Décollement" does not match well with that interpreted from the vertical incidence data. However, it does correspond generally with a zone of considerable structural complexity associated with a region of crustal detachment related to the Monashee Décollement. It may be that we are imaging

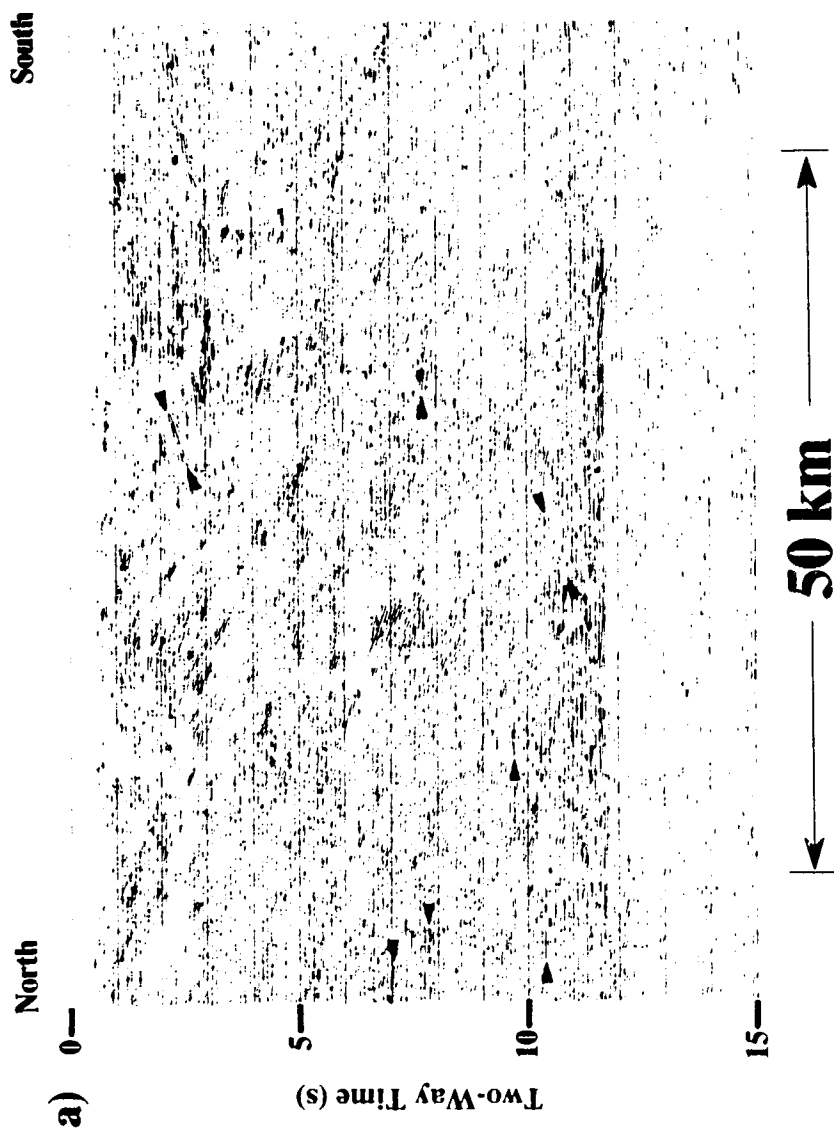


Figure 2.18 Migrated and coherency-filtered vibrator reflection line 6 [Cook et al., 1992]. Arrows indicate weak reflected events with dips opposed to the regional grain but consistent with refraction/wide-angle events. Compare with interpreted reflectivity shown with the Line 8 velocity model in Figure 2.19.

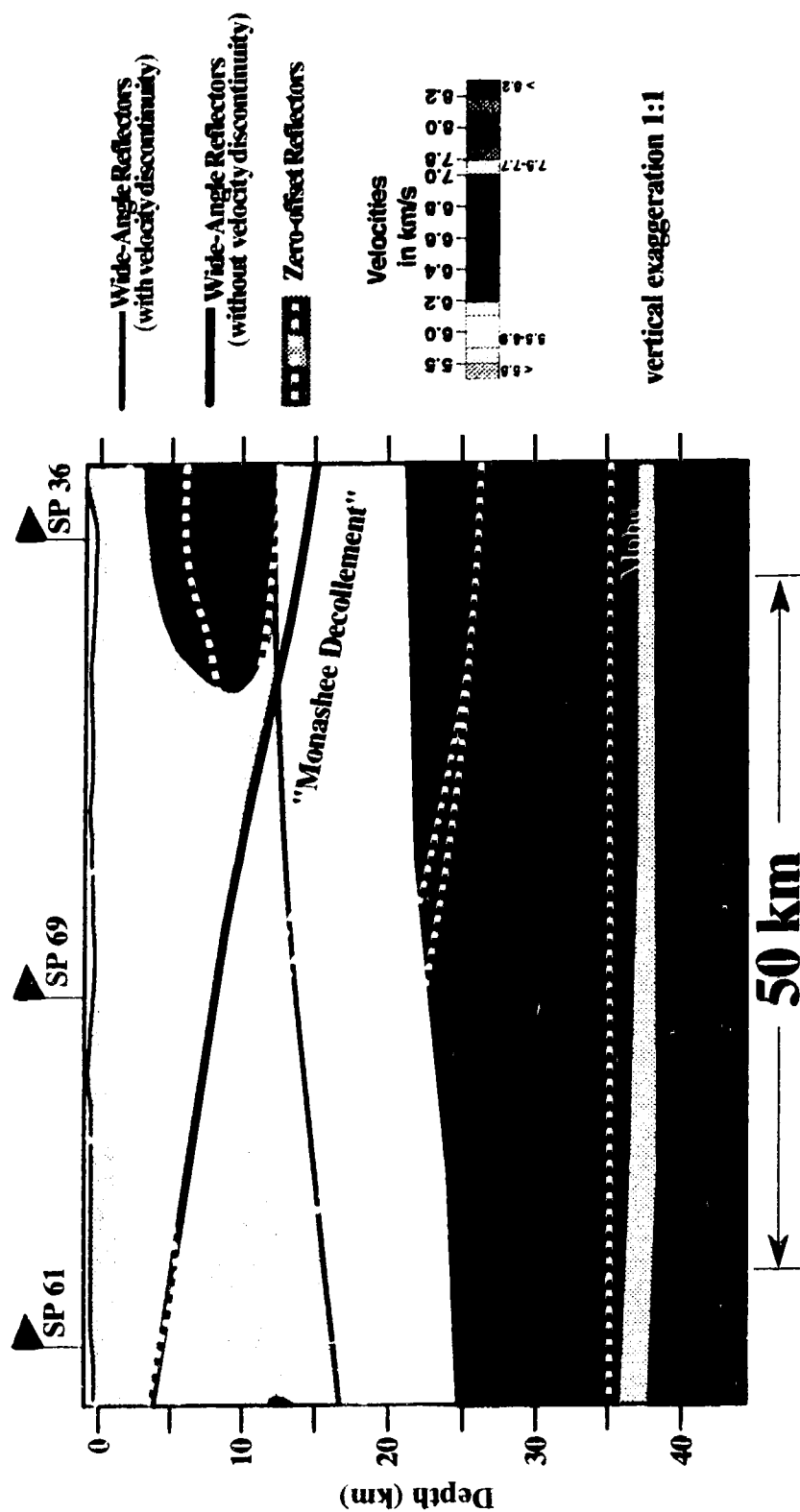


Figure 2.19 Comparison of zero-offset seismic reflection interpretation with refraction/wide-angle reflection interpretation of Line 8. Final SCoRE '90 line 8 velocity model coincident with line 6 reflection profile. The velocity model is given by color coded iso-velocity contours and solid lines for velocity discontinuities and interpreted shear zones. The dashed lines are the interpretation of the zero-offset reflections by Cook et al. [1992]. Depths are below sea level. GCSZ denotes the Gwillim Creek Shear Zone. The Monashee Décollement is a shear zone that was interpreted without reference to the existing velocity field and thus is allowed to cut across previously established velocity discontinuities.

different aspects of the deformational system. The shallower intra-crustal reflector, on the other hand, compares well with the location of the Gwillim Creek Shear Zone interpreted by *Cook et al.* [1992]. The iso-velocity lines also match the trends of the vertical incident reflectivity within the upper crust. The positions of the respective Mohos, at 35 km and greater, also match well within the errors involved.

However, there is marked discrepancy between the reflectivity trends presented by *Cook et al.* [1992] with the present interpretation in the middle to lower crust. There is little correspondence between the interpreted reflection data and the refraction/wide-angle constrained crustal boundaries. But, a close examination of reflection line 6 (Figure 2.18) shows that though the predominant reflectivity grain does dip north to south, there are un-interpreted, contradictory dips visible and even sub-horizontal reflections that can be correlated with the top of the lower crust as defined by the refraction data.

Line 19 of the Lithoprobe vertical incidence reflection program [*Cook et al.*, 1992] runs to the southwest, with its northeast end abutting refraction line 8 at approximately the location of shotpoint 32 (Figure 2.1). The interpretation of this reflection line shows the Monashee Décollement dipping to the southwest, which may be associated with the low velocities in the shallow crust interpreted from the refraction data between SP 32 and 33 (Figure 2.16). The depth to Moho, at 35 km, matches that of the refraction interpretation at the location of SP 32.

The study by *Zelt et al.* [1992] of SCoRE '89 refraction line 1 within the Intermontane Belt (Figure 2.1) shows a crust very similar to that interpreted for line 8. The mid crustal layer (10-15 km thick with a bottom at a depth of 23-25 km) has a velocity of 6.2 km s^{-1} , and local velocity inversions - 6.0 and 6.15 km s^{-1} with respect to 6.2 - 6.25 km s^{-1} in the upper crust immediately above. The lower crust has velocities of 6.5 to 7.0 and the upper mantle has velocities from 7.8 km s^{-1} at 33 km depth to 8.0 km s^{-1} at 45 km depth.

s^{-1} at 50 km. An intra-mantle reflector is interpreted at a depth of 50 km.

C. A. Zelt and D. J. White (manuscript in preparation, 1994) have a recent interpretation of SCoRE '90 line 9 which shares a shotpoint location (shotpoint 36 - Figure 2.1) with Line 8. Within the Omineca Belt, their work shows that crustal thickness is of the order of 36 km, upper crustal and mid crustal velocities are below 6.2 km s^{-1} while the lower crust has velocities between $6.5\text{-}6.7 \text{ km s}^{-1}$ with a positive velocity gradient. Upper mantle velocities are 7.9 km s^{-1} . At the line of intersection, the two velocity structures agree very well.

Line 7

The final velocity model of the crust and upper mantle for Line 7 is shown in Figure 2.17. The details of the velocity field for these profiles are shown as iso-velocity lines while wide-angle reflection boundaries are presented as solid lines. The color shading is coded to velocity values as indicated. The profile in Figure 2.17 is contoured beyond the range of seismic ray control by using constraints from other SCoRE wide-angle seismic studies [Zelt *et al.*, 1992,1993; Zelt and White, in preparation, O'Leary *et al.*, 1993].

During modelling the upper crust was divided into six sub-layers each with its own characteristic velocity and linear vertical velocity gradients based on the P_g amplitude properties. There is no evidence, other than that at the surface layer/basement boundary, for sharp velocity discontinuities between these sub units. These zones are understood not to necessarily be distinct geological layers, but only as indications of gross changes in the linear vertical velocity gradients.

The thin surface layer, whose average thickness is 300 m, has a mean velocity of 4.4 km s^{-1} with a high vertical velocity gradient of 0.28 s^{-1} . These parameters are also highly variable with velocities varying from less than 2.0 and up to 5.6 km s^{-1} and gradients ranging from a low value of 0.03 s^{-1} to a very high 1.0 s^{-1} .

The next 5 layers have average thicknesses of 2.3, 1.9, 2.6, 1.5 and 6.7 km respectively, average velocities of 5.9, 6.0, 6.1, 6.2 and 6.2 km s⁻¹ with respective average gradients of 0.10, 0.06, 0.02, 0.01 and 0.01 s⁻¹. Thus, within the upper crust, velocities increase and velocity gradients decrease with depth. The bottom of the upper crustal layer is between 12 and 16 km depth. Overall, the upper crust has a mean thickness of 15.3 km, an average velocity of just under 6.1 km s⁻¹, and an average vertical velocity gradient of 0.04 s⁻¹, decreasing from 0.3 to 0.01 s⁻¹.

Within the upper crust, we see a relatively heterogeneous pattern of velocities, as one would expect going across strike of two morphogeological belts. There are, in the middle of the profile, two low velocity trends that correlate, geometrically and spatially, to two crustal scale "Shear Zones", the Monashee Décollement (MD) and the Okanagan Valley Fault (OVF). Towards the west end of the line, there is an anomalous high-velocity plug in the upper crust. Here velocities are at least 0.4 km s⁻¹ higher than surrounding regions. The location of the high velocity anomaly corresponds to the position of the Nicola Horst, bounded by the Coldwater (CWF) and Quilchena Creek (QCF) Faults.

In the eastern part of the profile we interpret the middle crust to be a distinct seismological layer with respect to the upper and lower crust. It is between 7 and 12 km thick and has a relatively low velocity ranging from 5.9 to 6.2 km s⁻¹ and averaging less than 6.1 km s⁻¹. It is obvious that this layer exhibits a characteristic lower velocity than that of the upper crust. On this basis and with reference to the results of Line 8, we call this zone the Mid-Crustal Low Velocity Zone (LVZ). The top of the Mid-Crustal LVZ rises to the east from 15 km depth to 11 km. On the western end of the profile, however, the upper crustal high velocity plug coincident with the Nicola Horst, smoothly continues down into the middle and even lower crust. Mid-crustal velocities here increase from 6.3 to 6.6 km s⁻¹. Though there is good evidence of a reflecting boundary at the bottom of

the upper crust in this region [Zelt *et al.*, 1992], it is evident that crustal properties are quite different at the position of the horst.

The top of the lower crust is at depths of 23.5 to 25 km. Velocities range from 6.4-6.6 km s⁻¹ at the top to 6.5-7.0 km s⁻¹ at the base. Velocities decrease somewhat from east to west. The thickness of the lower crust is 10 km on average and it has a mean velocity gradient of greater than 0.01 s⁻¹. The bottom of the crust, the top of the crust/mantle transition zone, is located at a depth ranging from 31 to 36 km with an average of 34 km. The top of the 'Moho' has a pronounced dip from 32 km in the west to 40 km depth in the east. Velocities within the Moho transitional zone are ~7.5-7.7 km s⁻¹, as constrained by reflection amplitudes. The thickness of the transition region is variable, generally 0.2 to 0.8 km, but again is very poorly constrained by the data.

The upper mantle zone has been sampled to a depth of no more than 50 km. Velocities average 7.9 km s⁻¹ at the top and 8.1 km s⁻¹ at the bottom. The imaged portion of the upper mantle between 34 and 50 km has an average velocity of 8.0 km s⁻¹ with a velocity gradient of 0.01 s⁻¹. Note the well established lateral velocity gradient between the Coast and Intermontane belts on the west end of the profile

The average velocity of the crust for this profile is 6.2 km s⁻¹. This is less than the mean continental crustal velocity of 6.3-6.4 km s⁻¹ [Smithson *et al.*, 1981].

Figures 2.20 and 2.21 are a direct comparison between our seismic velocity model and the corresponding LITHOPROBE vertical incidence seismic reflection profiles [Cook *et al.*, 1992]. Figure 2.20 shows the actual seismic reflection data, while on a background of the color coded velocities, we have overlain the interpreted reflectivity with white dashed lines on Figure 2.21 where the two interpretations overlap. Again note that Cook *et al.* [1992] have converted from two-way traveltime to depth using only a constant crustal velocity of 6.0 km s⁻¹.

Earlier, in comparing reflection and refraction interpretations with respect to Line 8, we found that while there was good agreement in the upper crust, the comparisons

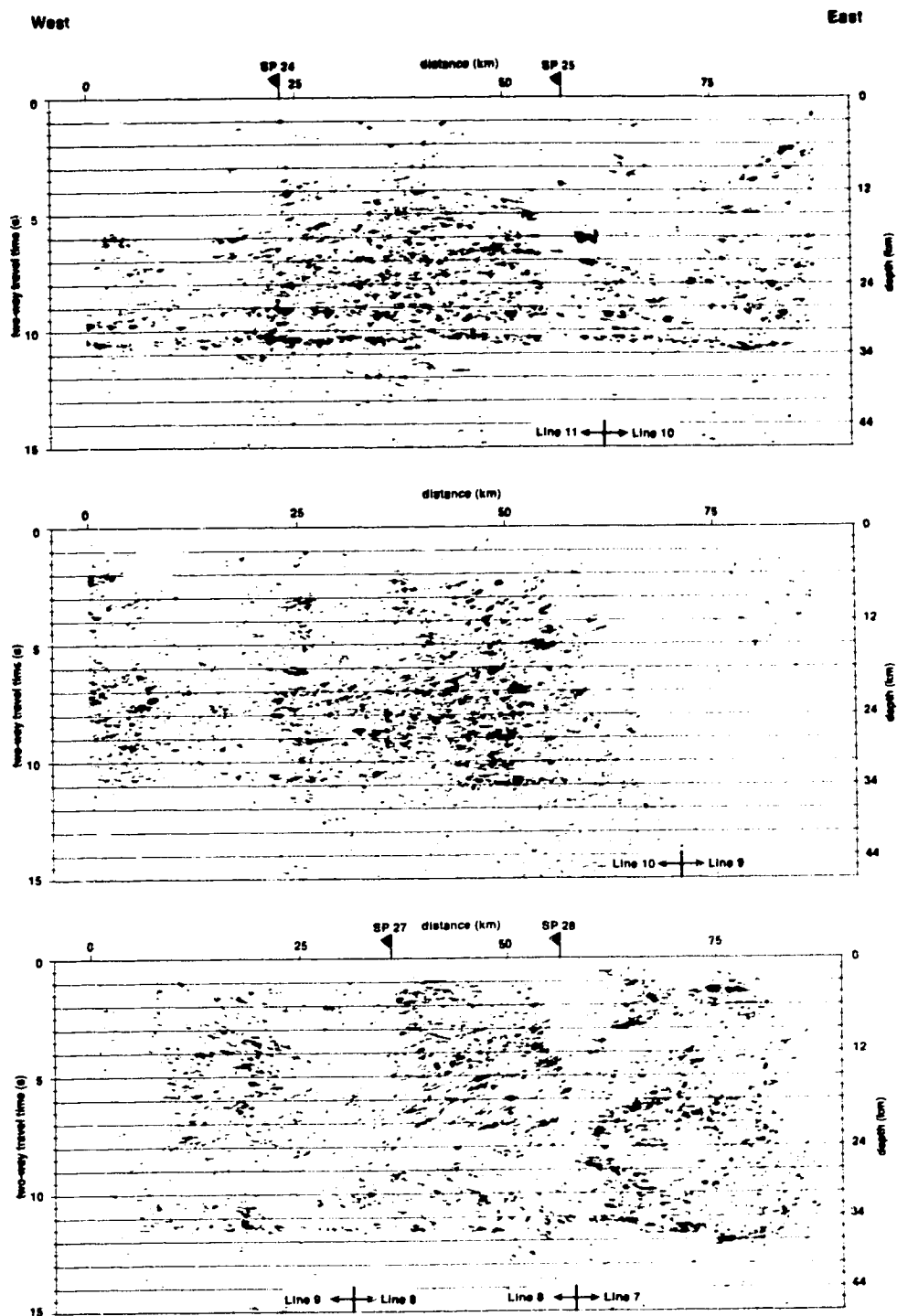


Figure 2.20 Migrated and coherency-filtered vibrator reflection lines 7 to 11 [Cook et al., 1992]. The combined profiles are shown in three panels, from west to east. Compare with the interpreted reflectivity shown with the Line 7 velocity model in Figure 2.21.

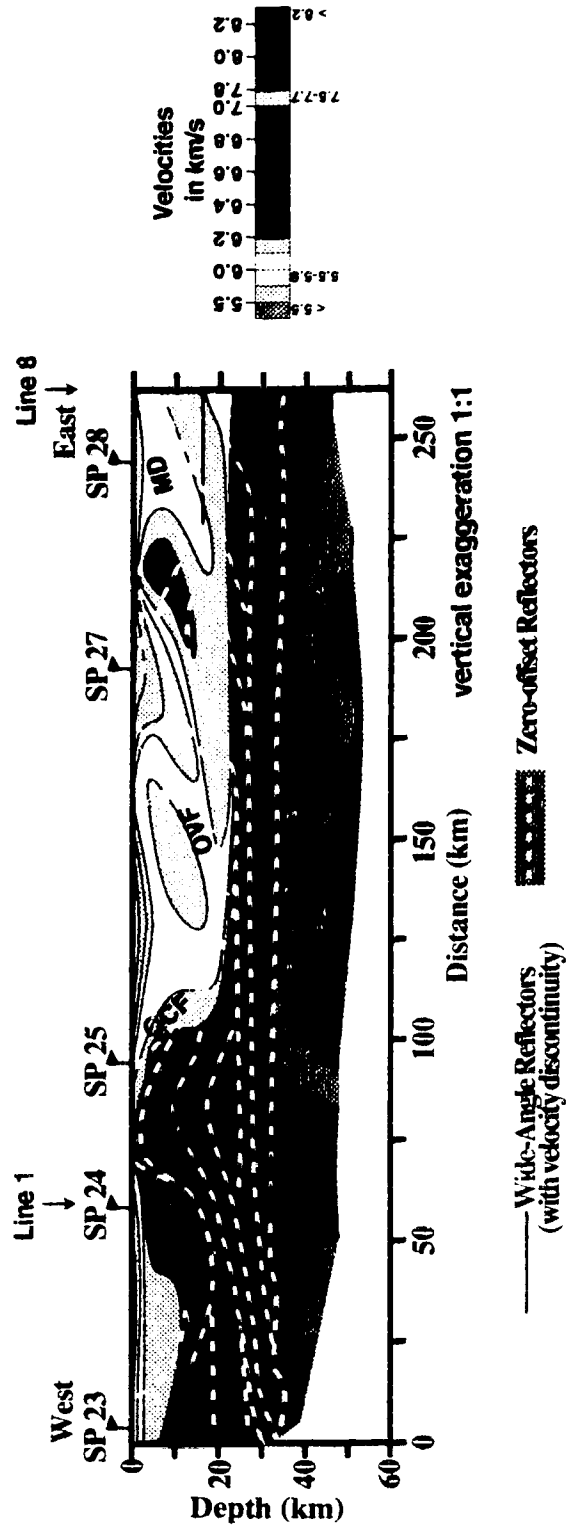


Figure 2.21 Line 7 final velocity model coincident with earlier acquired seismic reflection profiles directly compared with the interpreted reflectivity. The dashed white lines represent the reflection interpretation of Cook et al.[1992] while the velocity color code is given in the legend. 'CWF' is the Cold Water Fault, 'QCF' is the Quilchena Creek Fault, 'OVF' is the Okanagan Valley Fault and 'MD' is the Monashee Décollement.

were poor in the mid and lower crust. However, on Line 7 the agreement is remarkable. The pattern of reflectivity is closely matched by that of the velocity structure. In particular, note the layering of reflectivity and velocity trends in the region of the Nicola Horst, the soling of the reflectivity into the model's lower crustal layer and the correspondence of the reflection and refraction Mohos.

2.6 Discussion

Discussion of the final models (Figure 2.16 and 2.17) will center on the significance of the general velocity structure, features of the upper crust, comparisons with the vertical incidence reflection data and the implications of the velocity model as a whole with respect to other recent geophysical work.

The velocity model of the southeastern Cordillera, as illustrated by the present interpretation, seems to be anomalous with respect to much of the rest of northwestern North America. We can contrast the seismic velocity characteristics of the southern Canadian Cordillera with those of surrounding regions (Figure 2.22). In the Oregon Cascades (Figure 2.22a), *Leaver et al.* [1984] find a Moho at 45 km depth, velocities between 6.3 and 7.1 km s⁻¹ throughout most of the crust and upper mantle velocities of 7.7 km s⁻¹. *Catchings and Mooney* [1988] conclude that in the Columbia Plateau region (Figure 2.22b) the crust is 40 km thick, has high velocities in the middle and lower crust and a rather anomalous 8.4 km s⁻¹ upper mantle velocity. *Hawman et al.* [1990], *Holbrook* [1990], *Benz et al.* [1990] and *Catchings and Mooney* [1991] have interpreted the 1986 Program for Array Seismic Studies of the Continental Lithosphere Basin and Range experiment in northwestern Nevada (Figure 2.22c). They find a 31 to 32-km-thick crust, a 7.9 km s⁻¹ upper mantle, crustal velocities less than 6.2 km s⁻¹ in the mid crust and above, and, generally, less than 7.0 km s⁻¹ in the lower crust. *Hawman*

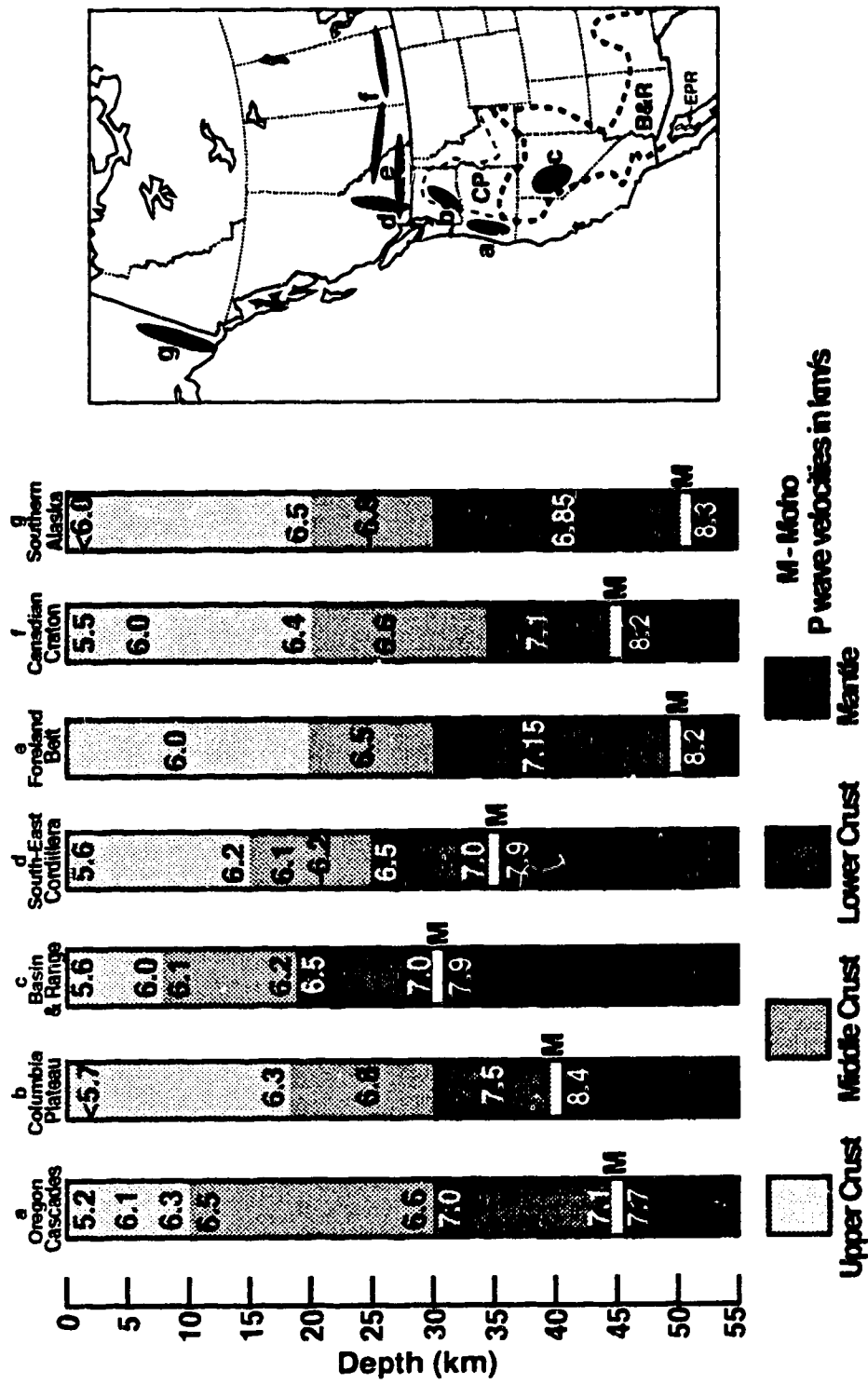


Figure 2.22 Velocity depth columns for several regions of western North America generalized from various studies cited in the text. Note similar characteristics between Basin and Range (panel c) and south-east Canadian Cordillera (panel d). The inset map shows approximate locations and orientations of the studies (B&R, Basin and Range; CP, Columbia Plateau; and EPR, East Pacific Rise).

et al. [1990] and *Catchings and Mooney* [1991] do interpret a 7.4 km s^{-1} lowermost crustal layer, but this may simply be the crust/mantle transition zone of *Benz et al.* [1990] and *Holbrook* [1990]. In the Foreland Belt (the Rocky Mountains) of Canada (Figure 2.22e) *Chandra and Cumming* [1972], *Bennet et al.* [1975] and C. A. Zelt and D. J. White (manuscript in preparation, 1994) show the crust to be 50 km thick with upper crustal velocities below 6.0 km s^{-1} , mid and lower crust velocities of 6.5 and 7.15 km s^{-1} , respectively, and upper mantle velocities of 8.2 km s^{-1} . *Chandra and Cumming* [1972] and *Kanasewich et al.* [1987] present seismic velocity structures of the North American craton in Western Canada (Figure 2.22f) using data from southern Alberta, Saskatchewan and Manitoba. Generally, the crust is 45 km thick with upper crust velocities up to 6.4 km s^{-1} , a 15-km-thick middle crust of 6.6 km s^{-1} , a lower crust below 35 km with a 7.1 km s^{-1} velocity and an upper mantle velocity of 8.2 km s^{-1} . In southern Alaska (Figure 2.22g), *Fuis et al.* [1991] interpret the North American crust, underthrust by the Pacific Plate, to be about 50 km thick and underlain by 8.3 km s^{-1} mantle. Upper crustal rocks have velocities increasing to 6.5 km s^{-1} , with approximately 6.8 km s^{-1} mid crustal and 6.85 km s^{-1} lower crustal material.

Definitely, the southeastern Canadian Cordillera (Figure 2.22d), as generalized from this study and the results of *Zelt et al.* [1992] and C. A. Zelt and D. J. White (manuscript in preparation, 1994), is anomalous with respect to the North American craton, to the Rocky Mountains, to the Cascade Ranges and to southern Alaska. The crust is thinner, and the crustal and upper mantle velocities are lower. The interpretation of Line 7 shows that these anomalous parameters of low velocity and thin crust are not only present in the Omineca Belt, but extend westward into the Intermontane Belt and eastward towards the Foreland Belt. Our region of study though, does have similarities to the seismic characteristics of the Basin and Range (Figure 2.22c), i.e. thin crust and low velocities in the crust and upper mantle. In addition, the southeast Cordillera has a thin

lithosphere [Wickens, 1971; Wickens, 1977] as does the Basin and Range [Thompson *et al.*, 1989; Smith *et al.*, 1989]. Thus, much of the southeastern Cordillera has Basin & Range characteristics.

One exception to the general trend of lower velocities in the upper and middle crust models is in the region of the Nicola Horst, on Line 7, where velocities in a plug-like structure are considerably higher than in the surrounding areas (Figure 2.17 and 2.21, between SP 24 and 25). The velocity trends here match extremely well the reflectivity patterns (Figure 2.20 and 2.21) imaged on seismic reflection profiles [Cook, *et al.*, 1992]. Thus, there is no doubt as to the exceptional nature of this characteristic. This feature with its higher velocity indicates that material was brought up from the lower crust.

An important feature of the upper crust in the Line 8 model is the Monashee Décollement (Figure 2.16). The trajectory of the trace of this fault intercepts the approximate location of the outcrop of the Monashee Décollement. On the iso-velocity display (Figure 2.16), one can see that lower velocity contours also dip into the shear zone, implying that low-velocity trends can be correlated with the structural disturbance caused by shear zones. If this is the case, then the lower velocities on the north end of the profile, between shotpoints 32 and 33, may be an indication of the apparent northward dip of the Monashee Décollement on the north end of the Monashee Complex (Figure 2.1).

Cook *et al.* [1992] have associated further reflectivity patterns with other major faults identified from geologic mapping. Comparison of the Line 7 velocity model with the reflectivity (Figure 2.20 and 2.21) shows that in the upper and mid crust there are spatial correspondences of crustal scale faults and shear zones (as identified from reflectivity) with low velocity trends. For instance, the association of a low velocity trend with the Monashee Décollement noted above is seen here as well - Figure 2.20 and 2.21, just below the position of shotpoint 28. Another correlation is with the Okanagan Valley Fault, just to the west of shotpoint 27.

The position of the Monashee Décollement reflector also seems to divide the north-south profile into two velocity regimes. On the Line 8 strike line (Figure 2.16), the velocities in the footwall of the Monashee fault zone tend to be lower than those of the hanging wall by 0.1 to 0.2 km s⁻¹. The trends of lower velocities in the footwall may be an indication of different rock properties juxtaposed on either side of the shear zone. *Cook et al.* [1992], with geologic constraints, interpret the foot wall of the Monashee Décollement to be North American cratonic rocks. However, there seems to be no such contrast evident across the Monashee Décollement on the cross-strike profile (Figure 2.17). Since the velocity differences are on the edge of the resolving power of the velocity measurements, one must be careful not to read too much into this characteristic. But the velocity differences along strike indicate that there may be different rock types on either side of the Monashee Décollement and that its footwall can be correlated with cratonic North America.

On Line 7, within the lower crust, there are higher velocity trends which thin out from east to west. *Cook et al.* [1992] suggest that a thin wedge of cratonic North America lies at the bottom of the crust and extends as far as the Fraser Fault (SP 23 on Figures 2.12b and 2.14). If one conjectures a correspondence between the higher seismic velocities in the lower crust with cratonic rocks, it is difficult to interpret the craton as lying much further west than the Okanagan Valley (just west of SP 27).

Zelt et al. [1993] and *O'Leary et al.* [1993] present seismic velocity models from SCoRE '89 (Line 3) and SCoRE '90 (Line 10) profiles west of our study area in the Coast Plutonic Complex. Their results are used to extend the western margins of our Line 7 model in Figures 2.12b and 2.14. On this basis, it is clear that the velocity characteristics of the crust in the Intermontane/Omineca region are different from those of the Coast Belt. In the Coast belt, velocities, especially in the upper and mid crust are much higher. The crust in the Coast Belt is also thicker by 2 to 3 km on average.

In contrast, there seems to be a lack of any seismic boundary between the Omineca and Intermontane Belts. This boundary should be seen at about the position of shotpoint 27 (Figures 2.12b and 2.14), but the velocity features are not significantly different on either side. The Intermontane and Omineca Belts are seismically quite similar to one another.

An important aspect of our work is the recognition of discrepancies between our Line 8 model and the vertical incidence interpretation, as discussed earlier. The reflection data of *Cook et al.* [1992] have considerable energy in the 10-56 Hz bandpass and has common reflecting point intervals of 25 m. In contrast, the SCoRE data has a peak frequency of approximately 5 Hz and receiver intervals no less than 1 km. Consequently, the reflection data have almost an order of magnitude better resolution temporally and 2 orders of magnitude spatially. The superior lateral and vertical resolution of the near vertical incidence reflection method allows it to image the short wavelength fabric of the crustal rocks that would be transparent to the refraction method [*Klemperer and Luetgert*, 1987]. Despite its low resolution the wide-angle refraction method is superior for measurement of velocities that the reflection method is insensitive to. It is probable that, in the middle and lower crust, the refraction data are sensing profound crustal velocity variations that have overprinted the structural fabric imaged by the reflection data.

There is also a possibility that discrepancies between the refraction/wide-angle reflection and vertical reflection interpretations may be due to anisotropy. For instance, much of the mis-position of the Monashee Décollement could be accounted for by 10% difference between vertical direction seismic velocities measured in the vertical incidence data and horizontal velocities sampled by the refraction experiment.

Holbrook [1990] also compares near-vertical and refraction/wide-angle interpretations within the Basin and Range Province. While finding a very good fit between reflection and refraction Moho, *Holbrook* [1990] notes that there are profound

differences shallower in the crust. There the pervasive deep crustal reflectivity does not correspond to any major boundary of the crustal velocity model. On the other hand, *Catchings and Mooney* [1991], interpreting the same Basin and Range data, show a refraction/wide-angle model that compares well with the near-vertical reflectivity.

The excellent comparison between Line 7 and the reflection interpretation (Figure 2.21), however, indicates that the situation is very complex. Perhaps there may be differences in the along-strike and cross-strike directions, that is lateral anisotropy. Or perhaps it may be only that the short (<75 km) overlap on Line 8 is not long enough to show the general correspondence of seismic reflection and refraction results. Whatever the reason, the question of the fit between the reflection and refraction data is an important one and will be the focus of future work which will require systematic re-processing and analysis of the reflection data.

Other recent geophysical work done in the Cordillera under the auspices of Lithoprobe is of considerable interest for the interpretation of our velocity model. *Jones et al.* [1992] have presented a qualitative interpretation of profiles of east-west magnetotelluric soundings across most of the southern Canadian Cordillera. In the Omineca Belt, resistive upper crust (>1000 Ω m) gives way to a shallow mid crust at 10 km depth with low resistivity (~150 Ω m) and then to a highly conductive lower crust (<10 Ω m). This low-resistivity lower crust is at variance with the lower crust of Intermontane Belt to the west, and the Foreland Belt to the east. This variation is interpreted to be due to varying porosity and/or salinity of fluids with additional conductivity enhancements due to partial melt in the crust beneath the eastern Omineca Belt correlated to a mantle upwelling. From their own magnetotelluric studies, *Gough and Majorowicz* [1992] attribute the relatively high conductivities of Cordilleran crustal rocks to water circulating within zones of differing fracture densities ultimately caused by an upwelling from the mantle.

Lewis et al. [1992] conclude that the central and eastern interior of southern

British Columbia (Intermontane and Omineca Belts) is a single heat flow province with a high reduced heat flow of 63 mW m^{-2} flowing into the upper crust from beneath, indicating a warm, thin lithosphere similar to that of the Basin and Range. Their calculations show that within the southern British Columbia interior, the 450°C isotherm lies between 10 and 15 km depth. They propose that seismically reflective zones seen in the LITHOPROBE reflection data are due to a thermally controlled layer of interconnected fluids in the middle crust. This reflectivity has also been suggested to correlate with the low crustal resistivities and a crustal porous layer. Deep crustal fluids would also have the effect of lowering the velocities that would be measured by seismic refraction experiments [Hyndman and Shearer, 1989; Hyndman and Klemperer, 1989].

Certainly, the low resistivities in the Omineca Belt [Jones *et al.*, 1992] do correlate in depth to the mid crustal LVZ. In general, the presence of water in the deep crust [Lewis *et al.*, 1992; Gough and Majorowicz, 1992] could be related to the velocity structure. However, the low crustal velocities could just as well be simply related to high crustal temperatures. Christensen [1979] and Christensen and Wepfer [1989] document the drop in compressional velocities of crustal type rocks at depth in temperature regimes similar to that of the southeastern Canadian Cordillera [Lewis *et al.*, 1992]. Christensen and Wepfer [1989] do expect velocity reversals in high heat flow regions like the southeastern Canadian Cordillera [Lewis *et al.*, 1992] and isotherms of 400°C and higher are where rock velocities at depth tend to drop dramatically [Christensen, 1979]. The hypothesis of deep crustal fluids, as well, contrasts with that of crustal graphite films giving rise to high conductivities in the lower crust [Frost *et al.*, 1989]. The correlation between a low resistive layer with our mid crustal LVZ does not necessarily imply the layer is fluid saturated, the correlation could simply be a coincidence of unrelated phenomena of graphite films and elevated temperatures at depth. Seismic velocity measurements cannot resolve the alternate interpretations of deep crustal fluids versus

graphite. Other explanations for low crustal velocities, high degrees of anisotropy due to the laminated nature of the Cordilleran crust for example, could be hypothesized as well.

Indeed, there is a high degree of correlation between the Line 7 seismic velocity model (Figure 2.16) and regional isotherms. Figure 2.23 shows a schematic of our final Line 7 model with selected crustal isotherms superimposed [Lewis *et al.*, 1992; T. J. Lewis, personal communication]. There is an apparent correspondence between the interpreted top of the middle crust (or top of the LVZ) with the 450°C isotherm. The shallowing of this seismic boundary is mirrored closely by the rise of that isotherm.

The lack of a seismically visible boundary between the Intermontane and Omineca superterrane and the correlation of velocities with heat may also be linked. Christensen and Wepfer [1989] expect velocity reversals in high heat flow regions like the southeastern Canadian Cordillera [Lewis *et al.*, 1992] and isotherms of 400°C and higher are where rock velocities at depth tend to drop dramatically [Christensen, 1979]. In other words, the heat flow in our region of study is expected to change the physical properties of the crustal rocks. Even the case of temperature controlled crustal fluids [Lewis *et al.*, 1992] simply means another type of temperature controlled change of physical properties. All of this implies overprinting of rock properties by heat, resulting in, first a decrease with depth of the velocity gradient and modification of upper crustal velocities to obliterate the velocity signature of a major crustal boundary, then a velocity inversion in the mid crust. This leads also to the implication that the physical properties of the crust are not immutable but can be and are altered.

Turning back to the Nicola Horst, it is noted that there seems to be little indication of crustal movements at the depth of the Moho. This is perhaps another expression of the mutability of the earth, where the almost certain deformations at the bottom of the crust have been smoothed out by the prevailing heat and pressure fields at depth.

Generally, the entire Line 8 and most of the Line 7 profiles consist of low

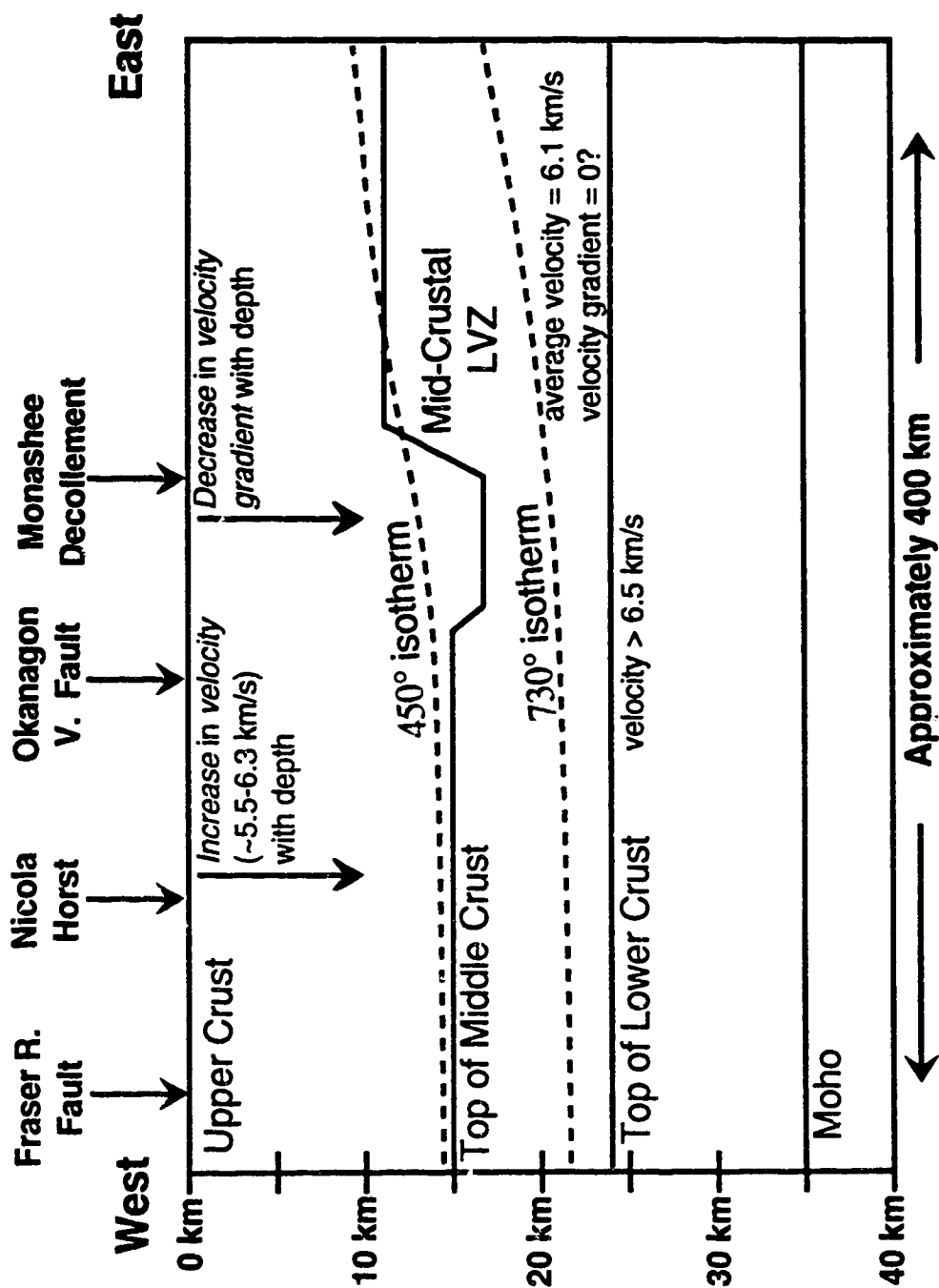


Figure 2.23 Schematic of Line 7 final velocity model compared with selected crustal isotherms (Lewis et al., 1992). Note the correspondence of the top of the LVZ with the 450° isotherm implying some temperature control to the crustal velocity field.

velocity rock, indicating that all of the southern Omineca and much of the Intermontane belt is made up of lower velocity crustal material. Velocities in the mantle underlying this same region are also lower than the average of northwest North America. If we can consider that the velocity field of the southeastern Cordillera is, in simple terms, a reflection of the temperature field, then one can conclude that a crust and upper mantle uniformly heated must be so heated from below. Coupled with the thin lithosphere in this region [Wickens, 1971; Wickens, 1977], this implies that the southeastern Cordillera is being heated by a source at depth. This can be related to the hypothesis by *Kanasewich* [1966] that the East Pacific Rise extends into the continent beneath the Basin and Range and beyond and the reiteration of the concept of mantle upwelling in the Cordillera by *Gough* [1986]. The nature of this heat source is beyond the resolution of our data and awaits more detailed and deeper geophysical experimentation.

2.7 Summary

An interpretation of the SCoRE '90 line 8 and line 7 seismic wide-angle reflection/refraction profiles across the Omineca and Intermontane belts of the southeastern Canadian Cordillera has established that the crust is relatively thin and has relatively low velocities. On line 8 the depth to Moho is 36 km on average while it is 35 km on line 7. The average crustal velocity is 6.2 km/s.

Along strike in the Omineca Belt the upper crust has average velocities from 5.6 km s⁻¹ near the surface to 6.2 km s⁻¹ to the top of the middle crust. Velocity gradients decrease with depth. There is a well-defined midcrustal low velocity layer, with an average velocity less than 6.1 km s⁻¹. Velocities in the lower crust, starting at about 24 km depth, range from 6.4 at the top to 6.8 km s⁻¹ at the base of the crust. A crust/mantle transition zone of 7.6-7.7 km s⁻¹ and thickness of 1 to 2 km can be interpreted. There is

an upper mantle zone bounded by an intramantle reflector at about 46-49 km depth, with velocities from 7.9 to 8.1 km s⁻¹. Higher-quality data or more sophisticated analysis of the current data would be required to show that this intramantle boundary is the base of the lithosphere.

Across strike through the Intermontane and Omineca belts velocities range up to a maximum of 6.4 km s⁻¹ in the upper crust, average less than 6.1 km s⁻¹ in the mid-crust and are between 6.5-6.9 km s⁻¹ in the lower crust. The Moho dips from 32 km depth in the west, to 40 km depth in the east of the profile. The upper mantle layer has velocities starting at 7.9 km s⁻¹ and averaging 8.0 km s⁻¹.

The models show the crust to be characterized by significant lateral changes in velocity which in the upper crust can be associated with large scale shear zones. Wide-angle reflections and velocity changes are associated with the Monashee Décollement, the Gwiilim Creek Shear Zone, the Okanagan Valley Fault and other crustal scale faults. Minor velocity differences between the footwall and hanging wall of the Monashee Décollement may be a reflection of the different origins of the rocks, but this is something resolved in one model, but not the other. Also, a high velocity plug in the upper and mid crust is identified with the Nicola Horst and the westernmost extent of the North American craton to just west of the Okanagan Valley may have been imaged by higher velocities in the lower crust.

There is a high degree of agreement between the velocity trends of the models with the reflectivity of coincident seismic reflection profiles suggesting the capability of high resolution refraction experiments to delineate local crustal anomalies. Where there are few similarities, mainly in a short section in the middle to lower crust, it is thought to be due to the different properties (broad-scale velocities versus short-wavelength reflectivity) sampled by the refraction and reflection seismic methods.

A correspondence is also noted between the velocity and thermal structures. Considering this correlation along with the seismically reflective nature of the crust and

the low electrical resistivities, we consider this to be not inconsistent with the hypothesis of porous crustal layers [Klemperer, 1987], as applied to the Cordillera by Lewis *et al.* [1992], although other hypotheses for high conductivities and low velocities cannot be ruled out. On the other hand, it may be that the region's high heat flow has simply altered the seismic velocity structure of the crust. In fact, the velocity profile may be a partial reflection of the regional temperature function which has overprinted the geological features of the crust.

The features of a relatively shallow Moho, low P_n velocity, and an intermediate crustal zone with low velocities, along with other geophysical interpretations shows the similarity of seismic characteristics of the Basin and Range. Also, the uniformly low velocities from surface to mantle suggests that the southeast Canadian Cordillera is currently undergoing heating from a source deeper within the mantle.

Chapter 3 Three-dimensional Cordilleran Refraction/Wide-Angle Reflection Analysis

3.1 Background and Data Acquisition

During the recording of the north-south refraction/wide-angle reflection profile through the Omineca Belt, 79 seismographs were deployed along an east-west line (labelled 'Line 6') just north of the U.S. border, and centered on Castlegar (Figure 3.1). The seismographs, all U.S. Geological Survey SCRs, recorded the shots of Line 8 in a broadside, or fan, geometry, giving a certain amount of three-dimensional coverage. The one exception to this is SP 37. The record of this shotpoint, the southernmost of line 8, is almost at the same longitude as the line of receivers, and as such is in effect an in-line, split-spread profile.

Besides the fan records, the in-line profiles of both SCoRE '89 (*Zelt et al.*, 1990) and SCoRE '90, provide a large degree of three-dimensional control over the southeastern Canadian Cordillera when looked at as a whole.

This chapter can be divided into three distinct parts. After a discussion of the data as a whole, SP 37 will be analysed independently, two records will be investigated to increase the resolution of three-dimensional Moho structure, and finally an anomalous arrival will be examined with respect to the possible structure of the upper mantle.

3.2 Data Characteristics

Of the eight shot records from Line 8, only four, SP 32 (Figure 3.2), SP 35 (Figure 3.3), SP 61 (Figure 3.4) and SP 37 (Figure 3.5) give any useful information. Figures 3.2 to 3.5 are plotted with color coded, true amplitudes (red for highest

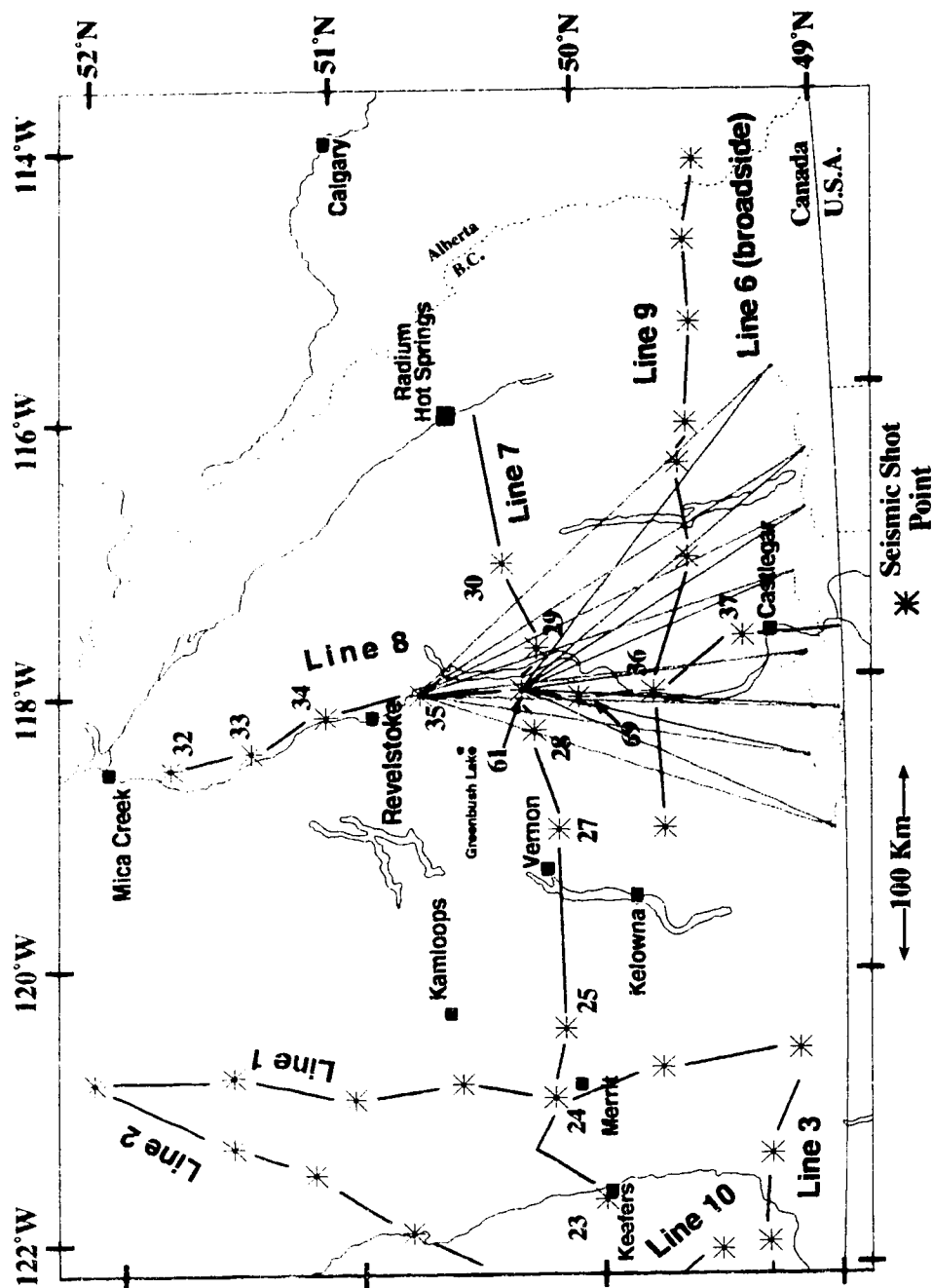


Figure 3.1 Lithoprobe's SCoRE '89 (lines 1, 2 and 3) and '90 (lines 6, 7, 8, 9 and 10) experiments give extensive three-dimensional coverage of the southeastern Canadian Cordillera. For the broadside records (line 6), SP 37 can be considered an in-line, split-spread profile. The other broadside records can be broken into smaller segments, each corresponding to an almost in-line path (as shown for SP 35 and 61) whose PmP arrivals can give point measurements of Moho depth away from the in-line models.

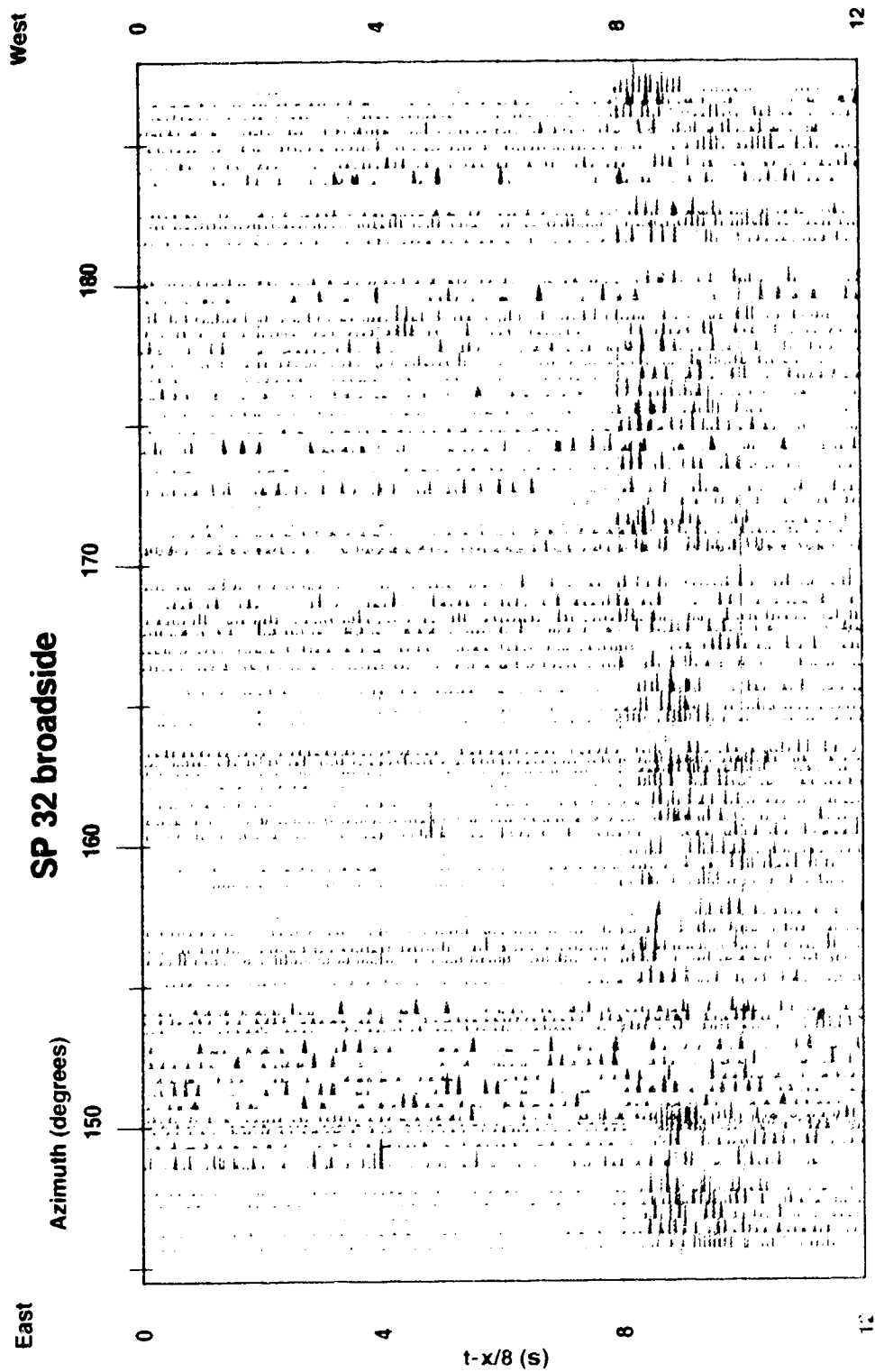


Figure 3.2 SP 32 broadside record. Data are plotted with color coded amplitudes and traces are plotted with respect to azimuth (direction) from shot to receiver. Note that there is only one, very strong, event at about 8.0 s reduced travel time.

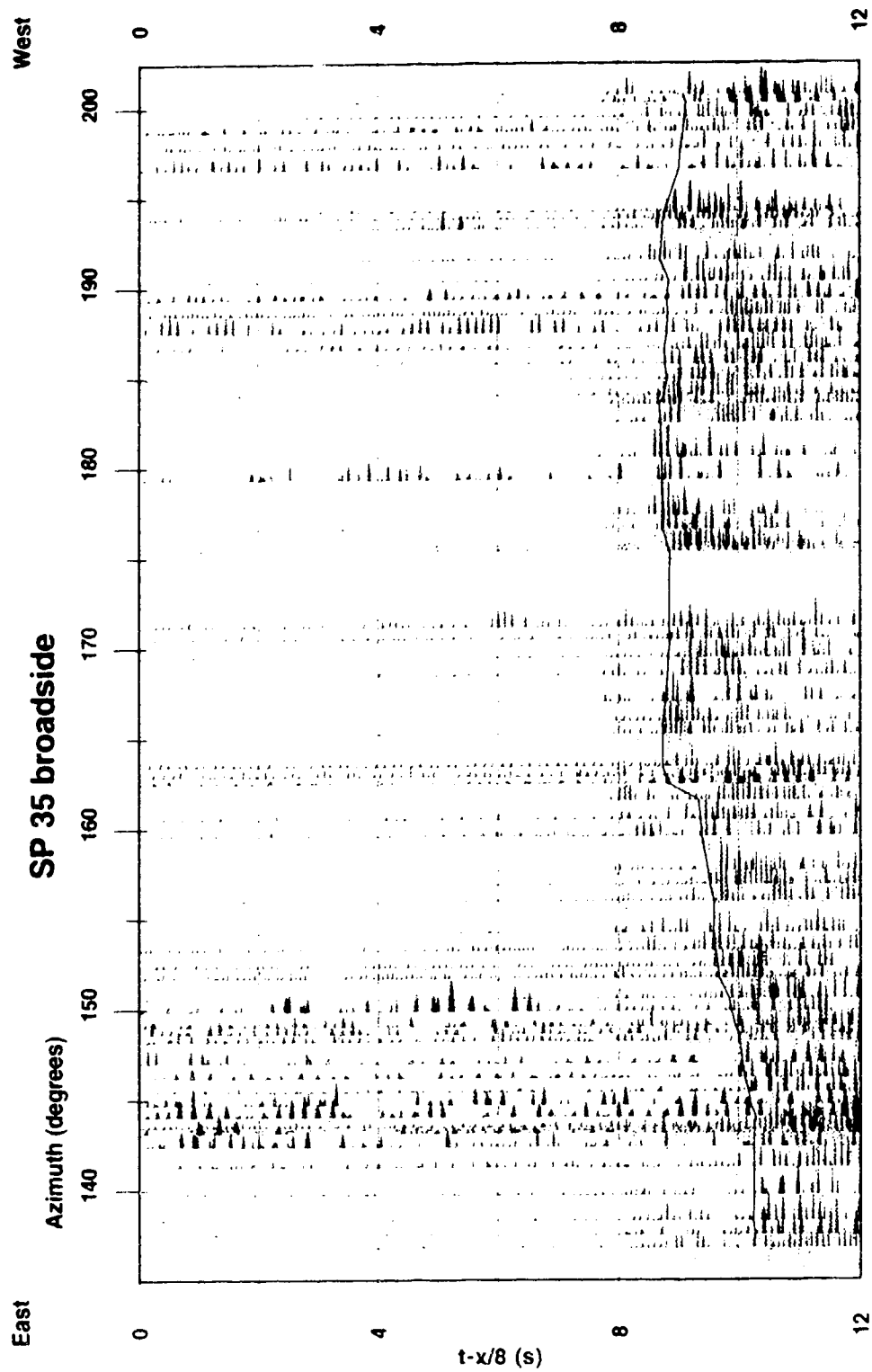


Figure 3.3 SP 35 broadside record. Data are plotted with color coded amplitudes and traces are plotted with respect to azimuth (direction) from shot to receiver. The line marks the interpreted time picks of the main event on this record.

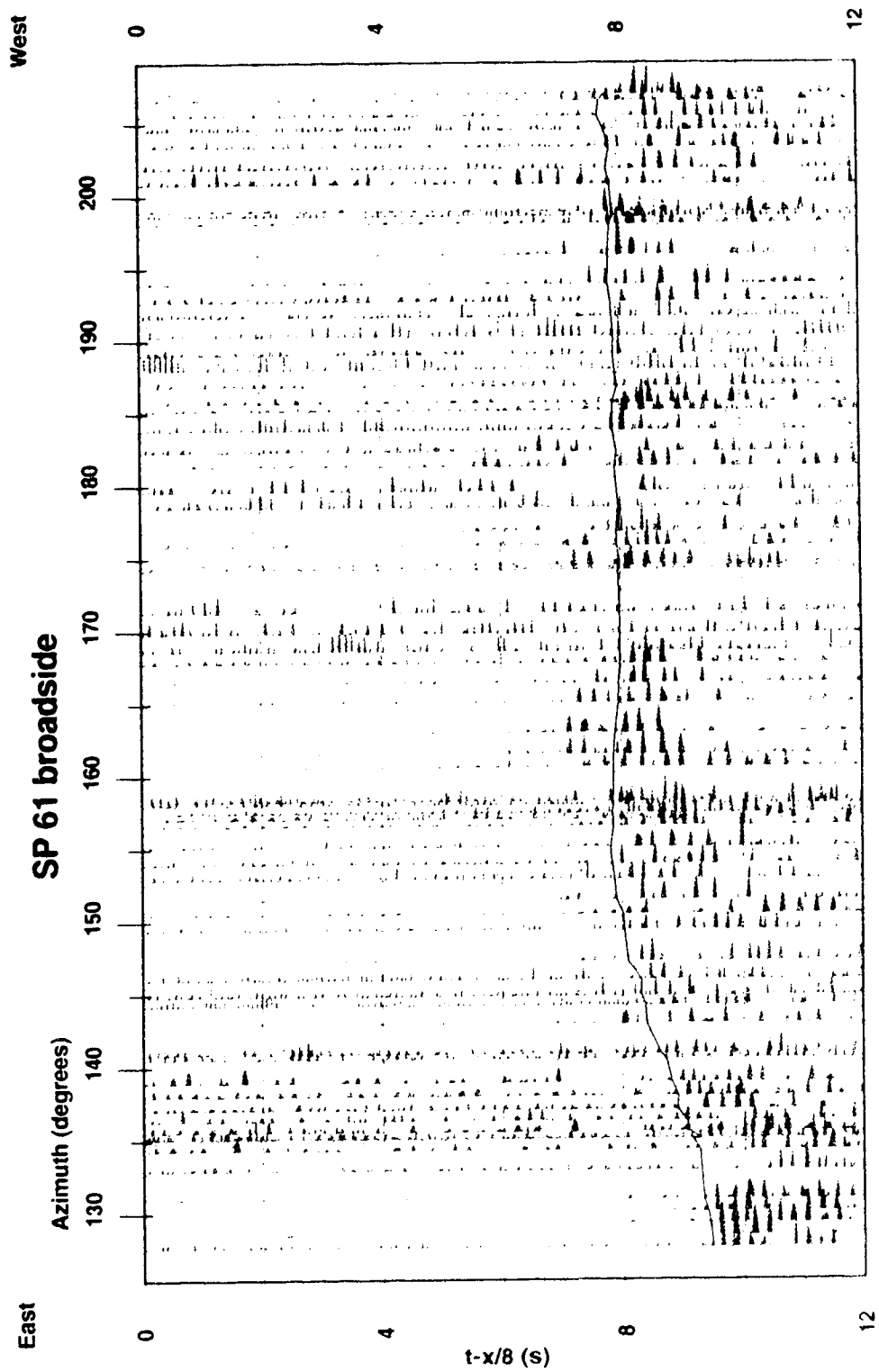


Figure 3.4 SP 61 broadside record. Data are plotted with color coded amplitudes and traces are plotted with respect to azimuth (direction) from shot to receiver. The line marks the interpreted time picks of the main event on this record.

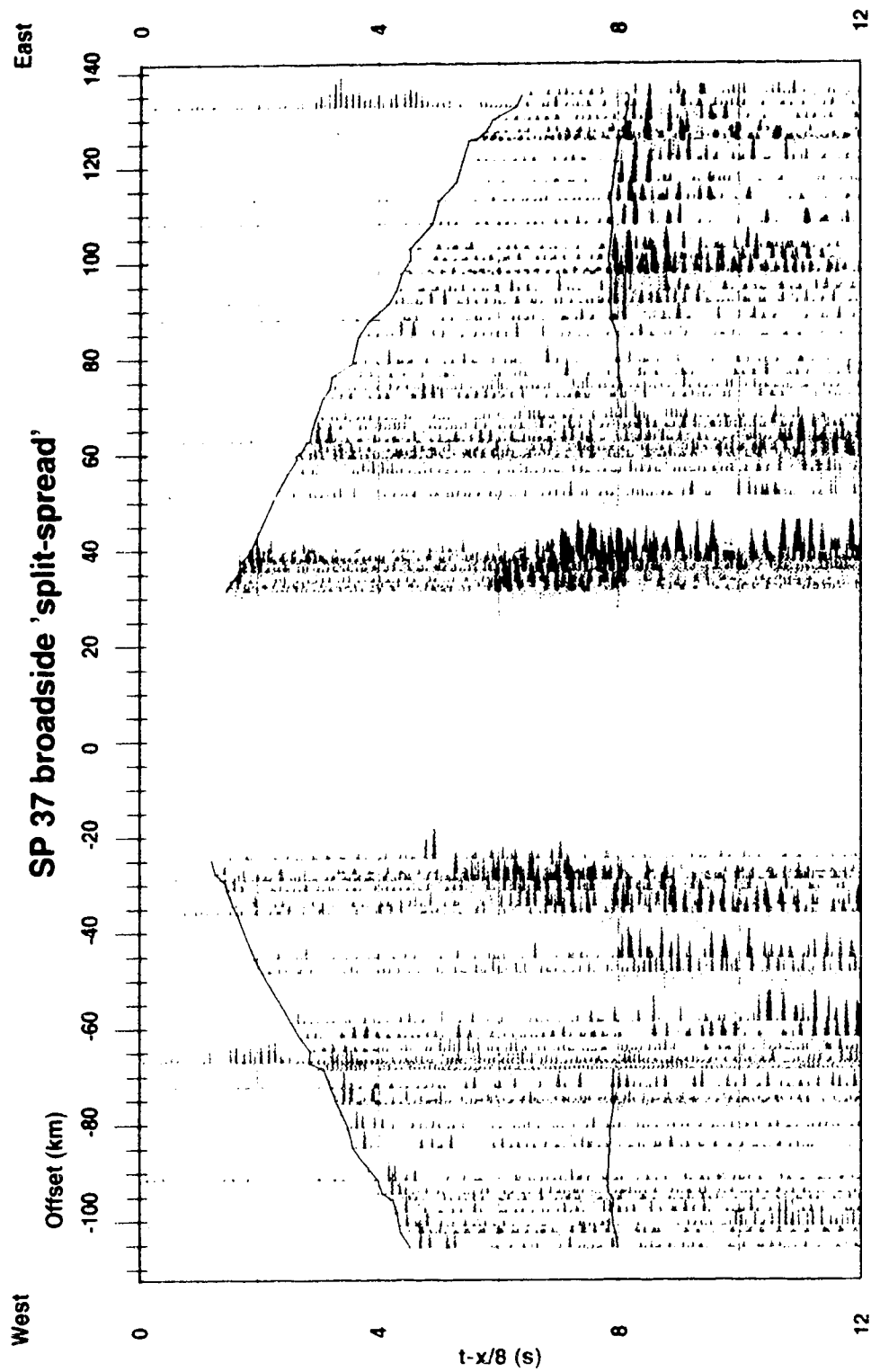


Figure 3.5 SP 37 broadside record. Data are plotted with color coded amplitudes and traces are plotted with respect to azimuth (direction) from shot to receiver. This record is close to being in an in-line, split-spread configuration. The lines mark the interpreted time picks of the main event on this record which are Pg and PmP.

amplitude, through yellow, green and finally blue for lowest amplitudes - all for the same polarity). The data are shown in the same way as are the in-line data of the previous chapter, with a reducing velocity of 8 km s^{-1} , but are here (Figures 3.2 to 3.4) instead plotted with respect to azimuth (direction from the shot to the receiver). Only SP 37 (Figure 3.5), due to its near to in-line, split-spread geometry, is shown plotted with respect to shot/receiver offset. Interpreted and picked arrival times for phases on SP 35, 61 and 37 are shown.

The other broadside shots can be seen in appendix 9, plotted in black and white.

The SP 32 record has one, relatively deep, continuous and strong arrival. It is seen at just below 8 s, reduced travel time (Figure 3.2) as a conspicuous increase in amplitude. It is the only recognized seismic phase in the record. A detailed discussion of the identification of this arrival is below, but it is interpreted to be a sub-moho reflection.

Both SP 35 and 61 (Figures 3.3 and 3.4) are similar. SP 35 has a deep, continuous, strong arrival - again recognized by an increase in amplitude - at 8.5 s, reduced time, and deeper. There is also a much weaker, less continuous phase at about 8 s. The SP 61 record has the strong phase at 8 s, reduced time, with the weaker, discontinuous arrival at 7 s. Again, a detailed discussion of phase identification is below, but the stronger arrival is most definitely P_mP (wide-angle reflection -WAR- from the Moho) while the weaker one is P_cP_2 (reflection from the mid crust/lower crust boundary).

The in-line SP 37 record (Figure 3.5) has two arrivals. There is no further discussion given to phase identification here since from experience with other SCoRE '90 records, one phase, on either side of the shot, is obviously P_g . The other arrival is an obvious P_mP phase on the east side of the shot. P_mP is also picked west of the shot, but this is a much more difficult pick.

3.3 Interpretation of split-spread record

The SP 37 split-spread record was analysed in the same manner as the previous in-lines (Chapter 2). First, a starting model was defined by extrapolating the extreme southern end of the Line 8 results to east and west.

Next, the data were examined for amplitude characteristics to constrain upper crustal layers and velocity gradients. Figure 3.6 shows the blocked off P_g amplitude curves for either side of the shot. Note that the inverse distance amplitude decrease has been corrected here. East of the shot, the amplitudes show a relatively large value, decreasing with offset, or in other words, with the depth penetration of the rays, signifying a decrease in the velocity gradient. West of the shot, there is very little amplitude change, inferring little change in velocity gradient with depth.

The initial model was modified with the aid of forward ray modelling [Zelt and Ellis, 1988]. Using the Line 8 for calibration, relative changes in linear velocity gradients were made to match the relative change in amplitudes. Then, layers were adjusted for depth till ray tracing matched the approximate offsets for amplitude changes.

At that point, traveltimes modelling and inversion [Zelt and Smith, 1992] was used to obtain the final velocity model. With only two phases identified, assumptions were very important. First, it was assumed that the upper crust velocity gradient below that region sampled by the P_g rays would be zero (similarly to Line 8). Further, it is postulated that a mid-crustal layer existed, whose velocity was the same or lower than the upper crust (again extrapolating from line 8). The inversion of P_g was relatively straight forward. But for P_mP , a further assumption on the actual mid-crustal velocity had to be made. Analysis of P_mP showed it likely that the Moho would be considerably deeper than in the north (in fact following the trend of a gentle dip from north to south revealed in the Line 8 analysis). So, there was a trade-off between low mid-crustal velocities and a deep Moho. It was finally decided that a mid-crustal velocity of 5.9 km/s was the lowest

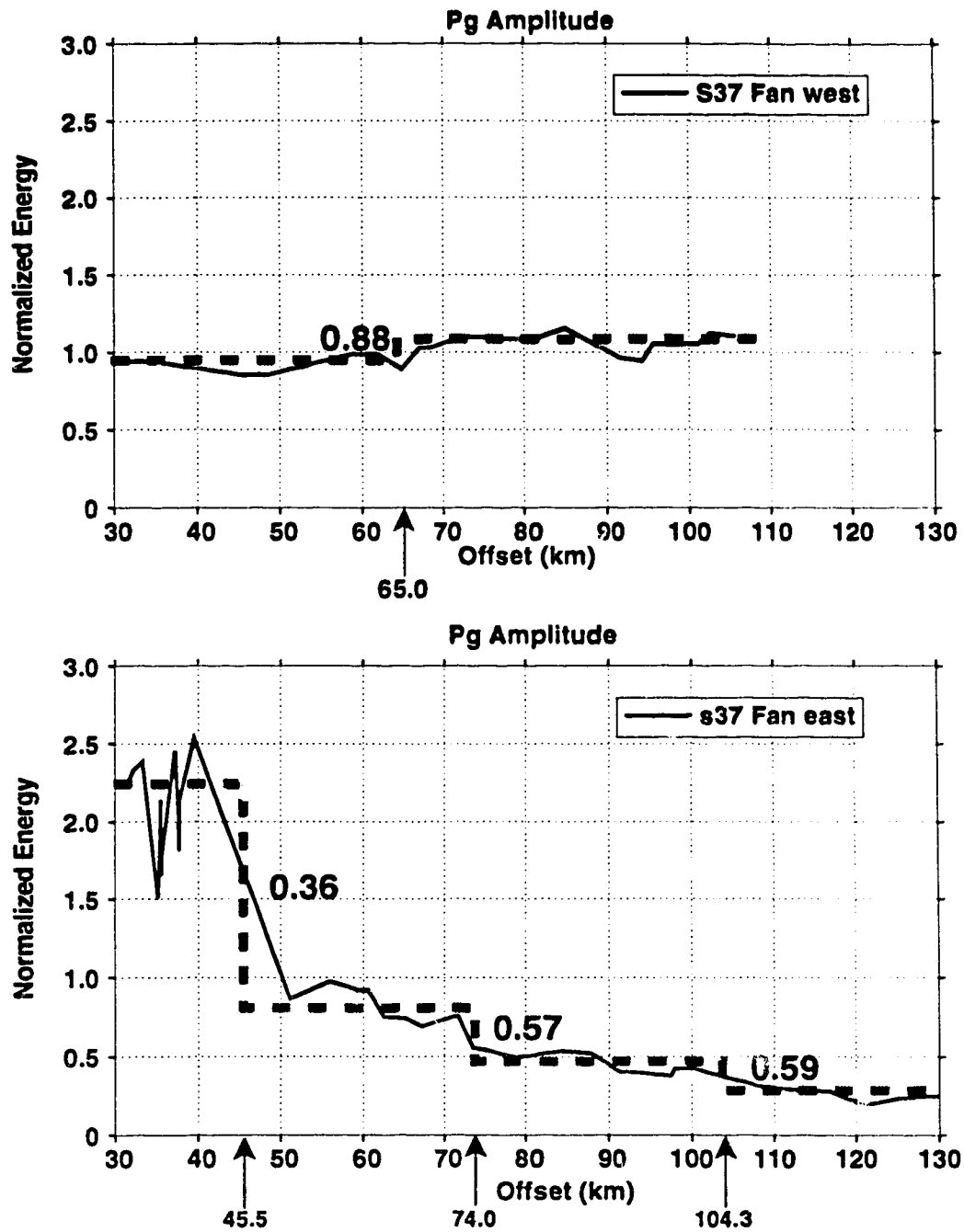


Figure 3.6 Amplitude vs. offset curves for Pg arrivals on SP 37 'split-spread' record. The amplitude curves are used to constrain the velocity gradients on either side of the shotpoint by equating relative changes in amplitude with corresponding relative changes in velocity gradients.

possible value giving the shallowest possible Moho at about 38 km. Higher velocities would result in a deeper Moho, but no more than 39-40 km with any reasonable mid-crustal value (less than 6.2 km/s).

With the above assumptions made, the inversion was carried out. For 109 total observations of P_g and P_mP , the final model gave a 0.1 s traveltime residual, comparable to the traveltime uncertainty of 0.1s, and a normalized χ^2 fit of 1.0 (Figure 3.7).

The velocity model, including values extrapolated from earlier results along strike, is shown in Figure 3.8. Upper crustal velocities are higher west of the shotpoint. The low velocity area to the east may be associated with the Kootenay Lake and Purcell Fault which the profile traverses, but with only one shotpoint and a paucity of observations, the model is poorly resolved. Lower crustal velocities are similar to those found on Lines 7 and 8. Perhaps the most important result is the observation that the Moho deepens to about 38 km near the U.S. border.

3.4 Measurement of crustal thickness from broadside records

The arrivals on SP 35 and 61 are identified by comparison with in-line data with similar offsets. Figure 3.9 shows the strong and continuous phase to be consistent with P_mP . That is, the arrival on the broadside records has similar reduced traveltimes as the P_mP arrivals on the in-line records. The shallower, discontinuous arrivals, by analogy with the in-line data, are P_cP_2 , the WAR from the top of the lower crustal layer.

Since the ray coverage of the broadside records is sparse, there is little velocity control. But measurement of Moho depth can be done by assuming a velocity model using the existing velocity structures interpreted earlier from the in-lines (and including the results of *Zelt and White* [in submission] from Line 9.

To make thing simpler, the broadside records were broken into several segments

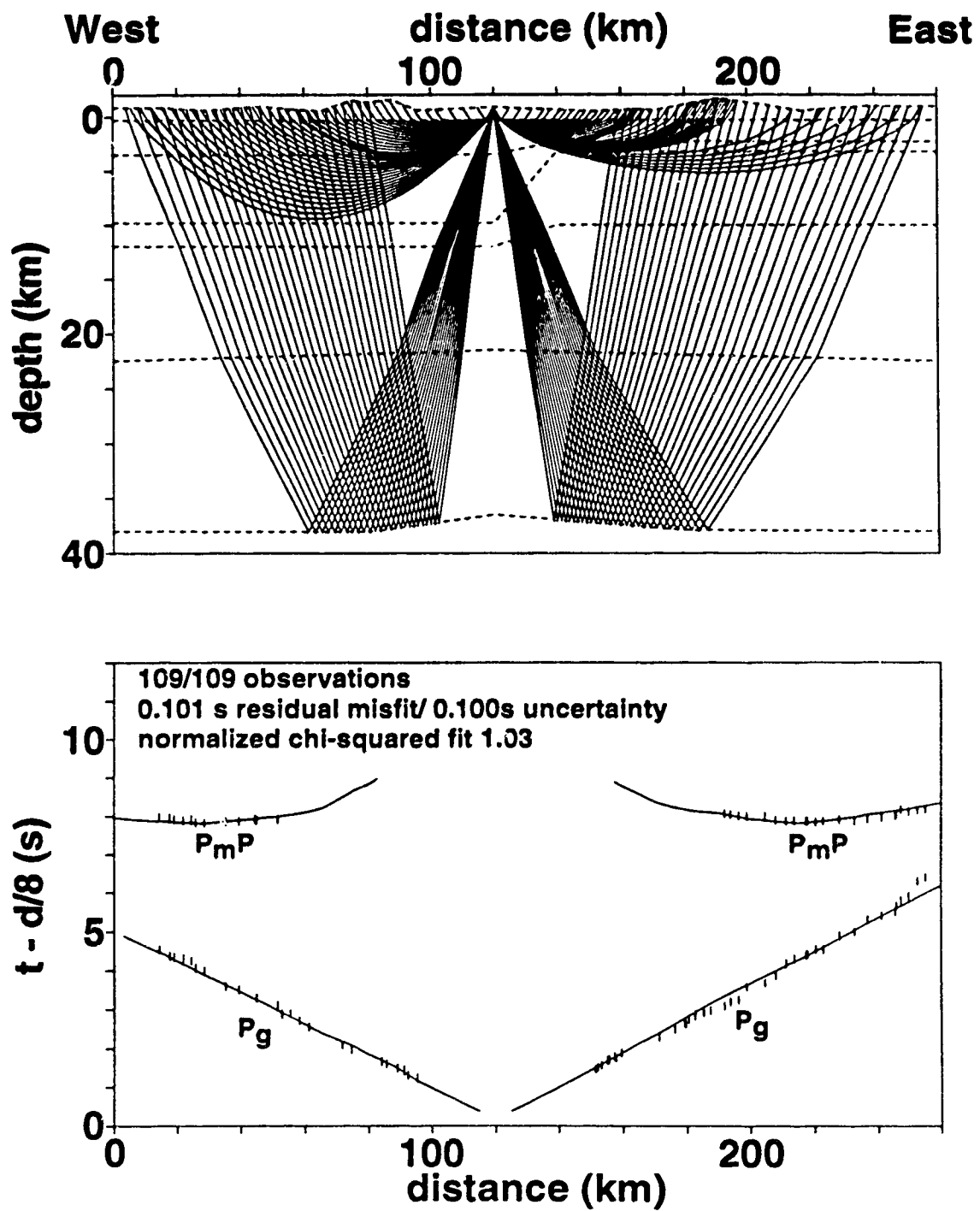


Figure 3.7 Theoretical (curve) and observed (vertical lines) traveltime fit for SP 37 'split-spread' record from final velocity model (see Figure 3.10).

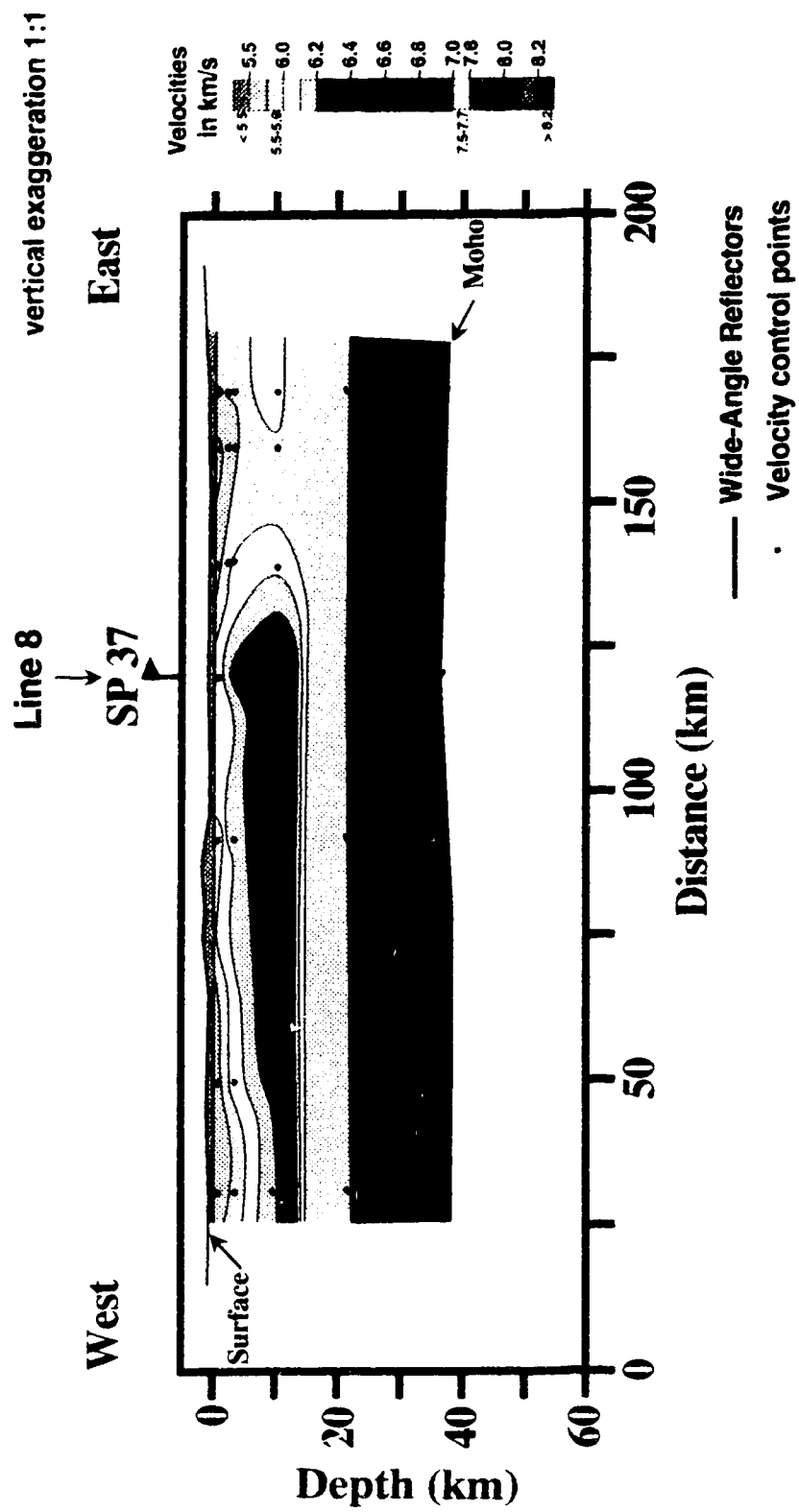


Figure 3.8 Final velocity model for SP37 broadside record. The velocity control points include values extrapolated from earlier SCoRE interpretations. The Moho near the U.S. border is significantly deeper than the area to the north.

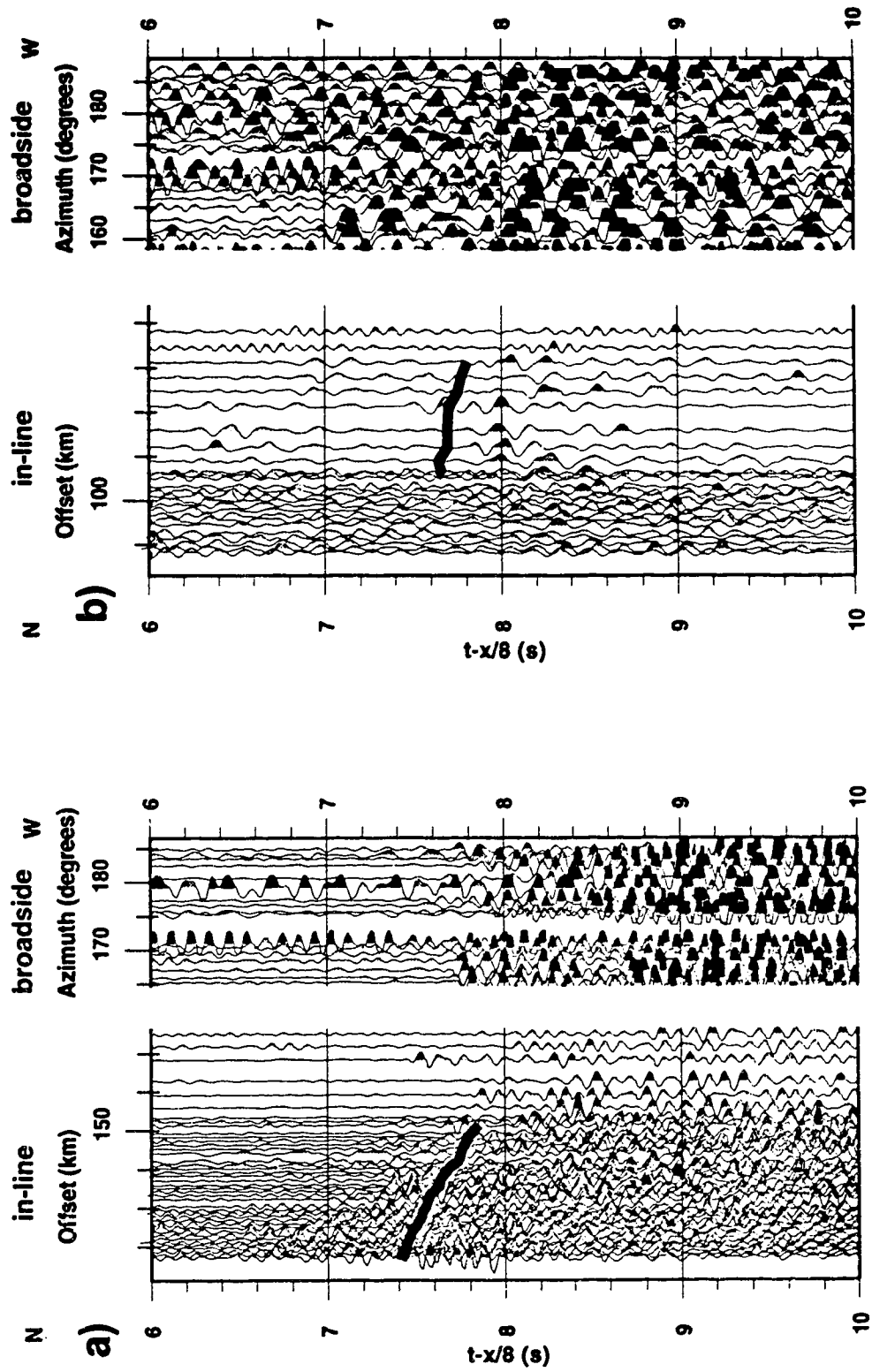


Figure 3.9 In-line and corresponding broadside traces for SP 35 (a) and 61 (b). The marked arrival on the in-lines is PmP. The in-line and broadside are shown juxtaposed near their intersections. Comparison shows the main arrival of both broadside records to be PmP, the WAR from the Moho. Shallower, discontinuous and weak arrivals are probably PcP2.

which were assumed to lie in straight line paths from the shot to the recorders (Figure 3.1). Velocity models for these fan segments were constructed from their geographical intersection with Lines 8, 7, 9 and the SP 37 split-spread. Then, forward ray trace modelling was done to match arrival times of this segmented data (Figure 3.10). This resulted in depth controls for the Moho in areas not covered by the in-line interpretations.

These depths, along with those from the previous chapter, and the results of *Zelt et al.* [1992], *Zelt et al.* [1993], *O'Leary et al.* [1993], *Zelt and White* [in preparation] and G. D. Spence [personal communication] were compiled to produce a depth to Moho map (Figure 3.11). Additional control points were obtained from various interpretations of the Project Edzoe Greenbush Lake shots [*Forsyth et al.*, 1974] and other seismic experiments. These include *Johnson and Couch* [1970], *Chandra and Cumming* [1972], *Hill* [1972], *Hales and Nation* [1973], *Bennet et al.* [1975], *Mereu et al.* [1977], and *Spence et al.* [1977]. Though these values did increase the contoured area, the lower resolution and reliability of these older surveys are indicated by a lack of coloring on the map.

Similarly, a compilation of average crustal velocities was mapped (Figure 3.12). There are fewer points on this map due to the lesser amount of variability of values and the lower reliability of velocity measurements of the older data.

Both these maps (Figure 3.11 and 3.12) can be compared to a map of the Bouguer gravity anomaly for the same area (Figure 3.13). It is assumed that the long wavelength Bouguer anomaly is sensitive to Moho depth. That is, a high gravity value is expected where the relatively high density mantle is closer to the surface while a lower value would be measured where the high density material is deeper.

The depth to Moho map (Figure 3.11) exhibits a general northwest-southeast trend, indeed as do the average crustal velocity and Bouguer gravity maps (Figures 3.12 and 3.13), corresponding the prevalent geologic strike of the region. As expected, the

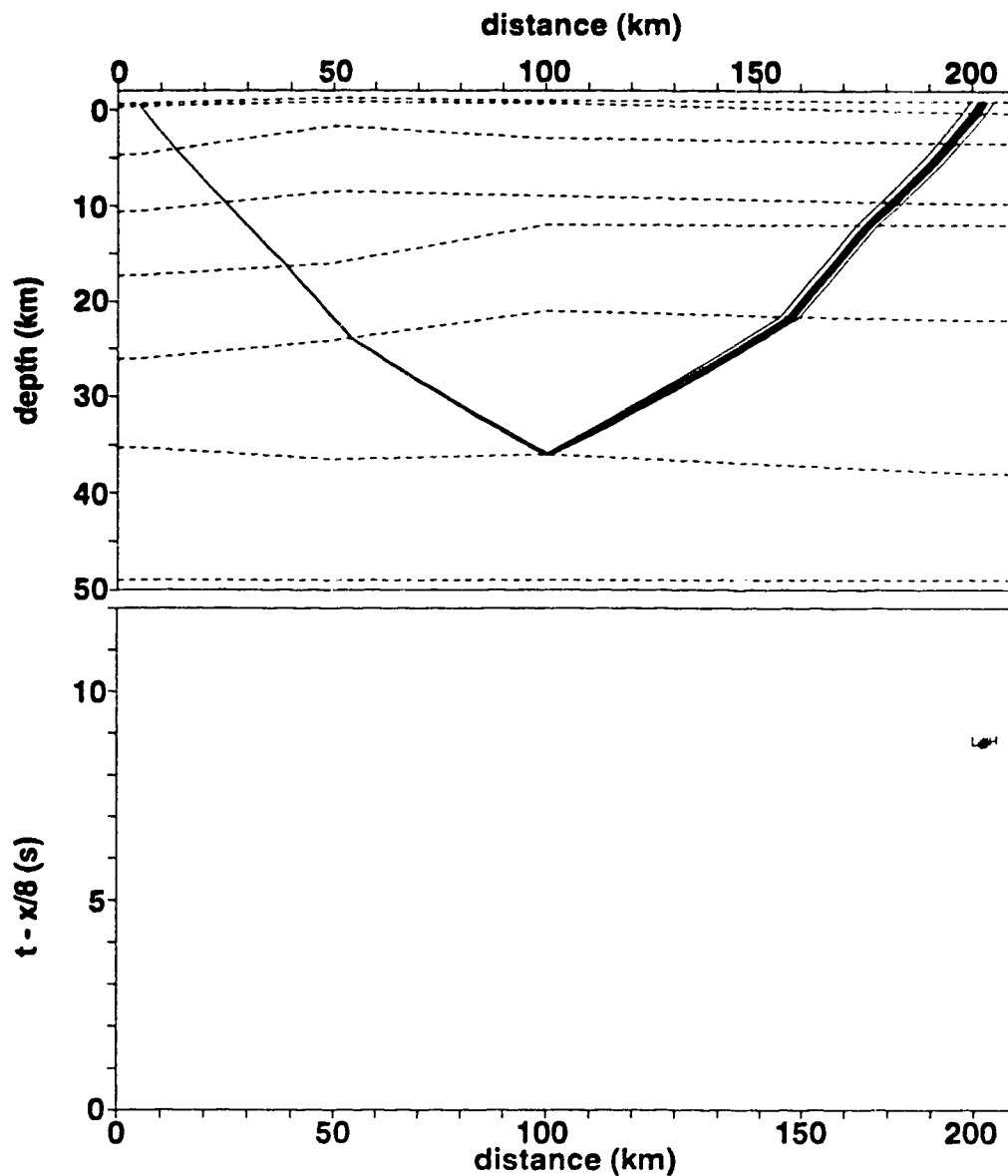


Figure 3.10 Example of interpretation of broadside data for depth to Moho measurement. This is for a segment of data on the east side of the fan profile of SP 35. The velocity model was made up from intersections of the fan profile with lines 7, 8, 9 and the split-spread model. A measurement to Moho was made by adjusting the depth of the reflecting area until a good fit to the observations was achieved.

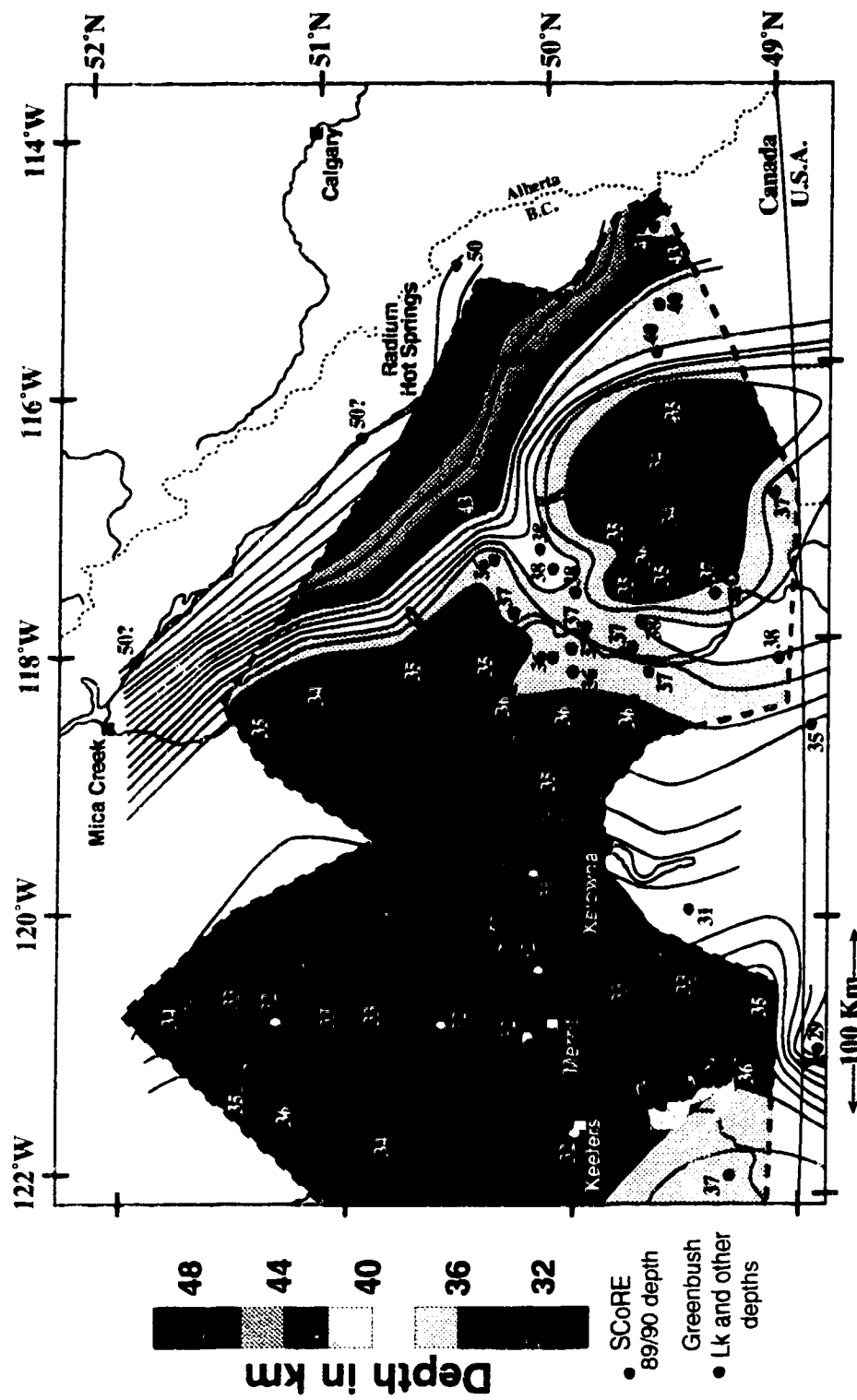


Figure 3.11 Map of depth to Moho in the southeastern Canadian Cordillera. All depths are below sea level. The colors indicate depth measurements from SCoRE 89 and 90 while contours outside are controlled by older estimates from the various Greenbush Lake and other experiments.

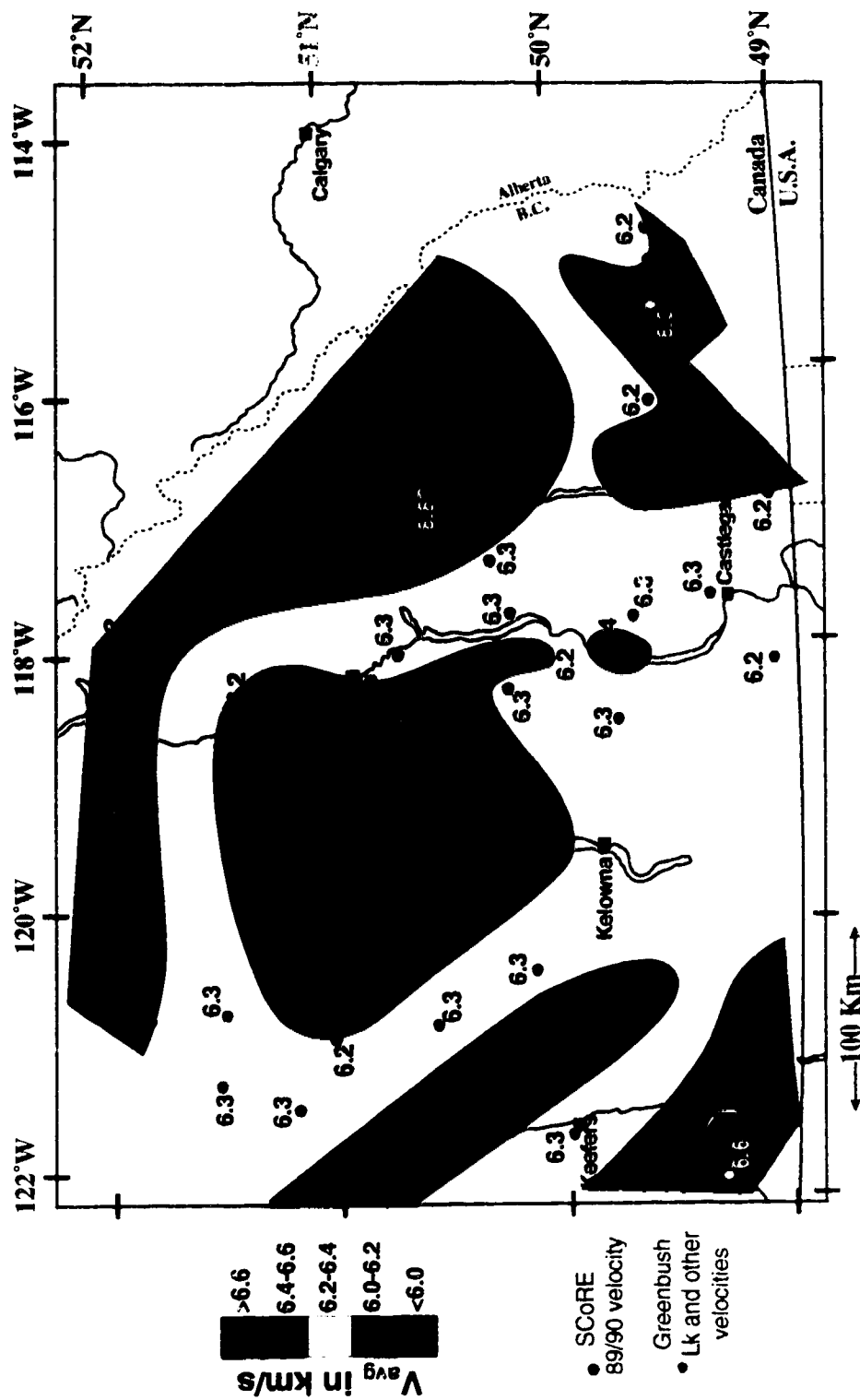


Figure 3.12 Map of average crustal velocity in the southeastern Canadian Cordillera in km/s. Contour interval is 0.2 km/s.

crust beneath the Foreland Belt/Rocky Mountains is quite thick, possibly reaching 50 km and greater (this region is mainly controlled by older measurements). Generally, the Moho depth decreases from 36-37 km on the western edge of the map, up to 30-33 km. in the middle of the Intermontane Belt (Merri/Kamloops region), gradually deepening to 37-38 km in the Southern Omineca Belt (Castlegar region) until a sharp increase in depth gradient entering the Foreland Belt (Radium Hot Springs region and west). There seems to be a slight tendency for an increase in Moho depth from North to South underneath both the Intermontane (south of Merrit) and especially the Omineca Belt (Revelstoke to Castlegar areas). Also, one can see an anomalous thinning of the crust centered on Kootenay Lake (northeast of Castlegar), which also shows up on the SP 37 split-spread as a low velocity region in the upper crust.

There are some general correlations between the Moho depth (Figure 3.11) and average crustal velocity (Figure 3.12) maps. The shallow Moho of the Intermontane and Omineca Belts (30-38 km) is matched by the 6.0 to 6.4 km/s average velocities. The increase in velocities, on the northeast and southwest corners seem to be associated with thickening of the crust in the Foreland and Coast Belts. The low velocity (6.0-6.2 km/s) regions in the middle of the map have a mild correlation with the shallower Moho depths of the Intermontane Belt. There is also a correspondence between the anomalously high Moho northeast of Calstlegar and lower crustal velocities.

Comparison of the Bouguer gravity map and the Moho depth map shows some correlation within the Intermontane Belt and into the Omineca Belt. There, along Line 1 and extending towards Line 8, the gravity tends to high values, suggesting the higher Moho seen on the depth map. The gravity measurements in the extreme southeast of British Columbia suggest a decrease in Moho depth. Though we have no seismic results there, there are indications that the crust may indeed be thinning.

On the other hand, there are negative correspondences between depth and gravity

as well. For instance, south of Castlegar, gravity hints at a thinning crust, whereas the depth map shows definite thickening. Perhaps this is an indication of the complex relationship between crustal thicknesses and density heterogeneities within the crust and mantle.

Another interesting comparison is with heat flow data. *Majorowicz et al.* [1993] show a heat flow contour map, compiled from *Lewis* [1991], and *Lewis et al.* [1985 and 1992], of the southeastern Canadian Cordillera. There is a heat flow high (120 mW m^{-1}) at 117°W and 49.5°N , centered on the depth anomaly over the Kootenay Lake, suggesting a link between a submantle heat source with the anomalously shallow Moho at this point. Other correlations with heat flow are difficult to see, again, perhaps, indicating the involved relationships between physical parameters.

3.5 Sub Moho arrivals and mantle structure

The SP 32 broadside record (Figure 3.2) has only one identifiable phase, a strong increase in amplitude at about 8s reduced time. The record, plotted with respect to shot to receiver azimuth, actually has 60 km of differential moveout between the traces. Over this amount, there is little or no systematic moveout, meaning that the apparent velocity is 8.0 km/s . With this apparent velocity, at this offset range (290 to 350 km), the arrival could possibly be P_n , or it may be an arrival from deeper in the mantle. It cannot be the phase P_m (Chapter 2) since that has an apparent velocity of 8.6 km/s and a reduced arrival time of about 7s at 300 km offset.

Figure 3.14 shows a comparison between the long offset traces of the SP 32 in-line record and the corresponding broadside data. P_n , with a 7.5 s arrival time, matches poorly with the broadside signal, unless one conjectures a change in the arrival trajectory due to, say, a step in the Moho. As it is, there is little comparison between the in-line P_n and the broadside arrival.

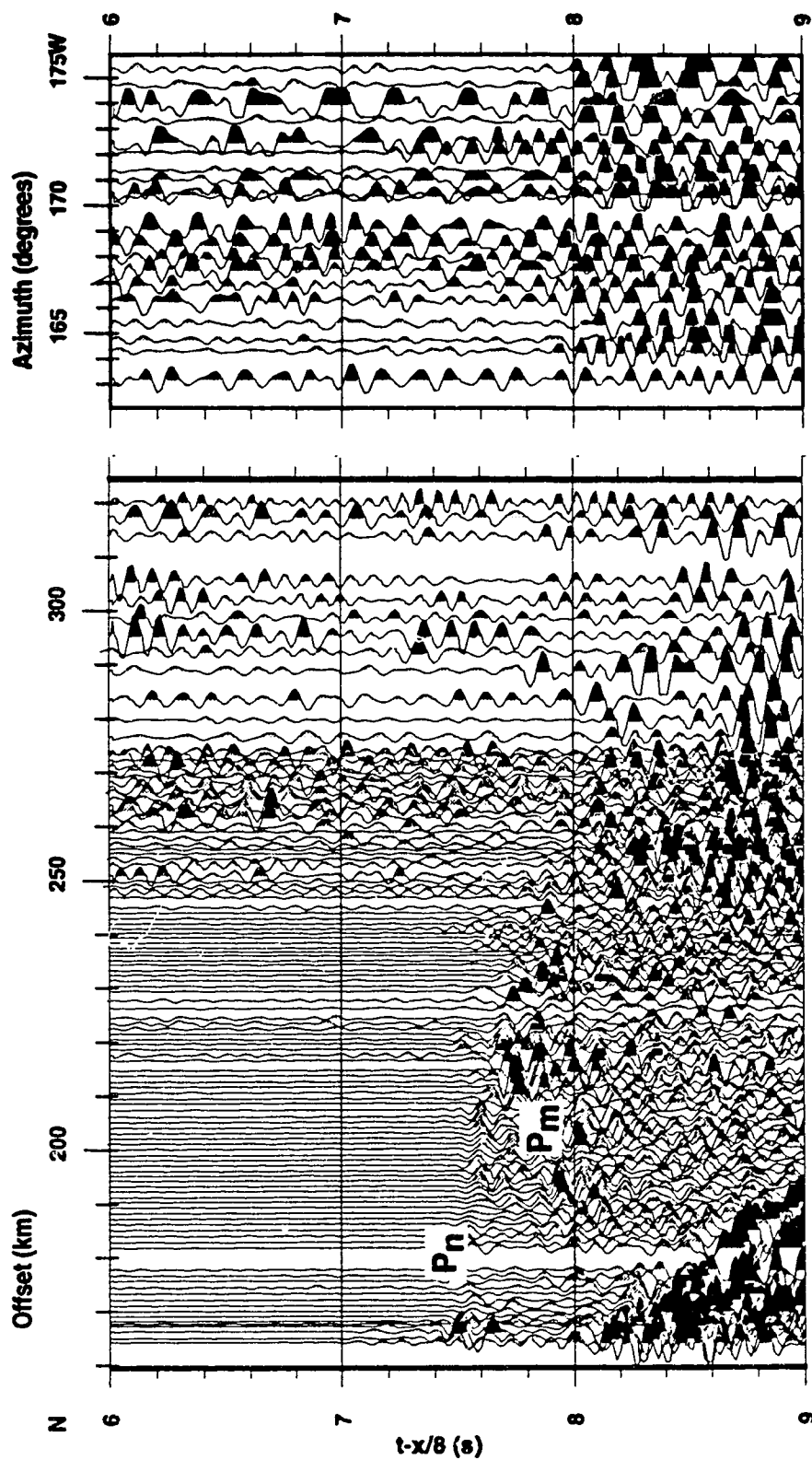


Figure 3.14 Parts of SP 32 in-line (left) and broadside (right) records. The broadside set corresponds to offsets centered about 300 km. There is very little similarity between the Pn arrival at 7.5 s and the 8 s arrival evident on the broadside data. It is interpreted that the broadside arrival is a WAR from deeper in the mantle.

As to the possibility of a step in the Moho changing the P_n trajectory, Figure 3.15a shows this. The Moho deepens from 36 km to 45.5. Broadside arrivals which straddle the intersection with the in-line profile are included with the P_n arrivals. Assuming the same velocities previously interpreted, we could put in a Moho step that would fit the hypothesis of the broadside picks being P_n . But, as in Figure 3.15b, this directly contradicts the evidence of the unambiguous P_mP pick from the SP 37 in-line profile, which clearly puts the Moho no deeper than 37 km. Analysis of the SP 37 split-spread, above, also contradicts this hypothesis. Finally, the gravity measurements (Figure 3.13) would predict, if anything, a shallow Moho on the southern end of Line 8.

Looking more closely at the SP 32 in-line record (Figure 3.16), one can see some shingling of arrivals below the P_m WAR. The apparent base of these signals is delineated in the figure by arrows. The path of a deeper WAR could include that of the horizontal arrivals at 290 km offset and greater from the broadside record.

This situation, including picks from this deep signal and the broadside is modelled in Figure 3.17. In the four models shown, the structure is that previously analysed for Line 8. The Moho is at 35-36 km and an upper mantle reflector is just above 50 km. Any number of velocities below the upper mantle reflector will match the arrivals picked from the in-line data, but only velocities below 8.1 km/s will match both those and the broadside picks. Considering the difficulties in picking the arrivals, it is impossible to choose between a velocity of 8.0 or 7.8 km/s. Other velocities are possible too by changing the depth of the reflector. The only thing that is clear is that it must be below 8.1 km/s - the average velocity of the uppermost mantle at the P_m reflector.

There are two implications of this analysis. First, it is an indication that the upper mantle, in the southeastern Canadian Cordillera, is at least moderately stratified. The mantle, as can also be seen in the previous chapter, is far from being composed of elastically homogeneous material. Second, a low velocity zone, of undetermined value,

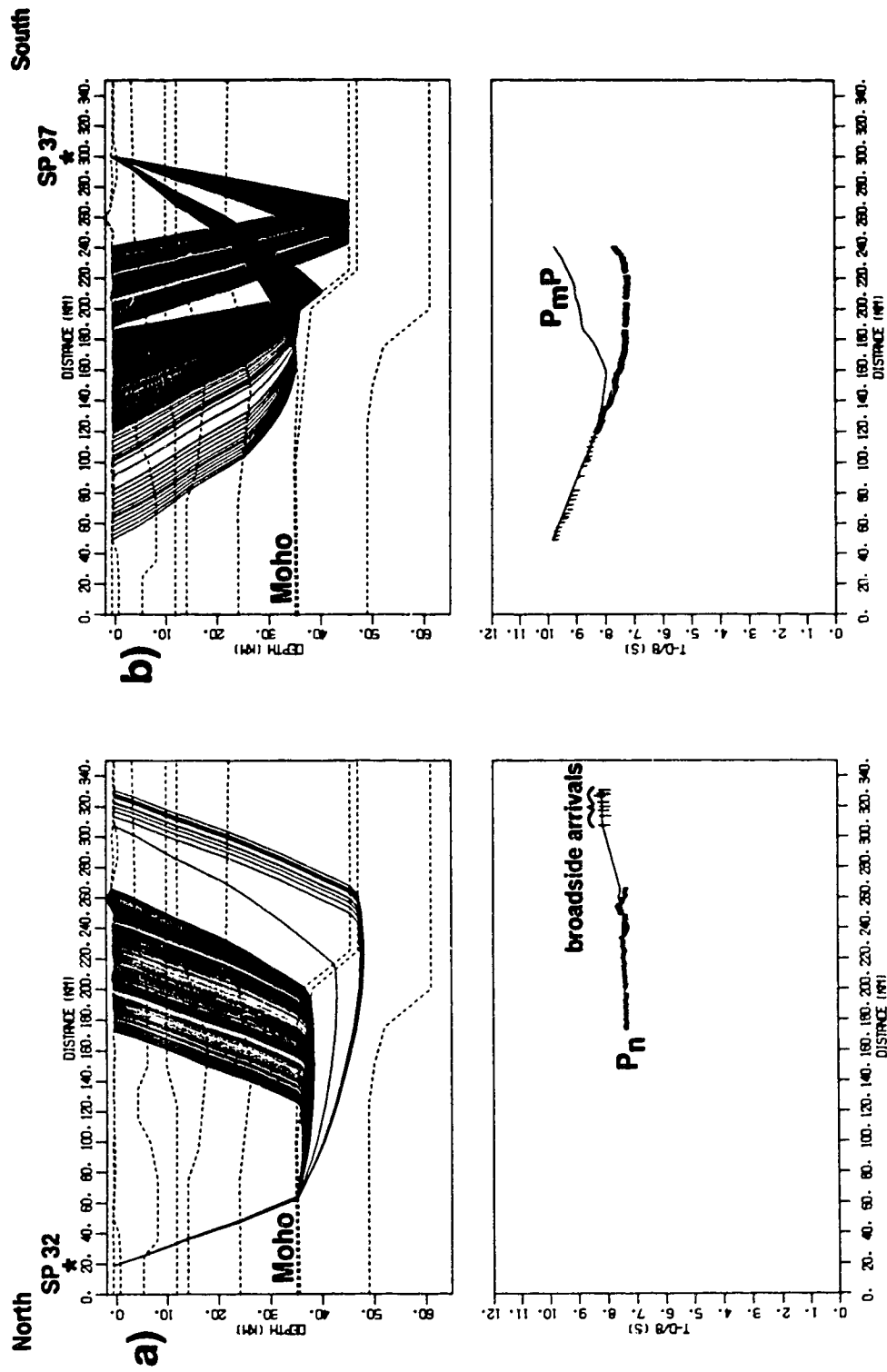


Figure 3.15 Hypothetical deepening of the Moho on Line 8. The 8 s (reduced time) SP 32 broadside arrivals could be interpreted as Pn, if there existed a step in the Moho as in a). But, this same step is inconsistent with PmP from SP 37, shown in b). It is thus likely that the broadside arrival is from well beneath the Moho.

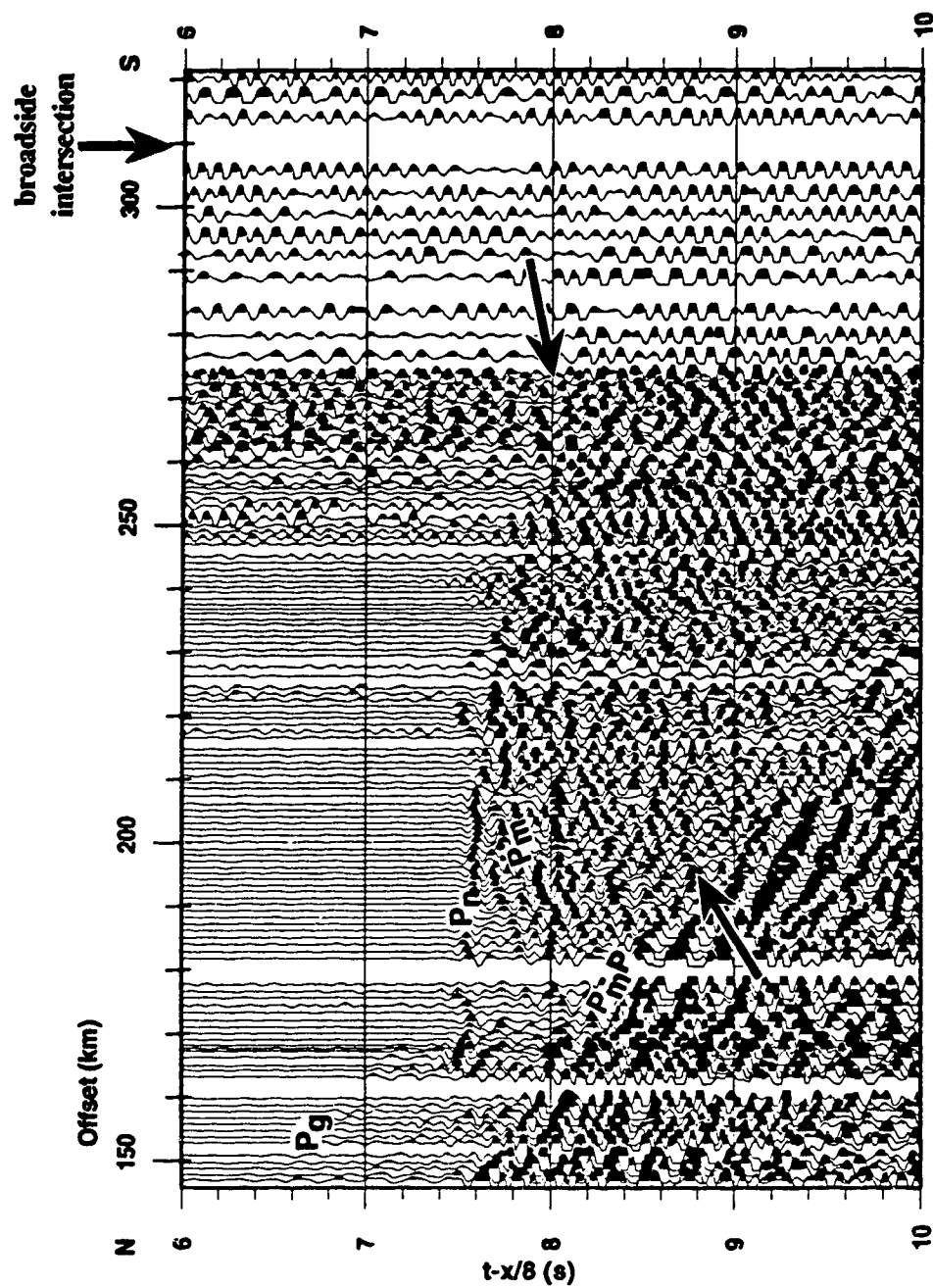


Figure 3.16 Blowup of SP 32 in-line record. Close examination shows a deep arrival (WAR) that is consistent with the phase seen on the corresponding broadside record at 8 s. Arrows mark this phase and the position of the intersection with the broadside recording line.

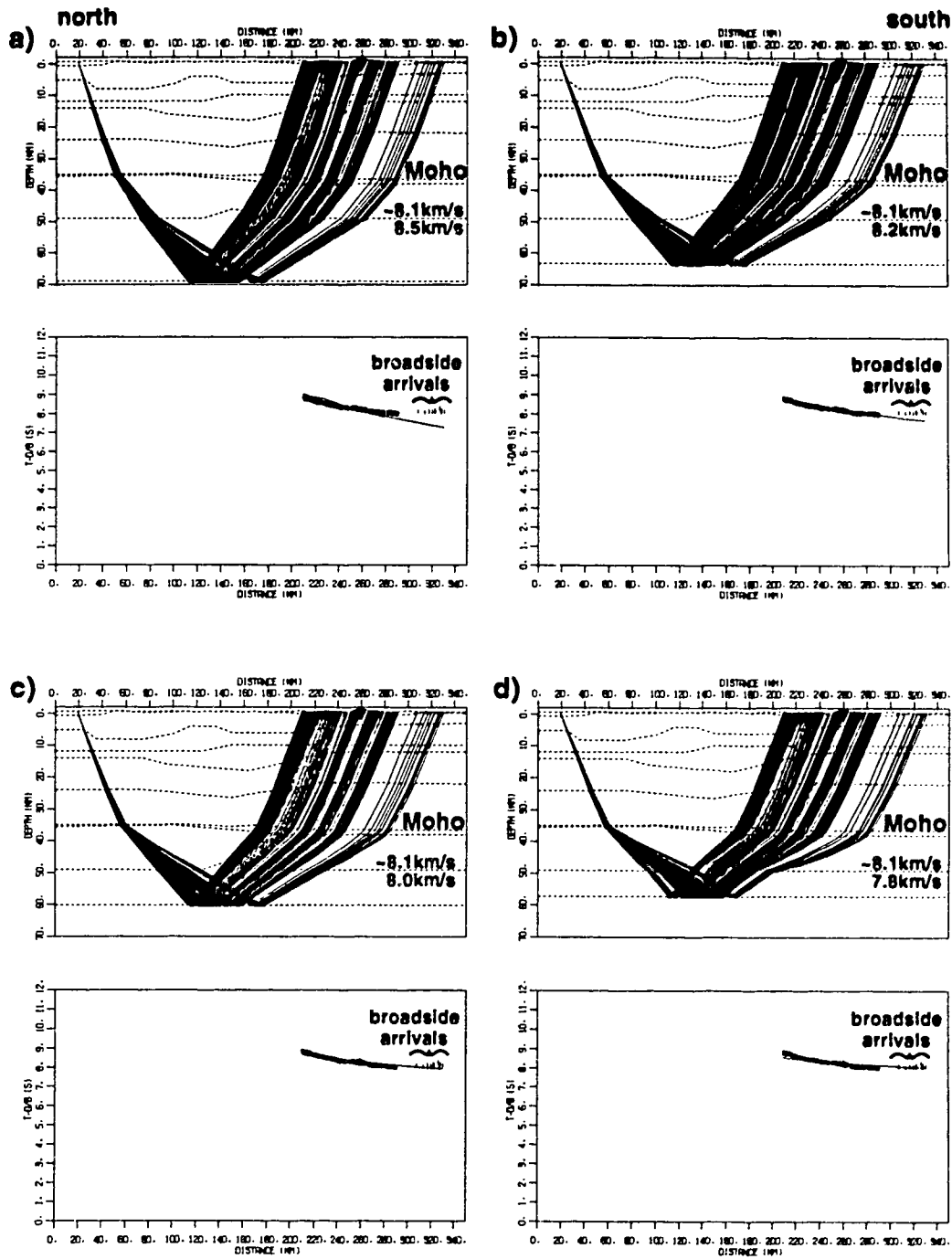


Figure 3.17 SP 32 deep broadside arrivals straddling the intersection with the in-line profile are modelled along with a deep arrival from the SP32 in-line data. Indications from the broadside record is that this arrival has no slope over an appreciable differential offset. Thus, only velocities less than 8.2 km/s are consistent with the data.

begins at about 50 km depth.

This last result, if one takes it to mean that the 50 km LVZ is the top of the asthenosphere, tends to confirm the estimates of lithospheric thickness in the Cordillera from surface wave studies by Wickens [1977] and is similar to the result of Zelt et al. [1992] who use amplitude analysis of their P_m phase to interpret a negative velocity contrast at the sub-Moho reflector. There is mounting evidence, largely circumstantial at this point, that the asthenosphere in the southeastern Cordillera is shallow and can be readily sensed by modern seismic experiments.

3.6 Summary

The three-dimensional broadside recording of the Line 8 shotpoints can be separated into three types. Shotpoint 37 is geometrically an in-line split spread which can be used to define a two dimensional, east-west, velocity profile just north of the Canadian/U.S. border. Two records (from SP 35 and 61) show good three-dimensional P_mP arrivals which can be used to increase the resolution of the crustal thicknesses in the southeastern Cordillera. Finally, a wide-angle reflection from well below the Moho gives us the possibility of defining lithospheric thickness.

The SP 37 analysis shows that in the upper crust, velocities are greater west of Castlegar than east. This may have some association with Kootenay Lake and the Purcell Fault. The depth to Moho is estimated to be almost 38 km, making it somewhat deeper than has been established further north. This is, however, on trend with the Moho dip that has been interpreted from Line 8.

The P_mP fan picks were used, in conjunction with other seismic refraction results, to map the depth to Moho and the average crustal velocity in the study area. The mapped results show a shallow Moho in the Intermontane Belt, deepening somewhat in the

Omineca Belt and falling quite quickly to possibly 50 km beneath the Foreland Belt. Lower average crustal velocities in the Intermontane Belt are somewhat correlatable with Moho depths, as are the Bouguer gravity results. There is an intriguing correspondence among a Moho high, low crustal velocity and a heat flow anomaly centered over Kootenay Lake, perhaps suggesting a heat source at depth (below the Moho).

The clear signal seen on the SP 32 broadside record was identified as being from below the upper mantle reflector interpreted earlier. The kinematic characteristics of this arrival on the in-line and broadside records suggest that it is a reflection from within a low velocity zone (< 8.1 km/s). The interpretation of these strong arrivals leads one to conclude that the base of the lithosphere is at 60 ± 5 km at the intersection of line 7 and 8. There is corroborative evidence for this from another refraction experiment and surface wave studies in the southern Cordillera. The data indicates that the top of the asthenosphere is shallow in the southeastern Cordillera and that modern refraction seismic experiments at distances of 300 km and more can determine important properties of the upper mantle.

Chapter 4 Seismic Power Density and Seismicity in Western Canada

4.1 Background

This chapter relates the seismicity of Western Canada to the geologic terranes and other tectonic elements making up this part of the continent. It makes use of both the usual method of displaying earthquake epicentral data and also a presentation in which the energy release during a 25 year period is transformed into a seismic power density map. The ultimate aim of this study is to be able to take the seismic and geologic characteristics of Western Canada and analyze them together under the constraints of new crustal models. These models will be derived from deep crustal seismic reflection and refraction data of current and future transects undertaken within the LITHOPROBE program.

It has been said that the seismicity of the earth is decidedly non-random and that though most of these seismic events occur at plate boundaries, a small but significant number do occur in continental interiors [Johnston, 1989]. Adams and Basham [1989] note that most of the area of the Canadian portion of the stable North American craton is aseismic but that there are several zones of intense seismicity and some distinct intracratonic seismic clusters [Milne *et al.*, 1978]. The tectonic setting with the Pacific, North America, Juan de Fuca and Explorer plates is summarized by Keen and Hyndman, [1979]. The Explorer and Juan de Fuca plates are separated by the Nootka fracture zone, a strike slip fault extending into Vancouver Island, with sinistral motion of 2 cm/yr. The convergence rate between the Juan de Fuca and the North American plate is 3.5 cm/yr while that between Explorer and North America is 1.4 cm/yr.

Most investigators [Sykes, 1978; Johnston, 1989, Adams and Basham, 1989] attribute intracratonic seismicity to reactivation of extensional rift zones. Talwani [1989a

and 1989b] concludes that seismic activity within plates is due to uniform stress fields reactivating old pre-existing faults. The consensus seems to be that intracratonic earthquakes must occur at zones of weakness which have been determined by the tectonic structure of the crust.

4.2 Western Canadian Seismicity

The pattern of seismicity in Western Canada is shown Figures 4.1 and 4.2 which are derived largely from the Canadian Earthquake Epicenter File, Geological Survey of Canada, and the U.S. Geological Survey, National Earthquake Information Center. Figure 4.1 shows those events that have occurred in the 25 year period between the beginning of 1964 and the end of 1988. All other seismic events recorded before 1964 are on Figure 4.2. The year 1964 is rather arbitrary for this separation, but it does serve to point out the increase in knowledge of intracratonic seismicity with the increase in seismic stations in the last quarter century. As the density of seismic stations is still low, the implication is that increased seismic monitoring would result in more detailed seismicity maps. The accuracy of the epicentral determinations is very variable over the whole map area and many events may be misplaced by 20 to 30 km. None of the events have been relocated since new crustal models are only now becoming available from the Lithoprobe field seismic refraction and reflection programs. The Southern Cordilleran phase of the Lithoprobe program, for instance, has over 1500 km of vibrator seismic reflection data along 16 lines and 2500 km of refraction data distributed among 8 lines, covering the area of interest (see Chapter 2 and 3).

The events shown in Figure 4.2 are important in showing that a number of very large earthquakes have occurred during the past century in areas where they have not recurred during the more recent past as seen in Figure 4.1. These include the 1949 magnitude 8 event near Seattle and the 1872 magnitude 8 event just south of the Canada-

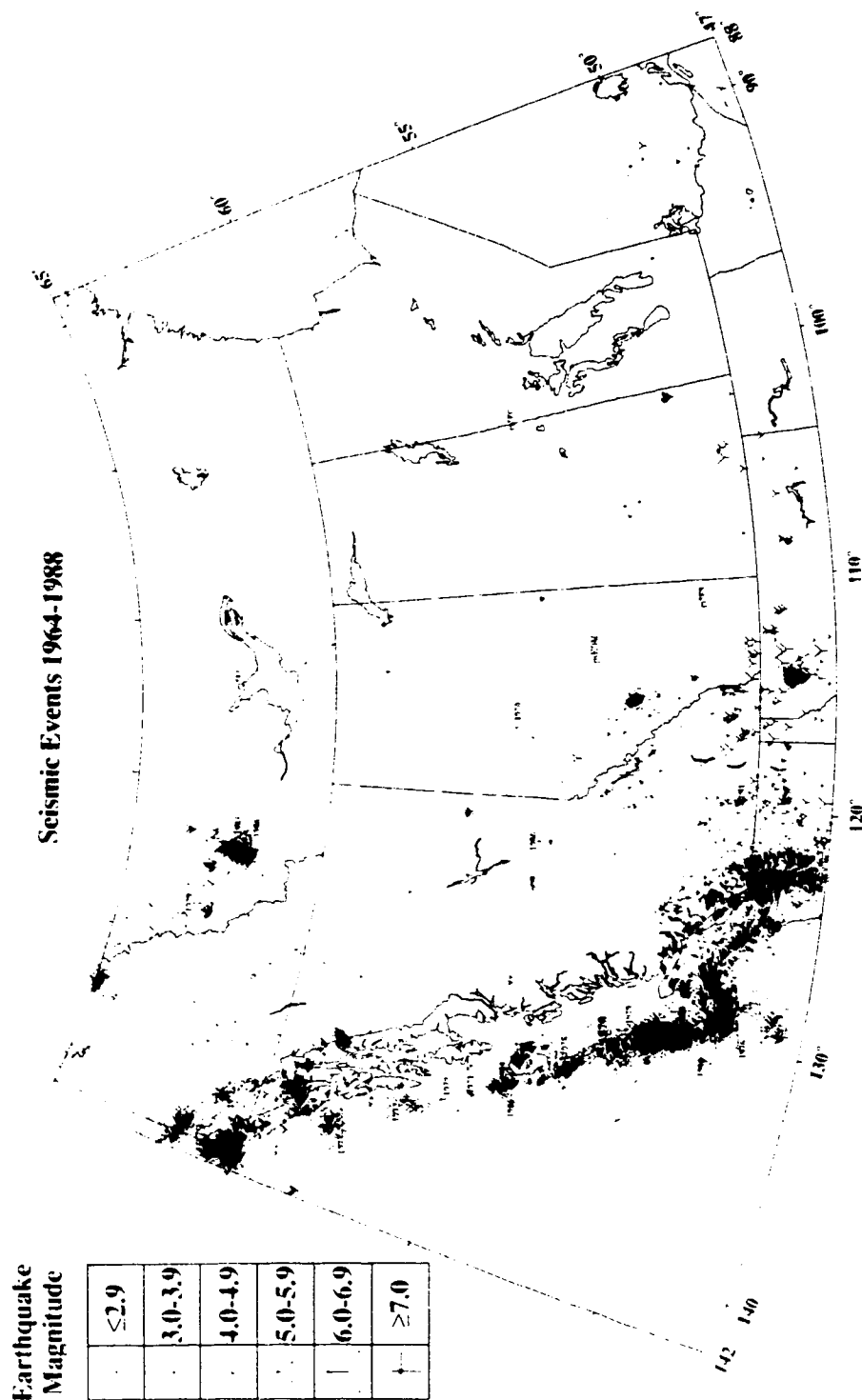


Figure 4.1 The seismicity in western Canada and adjacent regions for the 25 year interval 1964-1988. The primary data base is from the Geophysics Division of the Geological Survey of Canada, Seismological Service, Ottawa, Ontario and Sidney, B.C. and the United States Geological Survey, National Earthquake Information Center, Denver, Colorado.

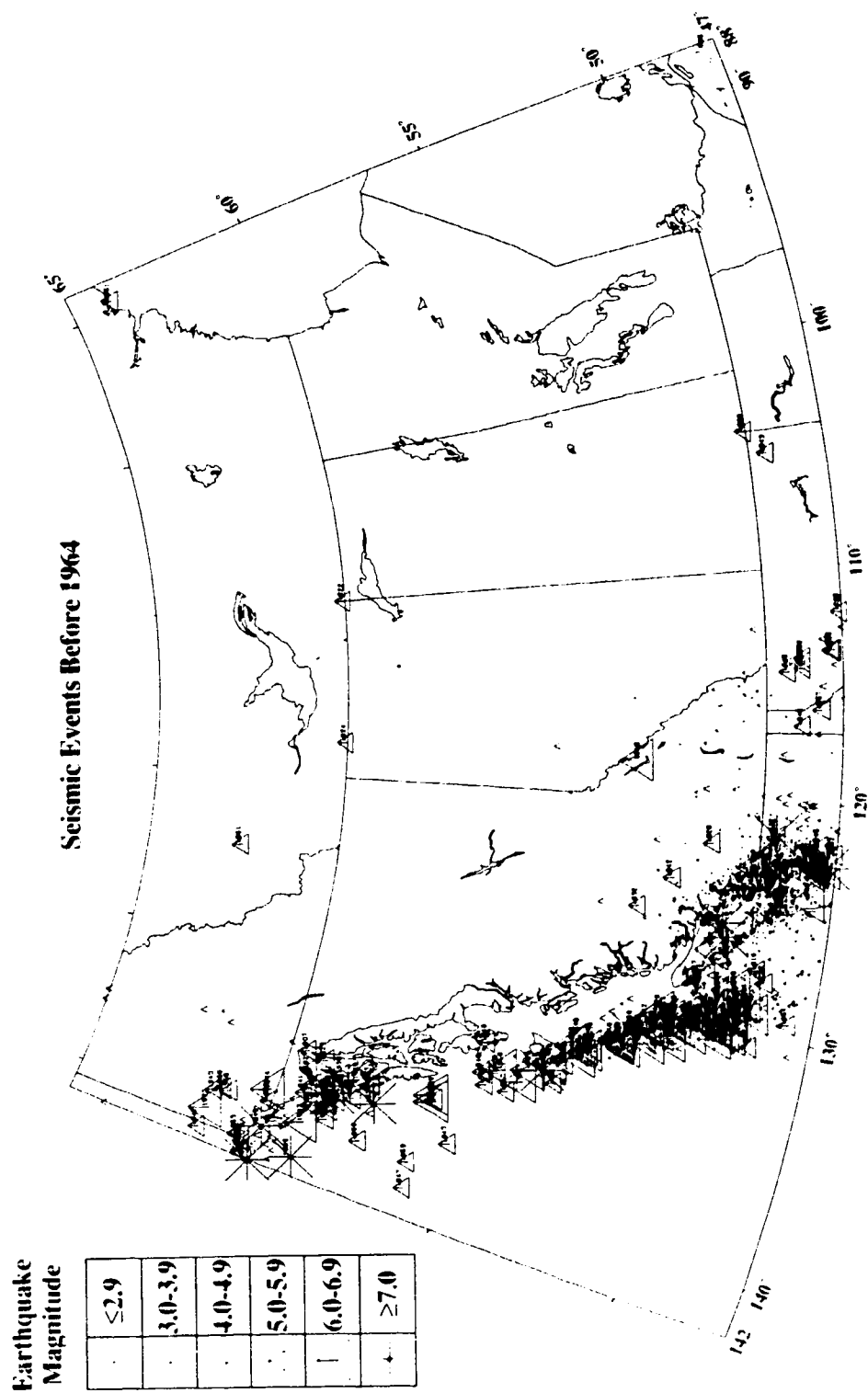


Figure 4.2 Earthquake events reported for the period prior to 1964.

USA border. In British Columbia there are the 1918 and 1946 events on Vancouver Island and the 1949 event on Queen Charlotte Island. The northwest triplet (1926, 1932 and 1943) fall close to either the Fraser or the Yalakom faults. The 1918 event in central B.C. is south of the Mica dam site on the Columbia River. In Alberta there is the 1957 event near Grande Prairie which indicates that the area was naturally unstable prior to the presumed induced event within the Snipe Lake Oil field in 1970. The two northern events on the Northwest Territories border in 1922 and 1924 events, plotted on latitude 60, are poorly located only from felt reports and may be related to minor current seismicity along the Great Slave Shear Zone. In Saskatchewan and northeastern North Dakota the 1909 and 1943 events are along a north-south trend of more recent microseismicity.

4.3 Seismic Power Density Map

Power density is the rate of energy release (Joules/s) per square meter. There is a recognized relationship between earthquake magnitude and energy release. By taking a simple energy magnitude relation such as the one by *Gutenberg and Richter* [1956]:

$$\log E = 11.4 + 1.5M_S$$

(where E is energy in ergs and M_S is the Richter magnitude from the epicenter file), each event magnitude is transformed to an estimate of radiated energy. The map area is then divided into equal-area, almost half degree bins and the energies over the 25 year sampling period are summed to get a total seismic energy release. Power density is obtained by dividing by the area and sampling period. It is possible to create more sophisticated spatial averaging using weights, overlapping bins or incorporating the dislocation area. For Western Canada and most parts of the world this does not seem justified since the recording stations are far apart and the epicenters for smaller events

may be in error by about 0.25° or more. Experiments at quadrupling or quartering the area does not change the pattern significantly on a contour map.

The plotted values (in Watts m⁻²) were contoured manually with the epicentral map as an underlay. This procedure achieves some spatial filtering and the result is not different significantly from computer contoured output which has some difficulty in accommodating the 12 orders of magnitude power differential. The final product is called a *Seismic Power Density Map* (Figure 4.3). The results are best displayed in colors which ranges from blue for 0 power density (i.e. totally aseismic) to red with greater than 10⁻⁴ W m⁻². This is comparable to the tens of mW m⁻² values of heat flow measurements. For a further comparison, the solar constant, the solar energy reaching the earth, is 1,350 W m⁻².

The largest values of power density, as expected, are along the trend marking the broad scale boundary between the oceanic Pacific, Explorer and Juan de Fuca plates and the continental North American lithosphere. Areas with no seismic activity on both the stable craton and within the Cordilleran area show up much more clearly on a seismic power density map. Further details will be discussed in conjunction with an examination of the structural elements of the area in question.

4.4 Seismicity And Tectonic Elements

The seismicity map in Figure 4.3 indicates the major zones of activity in Western Canada. Figure 4.4 shows the seismic power density compared with the terranes and tectonic elements of western Canada (from Figure 1.7). In the following discussion, I will be implicitly referring back to Figures 1.7 and 1.8. I will begin with a discussion of the very active plate boundaries and proceed eastward into the continent. The frequency and magnitude of earthquakes becomes less as one moves further way from this current portion of Cordilleran deformation. Yet, there is a significant amount of seismic activity

in the stable continental interior.

Most earthquakes in western Canada occur along the Pacific coast following the boundaries between the major lithospheric plates. On the seismic power density map there is a good correlation between high power density and major faults (Figure 4.4). For instance, the Queen Charlotte Fault and Juan de Fuca Ridge, taken to be the broad scale boundary between the Pacific and North American plates, show high power density trends. A listing of events by geographical area and date is instructive and is listed in Table 1. Note the continuous level of seismicity in the northwest from Alaska to the Queen Charlotte Sound and also a similar activity along the spreading centers between the Pacific plate and the Juan de Fuca plate in the south. The activity on Vancouver Island and the region in northern Washington state is quite different. There is an absence of similar large events in this region particularly during the 25 year period from 1965 to 1990. However there have been a large number of small and intermediate (magnitude 5 to 6.4) earthquakes along this zone during this last quarter century. This region would appear to display all the characteristics of a seismic gap. These gaps, that have previously been recognized along convergent and strike-slip boundaries [Fedotov, 1965; Mogi, 1968; Kelleher, 1970, 1972; Sykes, 1971; Kelleher *et al.*, 1973; Ohtake *et al.*, 1977; McCann *et al.*, 1979]. Large earthquakes generate rupture zones along plate boundaries and other zones of weakness but at any one time there are gaps in the spatial distribution of rupture zones. These gaps become the site of future seismic energy release in the form of large earthquakes.

The relatively good seismic network on the Pacific coast of Canada, by contrast with that of the interior, has established the relation between depth of earthquakes and the subducting Juan de Fuca plate. Figure 4.5 consists of a series of cross section showing earthquakes as a function of depth, as they are determined currently, in half degree strips from Latitude 47° to 52° N. The most reliable information in the Vancouver Island

Table 4.1 Large Earthquakes along the boundaries of the Pacific, Juan de Fuca, Explorer and North American Plates.

Year	Date	Magnitude	Latitude	Longitude	Comment
1899	Sept 4	8.2ML	60 N	142 W	Yukon-Alaska border
1899	Sept10	8.6 MS	60 N	140 W	Yukon-Alaska border
1899	Sept10	7.8MS	60 N	140 W	Yukon-Alaska border
1908	May 15	7.0 ML	59 N	141 W	Yukon-Alaska border
1944	Feb 3	6.5 ML	60.1 N	137.88 W	Yukon-Alaska border
1979	Feb 28	6.9 MS	60.64 N	141.60	Yukon-Alaska border
1927	Oct 24	7.1 ML	57.5 N	137 W	Alaska Panhandle
1958	July 10	7.9 ML	53.62N	133.27 W	Alaska Panhandle
1972	July 30	6.5 MB	56.8 N	135.7 W	Alaska Panhandle
1921	April 10	6.5 ML	54 N	134 W	Queen Charlotte Is
1948	Feb 28	6.5 ML	53.37 N	132.73 W	Queen Charlotte Is
1949	Aug 22	8.1 MS	53.6 2N	133.27W	Queen Charlotte Is
1912	Mar 11	6.5 ML	51. N	131.W	Queen Charlotte Sound
1929	May 26	7.0 ML	51.51 N	130.74 W	Queen Charlotte Sound
1956	Feb 19	6.5MS	51.61 N	131.37 W	Queen Charlotte Sound
1956	Dec 21	6.7 ML	51.29 N	130.6 W	Queen Charlotte Sound
1960	July 4	6.6 MS	51.79 N	131.19 W	Queen Charlotte Sound
1970	May 24	7.0 MS	51.77 N	130.76 W	Queen Charlotte Sound
1917	Dec 23	6.5 ML	50 N	128 W	N Vancouver Island
1918	Dec 6	7.0 ML	49.62 N	125.92 W	N Vancouver Island
1946	June 23	7.3 ML	49.76N	125.34	N Vancouver Island
1872	Dec 15	7.4 ML	48.6 N	121.4 W	N. Washington state
1949	Apr 13	7.1 ML	47.20 N	122.6 W	Seattle area
1965	Apr 29	6.5 ML	47.4 N	122.3 W	Seattle area
1914	July 21	6.5 ML	49 N	130 W	Juan de Fuca
1926	Nov 1	6.6 ML	48.75 N	128.50 W	Juan de Fuca
1939	Feb 8	6.5 ML	49.08 N	128.04 W	Juan de Fuca
1939	July 18	6.5 ML	49.01 N	129.22 W	Juan de Fuca
1946	July 18	6.5 ML	49.34 N	130.27 W	Juan de Fuca
1946	July 18	6.5 ML	49.54 N	129.71 W	Juan de Fuca
1976	Dec 20	6.7 MS	48.8 N	129.29 W	Juan de Fuca
1976	Dec 20	6.7 MS	49.02N	128.67W	Juan de Fuca
1980	Dec 17	6.8 MS	49.48 N	129.5 W	Juan de Fuca
1980	Dec 17	6.8 MS	49.52N	130.04 W	Juan de Fuca

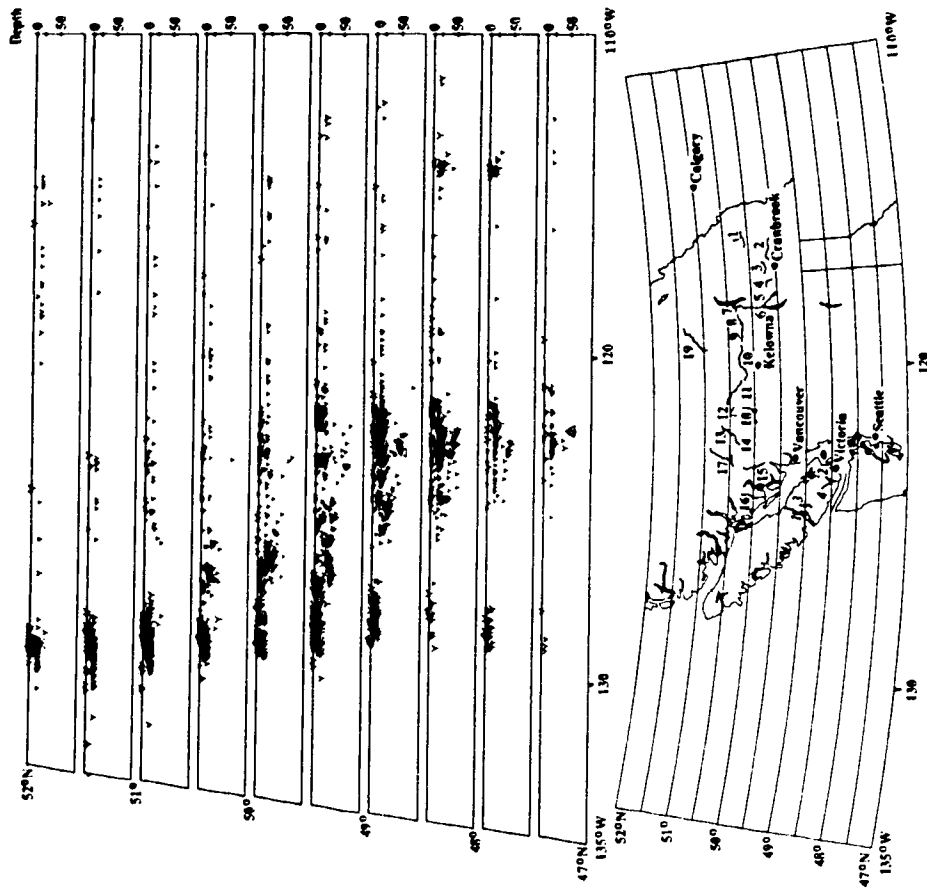


Figure 4.5 Cross sections showing the depth of earthquakes as located in 0.5 degree intervals from 47 degrees to 52 degrees N latitude. The depth to the Moho and other reflecting horizons are shown where there is reliable information. The index map shows latitude intervals and the locations of the LITHOPROBE seismic reflection lines.

area and the earthquakes associated with the Juan de Fuca subduction zone are clearly visible to depths of about 60 km on panels a to g. Seismic foci become deeper as one moves east.

There are prominent seismic power trends associated with the Coast Plutonic Complex, the region of the Fraser River Fault and the Northern Rocky Mountain Trench as well (Figure 4.4).

We can note, from Figure 4.3, that there are small earthquakes in the south central Cordillera that extend into the Interior Plains to the east. Some of these events appear to trend northeast to southwest, in opposition to the main Cordilleran northwest to southeast tendencies. These cratonic trends of the seismicity may then indicate the limits of the North American Basement. The craton would thus seem to extend to somewhere between the Arrow Lakes and the Okanagan Valley.

An aseismic region, associated with much of the Intermontane Belt (Figure 1.8, Figure 4.4), is very prominent. A smaller aseismic area, covering most of the Insular Belt is quite noticeable too. Less sizable aseismic zones can be found west of the Nahanni seismic belt.

As was mentioned above, northeast-southwest running trends in southeast British Columbia and southwest Alberta perhaps indicate the end of the North American craton. As well, there are indications of northeast-southwest trends in northern Alberta and in the Northwest Territories which can be related to the Great Slave Lake Shear Zone (Figures 1.7, 4.4).

There are other indications of seismic activity that are associated with interpreted Proterozoic suture zones [*Ross and Stephanson, 1989; Hoffman, 1989*] - most specifically with the Great Bear Terrane (Figures 1.7, 4.4).

In Figure 4.5, due to the sparseness of seismic stations in Western Canada, the depths of most of the events are very uncertain. Arbitrary depths have been assigned for

what are interpreted to be shallow, intermediate and deeper earthquakes. One notes that this has the effect of concentrating events in the shallow and deeper panels of Figure 4.5. Despite the uncertainties involved, if the depth solutions have any validity at all, it is clear that seismic events are restricted to the upper 20 km). A look at the crustal models derived from the SCoRE refraction data (Chapters 2 and 3) reveals that in this region failure occurs in the upper half of the crust. The Moho, from the seismic refraction data, is interpreted to be in the range of 35-38 km depth in southern British Columbia.

This discussion also points out the extent to which new crustal models of Western Canada are being developed. Interpretations of LITHOPROBE's Southern Cordillera reflection data and Southern Cordillera refraction programs are near completion. Extensive reflection and refraction profiling are underway in the Alberta Basement and Trans-Hudson Transects of the LITHOPROBE Phase III program. These new models, as they become available, will allow more accurate focal solutions.

4.5 Summary

A unique and innovative way of viewing seismicity has been presented. Earthquake activity has been mapped by a transformation and summation of magnitudes to power emission per area. This display for the western Canada has allowed a greater ease of comparison with the tectonic elements interpreted from geologic and geophysical studies. Correlations between the seismic power density with plate boundaries, terrane amalgamations, faults, and even possibly with buried cratonic margins has been noted. Though the original information is not particularly reliable (earthquake locations and depths, specifically), the method is promising for the study of earthquakes for the interpretation of crustal tectonics.

Chapter 5 Alberta basement seismic reflection transect

5.1 Background

The first stage of deep crustal seismic reflection profiling of Alberta was undertaken in the summer of 1992. As part of LITHOPROBE's Phase III Alberta Basement Transect, this marked the beginning of multi-disciplinary probing of the crust beneath the Western Canada Sedimentary Basin to study the origin of the continent and the influence of basement structure on the sedimentary section above [Ross *et al.*, in submission]. The innovative three-dimensional reflection and the velocity probe using a long-offset expanding spread experiments were made to complement the regular 2-D reflection profiling and were proposed by E. R. Kanasewich for Lithoprobe Phase III and the detailed planning carried out by me.

Veritas Geophysical Limited, of Calgary, obtained the contract for the seismic acquisition, which took place over a period of 29 days, from July 1 to July 29, 1992. As main contractor, Veritas sub-contracted line surveying, line clearing and clean-up operations. The Veritas crew consisted of about 35 people, working in 2 shifts for 24 hour per day operation. This was the first time that deep reflection studies had used as many as 480 detectors in a simultaneous recording program.

The two-dimensional reflection data were recorded in north-south and east-west profiles, numbered 1 to 10 from west to east and totalling 512.8 km. Lines 1, 3, 4, 6 and 8 were north-south while the other profiles were predominantly east-west. The lines followed the grid road system of Alberta, crossing the basement domains as near as possible perpendicular to strike (Figure 5.1). Line 1 started near Entwistle, west of Edmonton while the last profile, Line 10, the longest at over 150 km, finished at the Alberta-Saskatchewan border just northeast of Provost.

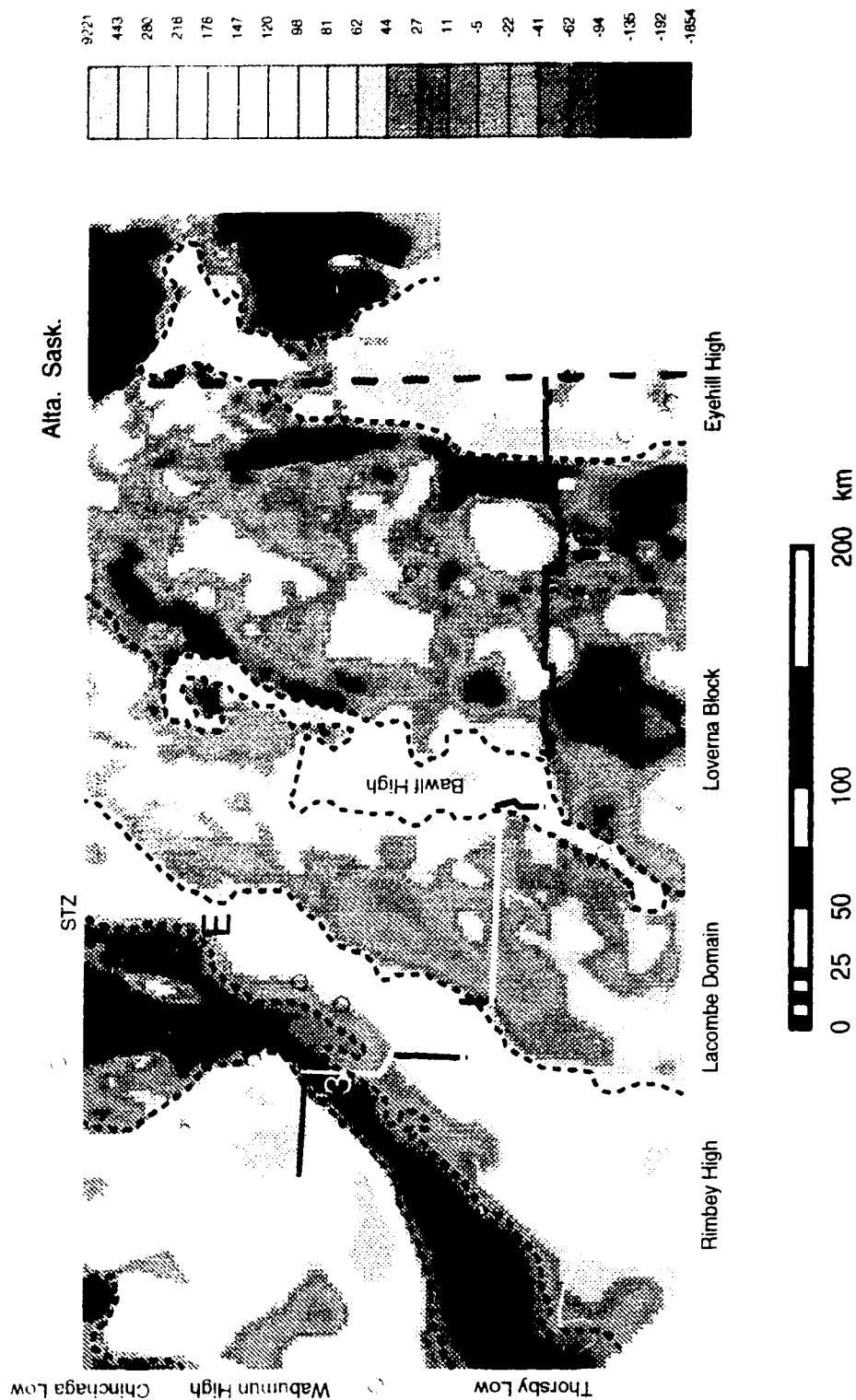


Figure 5.1 Map of the magnetic field signature of the crust over Alberta with the position of the Central Alberta seismic reflection lines. The interpreted geologic domains to the east of the Thorsby Low are all part of the Heame Province as seen in Figure 1.7. Magnetic data is from the Geological Survey of Canada with units of NanoTesla and a 2 km grid spacing. 'E' is the location of Edmonton and 'STZ' is the Snowbird Tectonic Zone.

The processing contract was awarded to Pulsonic Geophysical Ltd. of Calgary. They were supervised by us at the Seismology Laboratory and by scientists from the Continental Geoscience Division of the Geological Survey of Canada.

5.2 Two-dimensional profiling

The standard seismic reflection spread consisted of 240 receiver stations (Figure 5.2) in a straight line (480 receivers were used for special experiments, as described below). Each receiver station (Figure 5.3) was made up of nine (9) Oyo 20 DX 14 hz geophones (i.e. seismometers) per in-line array (i.e. 'string'). All geophones had 2" spike bases and were buried to reduce ambient noise (wind, for instance). The distance between geophones within a string was 5.25 m with a total array length of 42 m. This geophone group was centered on a receiver station. The group interval (that is, the distance from one receiver array midpoint to the next) was 50 m. The source (in this case mechanical vibrators - discussed below) interval was nominally 100 m (every two receiver stations). This resulted in an average 6000% CMP coverage (60 fold redundancy per common-mid-point). The spread configuration was an asymmetric split-spread - 3150 m maximum receiver/source offset on the west/north short end and a maximum 9150 m offset on the east/south long end.

For all the seismic lines, the surveying contractors gave UTM coordinates and elevation for each station to an absolute accuracy better than 50 m horizontally and 3 m in elevation and relatively better than 3 m horizontally and 0.6 m vertically between any 2 adjacent survey points.

Five Mertz Model 18, 44,000 lb peak force, buggy mounted vibrators were available (Figure 5.3) - four in use at any one time and the fifth for spare. The output vibrator signal was a 14 s linear sweep ranging from 10 to 56 hz. At each vibrator

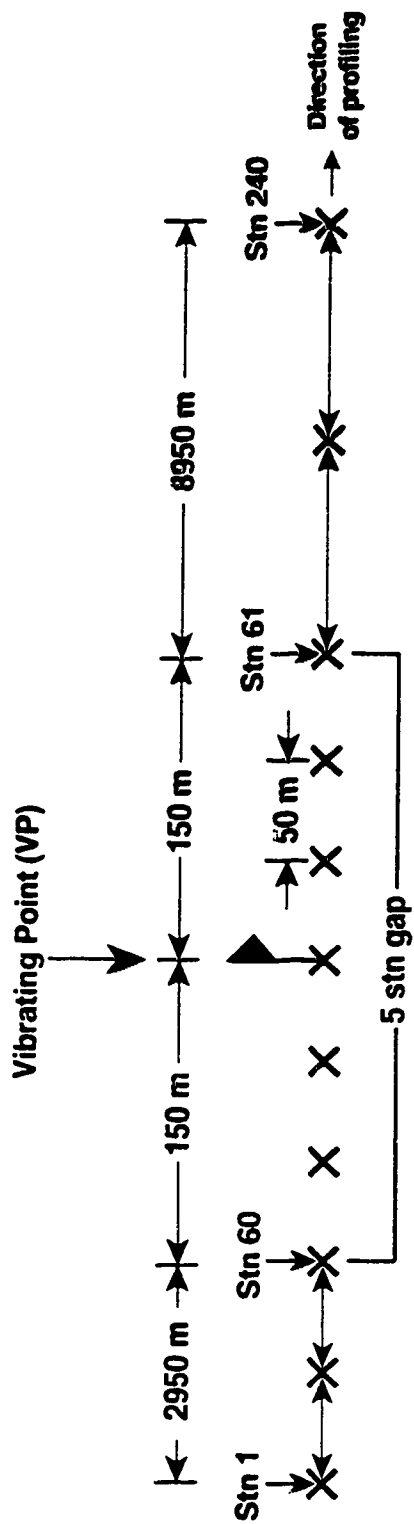


Figure 5.2 The standard seismic reflection spread geometry for Alberta Basement Transect profiling in 1992. There are 240 receiver stations every 50 m. The spread is termed an asymmetric split-spread with the source point (vibrating point - VP) located at one-third the distance down the spread (the first 60 stations). Maximum source to receiver offset is 3100 m on the short side and 9100 m on the long side. There is a five station gap (i.e. 5 dead channels) centered about the VP.

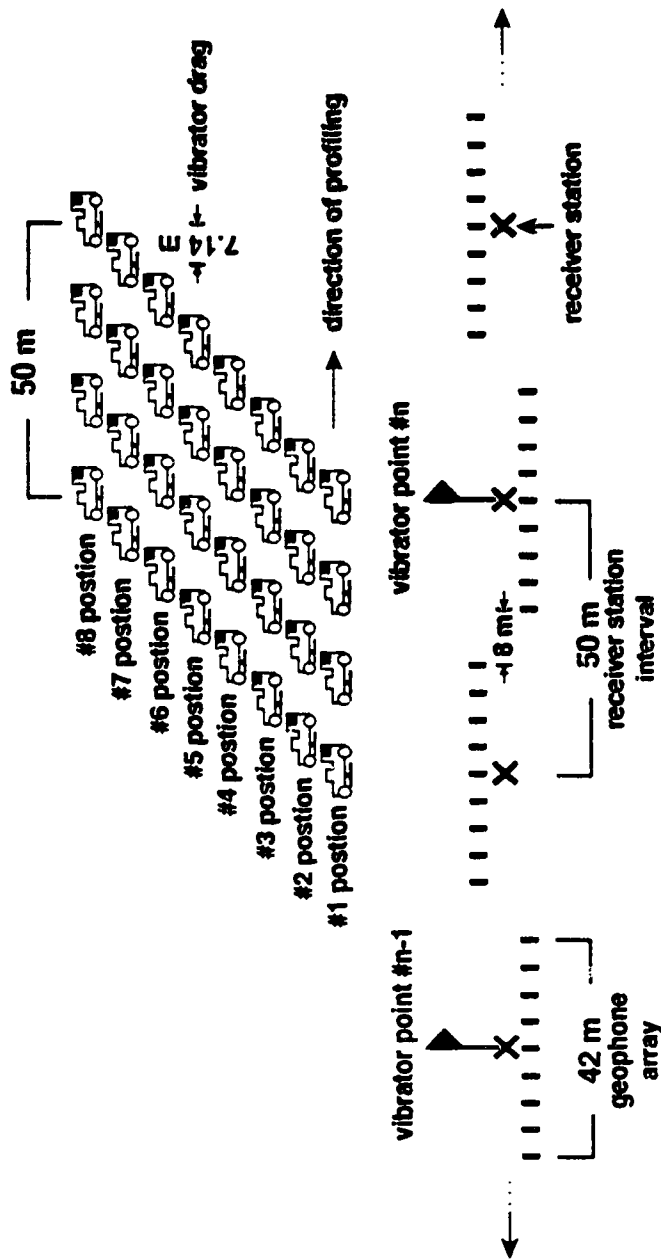


Figure 5.3 The standard seismic reflection geometry for Alberta Basement Transect profiling in 1992. Receiver stations consisted of a string of 9 buried geophones over 42 m. The nominal source interval was two station intervals (100m). With a 240 channel recording system, this gave an average 6000% CMP coverage. At each vibrating point (VP), a set of four vibrators would 'shake' eight times, moving up 7.14 m each time, symmetrically about the VP. The eight sweeps per VP were summed by the recording system to simulate a single source centered at the VP.

point, the vibrators would 'shake' eight times, moving up 7.14 m (vibrator 'drag') before each one. The suite of sweeps was centered on the vibrator point.

The Veritas crew recorded the seismic data with the I/O System One, a sophisticated cable telemetry seismograph. This instrument recorded data from the receiver stations, digitizing them with a 4 ms sampling interval, summed ('stacked') all eight sweeps of the vibrator suite to increase the strength of the relatively weak individual vibrator signals, and then performed a correlation of the data with the elongated vibrator signal to obtain sharp seismic pulses. The recording parameters included diversity stacking and burst editing, digital processes conducted simultaneously with recording which eliminated much of the cultural noise sources such as that produced by highway traffic. Standard frequency filtering included a 3 hz (12db/oct slope) to 90 hz (75db/octave slope) bandpass and a 60 hz notch filter (filtering out signals from electrical transmission lines). The noise reduction techniques and filtering, along with sophisticated vibrator synchronization monitoring ensured high quality data.

The final shot record stored on magnetic tape were 18 s long. In addition, at every few source points, uncorrelated records were written to tape for possible future extended correlation and analysis of very deep reflections.

Initially, over seven hours was needed for instrument and spread testing to check out the recording system and vibrator control and to decide on recording parameters.

In planning the experiment, the north-south, east-west grid road system of the Prairies had to be taken into account, creating at the same time problems and opportunities. The strike of the basement domains is north-east to south west. It is most appropriate to profile perpendicular to strike, but the extra costs (involving negotiations for private land access, line clearing, clean-up, etc.) involved in placing seismic lines across country was prohibitive. As well, Alberta provincial regulations hinder seismic operations on paved roads. Therefore, the lines had to be placed alternately on the north-

south and east-west gravel roads, making as close to possible a perpendicular crossing of geologic strike (Figure 5.1).

One problem involved in this is what happens at the intersection between perpendicular segments. Continuing shooting through bends ('crooked line') causes a smearing of the CMPs. Stopping a line in one direction, then beginning again immediately in the other direction means that the intersection point is poorly sampled due to the low fold at the ends of lines (in essence, the intersection is blank, no data is recovered from below it). This makes it difficult to correlate reflections from one line to the next. The proposed solution (Figure 5.4) was to acquire separate lines for each segment, to avoid CMP smearing, but to overshoot each linear segment so that the corner point (intersection) is CMP sampled by at least half the maximum nominal fold. An overlap of only 1.5 km, coupled with running the vibrators to the end of the lines with a stationary spread, ensured a minimum of 3000% coverage of the intersection point on each segment. This minimal increase in acquisition cost increased data quality and assured data continuity across the entire length of the profile.

During acquisition, Veritas encountered several problems of their own. On Line 2 (Figure 5.1), a road newly paved after scouting, required the moving of the vibrators onto a parallel road 2 miles away. The line was recorded on the planned road, but the vibrators 'shook' some distance to the south for a total length of 9.8 km. Other problems included the usual equipment breakdowns (which Veritas handled very efficiently), electrical storms (necessitating shutdown of system and disconnection of cables) and more than the usual vandalism (due to the length and exposed nature of the recording line on well-travelled roads - unusual in modern seismic acquisition in the petroleum industry) requiring reports to the local RCMP and the increased vigilance of the line crew. A River crossing was also necessary over the North Saskatchewan River (without a gap in coverage). Finally, vibrator damage required road grading in some areas.

Pulsonic Geophysical Ltd. of Calgary was contracted by LITHOPROBE to do the

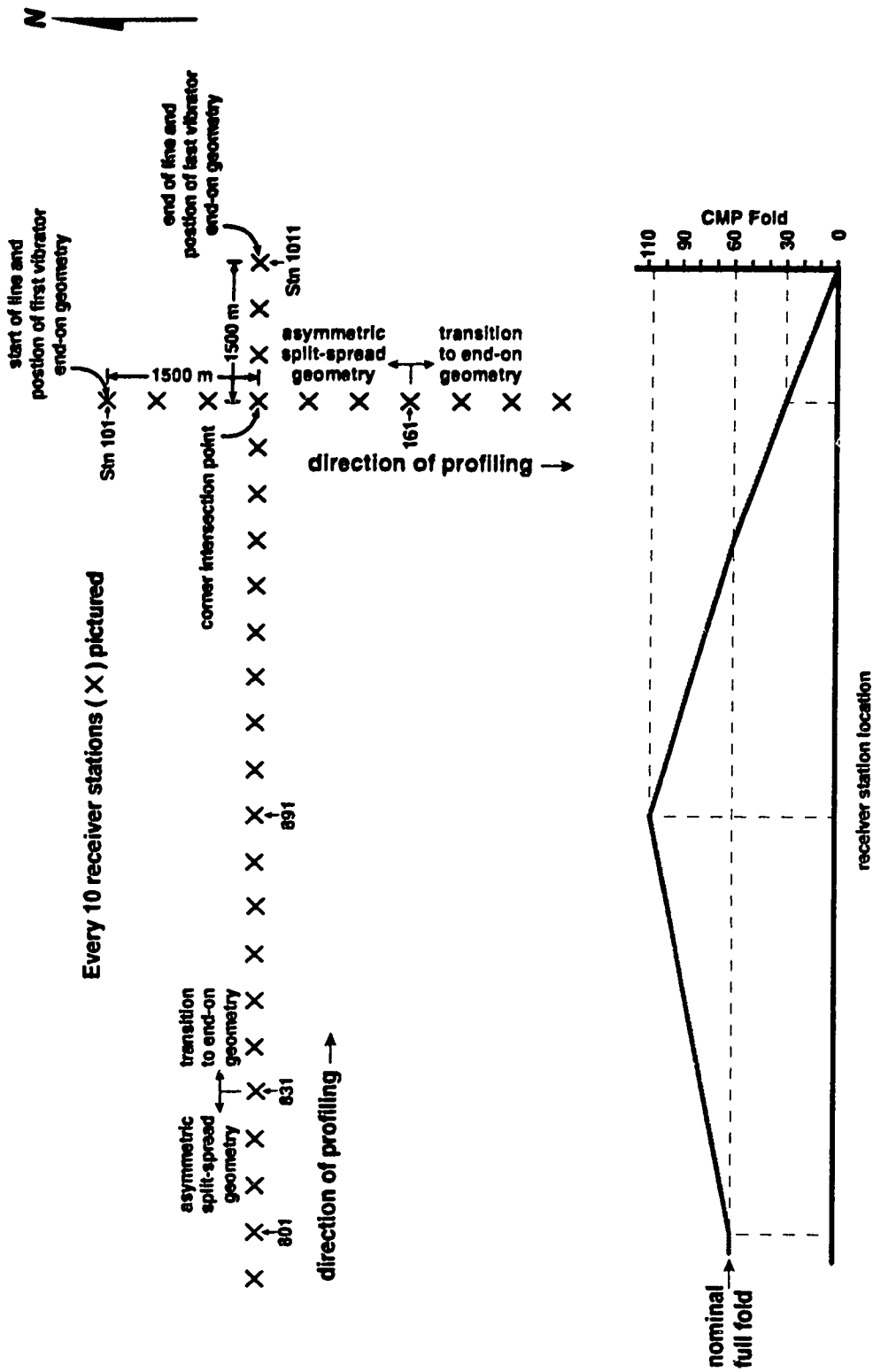


Figure 5.4 By shooting with a stationary receiver array at the beginning and end of each line (first and last vibrator points are off-end), one-half of the nominal fold can be achieved at intersection points with only a 1500 m overlap on each line. This ensures better continuity between lines without resorting to crooked line geometries and resultant smearing of CMPs.

initial processing of the standard reflection data under our supervision at the University of Alberta Seismology Laboratory as well as the Geological Survey of Canada in Ottawa. In addition, the Seismology Laboratory contracted Pulsonic to do the processing of the three-dimensional and expanding spread experiments.

On the basis of tests made on Line 1, Pulsonic designed a processing stream for the entire data set. For the most part, the processing sequence was similar to that applied to seismic reflection data in petroleum exploration. The initial steps included data format transformation, gain compensation and a zero to minimum phase conversion made necessary due to Pulsonic using software that assumes the seismic signal to be of a minimum phase type (vibrator data is of a zero phase type). Two different types of deconvolution were applied to increase the temporal resolution and balance the frequency spectrum over all the records.

In other LITHOPROBE projects, it has been found that static corrections (correcting for surface elevation and near surface velocity variations) is a key factor in obtaining superior seismic images. With that in mind, Pulsonic was required to apply 'refraction' static corrections, in which the first arrivals of the shot records are analysed to obtain detailed shallow velocity variations along the line. As well, surface-consistent residual statics were applied to fine tune reflector imaging.

Since the temporal range of the data was large, by petroleum exploration standards, and since velocity resolution in the shallow sedimentary section was of higher resolution compared to that in the basement, a two step velocity analysis was undertaken. This step was carefully monitored by us and the GSC. A thorough analysis of the upper 3 seconds of data, including constant velocity stacks and semblance velocity spectra displays, was done. The remaining 15 s of data was analysed by use of constant velocity stacks which was sufficient to obtain the coarse velocity values necessary for subsequent correction of the deeper data.

On the basis of velocity analysis, the data underwent normal-moveout (NMO) corrections (transforming the data into totally vertical incidence data) and trace muting (of non-reflection seismic arrivals) before the common-midpoint stack, which finally produced an interpretable seismic profile. Earlier tests had ascertained that the use of stacking velocities, as measured, was not able to properly image steeply dipping reflectors identified below the sedimentary column. So, a second stacked profile was produced which used artificially high stacking velocities for the data below the basement surface. This resulted in sections with enhanced dipping arrivals at the expense of sub-sedimentary horizontal events which, in any event, were interpreted to be multiple reflections masking the true geologic structure. A third set of profiles, combining both the low and high velocity stacks, was produced as well.

Post stack processing included the use of a random noise attenuation algorithm, automatic gain control scaling, finite-difference migration (to place dipping events back to their proper location) and final bandpass frequency filtering and scaling. The parameters for random noise attenuation and quality control of the migration steps were closely controlled by us and GSC scientists. Finite-difference wave equation migration (which allows a high degree of lateral and temporal velocity variation) simply used the earlier determined stacking velocity function, since more precise migration and velocity testing was beyond the budget of the commercial processing sequence.

The preliminary interpretation of the 1992 Alberta Basement Reflection experiment is given in *Ross et al.* [in submission]. The high quality of the recorded data and the careful processing steps resulted in superior seismic images - unambiguous, strong reflectivity is evident from the surface to 11-14 s, and laterally over all the profiles. The exceptional data imaged the crustal structures below the Phanerozoic sedimentary cover and shed light on the assembly of the Canadian craton in Proterozoic time. Crustal scale thrust imbrications and deflections of the crust/mantle boundary indicate the presence of a 1.8 billion year old orogenic belt underneath central Alberta.

Prominent reflections are observed throughout the entire 35-45 km thickness of the crust. Sets of dipping reflections seem to sole into a reflective zone in the lower crust at 12-14 s of seismic travel time. The base of the reflective zone is interpreted to be the crust/mantle boundary, or Moho. The geometry of the seismic reflectors indicates compressional deformation and crustal scale thrust imbrication. The eastern 300 km of the profile shows a west-northwest verging thrust belt along with an increase in Moho depth and inferred metamorphic grade into the stable craton region. In the western part of the profile, the reversal of the direction of thrusting and a Moho offset is associated with a gravity low which correlates to the subsurface extension of the Snowbird Tectonic Zone. The current information on the ages of Alberta basement rocks suggest that the orogenic features observed are part of a larger mountain building episode over 1000 km long.

5.3 Three-dimensional data

Besides making it unnecessary to use crooked-line geometry processing, the perpendicular segments also allowed for innovative, inexpensive acquisition of three-dimensional reflection data. This was done at what was termed '3-D corners'. Our only opportunity was at the corner created by the intersection of Lines 2 and 3 (Figure 5.1). Since planning had to be long term, the location was picked more on logistical than geophysical grounds.

Data acquisition was based on using, as much as possible, the existing field setup. At the end of the west-east Line 2, after the two-dimensional profiling was completed, the vibrators were placed on the north-south Line 3, leaving the recording spread on Line 2. 'Broadside' shots were then recorded, creating an east-west line of CMPs. As the vibrators moved in the south-north direction, the broadside recording created additional lines of CMPs. Then by vibrating on the west-east Line 2 and recording on Line 3 (as portrayed in Figure 5.5), after setting up the array for a new 2-dimensional profile, we

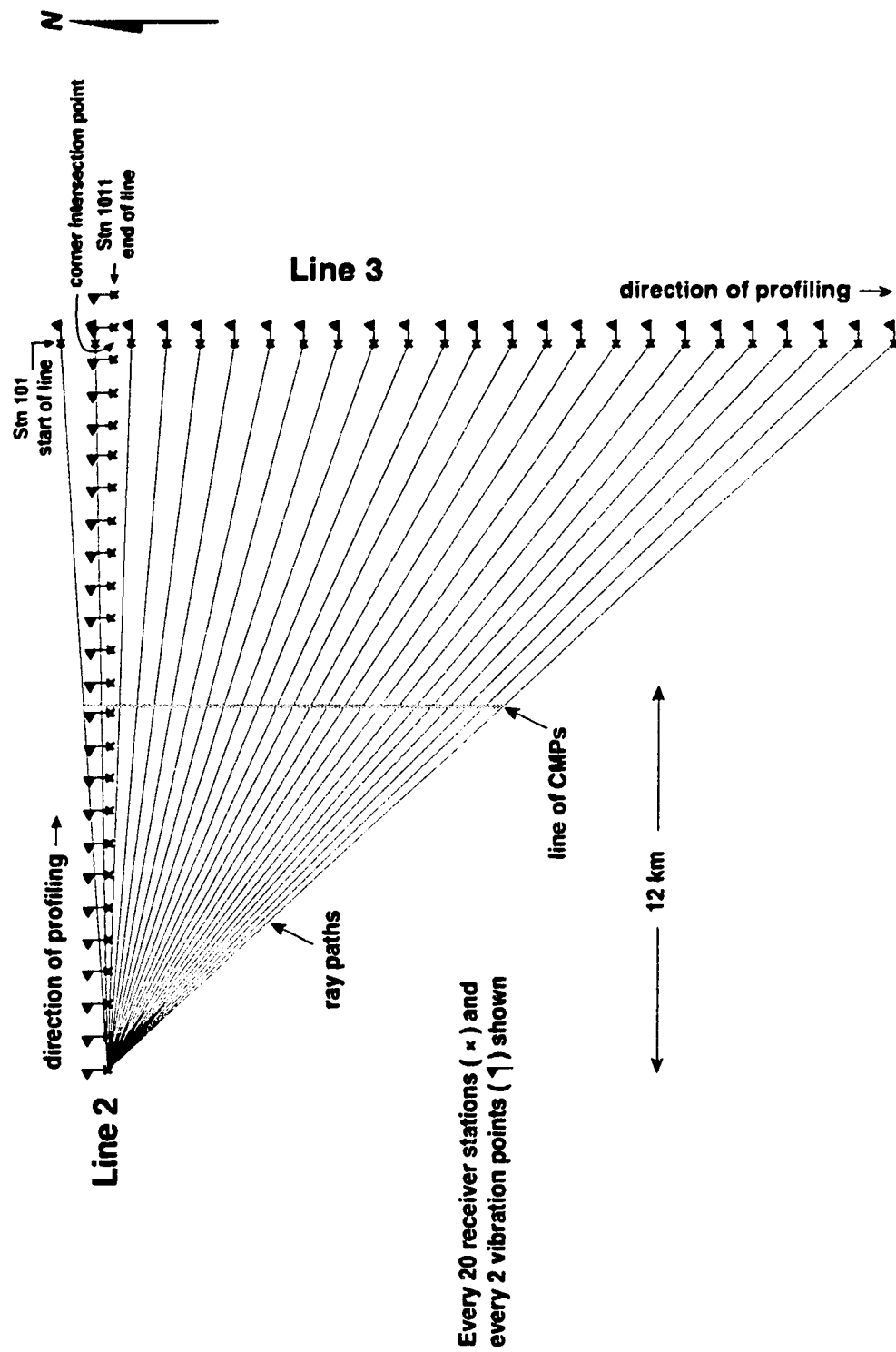
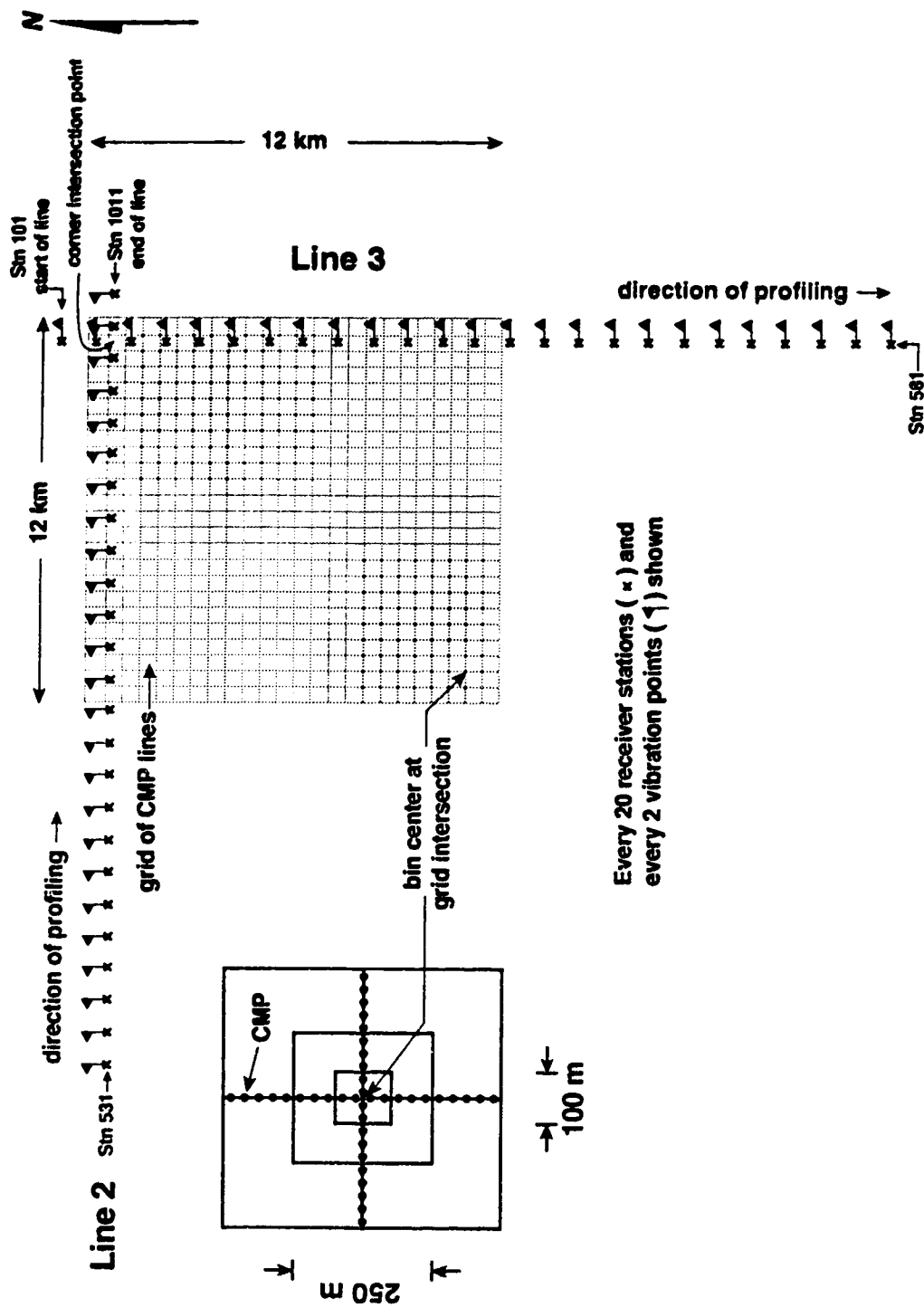


Figure 5.5 A set of vibrators on Line 2 recorded at the beginning of Line 3 (fan, or broadside geometry) will result in a line of common-mid-points(CMPs) parallel to the receiver line. Vibrators on Line 3 with recording on Line 2 gives a perpendicular line of CMPs. During field acquisition, 480 receivers were used for the special experiment.

obtained a set of north-south CMP lines. Thus we had a 3-dimensional grid of CMPs that could be bin stacked. Veritas was able to supply 480 channels for this experiment and with only 49 extra vibration points (minimal extra cost) on each perpendicular segment (VP interval was 500 m), we achieved a 49x49 grid of 2000% bins (250 m x 250 m), or a 121x121 grid of 800% bins (100 m x 100 m, in a 12 km x 12 km area (see Figure 5.6). The larger bins, of course, have a higher signal-to-noise ratio, but at the same time if there is any appreciable geological dip a certain amount of 'smearing' can be expected during summation. Smaller bins mitigate against that, at the expense of a smaller theoretical signal-to-noise ratio.

This special experiment (as well as the expanding spread described below) required VHF radio transmission (for control of vibrators) over distances much longer than required in the usual seismic reflection recording. During testing, Veritas discovered that the sweep start triggering tone was not regularly received by all vibrators at maximum vibrator/recorder distances. They solved this problem by mounting a large telescoping mast with a 6db gain directional antenna to the recorder, increasing reception to acceptable levels. With technical difficulties solved, acquisition proceeded normally.

A separate processing stream was followed for this special experiment. For instance, the three-dimensional data, had to have a three-dimensional geometry applied for sorting and stacking of traces into the appropriate bins. Two bin sizes, 250x250 m and 100x100 m, were used. The smaller bins were considered to image reflections better, despite their smaller fold, due to the smaller spatial spread - that is dip effects were less pronounced over a smaller area. Since the actual sites of VPs and recording stations are identical to the regular profiles, the same refraction derived and residual static corrections could be applied to the 3-dimensional data. A process of residual trim statics was also used to remove random static variations still in the data. Random noise attenuation, bandpass filtering and scaling, and a finite-difference migration were run



Every 20 receiver stations (x) and
every 2 vibration points (1) shown

Figure 5.6 With 480 receiver stations and a perpendicular line of 50 vibrator points, we get a 12kmX12km grid of CMPs. Three-dimensional stacking bins of 250mX250m have 2000% redundancy while 100mX100m bins have 800% fold but with less smearing due to geological dip.

after stack.

Figures 5.7 and 5.8 show migrated and coherency filtered (a method of simplifying the reflection profile, leaving only the stronger reflected energy) plots of Line 2 and 3, in whose east/north intersection corner lies the 3-dimensional data set. The Moho is interpreted to lie at 12-14 s (approximately 35-45 km depth), at the base of the zone of strong reflectivity.

Between 5-7 s there are a set of horizontal high amplitude arrivals of uncertain origin and significance [Ross *et al.*, in submission]. The reflective structure, seen on the east end of line 2, was recognized on the 3-d data as well and a top and bottom of the structure has been mapped by Dubuc [1994] and shown in Figures 5.9 and 5.10. The top of the structure has a depth differential (assuming 6000 m/s average crustal velocity) of 600 m and a northwest-southeast trend. The bottom of the structure has a 550 m variation in depth and a synformal structure. Neither trends, in present interpretations, have any correspondence with other geophysics, including aeromagnetics (Figure 5.1).

As well, the bottom of the crust has been picked (Figure 5.11). The time structure varies from 14 to 14.5 s over the 144 square km area, and there is a tendency towards deeper Moho to the east. But, the small area of the three-dimensional grid doesn't allow a great deal of interpretation of the Moho. It does point out, however, the possibilities of mapping deep structure with the three-dimensional reflection technique.

5.4 Velocity determination using long offset expanding spread data

In addition to the three-dimensional experiment, it was decided to investigate the possibility of using vibrators and reflection arrays to record longer offset data for increased velocity resolution. The desired offset for reliable velocity measurement to Moho depths, as a rule-of-thumb would be on the same order as the expected crustal

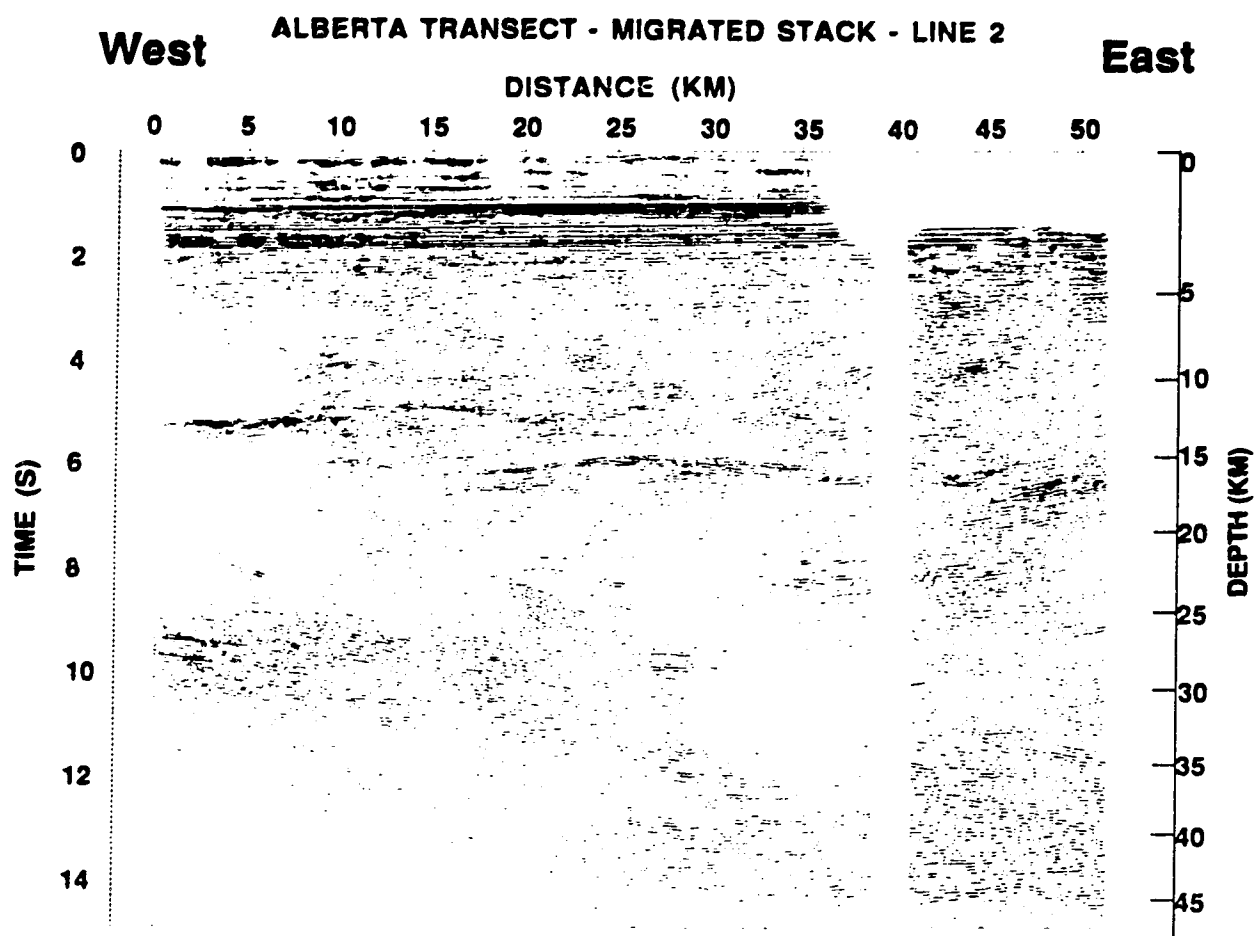


Figure 5.7 Migrated and coherency filtered line 2. The three-dimensional coverage is over the last 12 km (easternmost) of the profile.

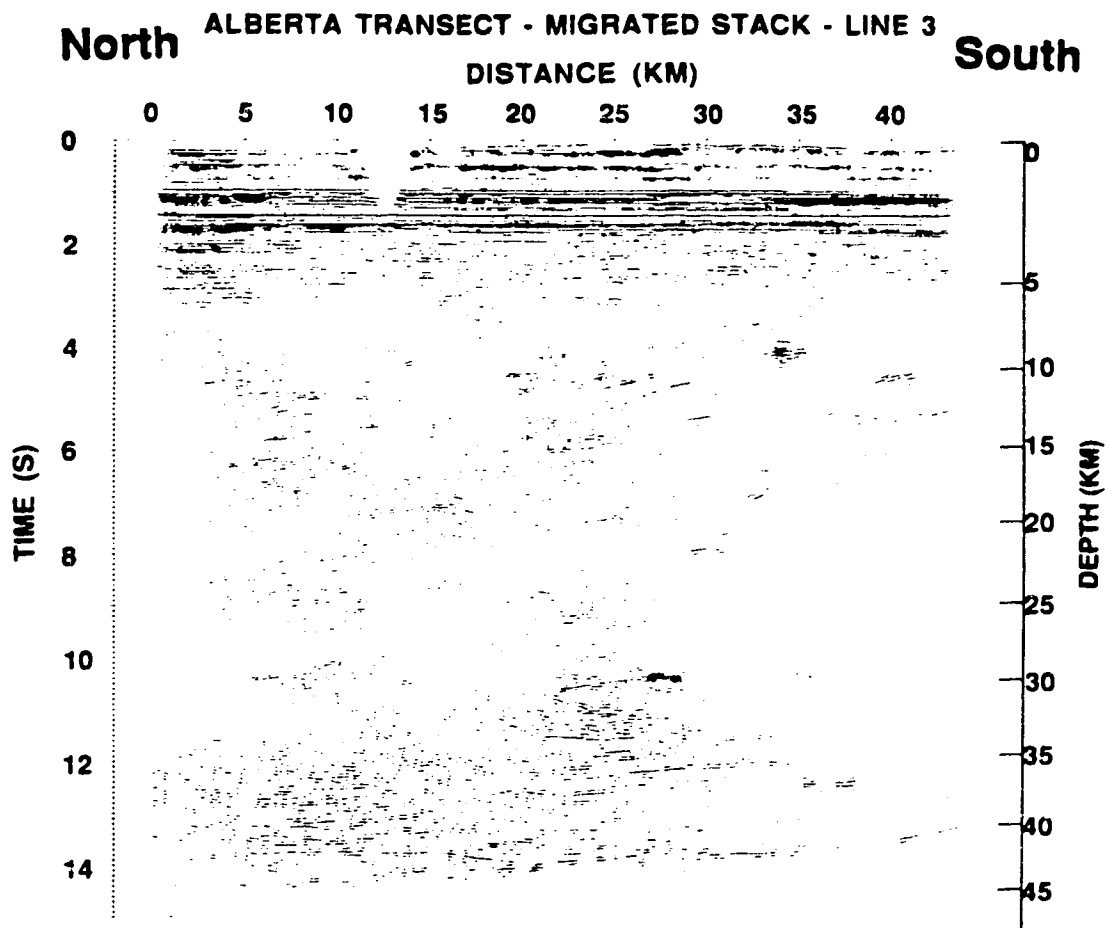


Figure 5.8 Migrated and coherency filtered line 3. The three-dimensional coverage is over the first 12 km (northernmost) of the profile.

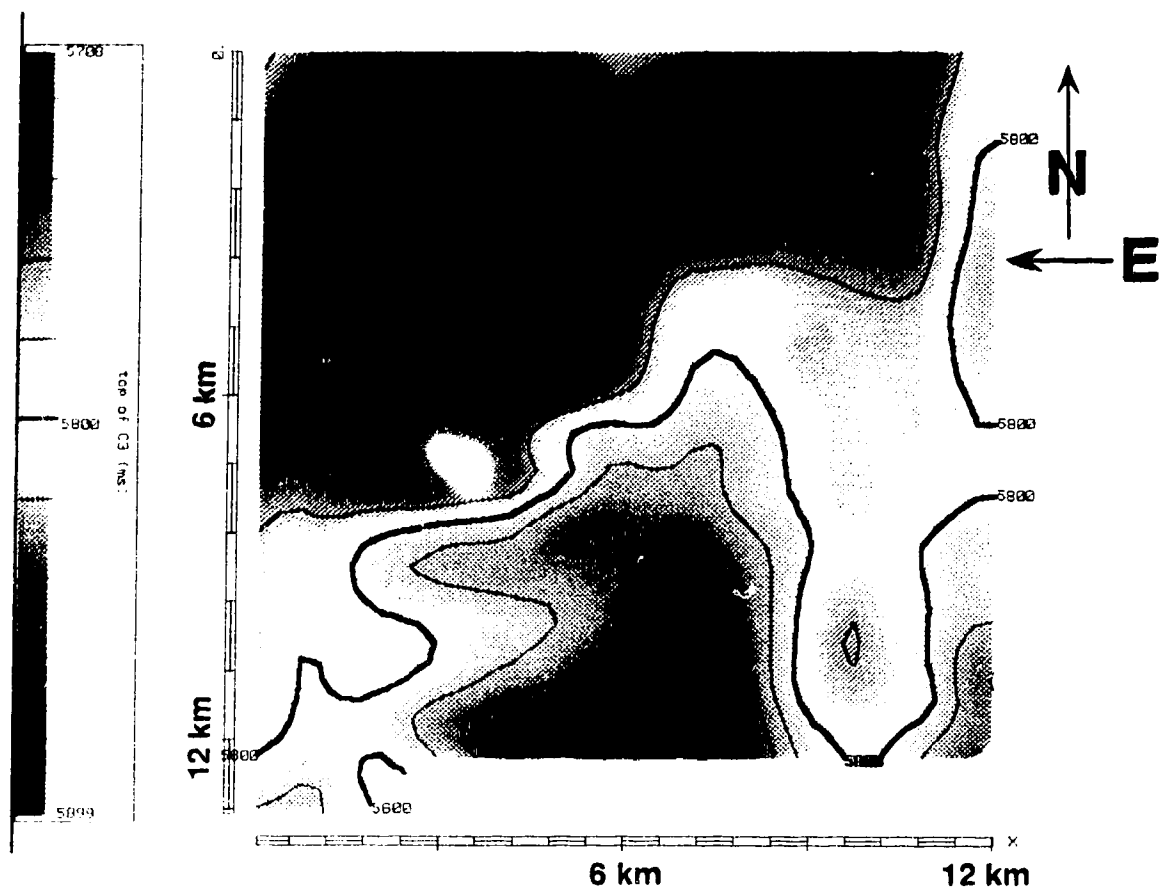
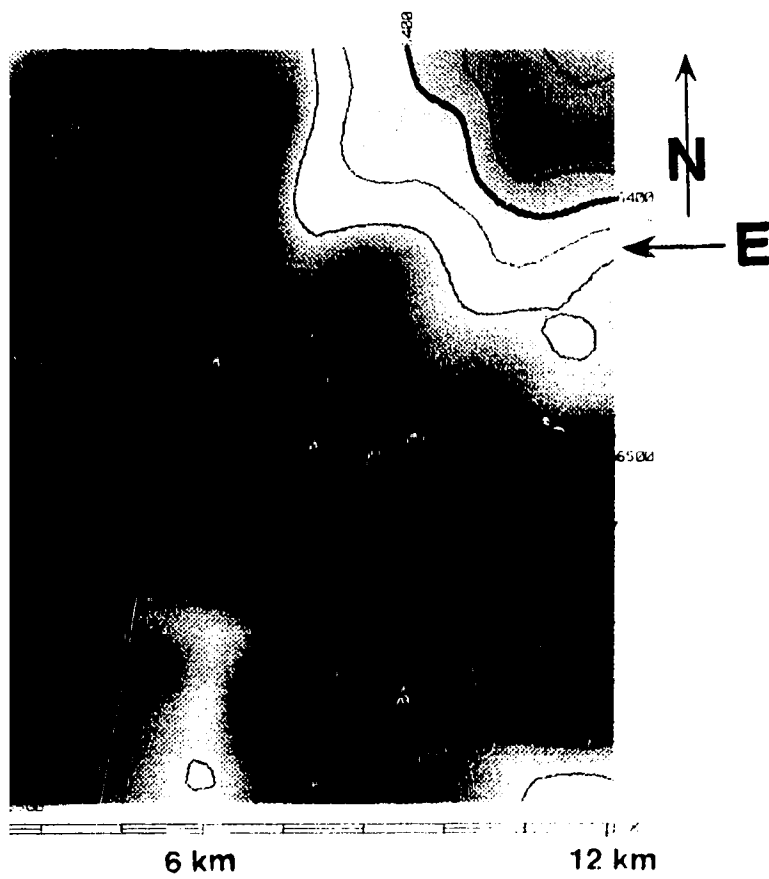


Figure 5.9 Time structure map of the top of the mid-crustal horizontal reflector imaged on the 3-d data set.



up of the bottom of the mid-crustal horizontal reflector

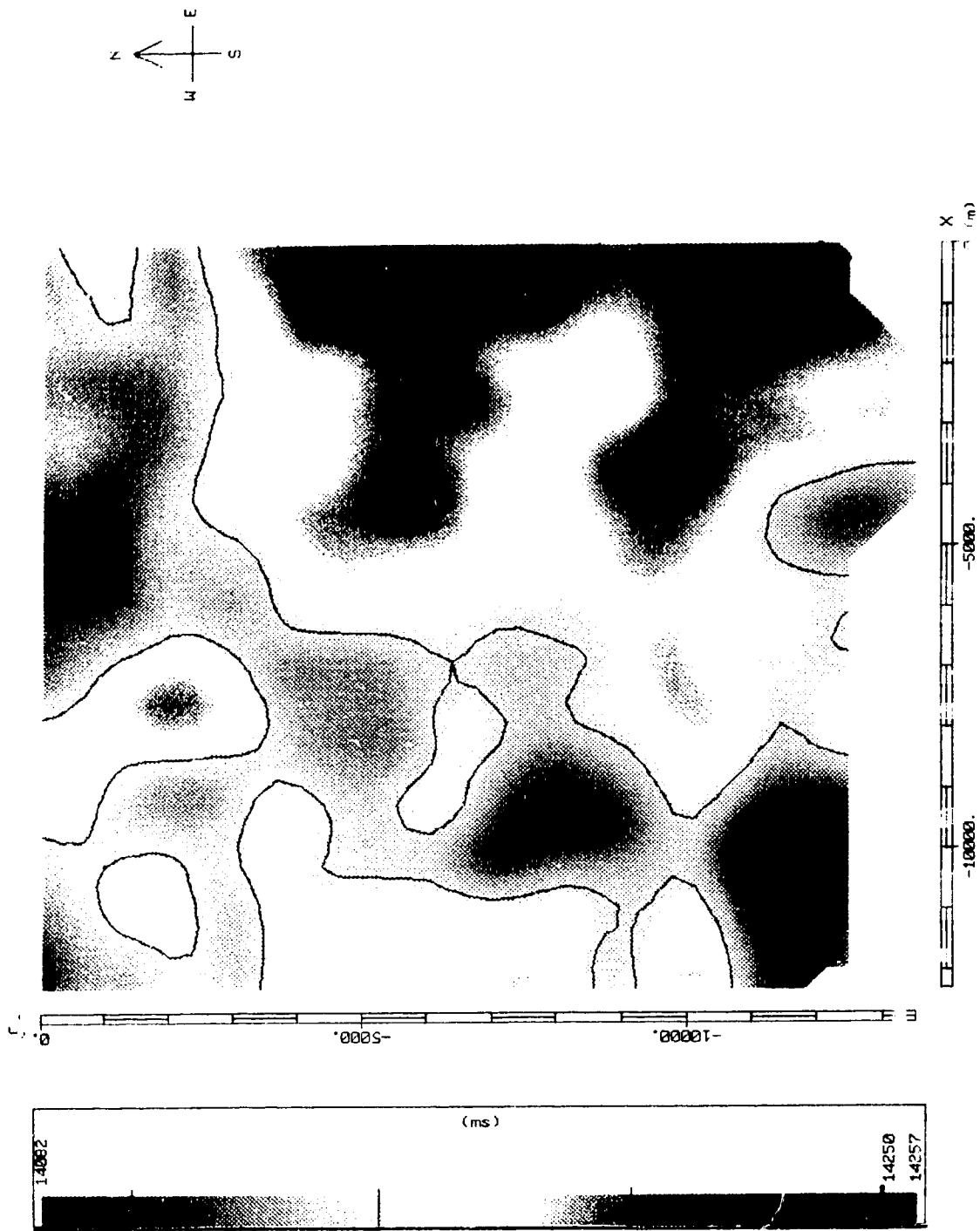


Figure 5.11 Time structure map of the bottom of the crust imaged on the 3-d data set.

thickness (40-45 km). The experiment was conducted by planning an expanding spread profile (ESP) that would be acquired along with the regular 2-D CMP profiling so as to keep the costs down. Line 7 (Figure 5.1) was chosen as the region for the experiment as it had the requisite length (at least 54 km). Veritas was again able to make 480 channels available for this experiment and had earlier solved technical problems involved in control of the vibrators over long distances.

The ESP was acquired in four stages during the normal recording of the regular Line 7 reflection profile. When, in the course of regular profiling, the live seismic spread reached the location of a planned ESP, the vibrators would move up to an appropriate ESP vibration point. After tape changes in the recording truck and ESP data acquisition, the vibrators would then move back to continue the standard CMP profiling until the spread reached the next ESP location, at which time the vibrators were again moved to the appropriate ESP vibration point (Figure 5.12).

With the 480 channel geometry (over 24 km of live recording line) we recorded reversed ESP coverage over 18 km with only 32 additional vibrating points. There were four stages - four ESP spread locations - for which 8 records each, at different offsets, were recorded. To acquire the desired offsets of 48 km required both straight line length and clear communications over 54 km.

The ESP, having identical VP and station sites as the regular profiling, could have the earlier derived static correction used directly. Much of the other processing was similar to that of the standard profiles. Besides producing a structure stack, Pulsonic also made several constant velocity stacks (where a single constant velocity was used for NMO corrections) which gave a first approximation to the crustal velocity field measured by the experiment.

As a preliminary interpretation of the velocity field underneath Line 7 (Figure 5.1 and 5.13), the constant velocity stacks were analysed to provide interval velocity with

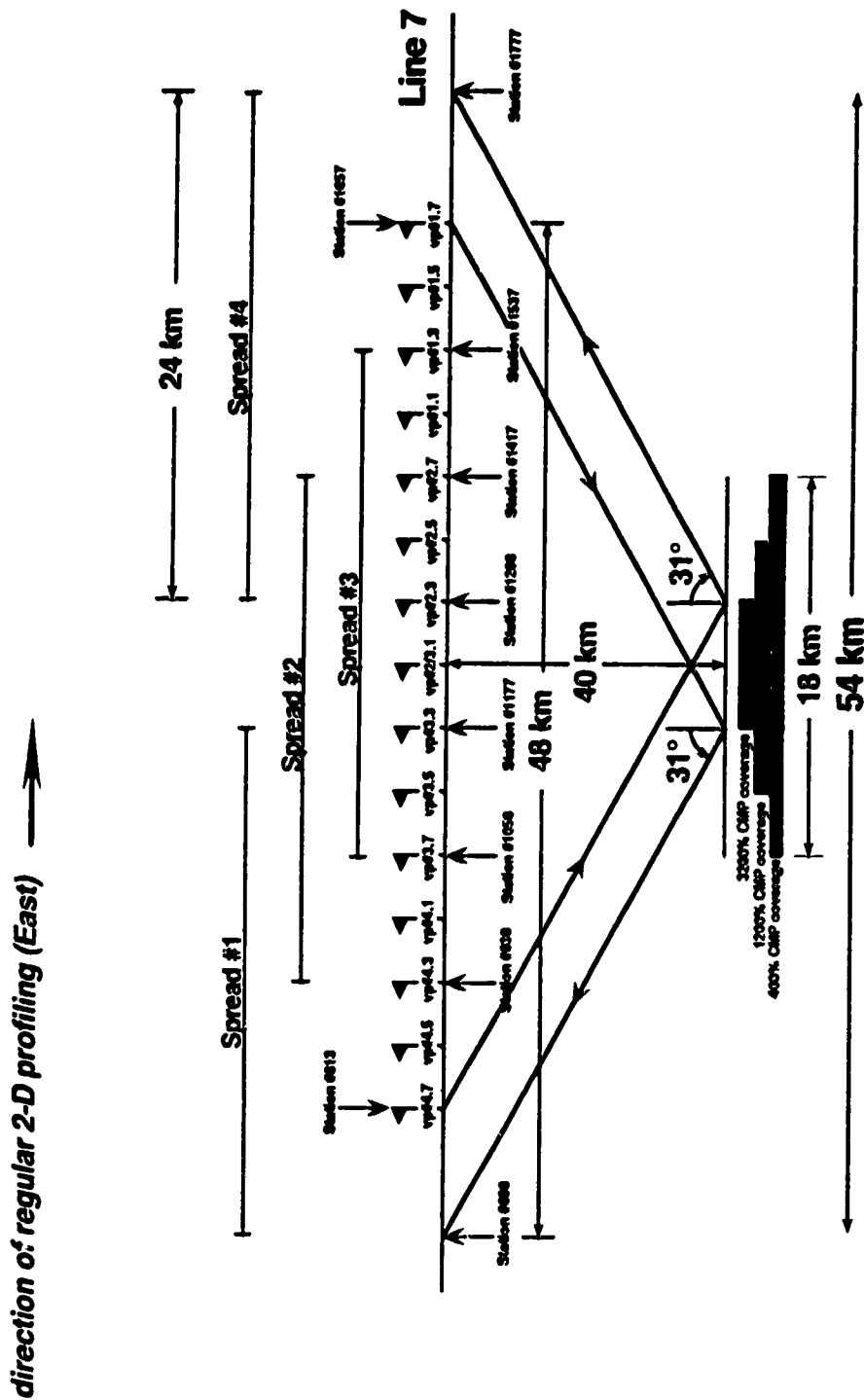


Figure 5.12 Schematic of expanding spread profile (ESP) acquired simultaneously with regular 2-D reflection profiling. When, during regular profiling, the recording spread reaches the location of a planned ESP spread, the vibrators are moved ahead to the appropriate ESP vibration points (VP). After recording the ESP records, the vibrators are moved back and the regular recording is resumed until the next ESP spread location is reached. Note that Spread #n corresponds to VP # n.1 to n.8. Also, each VP pictured is actually two independent VPs one station apart. This setup required a line at least 54 km long. Maximum source receiver offset is 48 km

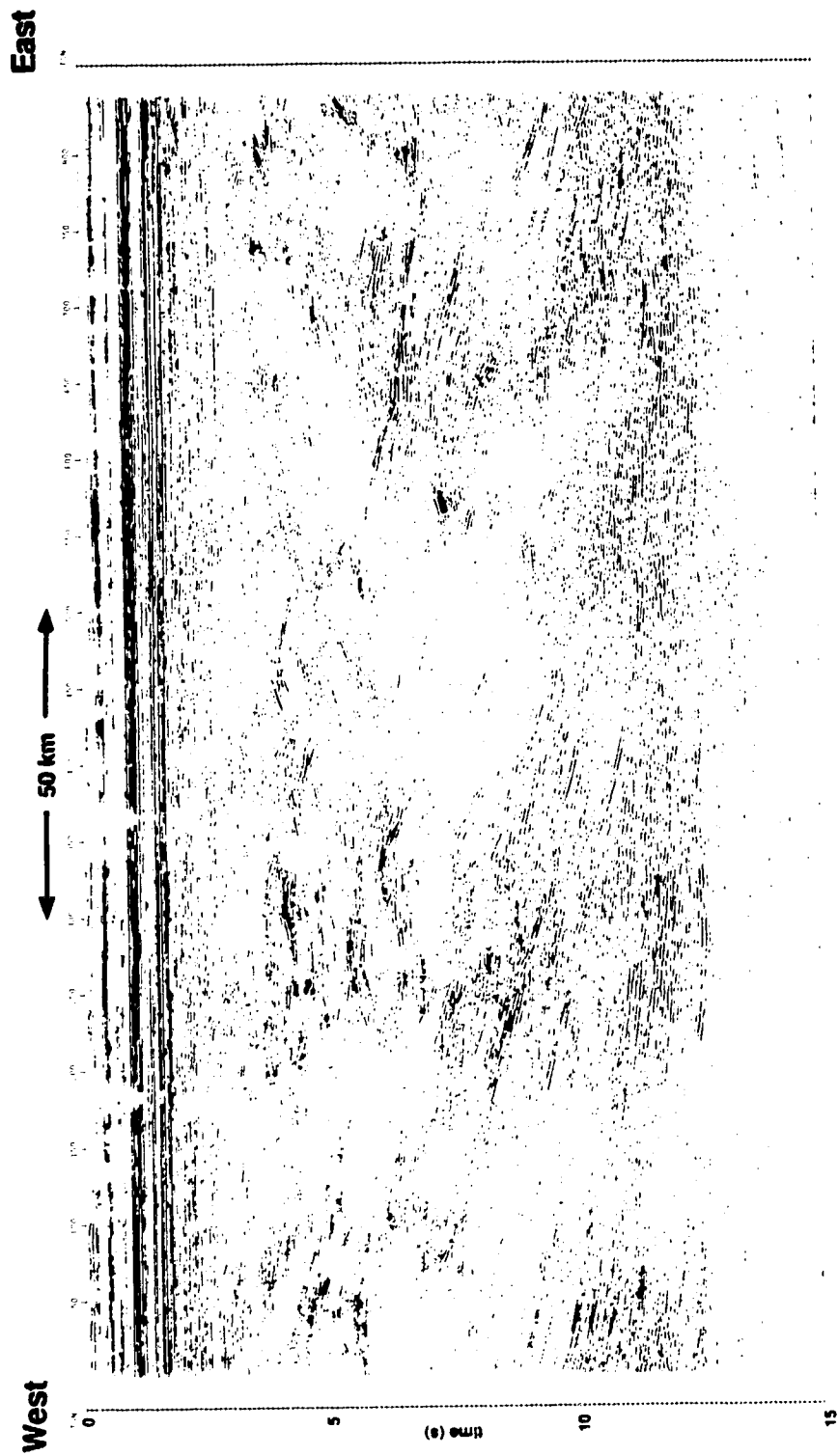


Figure 5.13 Migrated and coherency filtered line 7. The ESP coverage is over the 50 km marked at the top of the diagram.

depth. The root-mean-square velocity (V_{rms}) measured from the constant velocity stack sections can be transformed into interval velocities by use of the well known Dix formula [Dix, 1955]. The time/velocity information and calculated depths and interval velocities is given in Table 5.1 and plots of these values are shown in Figure 5.14.

Certainly, the velocities in Table 5.1 and Figure 5.14 do seem somewhat higher than expected from refraction data 200 km further to the south, looking at Figure 2.22f for example. The interval velocity of 7300 m/s between 8.7 and 11.6 km depth is high for crustal rocks at this depth. This interval, however, is associated with a distinctive region of layered reflections (Figure 5.13) which may indicate a mafic (i.e. high velocity) intrusion at that level. There is no magnetic high associated with Line 7 (Figure 5.1), but the depths in question may already be below the point at which the Curie temperature is reached. The average velocity of the entire crust, as calculated from Table 5.1, is 6.9 km/s. This is a high value, but it is still well within the range of global crustal average velocities of 5.8 to 7.0 km/s [Smithson *et al.*, 1981]. The crustal thickness is 42.9 km, which is not inconsistent with our previous estimates or compiled in Figure 2.22f. These calculations can only be considered as preliminary until a more sophisticated analysis can be carried out.

5.5 Summary

Careful planning and supervision of commercial seismic reflection acquisition and processing contractors has resulted in high quality seismic reflection and experimental data sets over central Alberta, the first of three Alberta Basement Transect reflection acquisition stages. The standard deep reflection profiling has imaged seismic reflectors which indicated that the Alberta basement rocks are the remnants of an early Proterozoic orogen.

Along with the 500 km of standard reflection data, an inexpensive method of three-dimensional data acquisition has succeeded in delineating a fuller structure of several prominent crustal reflectors. A second special experiment, a very wide aperture expanding spread has given a preliminary velocity structure in one region of the profiled crust. Here, indications are that crustal velocities may be somewhat higher than previously thought. Moho depth is measured to be at 43 km below the surface, the expected depth.

Table 5.1 Crustal velocity function for line 7 of the Alberta Basement Transect expanding spread profile

	Time (s)	V_{RMS} (m/s)	V_{INT}	Depth* (m)
1	0.0	2000		0
2	0.5	3000	2500	600
3	1.0	3500	3950	1600
4	2.0	4000	4450	3900
5	2.5	4500	6100	5400
6	3.6	5000	6000	8650
7	4.4	5500	7300	11600
8	6.6	6000	6900	19170
9	8.5	6250	7000	25800
10	10.5	6500	7450	33300
11	13.0†	6750	7700	42900
12	15.5	7000	8200	53150

* below datum level of 920 m

† Moho level

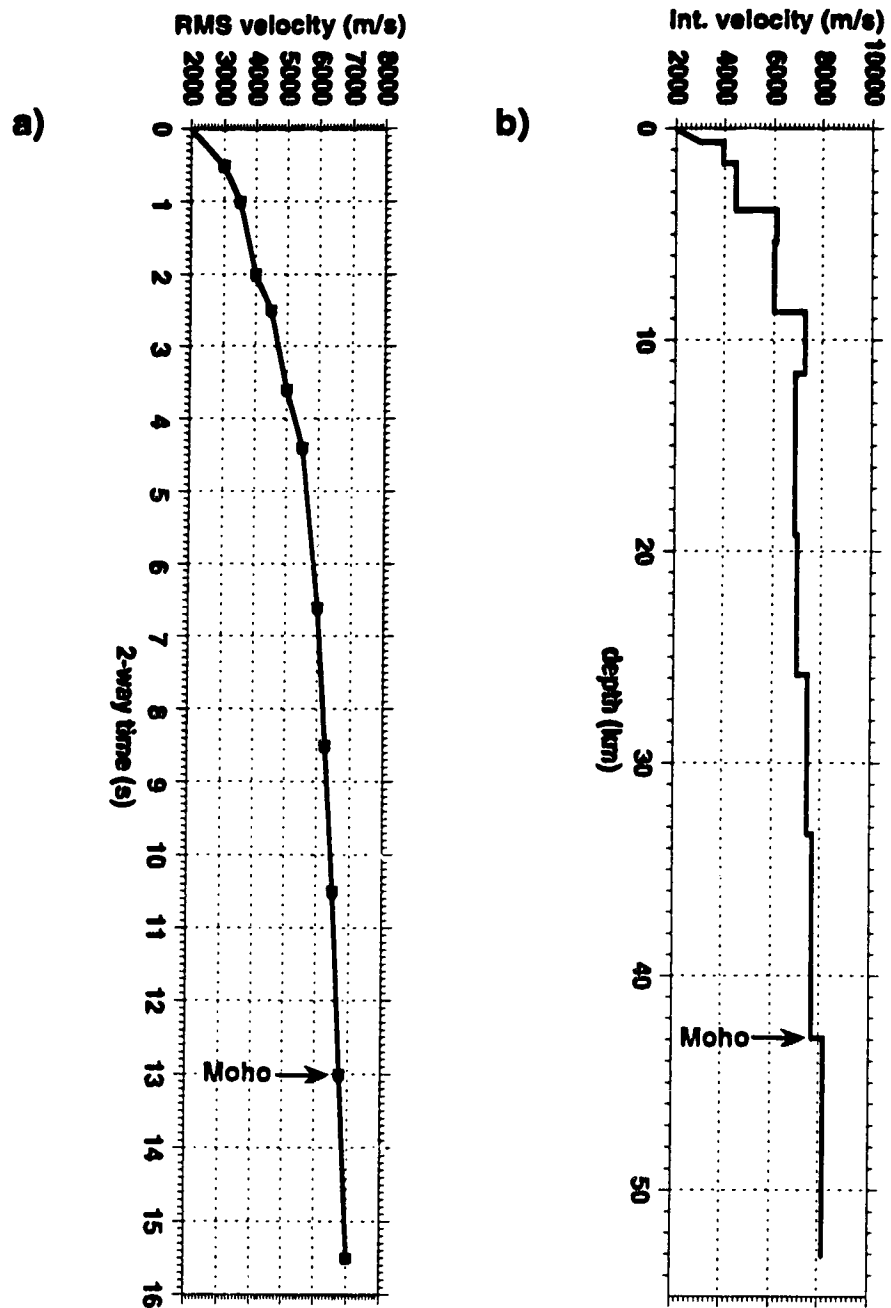


Figure 5.14 Plots of Alberta Basement Line 7 ESP a) root-mean-square velocity function and b) resulting interval velocity function from Table 5.1.

Chapter 6 Conclusion

6.1 Cordilleran Wide-Angle Experiments

The SCoRE '90 line 8 and line 7 seismic wide-angle reflection/refraction profiles indicate that in the southeastern Canadian Cordillera, the Moho lies at 35-36 km and that the average crustal velocity is 6.2 km/s. Both crustal thickness and average velocity are lower than in surrounding regions of North America. Generally, the crust thickens slightly from north to south, and more so from west to east. Velocity gradients decrease with depth in the upper crust, and a velocity inversion (low velocity zone) exists at the mid-crustal level over much of the south-eastern Cordillera. An upper mantle zone is also defined by the data, between 35-36 and 49 km depth. There is good agreement between the interpreted velocity field from the wide-angle data and the previously analyzed vertical incidence seismic reflection data. The given velocity models also fit well with other wide-angle results in the same and neighboring regions. For the most part, the imaged velocity structure establishes the similarities between the seismic response of the south-east Cordillera with that of the Basin and Range. Whether there are genetic similarities as well has not been entirely determined, though there are suggestions that related deep seated tectonic forces are influencing both regions.

A very significant part of the data analysis is the recognition of the correspondence between the velocity models and the thermal structure of the crust. It is evident that the region's high heat flow has, in some way, modified the elastic properties of the crust in such a way that the velocity profile is a partial reflection of the regional temperature profile.

This illustrates an important point concerning the geophysical study of any part of the earth. The low velocity zone, and its possible correspondence with heat flow, is not a

characteristic that can easily be imaged by the seismic reflection method. That is, interpretation of one type of data cannot reasonably be done without resort to data from other methods for more complete measurements of physical properties. It also shows that there is a good case, in such programs such as LITHOPROBE, to perhaps divert some of the massive resources budgeted to reflection profiling towards more sophisticated refraction/wide-angle studies and other geophysics (EM and heat flow, for instance).

Also significant is the observation that the considerable lateral velocity changes, especially in the upper crust, can be associated with large scale geologic structures. In fact, the often excellent agreement between the interpreted velocities and the reflectivity data suggests that high resolution refraction experiments have the ability to delineate local crustal anomalies.

One path of future research may lie in a more thorough investigation of the above claim. Though the spatial correlation between fault structures in the upper crust and low velocity anomalies is high, there is still some question whether the method employed here can resolve the features given the density of shotpoints and receivers. The question hinges on how wide the deformed zone about a fault or shear zone actually is, and by how much are the elastic parameters changed by the deformation. The question can be partly investigated by high resolution numerical modelling experiments using finite difference codes. Such codes, running on unix workstations have been developed at the University of Alberta Seismology Laboratory [Dai, 1993] and are fast enough to simulate long-offset seismic experiments through the upper crust. Such work is in the very initial stages, and not even preliminary results are available.

At any rate, it seems that wide-angle seismic experiments, such as SCoRE '90, are well on the way to bridging the gap between the traditional seismic exploration methods of refraction and reflection.

6.2 Cordilleran broadside experiment

The three-dimensional broadside records from the south-eastern Cordillera brought a certain amount of innovation to the SCoRE program. The extra east-west profile and the direct measurements of Moho depth, along with the two-dimensional results, allowed the compilation of a relatively high resolution map of Moho structure in this region. A map of such a type allowed the direct comparison of seismically derived characteristics with other geophysical maps in such a way not easily done with only information from cross-sections.

Perhaps more importantly, though, was the totally unexpected recording of a major sub-mantle seismic arrival. Analysis of this phase added another observation that corroborates the hypothesis of a very shallow lithosphere in our study area. And not only was it interesting to observe that this arrival was so obvious on broadside records and almost invisible on the in-line records, but it very clearly makes the point that unexpected results are often the hallmark of doing things a little differently. It is also clear that there is sufficient grist for further experiments in the future.

6.3 Seismic Power Density

The mapping of earthquake activity (seismicity) by a transformation to the density of power emission allows a greater ease of comparison with other geologic and geophysical compilations. Good correlations are made between aseismic regions and two major superterranes of the Cordillera and also between major faults and regions with high seismic energy emissions. The large uncertainties in some of the raw data (that is epicenters and magnitudes) only underscores the potential for seismic power density representations. As the number of seismic instruments increase, as the number of events

recorded increases, and as other geophysics increases the resolution of fundamental earth models used in epicentral determination, the power density map will become of higher resolution and of sharper focus. With increased reliability of the determination of focal depths, the technique could even be extended to the presentation of seismic power density profiles.

One striking advantage of the power density transformation over that of traditional seismicity maps, besides that of increased clarity, is the fact that the seismicity values are converted into a two-dimensional (even conceivably a three-dimensional) physical data sequence that is amenable to further digital processing, analysis and image enhancement. Some preparatory work at the University of Alberta Seismology Laboratory has already been done with first and second derivatives of the power density field.

6.4 Alberta Basement reflection experiments

High quality seismic reflection data from central Alberta have been obtained through careful attention to acquisition and processing parameters. As important as these reflection profiles are, possibly the special experiments were as important. It has been verified that useful three-dimensional reflection data can be recorded for crustal studies. It has equally been shown that crustal velocity information can be acquired with standard reflection profiling equipment, in an almost routine manner. Both three-dimensional and velocity information can be obtained relatively inexpensively.

Being the nature of an experiment, our experience also underlines the importance of reconnaissance surveys before planning special recordings. Both the three-dimensional and ESP spreads were located mainly on logistical grounds and though both data sets contain interesting information, study of the regular profiles shows where it would have been much more worthwhile to locate the experiments. More three-

dimensional and expanding spread work is planned for future Alberta Basement Transect profiles, and will be acquired after preliminary analysis of the regular profiling.

For the existing ESP data, upcoming work will include detailed, lateral semblance velocity analyses. As well, since the standard line 7 reflection profile shows a large number of reflection packages, the data can be analysed by ray-trace model based methods similar to the refraction/wide-angle interpretation in the south-east Cordillera.

A successful completion of the ESP work will mean the development of an alternative, low environmental impact, technique for measuring crustal velocities. It cannot yet replace refraction experiments, since it lacks deep penetrating refracted (turning) waves, but it could be viewed as another step in the synthesis of new crustal sensing methods from the reflection/refraction extremes.

Bibliography

- Abbot, H. L., On the velocity of transmission earth waves, *Amer. J. Sci. Arts, Ser. 3*, **15**, 178-184, 1878.
- Adams, John and Peter W. Basham, 1989, Seismicity and Seismotectonics of Canada's Eastern Margin and Craton, in *Earthquakes at North-Atlantic Passive Margins: Neotectonics and Postglacial Rebound*, edited by S. Gregersen and P. W. Basham, Kluwer Academic Publishers, Boston, p.355-370.
- Armstrong, R. L., Cordilleran metamorphic core complexes - from Arizona to southern Canada, *Annual Review of Earth and Planetary Sciences*, **10**, 129-154, 1982.
- Asudeh, I., R. Wetmiller and C. Spencer, The LithoSEIS User Manual. Geological Survey of Canada Open File No. 2679, 1993.
- Atwater, Tanya, Implications of plate tectonics for the cenozoic tectonic evolution of western North America, *Geological Society of America Bulletin*, v. **81**, p. 3513-3536, 1970.
- Atwater, Tanya, Plate tectonic history of the northeast Pacific and western North America, in *The Geology of North America, The Eastern Pacific Ocean and Hawaii*, Volume N, edited by E. L. Winterer, D. M. Hussong and R. W. Decker, Geological Society of America, Boulder, p. 21-72, 1989.
- Atwater, Tanya and Jeff Severinghaus, 1989, Tectonic Maps of the Northeast Pacific, in *The Geology of North America: The Eastern Pacific Ocean and Hawaii*, Volume N, edited by E. L. Winterer, Donald M. Hussong and Robert W. Decker, Geological Society of America, Boulder, p.15-20.
- Avé Lallemant, H. G. and J. S. Oldow, Early mesozoic southward migration of cordilleran transpressional terranes, *Tectonics*, **7**, 1057-1075, 1988.
- Basham, P. W., Weichert, D. H., Anglin, F. M. and Berry, M. J., New probabilistic strong seismic ground motion maps of Canada, *Bull. Seismol. Soc. Am.*, **75**, 563-595, 1985.
- Berry, M. J., W. R. Jacoby, E. R. Niblett and R. A. Stacey, A review of geophysical studies in the Canadian Cordillera, *Can. J. Earth Sci.*, **8**, 788-801, 1971.
- Berry, M. J. and D. A. Forsyth, Structure of the Canadian Cordillera from seismic refraction and other data, *Can. J. Earth Sci.*, **12**, 182-208, 1975.
- Bennet, G. J., R. M. Clowes, and R. M. Ellis, A seismic refraction survey along the southern Rocky Mountain Trench, *Bull. Seismol. Soc. Am.*, **68**, 37-54, 1975.

- Benz, H. M., R. B. Smith, and W. D. Mooney, Crustal structure of the northwestern Basin and Range province from the 1986 Program for Array Seismic Studies of the Continental Lithosphere seismic experiment, *J. Geophys. Res.*, **95**, 21,823-21,842, 1990.
- Bullen, K. E., *An introduction to the theory of seismology*, Cambridge University Press, Cambridge, 381 pp., 1963.
- Burianyk, M. J. A., E. R. Kanasewich, R. M. Ellis, and R. M. Clowes, *SCoRE '90: southern Cordillera refraction experiment field report and data set description*, Lithoprobe Rep. 21, 30 pp. LITHOPROBE Secretariat, University of British Columbia, Vancouver, 1992.
- Burianyk, M. J. A., E. R. Kanasewich and N. Udey, Crustal velocity structure of the Omineca and Intermontane belts, southeastern Canadian cordillera, in submission.
- Carr, S. D., R. Parrish, and R. L. Brown, Eocene structural development of the Valhalla Complex, southeastern British Columbia, *Tectonics*, **7**, 75-196, 1987.
- Catchings, R. D. and W. D. Mooney, Crustal structure of the Columbia Plateau: Evidence for continental rifting, *J. Geophys. Res.*, **93**, 459-474, 1988.
- Catchings, R. D. and W. D. Mooney, Basin and Range crustal and upper mantle structure, northwest to central Nevada, *J. Geophys. Res.*, **96**, 6247-6267, 1991.
- Chandra, N. N., and G. L. Cumming, Seismic refraction studies in western Canada, *Can. J. Earth Sci.*, **9**, 1099-1109, 1972.
- Christensen, N. I., Compressional wave velocities in rocks at high temperatures and pressures, critical thermal gradients and crustal low-velocity zones, *J. Geophys. Res.*, **84**, 6849-6857, 1979.
- Christensen, N. I., and W. W. Wepfer, Laboratory techniques for determining seismic velocities and attenuations, with applications to the continental lithosphere, in Geophysical framework of the continental United States, edited by L. C. Pakiser and W. D. Mooney, *Mem. Geol. Soc. Am.*, **172**, 91-102, 1989.
- Clowes, R. M. (editor), *LITHOPROBE Phase IV Proposal - Studies of the Evolution of a Continent*, LITHOPROBE Secretariat, University of British Columbia, Vancouver, 290 pp., 1993.
- Coney, P. J., D. L. Jones, and J. W. H. Monger, Cordilleran suspect terranes, *Nature*, **288**, 329-333, 1980.
- Cook, F. A., A. G. Green, P. S. Simony, R. A. Price, R. Parrish, B. Milkereit, P. L.

- Gordy, R. L. Brown, K. C. Coffin, and C. Patenaude, Lithoprobe seismic reflection structure of the southeastern Canadian Cordillera: Initial results, *Tectonics*, **7**, 157-180, 1988.
- Cook, F. A., J. L. Varsek, R. M. Clowes, E. R. Kanasewich, C. S. Spencer, R. R. Parrish, R. L. Brown, S. D. Carr, B. J. Johnson, and R. A. Price, Lithoprobe crustal reflection cross section of the southern Canadian Cordillera 1: Foreland thrust and fold belt to Fraser River fault, *Tectonics*, **11**, 12-35, 1992.
- Cumming, W. B., R. M. Clowes, and R. M. Ellis, Crustal structure from a seismic refraction profile across southern British Columbia, *Can. J. Earth Sci.*, **16**, 1024-1049, 1979.
- Cerveny, V., Molotkov, I and Psencik, I., *Ray method in seismology*, Charles University Press, 1977.
- Dai, Nanxun, Finite difference simulation and imaging of seismic waves in complex media, unpublished Ph.D. thesis, University of Alberta, 1993.
- Davis, E. E. and T. J. Lewis, Heat Flow in a Back-Arc Environment: Intermontane and Omineca Crystalline Belts, Southern Canadian Cordillera, *Can. J. Earth Sci.*, **21**, 715-726, 1984.
- Debiche, M. G. A. Cox and D. Engebretson, The motion of allochthonous terranes across the north Pacific basin, *Geol. Soc. Am, Special Paper*, **207**, 49 pp., 1987.
- Dix, C. H., Seismic velocities from surface measurements, *Geophysics*, **20**, 68-86, 1955.
- Dobrin, M. B. and Savit, C. H., *Introduction to Geophysical Prospecting*, 4th ed., McGraw-Hill, New York, 1988, 867 pp.
- Dubuc, G., Alberta basement lithoprobe transect three-dimensional seismic imaging of mid-crustal structures, unpublished M.Sc. project report, University of Alberta, Spring, 1994.
- Eaton, Gordon P., The Basin and Range province: origin and tectonic significance, *Annual Review of Earth and Planetary Sciences*, **10**, 409-440, 1982.
- Engebretson, David C., Allan Cox and Richard G. Gordon, Relative motions between oceanic and continental plates in the Pacific basin, *Geological Society of America, Special Paper*, **206**, 59 pp., 1985.
- Fedotov, S. A., Regularities of the distribution of strong earthquakes in Kamchatka, the Kurile Islands and northeastern Japan, *Tran. Acad. of Sci. USSR, Inst. Phys Earth*, **36**, 66-93, 1965.

- Fessenden, R., Methods and apparatus for locating ore bodies, U.S. Patent Application, January 15, 1917.
- Forsyth, D. A., M. J. Berry and R. M. Ellis, A refraction survey across the Canadian Cordillera at 54°N, *Can. J. Earth Sci.*, **11**, 533-548, 1974.
- Frost, B. R., W. S. Fyfe, K. Tazaki, and T. Chan, Grain-boundary graphite in rocks and implications for high electrical conductivity in the lower crust, *Nature*, **340**, 134-136, 1989.
- Fuis, G. S., E. L. Ambos, W. D. Mooney, N. I. Christensen, and E. Geist, Crustal structure of accreted terranes in southern Alaska, Chugach Mountains and Copper River Basin, from seismic refraction results, *J. Geophys. Res.*, **96**, 4187-4227, 1991.
- Fowler, C. M. R., *The Solid Earth, an Introduction to Global Geophysics*, Cambridge University Press, New York, 1990, 472 pp.
- Fuchs, K. and G. Muller, Computation of synthetic seismograms with the reflectivity method and comparison with observations, *Geophys. J. R. Astr. Soc.*, **23**, 417-433, 1971.
- Gabrielse, H., Major dextral transcurrent displacements along the northern Rocky Mountain Trench and related lineaments in north-central British Columbia, *Geol. Soc. Am. Bull.*, **96**, 1-14, 1985.
- Gabrielse, H., and C. J. Yorath, DNAG #4, The Cordilleran Orogen in Canada, *Geosci. Can.*, **16**, 67-83, 1989.
- Giese, P., C. Prodehl and A. Stein (Eds.), *Explosion seismology in central Europe; data and results*, Springer-Verlag, Berlin, 429 pp., 1976.
- Geological Survey of Canada, Geophysics Division, 1989, Canadian Earthquake Epicenter catalog.
- Gough, D. I., Mantle upflow tectonics in the Canadian Cordillera, *J. Geophys. Res.*, **91**, 1909-1919, 1986.
- Gough, D. I. and Gough, W. I., Stress Near the Surface of the Earth, *Ann. Rev. Earth Planet. Sci.*, **15**, 545-566, 1987.
- Gough, D. I., and J. A. Majorowicz, Magnetotelluric soundings, structures and fluids in the southern Canadian Cordillera, *Can. J. Earth Sci.*, **29**, 609-620, 1992.
- Gutenberg, B. and Richter, C. F., Magnitude and energy of earthquakes, *Annali di*

Geofisica, 9, 1-15, 1956.

Gutenberg, B. and Richter, C. F., *Seismicity of the earth and associated phenomena*, Princeton University Press, Princeton, 273 pp. 1949.

Hales, A. L., and J. B. Nation, A seismic refraction survey in the northern Rocky Mountains: More evidence for an intermediate crustal layer, *Geophys. J. R. Astr. Soc.*, **35**, 381-399, 1973.

Hawman, R. B., R. H. Colburn, D. A. Walker and S. B. Smithson, Processing and inversion of refraction and wide-angle reflection data from the 1986 Nevada PASSCAL experiment, *J. Geophys. Res.*, **95**, 4657-4691, 1990.

Hoffman, Paul F., United plates of America, the birth of a craton: early proterozoic assembly and growth of Laurentia, *Ann. Rev. Earth Planet. Sci.*, **16**, 543-603, 1988.

Hoffman, Paul F., Precambrian geology and tectonic history of North America, in *The geology of North America - an overview*, ed. A.W. Bally and A. R. Palmer, *Geol. Soc. Am., The Geology of North America*, v. A, 447-512, 1989

Holbrook, S. W., The crustal structure of the northwestern Basin and Range province, Nevada, from wide-angle seismic data, *J. Geophys. Res.*, **95**, 21,843-21,869, 1990.

Hyndman, R. D., and Klemperer, S. L., Lower-crustal porosity from electrical measurements and inferences about composition from seismic velocities, *Geophys. Res. Lett.*, **16**, 255-258, 1989.

Hyndman, R. D., and P. M. Shearer, Water in the lower continental crust: Modeling magnetotelluric and seismic reflection results, *Geophys. J. Int.*, **98**, 343-365, 1989.

Irving, E. and P. J. Wynne, Paleomagnetic evidence for motions of parts of the Canadian Cordillera, *Tectonophysics*, **187**, 259-275, 1991.

Johnson, S. H. and R. W. Couch, Crustal structure in the north Cascade Mountains of Washington and British Columbia from seismic refraction measurements, *Bull. Seismol. Soc. Am.*, **60**, 1259-1269, 1970.

Johnston, Arch C., 1989, The Seismicity of 'Stable Continental Interiors', in *Earthquakes at North-Atlantic Passive Margins: Neotectonics and Postglacial Rebound*, edited by S. Gregersen and P. W. Basham, Kluwer Academic Publishers, Boston, p.299-327.

Jones, A. G., D. I. Gough, R. D. Kurtz, J. M. DeLaurier, D. E. Boerner, J. A. Craven, R.

- G. Ellis and G. W. McNeice, Electromagnetic images of regional structure in the southern Canadian Cordillera, *Geophys. Res. Lett.*, **12**, 2373-2376, 1992.
- Junger, A., Deep basement reflections in Big Horn County, Montana, *Geophysics*, **16**, 499-510, 1951.
- Kanasewich, E. R. and G. L. Cumming, Near vertical incidence seismic reflections from the 'Conrad' discontinuity, *J. Geophys. Res.*, **70**, 3441-3446, 1965.
- Kanasewich, E. R., Deep Crustal Structure under the Plains and Rocky Mountains, *Can. J. Earth Sci.*, **3**, 937-945, 1966.
- Kanasewich, E. R., Z. Hajnal, A. G. Green, G. L. Cumming, R. F. Mereu, R. M. Clowes, P. Morel-A-L'Huissier, S. Chiu, C. G. Macrides, M. Shahriar, and A. M. Congram, Seismic Studies of the crust under the Williston Basin, *Can. J. Earth Sci.*, **24**, 2160-2171, 1987.
- Kanasewich, E. R. and S. K. Chiu, Least-squares inversion of spatial seismic refraction data, *Bull. Seismo. Soc. Am.*, **75**, 865-880, 1985.
- Kanasewich, E. R., M. J. A. Burianyk, R. M. Ellis, R. M. Clowes, D. J. White, T. Côté, D. A. Forsyth, J. H. Luetgert and G. D. Spence, Crustal Velocity Structure of the Omineca Belt, Southeastern Canadian Cordillera, *J. Geophys. Res.*, **99**, 2653-2670, 1994.
- Karcher, J. C., The reflection seismograph: its invention and use in the discovery of oil and gas fields, *Geophysics: The Leading Edge of Exploration*, No. 11, **6**, 10-19, November, 1987.
- Keen, C. E. and R. D. Hyndman, Geophysical review of the continental margins of eastern and western Canada, *Can. J. Earth Sci.*, **16**, 712-747, 1979.
- Kelleher, J. A., Space-time seismicity of the Alaska-Aleutian seismic zone. *J. Geophys. Res.*, **75**, 5745-5756, 1970.
- Kelleher, J. A., Rupture zones of large South American earthquakes and some predictions. *J. Geophys. Res.*, **77**, 2087-2103, 1972.
- Kelleher, J. A., Sykes, L. R. and Oliver, J., Possible criteria for predicting earthquake locations and their application to major plate boundaries of the Pacific and Caribbean. *J. Geophys. Res.*, **78**, 2547-2585, 1973.
- Klemperer, S. L., A relation between continental heat flow and the seismic reflectivity of the lower crust, *J. Geophys.*, **61**, 1-11, 1987.

- Klemperer, S. L. and J. H. Luetgert, A comparison of reflection and refraction processing and interpretation methods applied to conventional refraction data from coastal Maine, *Bull. Seismol. Soc. Am.*, **77**, 614-630, 1987.
- Kohler, W. M, Seismic cassette recorder (SCR) playback and digitizing system for IBM AT compatible computers, United States Department of the Interior Geological Survey, Open-File Report 90-99, Menlo Park, 46 pp., 1990.
- Lambert, R. St. J. and V. E. Chamberlain, Cordillera revisited, with a three-dimensional model for Cretaceous tectonics in British Columbia, *J. Geol.*, **96**, 47-60, 1988.
- Leaver, D. S., W. D. Mooney, and W. M. Kohler, A seismic refraction study of the Oregon Cascades, *J. Geophys. Res.*, **89**, 3121-3134, 1984.
- Lewis, T. J., Heat flux in the Canadian Cordillera, In: D. B. Simmons, E.R. Engdahl, D. Blackwell and D. Schwartz (Eds.), *Neotectonics of North America*, Geol. Soc. Am., Decade Map Volume. 1992.
- Lewis, T. J., A. M. Jessop and A. S. Judge, Heat flux measurements in southwestern British Columbia: the thermal consequences of plate tectonics, *Can. J. Earth Sci.*, **22**, 1262-1273, 1985.
- Lewis, T. J, W. H. Bentkowski and R. D. Hyndman, Crustal temperatures near the LITHOPROBE southern Cordilleran transect, *Can. J. Earth Sci.*, **29**, 1197-1214, 1992.
- McCann, W. R., Nishenko, S. P., Sykes, L. R. and Kraus, J., Seismic gaps and plate tectonic: seismic potential for major boundaries., *Pure App. Geoph.*, **117**, 1082-1147, 1979.
- Majorowicz, J. A. and D. Ian Gough, Crustal Structures from MT Soundings in the Canadian Cordillera, *Earth Planet. Sci. Lett.*, **102**, 444-454, 1991.
- Majorowicz, J. A., D. I. Gough and T. J. Lewis, Correlation between the depth to the lower-crustal high conductive layer and heat flow in the Canadian cordillera, *Tectonophysics*, **225**, 49-56, 1993.
- Mallet, R., On the dynamics of earthquakes; being an attempt to reduce their observed phenomena to known laws of wave motion in solids and fluids, *Trans. R. Irish Acad.*, **21**, 50-106, 1848.
- Mallet, R., Second report on the facts of earthquake phenomena, *Brit. Assoc. Adv. Sci.*, **21**, 272-320, 1851.
- Mallet, R., Account of experiments made at Holyhead, *Philosophical Transactions of the Royal Society of London*, **151**, 655-679, 1861.

- Meissner, Rolf, *The continental crust, a geophysical approach*, Vol. 34 of International Geophysics Series, W. L. Donn, ed., Academic Press Inc., Toronto, 1986, 426 pp.
- Menke, W., *Geophysical Data Analysis: Discrete Inverse Theory*, revised edition, Academic Press, Inc., Toronto, 1989.
- Mereu, R. F., S. C. Majumdar and R. E. White, The structure of the crust and upper mantle under the highest ranges of the Canadian Rockies from a seismic refraction survey, *Can. J. Earth Sci.*, **14**, 196-208, 1977.
- Milne, J., *Earthquakes*, Appleton, New York, 1899.
- Milne, W. G., Rogers, G. C., Riddihough, G. A., McMechan, G. A., and Hyndman, R. D., Seismicity of Western Canada. *Can. J. Earth Sci.*, **15**, 1170-1193, 1978.
- Mintrop, L., *On the history of the seismic method for the investigation of underground formations and mineral deposits*, Seismos, Hannover, 1931.
- Milsom, J., *Field geophysics*, Halstead Press, New York, 182 pp., 1989.
- Mogi, K., 1968, Some features of recent seismic activity in and near Japan, 1. *Bull. Earthquake Res. Inst. Tokyo*, **46**, 1225-1236.
- Mogi, K., Two kinds of Gaps, *Pure Appl. Geoph.*, **117**, 1172-1186, 1979.
- Monger, J. W. H. and Ross, C. A., Distribution of Fusulinaceans in the Western Canadian Cordillera, *Can. J. Earth Sci.*, **8** : 259-278, 1971.
- Monger, J. W. H. and E. Irving, Northward displacement of north-central British Columbia, *Nature*, **285**, 289-294, 1980.
- Monger, J. W. H., Geology of the Ashcroft map-area, southwestern British Columbia., *Geol. Surv. Can. Paper* 82-1A, 293-297, 1982.
- Monger, J. W. H., R. A. Price and D. J. Tempelman-Kluit, Tectonic Accretion and the Origin of the Two major metamorphic and Plutonic Welts in the Canadian Cordillera, *Geology*, **10** : 70-75, 1982.
- Monger, J. W. H., Cordilleran tectonics: a Canadian perspective, *Bull. Soc. Geol. France*, **26**, pp. 255-278, 1984.
- Monger, J. W. H., Clowes, R. M., Price, R. A., Simony, P. S., Riddihough, R. P. and Woodsworth, G. J., B-2 Juan de Fuca Plate to Alberta plains. *Geol. Soc. Am., Continent/Ocean Transect* no. 7, 1985.

- Murphy, J. M., G. S. Fuis, A. R. Levander, W. J. Lutter, E. E. Criley, S. A. Henrys, I. Asudeh, and J. C. Fowler, Data report for the 1990 seismic reflection/refraction experiment in the Brooks Range, Arctic Alaska, United States Department of the Interior Geological Survey, Open-File Report 93-265, Menlo Park, 128 pp., 1993.
- Murphy, J. M., USGS FM cassette seismic-refraction recording system, United States Department of the Interior Geological Survey, Open-File Report 88-570, Menlo Park, 43 pp., 1988.
- Ohtake, M. T., Matumoto, T., and Lathan, G. V., Seismicity gap near Oaxaca, Southern Mexico as a probable precursor to a large earthquake. *Pure and Applied Geophysics*, 115, 375-385, 1977.
- Oldow J. S., A. W. Bally, H. G. Avé Lallemant, and W. P. Leeman, Phanerozoic evolution of the North American Cordillera; United States and Canada, in *The Geology of North America: An Overview, The Geology of North America Volume A*, edited by A. W. Bally and A. R. Palmer, Geological Society of America, Boulder, 139-232, 1989.
- O'leary, D. M., R. M. Clowes and R. M. Ellis, Crustal Velocity Structure in the Southern Coast Belt, British Columbia, *Can. J. Earth Sci*, 30, 2389-2403, 1993.
- Parrish, R. R., S. D. Carr, and D. L. Parkinson, Eocene extensional tectonics and geochronology of the southern Omineca Belt, British Columbia and Washington, *Tectonics*, 7, 181-212, 1988.
- Potter, C. J., Sanford, W. E., Yoos, T. R., Prussen, E. I., Keach II, R. W., Oliver, J. E., Kaufman, S. and Brown, L. D., COCORP deep seismic reflection traverse of the interior of the North American Cordillera, Washington and Idaho: implications for orogenic evolution. *Tectonics*, 5, 1007-1025, 1986..
- Potter, C. J., Origin, accretion, and post accretionary evolution of the Bridge River terrane, southwest British Columbia. *Tectonics*, 5, 1027-1041, 1986.
- Price, Raymond A. and Dugald M. Carmichael, Geometric test for late cretaceous-paleogene intracontinental transform faulting in the Canadian cordillera, *Geology*, 14, pp. 468-471, 1986.
- Read, P. B. and R. L. Brown, Columbia River fault zone: southeastern margin of the Shuswap and Monashee complexes, southern British Columbia, *Can. J. Earth Sci.*, 18, 1127-1145, 1981.
- Ross, G. M. and R. A. Stephenson, Crystalline Basement: The Foundations of Western Canada Sedimentary Basin, in *Western Canada Sedimentary Basin - A Case Study*, edited by B. D. Ricketts, Canadian Society of Petroleum Geologists,

Calgary, 320 pp, 1989.

- Ross, G. M., R. R. Parrish, M. E. Villeneuve, and S. A. Bowring, Geophysics and geochronology of the crystalline basement of the Alberta basin, western Canada, *Can. J. Earth Sci.*, **28**, 512-522, 1991.
- Ross, G. M., B. Milkereit, E. R. Kanasewich, D. W. Eaton, D. J. White, M. J. A. Burianyk and J. Mariano, Paleoproterozoic collisional orogen beneath western Canada sedimentary basin imaged by Lithoprobe crustal seismic reflection data, submitted to *Geology*, April, 1994.
- Schermer, Elizabeth R., David G. Howell and David L. Jones, The origin of allocthonous terranes: perspectives on the growth and shaping of continents, *Ann. Rev. Earth Planet. Sci.*, **12**, 107-131, 1984.
- Schoenberger, Michael (ed.), Special Issue on Seismic Signal Processing, *Proceedings of the IEEE*, **72**, 1984.
- SEG, *Digital tape standards*, Society of Exploration Geophysicists, Tulsa, 65 pp., 1980.
- SEG, *Positional data exchange formats standard*, Society of Exploration Geophysicists, Tulsa, 65 pp., 1983.
- Smith, R. B., W. C. Nagy, K. A. Julander, J. J. Viveiros, C. A. Barker, and D. G. Gants, Geophysical and tectonic framework of the eastern Basin and Range - Colorado Plateau-Rocky Mountain transition, in Geophysical framework of the continental United States, edited by L. C. Pakiser and W. D. Mooney, *Mem. Geol. Soc. Am.*, **172**, 205-233, 1989.
- Smithson, S. B., R. A. Johnson, and Y. K. Wong, Mean crustal velocity: A critical parameter for interpreting crustal structure and crustal growth, *Earth Planet. Sci. Lett.*, **53**, 323-332, 1981.
- Spence, G. D., R. M. Clowes and R. M. Ellis, Depth limits on the M discontinuity in the southern Rocky Mountain Trench, Canada, *Bull. Seismol. Soc. Am.*, **67**, 543-546, 1977.
- Spencer, C., I. Asudeh and T. Cote, SEG_Y_LDS Version 2.0 Format Reference Document, GSC Internal Report., 17 pp., 1989.
- Sykes, L. R., Intraplate Seismicity, Reactivation of Preexisting Zones of Weakness, Alkaline Magmatism, and Other Tectonism Postdating Continental Fragmentations, *Rev. Geoph. Space Phys.*, **16**, 621-688, 1978.
- Talwani, Pradeep, Seismotectonics in the Southeastern United States, in *Earthquakes at North-Atlantic Passive Margins: Neotectonics and Postglacial Rebound*, edited

- by S. Gregersen and P. W. Basham, Kluwer Academic Publishers, Boston, p.371-392, 1989a.
- Talwani, Pradeep, Characteristic Features of Intraplate Earthquakes and the Models Proposed to Explain Them, in *Earthquakes at North-Atlantic Passive Margins: Neotectonics and Postglacial Rebound*, edited by S. Gregersen and P. W. Basham, Kluwer Academic Publishers, Boston, p.563-579, 1989b.
- Telford, W. M., Geldart, L. P., and Sherrif, R. E., *Applied Geophysics*, 2nd ed., Cambridge University Press, New York, 1990, 770 pp.
- Thompson, G. A., R. Catchings, E. Goodwin, S. Holbrook, C. Jarchow, C. Mann, J. McCarthy, and D. Okaya, Geophysics of the western Basin and Range province, Geophysical framework of the continental United States, edited by L. C. Pakiser and W. D. Mooney, *Mem. Geol. Soc. Am.*, **172**, 177-203, 1989.
- Varsek, J. L., F. A. Cook, R. M. Clowes, J. M. Journeay, J. W. H. Monger, R. R. Parrish, E. R. Kanasewich and C. S. Spencer, Lithoprobe crustal reflection structure of the southern Canadian Cordillera 2: coast mountains transect, *Tectonics*, **12**, 334-360, 1993.
- Williams, Harold, Paul F. Hoffman, John F. Lewry, James W. H. Monger and Toby Rivers, Anatomy of North America: thematic geologic portrayals of the continent, *Tectonophysics*, **187**, 117-134, 1991.
- Villeneuve, M. E., G. M. Ross, R. J. Th  rialut, W. Miles, R. R. Parrish, and J. Broome, Tectonic subdivision and U-Pb geochronology of the crystalline basement of the Alberta Basin, Western Canada, *Geol. Surv. Can. Bull.* 447, 1993.
- Wheeler, J. O. and P. McFeeley, Tectonic Assemblage Map of the Canadian Cordillera and adjacent parts of the United States of America, scale 1:2 000 000, Geol. Surv. Can., Map 1712A, 1991.
- Wheeler, J. O., A. J. Brookfield, H. Gabrielse, J. W. H. Monger, H. W. Tipper and G. J. Woodsworth, Terrane map of the Canadian Cordillera, scale 1:2 000 000, Geol. Surv. Can., Map 1713A, 1991.
- Wickens, A. J., Variations in lithospheric thickness in Canada, *Can. J. Earth Sci.*, **8**, 1154-1162, 1971.
- Wickens, A. J., The upper mantle of southern British Columbia, *Can. J. Earth Sci.*, **14**, 1100-1115, 1977.
- Yilmaz, Ozdogan, *Seismic Data Processing*, SEG, Tulsa, 526 pp., 1987.

- Zelt, B. C., R. M. Ellis, and R. M. Clowes, 1990, SCoRE '89: The southern Cordillera refraction experiment-Description of dataset,.. LITHOPROBE Rep. 21, LITHOPROBE Secretariat, University of British Columbia, Vancouver, 36 pp, 1990.
- Zelt, B. C., R. M. Ellis, R. M. Clowes, E. R. Kanasewich, I. Asudeh, J. H. Luetgert, Z. Hajnal, A. Ikami, G. D. Spence, and R. D. Hyndman, Crust and upper mantle velocity structure of the Intermontane Belt, southern Canadian Cordillera, *Can. J. Earth Sci.*, **29**, 1530-1548, 1992.
- Zelt, B. C., R. M. Ellis and R. M. Clowes, Crustal velocity structure in the eastern and southernmost Coast belts, Canadian Cordillera, *Can. J. Earth Sci.*, **30**, 1014-1027, 1993.
- Zeit, C. A., and R. M. Ellis, Practical and efficient ray tracing in two- dimensional media for rapid travel time and amplitude forward modeling, *Can. J. Expl. Geophys.*, **24**, 16-31, 1988.
- Zelt, C.A., and R. B. Smith, Seismic travelttime inversion for 2-D crustal velocity structure, *Geophys. J. Int.*, **108**, 16-34, 1992.
- Zelt, C.A. and D.J. White, Crustal structure of the southeastern Canadian Cordillera from wide-angle seismic data, in preparation.
- Zoback, Mary Lou and Mark Zoback, State of Stress in the Conterminous United States, *J. Geoph. Res.*, **85**, 6113-6156, 1980.
- Zoback, Mary Lou , Nishenko, S. P., Richardson, R. M., Hasegawa, H. S. and Zoback, M. D., Mid-plate stress, deformation, and seismicity. *The Geology of North America, Vol M.*, Chapter 18. The Western North Atlantic Region, Geological Society of America, 297-312, 1986.
- Zverev, S. M. (Ed.), *Problems in Deep Seismic Sounding*, Consultants Bureau, New York, 166 pp., 1967.

Appendices

Appendix 1 SCoRE '90 Schedule

Monday, August 6

a) Pickup of GSC equipment at Ferry terminal in Tacoma, Washington (after Alaska experiment). b) Arrival of unlicensed shooters in Vancouver. c) Departure of some UBC people to Clearwater Lake.

Tuesday, August 7

a) BC blaster's licence exams for unlicensed shooters at 9 am. b) Setup GSC base at UBC - Dept. of Geophysics and Astronomy.

Wednesday, August 8

a) Arrival of most other participants in Vancouver/UBC. b) General briefing in evening. c) Setup base in Clearwater Lake.

Thursday, August 9

a) USGS set up base at UBC - Dept. of Geophysics and Astronomy. b) Begin deployment of **LINE 10** from Clearwater Lake (helicopter, boat and road). c) Begin helicopter deployment of **LINE 10** from Vancouver.

Friday, August 10

a) Complete deployment of **LINE 10** from Clearwater Lake. b) Complete deployment of **LINE 10** with USGS and remaining GSC instruments. c) **Shoot LINE 10 overnight** (i.e. starting 12:00 midnight PDT, August 11 - 0700 UT, August 11).

Saturday, August 11

a) Begin pickup of **LINE 10**. b) Upload lunchboxes in Clearwater and Vancouver bases.

Sunday, August 12

a) Finish uploading lunchboxes. b) Begin packing up Clearwater and Vancouver bases for move to Castlegar. c) Leave for Castlegar. d) USGS digitize and instrument repair cycle (in Vancouver).

Monday, August 13

a) Begin setting up base in Castlegar. b) USGS move to Merrit/Boston Bar/Hope.

Tuesday, August 14

a) Finish setting up base. b) Personnel training (LithoSEIS for deployers). c) USGS program instruments. d) Begin downloading and deployment of **LINE 7** with Canadian instruments.

Wednesday, August 15

a) Finish downloading and deploying **LINE 7** with Canadian instruments. b) USGS deploy instruments. c) **Shoot LINE 7 overnight** (i.e. starting 12:00 midnight PDT, August 16 - 0700 UT, August 16).

Thursday, August 16

a) Begin pick-up of Canadian lunchboxes. b) Begin upload of lunchboxes. c) USGS pick up instruments.

Friday, August 17

a) Continue upload. b) USGS travel from Merrit/Boston Bar/Hope to Castlegar.

Saturday, August 18

a) Begin download and deployment of Canadian lunchboxes on **LINE 8**. b) USGS digitize and instrument repair cycle.

Sunday, August 19

a) Complete download and deployment of Canadian lunchboxes on LINE 8. b) USGS program and deploy instruments on LINE 8. c) Shoot LINE 8 overnight (i.e. starting 12:00 midnight PDT, August 20 - 0700 UT, August 20).

Monday, August 20

a) Begin pick-up of Canadian lunchboxes. b) Begin upload of lunchboxes. c) USGS pick up instruments.

Tuesday, August 21

a) Continue upload of Canadian lunchboxes. b) Begin download and deployment of Canadian instruments on LINE 9. c) USGS digitize and instrument repair cycle. d) USGS travel to Kimberley/Blairmore.

Wednesday, August 22

a) Continue download and deployment of Canadian lunchboxes on LINE 9. b) USGS travel and deploy instruments on LINE 9. c) Shoot LINE 9 overnight (i.e. starting 12:00 midnight PDT, August 23 - 0700 UT, August 23).

Thursday, August 23

a) Leave instruments out for another night b) Backup - Shoot LINE 9 SHOTPOINT 44 overnight (i.e. at 12:00 midnight PDT, August 24 - 0700 UT, August 24).

Friday, August 24

a) Begin pick-up of Canadian lunchboxes. b) Begin upload of lunchboxes. c) USGS pick up instruments and travel to Castlegar. d) Finish upload Canadian lunchboxes. e) USGS digitization, repair cycle, etc. f) begin packing up Castlegar base.

Saturday, August 25

a) Finish up uploading, archiving, digitization and packing up. b) leave Castlegar.

Appendix 2 SCoRE '90 Participants

- 1) Michael Burianyk (U of A) - Organizer
- 2) Ernest Kanasevich (U of A) - Scientist and Principal Investigator
- 3) Greg Purdue (U of A) - Line scout, deployer, shooter's helper
- 4) Lindsey Brady (U of A) - Line scout, deployer, shooter's helper
- 5) Sotiris Kapotas (U of A) - Deployer, shooter's helper
- 6) Nanxun Dai (U of A) - Deployer, shooter's helper
- 7) Laurence Le (U of A) - Deployer, shooter's helper
- 8) Joe Stuhec (U of A) - Deployer, shooter's helper
- 9) Len Tober (U of A) - Technician, line scout, deployer, shooter's helper
- 10) Jay Haverstock (U of A) - Technician, deployer, shooter's helper
- 11) George Spence (UVic) - Scientist and deployer
- 12) Nancy McLean (UVic) - Deployer, shooter's helper
- 13) Jack Arnold (U of S) - Technician, shooter
- 14) Alex Bezdan (U of S) - shooter
- 15) Doug Neilson (U of S) - shooter
- 16) Bob Ellis (UBC) - Scientist
- 17) Ron Clowes (UBC) - Scientist
- 18) Brad Isbell (UBC) - Line scout, deployer, shooter's helper
- 19) Barry Zelt (UBC) - Line scout, deployer, shooter's helper
- 20) Sukhi Hundal (UBC) - Deployer, shooter's helper
- 21) Audrey Willet (UBC) - Deployer, shooter's helper
- 22) Li Sun (UBC) - deployer, shooter's helper

- 23) Sonya Dehler (UBC) - Deployer
- 24) John Hole (UBC) - Deployer, shooter's helper
- 25) John Fraser (UBC) - deployer, shooter's helper
- 26) Bo Chandra (UBC/Consultant) - shooter
- 27) Peter Carroll (LITHOPROBE) - Shotpoint coordinator
- 28) Don White (GSC) - Scientist and lab crew
- 29) Tim Côté (GSC) - Lab chief
- 30) Dave Forsyth (GSC) - Scientist and shooter
- 31) Blake Wright (GSC) -lab technician
- 32) Tim Cartwright (GSC) -Technician, lab crew, deployer
- 33) Rebecca Irving (GSC) - Lab crew, deployer, shooter's helper
- 34) Emmanuel Saydeh (GSC) - Lab crew, deployer, shooter's helper
- 35) Jim Luetgert (USGS) - Scientist and shooter
- 36) Ron Kaderabek (USGS) - Electronics technician and shooter
- 37) Rufus Catchings (USGS) - Scientist , deployer, shooter's helper
- 38) Joseph Cotton (USGS) - Deployer, shooter
- 39) Mark Goldman (USGS) - Deployer, computer
- 40) Lynn Dietz (USGS) - Deployer, shooter's helper
- 41) Bob McClearn (USGS) - Technician, deployer, shooter's helper
- 42) Cliff Gill (USGS) -Deployer, shooter's helper

Appendix 3 SCoRE '90 Shotpoint List

(Shotpoint number, shotpoint name, closest receiver location, NTS map number, number of holes and size of shot)

LINE 7

SP 23 Keefers	(R7701)	NTS 92I/4	2 holes - 1800 kg (SCoRE '89 SP 7)
SP 24 Lower Nicola	(R7702)	NTS 92I/2	1 hole - 200 kg (SCoRE '89 SP 2)
SP 25 Quilchena	(R7457)	NTS 92I/1	1 hole - 200 kg
SP 27 Lumby	(R7721)	NTS 82L/3	1 hole - 800 kg
SP 28 Cherry Creek	(R7723)	NTS 82L/8	1 hole - 200 kg
SP 29 Nakusp	(R7725)	NTS 82K/5	1 hole - 200 kg
SP 30 Lardeau River	(R7726)	NTS 82K/7	3 holes - 2000 kg

LINE 8

SP 32 Big Mouth Crk	(R8001)	NTS 82M/15	2 holes - 1800 kg
SP 33 Downie Creek	(R8016)	NTS 82M/8	1 hole - 200 kg
SP 34 Sale Creek	(R8301)	NTS 82M1	1 hole - 200 kg
SP 35 Cranberry Crk	(R8058)	NTS 82L/16	1 hole - 800 kg
SP 61A Arrow Park	(R8302)	NTS 82L/8	1 hole - 200 kg
SP 61B Arrow Park	(R8302)	NTS 82L/8	1 hole - 200 kg
SP 69 Whatshan Lk	(R8128)	NTS 82L/1	1 hole - 200 kg
SP 36 Applegrove	(R8303)	NTS 82E/16	1 hole - 200 kg <i>Site shared with Line 9</i>
SP 37 Norns Crk	(R8210)	NTS 82F/5	2 holes - 1800 kg

LINE 9

SP 38 Big White Mtn.	(R0800)	NTS 82E/14	2 holes - 1800 kg
SP 36 Applegrove	(R1101)	NTS 82E/16	1 hole - 200 kg <i>Site shared with Line 8</i>
SP 75 Kokanee Crk	(F1102)	NTS 82F/11	1 hole - 200 kg
SP 40 Redding Crk	(R0943)	NTS 82F/9	1 hole - 200 kg
SP 41 St. Mary Lk	(R0963)	NTS 82F/9	1 hole - 800 kg
SP 42 Horseshoe Lk	(R1105)	NTS 82G/12	1 hole - 200 kg

SP 43 Hosmer Crk	(R1106)	NTS 82G/10	1 hole - 200 kg
SP 44 Byron Crk	(R1085)	NTS 82G/9	2 holes - 1800 kg

LINE 10

SP 46 Mystery Crk	(R2001)	NTS 92H/5	3 holes - 2500 kg
SP 47 Gowan Crk	(R2049)	NTS 92G/16	1 hole - 200 kg
SP 48 Pemberton	(R2102)	NTS 92J/7	1 hole - 200 kg
SP 49 Salal Crk	(R2153)	NTS 92J/1	1 hole - 800 kg
SP 50 Tatlayoko Lk	(R2248)	NTS 92N/9	1 hole - 400 kg
SP 51 Miner Lk	(R2302)	NTS 92 N/15	2 holes - 1800 kg

In addition for Line 7:

SP 26 Bouleau Mntn NTS 82L/5 1 hole-200 kg drilled but not found or fired

Appendix 4 Number of Shotholes and Quantity of Explosives

Line 7	7 SPs total:	4 holes (4 x 140') x 900 kg	560'	3600kg
		1 hole (1 x 140') x 800 kg	140'	800kg
		6 holes (6 x 100') x 200 kg	<u>600'</u>	<u>1200kg</u>
			1300'	5600kg
Line 8	8 SPs total:	4 holes (4 x 140') x 900 kg	560'	3600kg
		1 hole (1 x 140') x 800 kg	140'	800kg
		6 holes (6 x 100') x 200 kg	<u>600'</u>	<u>1200kg</u>
			1300'	5600kg
Line 9	8 SPs total	4 holes (4 x 140') x 900 kg	560'	3600kg
		1 hole (1 x 140') x 800 kg	140'	800kg
		5 holes (5 x 100') x 200 kg	<u>500'</u>	<u>1000kg</u>
			1200'	5400kg
Line 10	6 SPs total:	4 holes (4 x 140') x 900 kg	560'	3600kg
		1 hole (1 x 140') x 700 kg	140'	700kg
		1 hole (1 x 140') x 800 kg	140'	800kg
		1 hole (1 x 100') x 400 kg	100'	400kg
		2 holes (2 x 100') x 200 kg	<u>200'</u>	<u>400kg</u>
			1140'	5900kg

This is a total of 4,940' of holes drilled and 22,500kg of explosives used.

Appendix 5 Detailed Shothole Locations and Shot times

NOTE: all times are UT (i.e. not local time)

Shot 23 charge size: 1800 kg

day	year	hour	min	sec	µsec
228	1990	6	59	59	999001

lat	long	elev(m asl)	depth(m)
deg min	deg min		
50 0.3067	121 35.9383	337	42.0

<u>Shot 24</u>						charge size: 200kg
day	year	hour	min	sec	μsec	
228	1990	12	59	59	999001	
lat		long		elev(m asl)	depth(m)	
deg	min	deg	min			
50	18.6233	120	53.7500	1053	42.0	

<u>Shot 25</u>						charge size: 200 kg
day	year	hour	min	sec	μsec	
228	1990	7	2	0	0	
lat		long		elev(m asl)	depth(m)	
deg	min	deg	min			
50	11.1076	120	24.5480	789	30.0	

<u>Shot 27</u>						charge size: 800 kg
day	year	hour	min	sec	μsec	
228	1990	7	8	0	32000	
lat		long		elev(m asl)	depth(m)	
deg	min	deg	min			
50	12.4909	119	01.1416	590	42.0	

<u>Shot 28</u>						charge size: 200 kg
day	year	hour	min	sec	μsec	
228	1990	13	4	0	11000	
lat		long		elev(m asl)	depth(m)	
deg	min	deg	min			
50	18.1088	118	19.2295	1050	42.0	

<u>Shot 29</u>						charge size: 200 kg
day	year	hour	min	sec	μsec	
228	1990	7	5	59	985001	
lat		long		elev(m asl)	depth(m)	
deg	min	deg	min			
50	16.9632	117	44.6695	814	30.0	

<u>Shot 30</u>						charge size: 2000kg
day	year	hour	min	sec	μsec	
228	1990	7	12	0	76000	
lat		long		elev(m asl)	depth(m)	
deg	min	deg	min			
50	25.03	117	08.45	688	42.0	

Shot 32 charge size: 1800 kg

day	year	hour	min	s	ec	μsec		
232	1990	7	2		0	0		
	lat			long		elev(m asl)	depth(m)	
deg	min		deg	min				
51	49.4545		118	32.1687		648	42.0	

Shot 33 charge size: 200 kg

day	year	hour	min	s	sec	μsec		
232	1990	7	4		0	37000		
	lat			long		elev(m asl)	depth(m)	
deg	min		deg	min				
51	29.1471		118	26.0025		807	30.0	

Shot 34 charge size: 200 kg

day	year	hour	min	s	sec	μsec		
232	1990	11	0		0	46000		
	lat			long		elev(m asl)	depth(m)	
deg	min		deg	min				
51	10.2900		118	11.4860		800	30.0	

Shot 35 charge size: 800 kg

day	year	hour	min	s	sec	μsec		
232	1990	7	6		0	77000		
	lat			long		elev(m asl)	depth(m)	
deg	min		deg	min				
50	46.7780		118	2.9770		636	42.0	

Shot 61a charge size: 200kg

day	year	hour	min	s	sec	μsec		
232	1990	7	0		0	2000		
	lat			long		elev(m asl)	depth(m)	
deg	min		deg	min				
50	21.050		118	2.091		702	30.0	

note: there are two shotpoints 61 (61a and 61b) shot at the same location but at different times

Shot_61b charge size: 200 kg

day	year	hour	min	sec	μsec		
232	1990	7	12	0	2000		
lat		long		elev(m asl)		depth(m)	
deg	min	deg	min				
50	21.050	118	2.091		702		30.0

note: this is the second shotpoint 61 (same location,different shot time)

Shot_62 charge size: 200 kg

day	year	hour	min	sec	msec		
232	1990	11	2	0	2000		
lat		long		elev(m asl)		depth(m)	
deg	min	deg	min				
50	6.56	118	5.64		462		30.0

Shot_36 charge size: 200 kg

day	year	hour	min	sec	μsec		
232	1990	7	7	59	990000		
lat		long		elev(m asl)		depth(m)	
deg	min	deg	min				
49	47.9620	118	04.1884		429		30.0

note: there is a second shotpoint 36, same location as this one, but at a different time

Shot_36 charge size: 200 kg

day	year	hour	min	sec	μsec		
235	1990	7	2	0	32000		
lat		long		elev(m asl)		depth(m)	
deg	min	deg	min				
49	47.9620	118	04.1884		429		30.0

note: this is a second shotpoint 36, same location as last one, but at a different time

Shot_37 charge size: 1800 kg

day	year	hour	min	sec	μsec		
232	1990	7	10	0	0		
lat		long		elev(m asl)		depth(m)	
deg	min	deg	min				
49	25.0856	117	42.3707		875		42.0

Shot 38 charge size: 1800 kg

day	year	hour	min	sec	μsec		
235	1990	7	0	0	32000		

lat		long		elev(m asl)	depth(m)
deg	min	deg	min		
49	45.9012	119	01.1086	1498	42.0

Shot 75 charge size: 200 kg

day	year	hour	min	sec	μsec		
235	1990	7	4	0	0		

lat		long		elev(m asl)	depth(m)
deg	min	deg	min		
49	38.3592	117	09.0228	841	30.0

Shot 40 charge size: 200 kg

day	year	hour	min	sec	μsec		
235	1990	10	59	59	980000		

lat		long		elev(m asl)	depth(m)
deg	min	deg	min		
49	39.7825	116	29.5937	1266	30.0

Shot 41 charge size: 800 kg

day	year	hour	min	sec	μsec		
235	1990	7	5	59	984000		

lat		long		elev(m asl)	depth(m)
deg	min	deg	min		
49	37.217	116	13.016	1053	42.0

Shot 42 charge size: 200 kg

day	year	hour	min	sec	μsec		
235	1990	11	2	0	0		

lat		long		elev(m asl)	depth(m)
deg	min	deg	min		
49	34.841	115	31.197	884	30.0

Shot 43 charge size: 200 kg

day	year	hour	min	sec	μsec		
235	1990	7	8	0	0		

lat		long		elev(m asl)	depth(m)
deg	min	deg	min		
49	34.950	114	56.947	1169	30.0

Shot 44 charge size: 1800 kg

day	year	hour	min	sec	μsec		
236	1990	7	0	0	34000		

lat		long		elev(m asl)	depth(m)
deg	min	deg	min		
49	30.9780	114	23.7418	1512	42.0

Shot 46 charge size: 2500 kg

day	year	hour	min	sec	μsec		
223	1990	7	8	0	11000		

lat		long		elev(m asl)	depth(m)
deg	min	deg	min		
49	30.8658	121	55.64461	375.0	42.0

Shot 47 charge size: 200 kg

day	year	hour	min s	ec	μsec		
223	1990	7	6	0	2000		

lat		long		elev(m asl)	depth(m)
deg	min	deg	min		
49	55.3704	122	21.89819	100.0	32.0

Shot 48 charge size: 200 kg

day	year	hour	min	sec	μsec		
223	1990	7	4	0	36000		

lat		long		elev(m asl)	depth(m)
deg	min	deg	min		
50	22.5678	122	50.877	221.0	30.0

Shot 49 charge size: 800 kg

day	year	hour	min	sec	μsec		
223	1990	7	2	0	5000		

lat		long		elev(m asl)	depth(m)
deg	min	deg	min		
50	41.1996	123	30.399	716.0	42.0

Shot 50 charge size: 400 kg

day	year	hour	min	sec	μsec		
223	1990	7	0	0	12000		

lat		long		elev(m asl)	depth(m)
deg	min	deg	min		
51	28.8	124	24.6936	830.0	30.0

<u>Shot 51</u>		charge size: 1800 kg			
day	year	hour	min	sec	μsec
223	1990	11	0	0	21000
lat		long		elev(m asl)	depth(m)
deg	min	deg	min		
51	54.1866	124	57.8046	1388.0	42.0

Appendix 6 SCoRE '90 Shotpoint Environmental Requirements

COGLA Regulations for shothole clearance

For residence or area of public congregation or water well:

$$D = \text{Sqrt}(E) * 45.0$$

For oil or gas pipeline (measure from the centre line of the pipeline) and an oil or gas well:

$$D = \text{Sqrt}(E) * 22.6$$

where E is charge weight (in Kilograms) and D is distance (i.e. clearance) from shotpoint to structure in meters.

On this basis required clearances were:

2000m for 1800 kg
1300m for 800 kg
640m for 200 kg

EMR- Office of Environmental Affairs (OEA) Conditions for Approval

- 1) The 200 and 800 kg. explosive charges are not to be detonated closer than 650 m (preferably 1000 m) from fish-bearing waters.
- 2) The 1800 kg. charges are not to be detonated closer than 1500 m (preferably 2000 m) from fish-bearing waters.
- 3) No run-off, drill cuttings, drilling muds, or any other effluent, including solid waste, from the land clearing, road construction, drilling or detonation operations are to be released or placed in such a manner to allow release into fish-bearing waters or fish habitats.
- 4) Municipalities' mayors must be informed of the seismic work that will be done in their areas. The information should be provided to them prior to the beginning of the work.

Appendix 7 SCoRE '90 Receiver Site Names

NB: Note that numbers in *bold italics* refer to sites recorded by USGS instruments.

LINE 5 (Spatial Array - recorded only during deployments for lines 7 and 9)

5310 (Line 7 deployment only), 5311 (Line 9 deployment only), 5214, 5216, 5218, 5249 - 5252 (Line 7 and 9 deployments simultaneously), 5243 - 5247, 5256 - 5260 (Line 9 deployment only).

Total: 19 (maximum possible number of traces for each shot record of Line 5)

LINE 6 (Broadside Array - recorded only during deployment for Line 8)

6222 - 6300

Total: 79 (maximum possible number of traces for each shot record of Line 6)

LINE 7

7400 - 7505, 7506 - 7605, 7611 - 7632, 7634 - 7649, 7655 - 7672, 7679 - 7687, 7701, 7702, 7703 - 7714, 7721, 7723, 7724, 7725, 7726

Total: 290 (maximum possible number of traces for each shot record of Line 7)

Closest receiver to shotpoint - SP23(*R7701*), SP24(*R7702*), SP25(*R7457*), SP27(*R7721*) SP28(*R7723*), SP29(*R7725*), SP30(*R7726*)

LINE 88001 - 8113, 8117 - 8161, 8163 - 8180, ~~8181 - 8221~~, 8301, 8302, 8303, 8311**Total:** 221 (maximum possible number of traces for each shot record of Line 8)**Closest receiver to shotpoint -** SP32(R8001), SP33(8016), SP34(R8301), SP35(8058), SP61(R8302), SP69(R8128), SP36(R8303), SP37(~~R8210~~)**LINE 9**

0800 - 0803, 0805 - 0816, 0163 - 0196, 0853 - 0901, 0906 - 0920, 0928 - 0968,

~~0969 - 1028, 1033 - 1044, 1046 - 1088~~, 1101 - 1104, ~~1105 - 1106~~**Total:** 276 (maximum possible number of traces for each shot record of Line 9)**Closest receiver to shotpoint -** SP38(R0800), SP36(R1101), SP75(R1102), SP40(R0943), SP41(R0963), SP42(~~R1105~~), SP43(~~R1106~~), SP44(~~R1085~~)**LINE 10**2001 - 2027, ~~2028 - 2055, 2057 - 2070, 2072 - 2084, 2086, 2088 - 2103, 2105 - 2109, 2111 - 2125, 2127 - 2144~~, 2148 - 2203, 2205 - 2246, 2248, 2249, 2252 - 2300, 2302, 2304, 2306, 2308**Total:** 290 (maximum possible number of traces for each shot record of Line 10)**Closest receiver to shotpoint -** SP46(R2001), SP47(~~R2049~~), SP48(~~R2102~~), SP49(R2153), SP50(R2248), SP51(R2302)**Appendix 8 Deployment and Shooting Schedule**

Deployment	Shotpoint	Size (Kg)	Date	Time (PDT)	Shooter
1*	46	2500	August 11	12:08am (0708UT)	B. Chandra
1*	47	200	August 11	12:06am (0706UT)	J. Luetgert
1*	48	200	August 11	12:04am (0704UT)	A. Bezdan
1*	49	800	August 11	12:02am (0702UT)	D. Neilson
1*	50	400	August 11	12:00am (0700UT)	J. Arnold
1*	51	1800	August 11	04:00am (1100UT)	J. Arnold
2†	23	1800	August 16	12:00am (0700UT)	J. Luetgert
2†	24	200	August 16	06:00am (1300UT)	J. Luetgert
2†	25	200	August 16	12:02am (0702UT)	R. Kaderabek
2†	27	800	August 16	12:08am (0708UT)	A. Bezdan
2†	28	200	August 16	06:04am (1304UT)	B. Chandra
2†	29	200	August 16	12:06am (0706UT)	D. Neilson
2†	30	2000	August 16	12:12am (0712UT)	J. Arnold
3@	32	1800	August 20	12:02am (0702UT)	J. Luetgert
3@	33	200	August 20	12:04am (0704UT)	A. Bezdan
3@	34	200	August 20	04:00am (1100UT)	A. Bezdan
3@	35	800	August 20	12:06am (0706UT)	J. Arnold
3@	61A	200	August 20	12:00am (0700UT)	D. Forsyth
3@	61B	200	August 20	12:12am (0712UT)	D. Forsyth
3@	69	200	August 20	04:02am (1102UT)	D. Forsyth
3@	36	200	August 20	12:08am (0708UT)	D. Neilson
3@	37	1800	August 20	12:10am (0710UT)	R. Kaderabek
4#	38	1800	August 23	12:00am (0700UT)	D. Forsyth
4#	36	200	August 23	12:02am (0702UT)	A. Bezdan
4#	75	200	August 23	12:04am (0704UT)	R. Kaderabek
4#	40	200	August 23	04:00am (1100UT)	D. Neilson

4#	41	800	August 23	12:06am (0706UT)	D.Neilson
4#	42	200	August 23	04:02am (1102UT)	J. Luetgert
4#	43	200	August 23	12:08am (0708UT)	J. Luetgert
4#	44	1800	August 24	12:00am (0700UT)	J. Arnold

* Line 10

† Line 7 and part of spatial array

@ Line 8 and broadside array

Line 9 and part of spatial array

Appendix 9 SCoRE '90 Shot Profiles

The following pages have plots of all shot records for Lines 7, 8 and 6 (broadside). For each record of lines 7 and 8, there are two plots, one without and one with arrival picks. The broadside records are only shown without arrival picks.

